FAKULTÄT FÜR MEDIZIN DER TECHNISCHEN UNIVERSITÄT MÜNCHEN

Lehrstuhl für Medizinische Mikrobiologie, Immunologie und Hygiene

Immune factors guiding *Listeria monocytogenes* infection

Steven Phillip Broadley

Vollständiger Abdruck der Fakultät für Medizin der Technischen Universität München zur Erlangung des akademischen Grades eines

Doktors der Naturwissenschaften

genehmigten Dissertation.

Vorsitzender: Univ.-Prof. Dr. M. Göttlicher

Prüfer der Dissertation:

1. Univ.-Prof. Dr. D. Busch
2. apl. Prof. Dr. Th. M. Fuchs

Die Dissertation wurde am 15.09.2015 bei der Technischen Universität München eingereicht und durch die Fakultät für Medizin am 16.12.2015 angenommen.

Summary

Under normal conditions blood is sterile. Should bacteria reach the bloodstream, they must be removed rapidly to prevent the development of life-threatening diseases. Two organs dominate clearance of bacteria from the bloodstream: the liver, primarily known for destruction of pathogens, and the spleen, where antigen is used to prime long-lasting immune responses. Systemically circulating *Listeria monocytogenes* (*L.m.*) have been reported to bind murine blood platelets dependent on complement factor 3 (C3) and the platelet receptor Glycoprotein Ib (GPIb). Disruption of binding resulted in a faster clearance of *L.m.* from the bloodstream. The aim of this thesis was to investigate the process of *L.m.* – platelet complex formation and how binding to platelets alters the fate of systemically circulating *L.m.*.

Light transmission platelet aggregometry revealed the process of *L.m.* – platelet interaction to consist of three distinct phases: I) Opsonization of *L.m.* with C3, II) formation of *L.m.* – platelet complexes dependent on C3 and GPIb, and III) activation and aggregation of platelets around complexed *L.m.* dependent on Immunoglobulin G. Utilizing 2-photon intravital imaging, novel positron-emission tomography and flow cytometry analysis it was found that clearance of systemically circulating *L.m.* is predominantly facilitated by hepatic Kupffer cells, who utilize two distinct mechanisms for the clearance of either non-platelet bound *L.m.* or *L.m.* – platelet complexes from the circulation: Uptake of non-platelet bound *L.m.* was found to depend on class A scavenger receptors (SRA), while uptake of *L.m.* – platelet complexes depended on the complement receptor of the immunoglobulin superfamily (CRIg). SRA-mediated clearance was found to be more efficient in the uptake and destruction of *L.m.* than its CRIg dependent counterpart. The slower clearance of *L.m.* – platelet complexes led to increased localization of *L.m.* to other organs, especially the spleen. CRIg-mediated clearance of bacteria-platelet complexes was also observed after systemic infection with other Gram (+) and Gram (-) bacteria, such as *Enterococcus faecalis* and *Escherichia coli*. A lack of clearance of *L.m.* – platelet complexes led to bacterial localization to the lung, indicating that aggregation of platelets around *L.m.*, as had been observed *in vitro*, possibly led to the formation of microthrombi.

Taken together, the data presented in this thesis indicate following process: After systemic infection Kupffer cells rapidly remove and destroy non-platelet bound *L.m.* from the circulation via SRA-mediated uptake. A portion of circulating *L.m.* binds to platelets, shifting hepatic clearance to CRIg-dependent uptake. CRIg-mediated clearance of *L.m.* from the bloodstream is slower than initial SRA-mediated clearance, thus allowing a small but important amount of bacterial localization to the spleen, where the antigen is used to prime adaptive immune responses.

Zusammenfassung

Normalerweise ist Blut steril. Gelangen Bakterien in die Blutbahn, müssen sie schnellstmöglich entfernt werden um lebensgefährliche Krankheiten zu vermeiden. Bakterien werden hauptsächlich von zwei Organen aus der Blutbahn gefiltert: Der Leber, in der Bakterien zerstört werden, und der Milz, in der bakterielles Antigen zur Ausbildung einer lang anhaltenden Immunantwort genutzt wird. Es wurde gezeigt, dass in der Maus systemisch zirkulierende *Listeria monocytogenes* (*L.m.*) Blutplättchen mittels Komplementfaktor 3 (C3) und dem Plättchen-Rezeptor Glykoprotein Ib (GPIb) binden. Wurde diese Komplexbildung durch Plättchen, C3 oder GPIb Defizienz unterbunden, so wurden zirkulierende *L.m.* schneller aus der Blutbahn entfernt als im Wildtypen. Ziel dieser Dissertation war es, Vorgänge und Auswirkungen der Komplexbildung zwischen *L.m.* und Plättchen zu untersuchen.

Licht-Transmissions-Aggregometrie zeigte, dass die Interaktion zwischen *L.m.* und Plättchen aus drei individuellen Phasen besteht: I) Der Opsonisierung von *L.m.* mit C3, II) Der Bildung von *L.m.*-Plättchen Komplexen abhängig von C3 und GPIb und III) Der Aktivierung und Aggregation von Plättchen um gebundene *L.m.* abhängig von Immunoglobulin G (IgG). Mittels intravitaler 2-Photonenmikroskopie, Positronen-Emissions-Tomographie und Durchfluss-zytometrie wurde herausgefunden, dass Kupffer-Zellen der Leber den Großteil zirkulierender *L.m.* aus dem Blut entfernen, wobei zwei verschiedene Mechanismen die Aufnahme von freien *L.m.* und *L.m.*-Plättchen-Komplexen bewerkstelligten: Während freie *L.m.* in Abhängigkeit von Klasse A Scavenger Rezeptoren (SRA) aufgenommen wurden, war die Aufnahme von *L.m.* – Plättchen-Komplexen abhängig von dem Komplementrezeptor der Immunoglobulin Superfamilie (CRIg). Die Entfernung freier *L.m.* aus der Blutbahn mittels SRA geschah schneller als die Entfernung komplexgebundener *L.m.* mittels CRIg und zerstörte *L.m.* effektiver. Durch die langsamere Komplexentfernung gelangen Bakterien zu anderen Organen, insbesondere zur Milz. CRIg-abhängige Aufnahme von Bakterien-Plättchen-Komplexen wurde ebenfalls nach systemischer Infektion mit anderen Gram (+) und Gram (-) Bakterien beobachtet, wie z.B. *Ent. faecalis* oder *E. coli*. Ohne CRIg-vermittelte Aufnahme von *L.m.*-Plättchen-Komplexen kam es zu einer Lokalisation von *L.m.* in der Lunge, was darauf hindeutet, dass Plättchenaktivierung und -aggregation um gebundene *L.m.* die Bildung von Mikrothrombi bedingen könnte.

Zusammenfassend deuten die Ergebnisse dieser Dissertation auf folgenden Ablauf hin: Nach systemischer Infektion entfernen Kupffer-Zellen rasch freie *L.m.* mittels SRA. Ein Teil der *L.m.* bindet an Plättchen und wird mittels CRIg von den Kupffer-Zellen entfernt. *L.m.* Aufnahme durch CRIg ist langsamer als durch SRA und ermöglicht so einem kleinen Teil der *L.m.* das Erreichen der Milz, wo das bakterielle Antigen zur Generierung einer adaptiven Immunantwort verwendet wird.

Table of contents

List of figures, tables and illustrations

List of abbreviations

°C	Degrees Celsius
A	Ampere
ActA	actin assembly inducing protein
ADP	adenosine diphosphate
ASGR	asialoglycoprotein receptor
Bf	factor B
BHI	brain heart infusion
Bq	Bequerel
BSA	bovine serum albumin
C	complement factor
Ca^{2+}	calcium
CD	cluster of differentiation
CFSE	carboxyfluorescein succinimidyl ester
CFU	colony forming units
CMTMR	chloromethyl benzoylamino tetramethylrhodamine
CR	complement receptor
CRD	carbohydrate recognition domain
CT	computed tomography
DC	dendritic cell
DNase	deoxyribonuclease
EDTA	ethylene diamine tetraacetate
FACS	fluorescence-activated cell sorting
FCS	fetal calf serum
FDG	fluordeoxyglucose
fH	factor H
FITC	fluorescein isothiocyanate
FSC	forward scatter
g	gram
GlcNac	N-acetylglucosamine
GP	glycoprotein
h	hour
HEPES	hydroxyethyl piperazine ethanesulfonic acid
ID	injected dose

Ig	immunoglobulin
l	litre
L.m.	*Listeria monocytogenes*
LLO	Listeriolysin O
LPS	lipopolysaccharide
LTA	lipoteichoic acid
Mg^{2+}	magnesium
min	minute
M	molar
MMF	medetomidin/midazolam/fentanyl
Mn^{2+}	manganese
OD	optical density
PAMP	pathogen associated molecular pattern
PBS	phosphate buffered saline
PET	positron emission tomography
PI	propidium iodide
Poly(C)	polycytidylic acid
Poly(I)	polyinosinic acid
PPP	platelet poor plasma
PRP	platelet rich plasma
PRR	pattern recognition receptor
ROI	region of interest
s	second
SD	standard deviation
SEM	standard error of the means
SRA	class A scavenger receptor
SSC	side scatter
TLR	toll-like receptor
v/v	volume per volume
vWF	von-Willebrandt factor
w/v	weight per volume
WT	wild-type

1 Introduction

Infections of the bloodstream allow bacteria to spread rapidly throughout the body, which in turn may lead to serious diseases, such as infectious endocarditis and meningitis or sepsis (Miniño *et al.,* 2011). Such an infiltration of the bloodstream can arise from disseminating infections, surgical interventions or the use of intravenous catheters. Additionally, even though the bloodstream of healthy humans is generally thought to be sterile, mundane activities such as brushing one's teeth have been shown to lead to transient bacteraemia (Bone, 1991). Main threats of bacteraemia are not only the spread of bacteria throughout the body, but also the induction of an uncontrolled immune reaction to circulating bacteria. This condition is termed sepsis and is associated with fever, leucocytosis and in severe cases organ failure and death (Cohen, 2002). Sepsis was responsible for nearly 36,000 death in the US in the year 2008 alone (Miniño *et al.,* 2011). To prevent bacterial dissemination and the formation of sepsis the immune system must both rapidly clear bacteria from the bloodstream while at the same time induce the formation of a robust adaptive immune response, to maximise protection in the case of reinfection. Rapid clearance of circulating bacteria is facilitated in bulk by phagocytic cells of the innate immune system, of which the largest population in the body is present in the liver (Nemeth *et al.,* 2009).

1.1 Liver morphology

The liver is both the largest solid organ and the largest gland in the body, is a metabolic centre for carbohydrate and lipid metabolism, has an important role in bile formation, detoxification of exo- and endogenous compounds and also acts as a first filter for pathogens arriving from the gut via the portal vein (Jones and Spring-Mills, 1984). Apart from the portal vein, which carries nutrient rich blood from the gut to the liver, it receives oxygenated blood via the hepatic artery, giving it a dual blood supply. These two blood supplies are mixed upon entering the liver lobules, hexagonally shaped functional subunits of the liver parenchyma (Gumucio *et al.,* 1994). The blood flows from the outer portal fields through the liver sinusoids to the central vein. These sinusoids are lined with highly fenestrated endothelia and liver resident macrophages known as Kupffer cells (Jones and Spring-Mills, 1984; Wake *et al.,* 1989). Between the sinusoids and hepatocytes lies the perisinusoidal space, also known as the space of Disse. This space is filled with blood plasma, which can pass through the fenestrated endothelium cells, to supply hepatocytes with nutrients (Phillips *et al.,* 1987; Bouwens *et al.,* 1992). The space of Disse also contains hepatic stellate cells, which act as storage location of fat and fat soluble vitamins, such as vitamin A (Wake, 1980; Moriwaki *et al.,* 1988). Additionally, the liver is the organ tasked with the production of a large number of systemically

circulating complement proteins (Alper *et al.,* 1969; Ramadori *et al.,* 1984), an important first line of defence against pathogens that have reached the bloodstream.

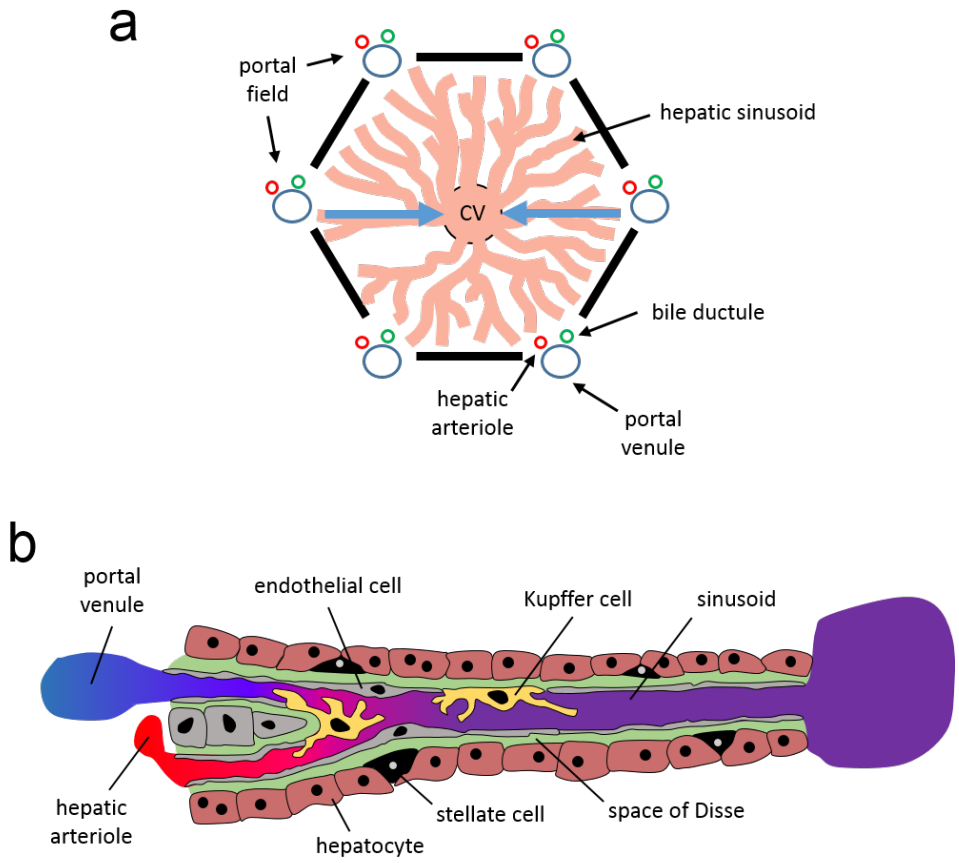

Illustration 1-1 Morphology of the liver
(a) Schematic representation of a liver lobule. Lobules are demarcated by six portal fields containing a hepatic arteriole carrying oxygen rich blood, a portal venule, carrying nutrient rich blood and a bile duct. The blood is mixed in the hepatic sinusoids and flows from the portal fields to the central venule (CV) located at the centre of the lobule. **(b)** Schematic representation of a hepatic sinusoid. Venous (blue) and arterial blood (red) are mixed upon entry into the sinusoid, which is lined with the sinusoidal cell layer consisting of endothelial cells and Kupffer cells. Hepatocytes and stellate cells are separated from the sinusoidal cell layer by the space of Disse. Adapted from (Frevert, 2004)

1.2 The complement system

The complement system is an essential part of the innate immune system and was discovered in the late 19th century as a heat-labile component of plasma that improved the opsonization of bacteria with antibodies and allowed certain bacteria to be lysed (Buchner, 1894; Bordet, 1895). The term complement was then introduced by Paul Ehrlich, who correctly postulated these heat-labile proteins to complement the action of immune cells in the defence against pathogens (Ehrlich, 1904). The complement system consists of over 30 plasma proteins that react with each other to label particles foreign to the body and induce inflammatory responses that help counteract infection (Murphy *et al.,* 2014). Complement proteins are primarily produced in the liver by hepatocytes and then circulate systemically in large numbers (Alper *et al.,* 1969; Gasque, 2004), but can also be produced on a local level by other cell populations such as monocytes, macrophages, epithelial cells or fibroblasts (Morgan and Gasque, 1997).

Three distinct pathways have been described in which complement can be activated and deposited on the surface of pathogens:

The classical pathway of complement activation can be activated in two ways, both mediated by the complement factor 1 (C1) via its subunit C1q. C1q can either bind directly to a particle's surface, recognizing polyanionic ligands or also phosphatidylserine exposed on apoptotic cells (Sontheimer *et al.,* 2005; Paidassi *et al.,* 2008b; Paidassi *et al.,* 2008a) or it can recognize formed antigen:antibody complexes and bind to the constant region of IgG or IgM antibodies (Burton *et al.,* 1980; Emanuel *et al.,* 1982). Binding of C1q activates the serine proteases C1r and C1s, which in turn cleave complement factor 4 (C4) and complement factor 2 (C2). This leads to the formation of the classical complement factor 3 (C3)-convertase C4bC2b.

The lectin pathway of complement activation is initiated by the binding of mannose-binding-lectin (MBL), a protein which is structurally very similar to C1q (Kjaer *et al.,* 2013), to mannose-containing carbohydrate structures on the surface of pathogens (Fujita, 2002; Matsushita and Fujita, 2002). This recognition in turn activates the proteases mannose-binding-lectin associated protease 1 and 2. These activated proteases then, in an analogue fashion to the classical pathway of complement activation, cleave C4 and C2 to the C3-convertase C4bC2b.

The third pathway of complement activation is the alternative pathway. Different from the classical and lectin pathways, this pathway does not require a pathogen-binding protein for the formation of a C3 convertase. It can be initiated directly by the surface of pathogens (Dierich *et al.,* 1973) or by the spontaneous hydrolysis of C3 to C3(H_2O) which in turn binds to complement factor B (Bf). This binding induces the cleavage of fB to Ba and Bb forming the fluid phase C3-convertase C3(H_2O)Bb (Pangburn *et al.,* 1981). The convertase then highly efficiently cleaves surrounding C3 to C3b, which in part then covalently attaches to the foreign

surface. There C3b can again bind fB, induce its cleavage and form the alternate pathway C3-convertase C3b,Bb.

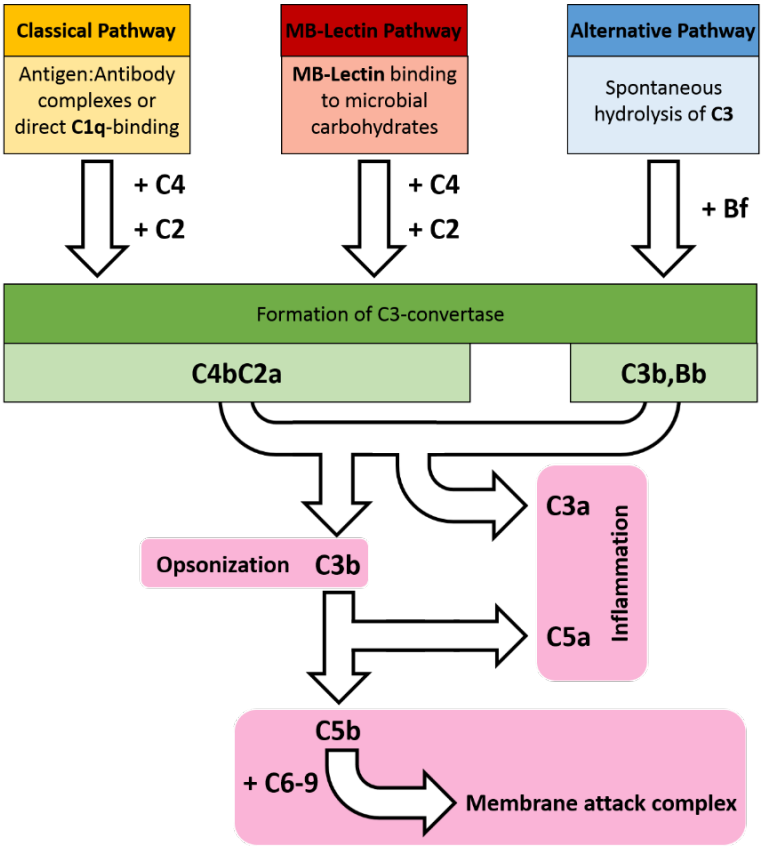

Illustration 1-2 Pathways of complement activation
Classical complement activation begins by the binding of C1q to a surface. This can be facilitated by recognition of antigen:antibody complexes or direct binding of C1q to specific ligands, e.g. polyanionic ligands. MB-Lectin complement activation is induced by the binding of MB-Lectin to exposed carbohydrates and alternative complement activation relies on spontaneous hydrolysis of C3 to C3(H_2O). All three pathways lead to the formation of a C3-convertase: Classical and MB-Lectin pathway recruit C4 and C2 to form the convertase C4bC2a, while the alternative pathway recruits Bf to form the convertase C3b,Bb. These convertases lead to cleavage of C3 to C3a and C3b. C3a acts as an anaphylatoxin, while C3b can bind foreign surfaces and thus tag them for phagocytosis (opsonization) or bind the formed C3 convertase to form a C5 convertase, leading to the proteolytic processing of C5 to C5a and C5b. C5a acts again as anaphylatoxin, while C5b recruits the terminal complement components C6-9 to form the membrane attack complex.

All three pathways converge at this stage in which C3 is cleaved via a C3-convertase. C3 consists of two chains, termed α and β, which are linked by disulphide bonds (Bokisch *et al.,* 1975). Cleavage of the α-chain results in C3a, which acts as an anaphylatoxin in that it induces inflammation and chemotaxis, and C3b, which binds to the pathogen surface and tags it for phagocytosis by cells of the innate immune system, a process termed opsonization (Bokisch *et al.,* 1969). C3b furthermore is necessary for the formation of the C5 convertase, which cleaves complement factor 5 (C5) into C5a, a peptide with strong chemotactic and inflammatory abilities (Snyderman *et al.,* 1970), and C5b. C5b then mediates the formation of

the membrane-attack-complex by recruiting complement factors 6-9 to the pathogen surface (Kolb *et al.,* 1972; Kolb and Muller-Eberhard, 1973), the cytolytic product of the complement cascade capable of causing osmotic lysis certain pathogens or cells by forming a transmembrane channel on the pathogen (Leslie and Nielsen, 2004).

All three pathways of complement activation have various proteins to regulate the location at which C3b can be deposited to protect endogenous cells. The complement receptor 1 (CR1), complement factor H (fH) and the membrane bound protein decay accelerating factor compete with Bb for binding to C3b and can act as cofactors to complement factor I (fI), which cleaves C3b into iC3b (Burge *et al.,* 1981; Farries *et al.,* 1990; Weisman *et al.,* 1990). iC3b is no longer capable of facilitating complement activation, but still can bind to complement receptors (Lambris, 1988). fI can subsequently further degrade iC3b to C3d(g) and C3d. Both C3d(g) and C3d are no longer recognized by phagocytic receptors, but have been shown to induce the generation of antibodies against opsonized antigen (Dempsey *et al.,* 1996). Recent evidence has also shown that von-Willebrand-factor (vWF) can also act as a cofactor to fI (Feng *et al.,* 2015). Since pathogens lack these regulatory proteins, the convertase C3b,Bb can be formed and persist on their surface. Additionally, factor P can also be deposited onto pathogen surfaces and stabilizes the convertase (Pangburn and Muller-Eberhard, 1984).

1.3 Phagocytic receptors

Phagocytosis describes the process of engulfment of a solid particle, such as a bacterium, by a cell and was first described by Elie Metchnikoff (Metchnikoff, 1893). Bacteria are internalized into a membrane-enclosed vesicle called phagosome, which is subsequently acidified and fuses with lysosomes in an effort to destroy the contained bacteria (Murphy *et al.,* 2014). The process of phagocytosis is induced by cell surface receptors that recognize either a pathogen directly or immune proteins deposited on its surface.

1.3.1 Complement receptors

Complement opsonization is the labelling of targets with C3b and its proteolytic products iC3b, C3c and C3d(g) for phagocytosis or recognition by cells of the mononuclear phagocyte system (van Furth *et al.,* 1972; van Furth, 1980, 1989) or polymorphonuclear leukocytes (Wood *et al.,* 1951; Moore *et al.,* 1978) via complement receptors (Ross and Medof, 1985). Five C3-recognizing complement receptors grouped into three structural families have been described: the short consensus repeat molecules CR1 and complement receptor 2 (CR2), the

β_2-integrin family members complement receptor 3 (CR3) and complement receptor 4 (CR4) and the immunoglobulin superfamily member complement receptor of the immunoglobulin superfamily (CRIg) (van Lookeren Campagne *et al.,* 2007).

CR1 is known to have a high affinity for the proteolytic complement products C3b and C4b (Krych-Goldberg and Atkinson, 2001). In humans and primates, its main function is to capture immune complexes on erythrocytes, which are then cleared by monocytes in liver and spleen (Emlen *et al.,* 1992; Taylor *et al.,* 1997). Although it is expressed on all human peripheral blood cells excluding platelets, T-cells and NK-cells, it has been shown to only play a role in phagocytosis by neutrophil granulocytes (Sengelov *et al.,* 1994). It can also act as a potent inhibitor of both the classical and alternative pathway of complement activation (Burge *et al.,* 1981; Farries *et al.,* 1990; Weisman *et al.,* 1990).

CR2 is described as the principal complement receptor that enhances B cell immunity and can bind iC3b, C3d(g) and C3d (Weis *et al.,* 1984). Uptake of antigen via CR2 into B-cells lowers their activation threshold and induces cell survival signals (Matsumoto *et al.,* 1991). CR2 is also expressed on follicular dendritic cells in both human and mouse (Reynes *et al.,* 1985; Molina *et al.,* 1996). Follicular dendritic cells are cells unique to primary and secondary lymphoid organs specialized in trapping opsonized antigen and presenting this antigen to B-cells (Banchereau and Steinman, 1998). CR2 is encoded by the same gene as CR1 in mice, but after transcription is formed by alternate splicing (Kurtz *et al.,* 1990).

CR3 and CR4 are both heterodimeric receptors sharing a common β-chain (CD18). The α-subunit of CR3 is CD11b, while the α-subunit of CR4 is CD11c. As part of the integrin family both receptors not only have phagocytic capacities, but also act in leukocyte trafficking, cell adhesion and stimulation (Ross, 2000). CR3, also known as Mac-1, is expressed on monocytes, macrophages, polymorphonuclear cells, NK cells and certain minor subsets of B-cells and T-cells in humans (Ross and Vetvicka, 1993). In mice it is expressed on monocytes, polymorphonuclear cells, NK-cells and certain subsets of tissue resident macrophages, such as splenic marginal zone macrophages or hepatic Kupffer cells (Gordon *et al.,* 1992). It not only recognizes iC3b and C3dg, but can also bind bacterial cell wall components directly, like lipopolysaccharide (LPS) or β-glucan, and thus act as a pattern recognition receptor (Ross and Vetvicka, 1993; Gregory and Wing, 2002).

CRIg, also known as Z39Ig, as which it was first described (Langnaese *et al.,* 2000) is not expressed on circulating cells and can only be found on Kupffer cells of the liver, interstitial macrophages of the heart, synovial lining macrophages in joints and on foam cells in atherosclerotic plaques (Helmy *et al.,* 2006; Lee *et al.,* 2006; Vogt *et al.,* 2006). It can bind C3b, iC3b and C3c and is the only complement receptor to recognize the β-chain of C3 (Wiesmann *et al.,* 2006).

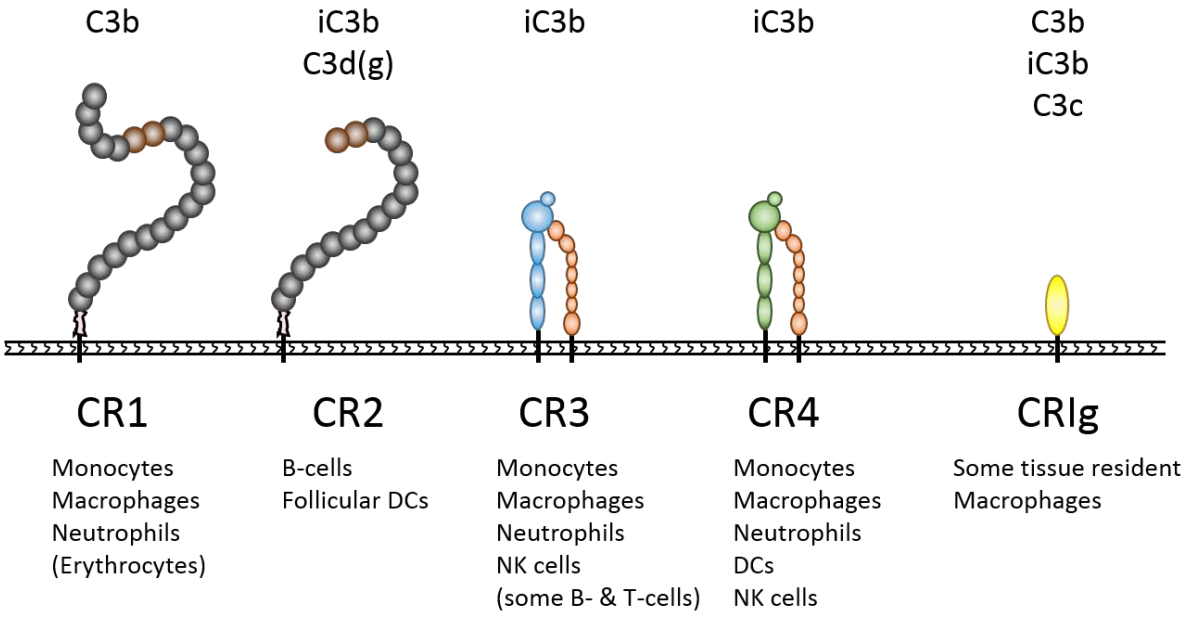

Illustration 1-3 Complement receptors
CR1 in humans is expressed on most blood cells and recognizes C3b, whereas murine CR1 is a splice variant of **CR2** and is expressed on B-cells and follicular DCs, like is CR2. Murine CR1/2 recognizes C3b, proteolytically inactivated iC3b and the cleaved C3d(g). Both CR1 and CR2 consist of short consensus repeat modules. **CR3 and CR4** both are integrins, heterodimerically consisting of the β_2-chain (CD18) and a varying α-chain. CR3s α-chain consists of CD11b (α_M) and CR4s consists of CD11c (α_X). CR3 is expressed on most phagocytic cell populations, whereas CR4 is mostly only expressed on these populations after activation of the phagocytes, the exception being dendritic cells, where it is expressed constantly. Both CR3 and CR4 recognize and bind iC3b. **CRIg** is a type I transmembrane Ig superfamily protein receptor expressed only on certain populations of tissue resident macrophages. It has been shown to recognize C3b, iC3b and C3c. Adapted from (He *et al*., 2008)

1.3.2 Pattern recognition receptors

Innate immunity cannot only be mediated via the phagocytosis of complement-opsonized particles, but also by the direct recognition of so called pathogen associated molecular patterns (PAMPs). This is facilitated by pattern recognition receptors (PRRs) that recognize unique and conserved molecular patterns on pathogens. These patterns are highly conserved through evolution because they are essential for the survival of pathogens and include formylated peptides, lipopolysaccharide (LPS) and lipoteichoic acid (LTA) of Gram (-) and Gram (+) bacteria respectively, mannan of the yeast cell wall, or double stranded RNA found for instance in certain viruses (Aderem and Underhill, 1999). In the context of this thesis, membrane-bound PRRs implicated in recognizing bacterial PAMPs will in the following be shortly introduced.

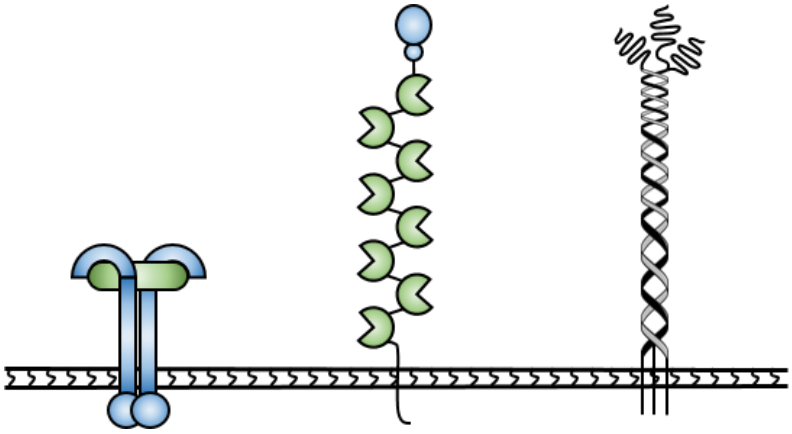

Illustration 1-4 Extracellular pattern recognition receptors with the capacity to recognize bacteria
Families of pattern recognition receptors reported to recognize bacterial PAMPs are Toll-like receptors such as TLR4 (left), C-type lectins such as the Mannose receptor (middle) and Scavenger receptors, such as SRA-I (right).

1.3.2.1 Toll-like receptors

Toll receptors were first described in *Drosophila melanogaster*, where they were crucial for the innate immune response against infecting fungi (Lemaitre *et al.,* 1996). 13 mammalian analogues, termed Toll-like receptors (TLR), have been identified to date, of which 10 are expressed in humans and 13 in mice (Uematsu and Akira, 2006; Takeuchi and Akira, 2010; Oldenburg *et al.,* 2012). TLRs consist of an intracellular domain similar to that of the interleukin-1 receptor family, which is required for intracellular signalling, and an extracellular leucine-rich repeat domain responsible for the recognition and binding of PAMPs (Akira, 2006).

TLRs 1, 2, 4, 5, 6, 9, 11 and 13 have been shown to recognize bacterial proteins and upon binding induce signalling leading to various immune responses, including cytokine production and dendritic cell maturation (Akira, 2004). TLR 1, 2 and 6 are structurally related and recognize bacterial peptidoglycan, di- and triacylpeptides (Takeuchi *et al.,* 2001; Takeuchi *et al.,* 2002; Akira, 2004). TLR 4 can bind lipid A, an integral component of bacterial LPS (Shimazu *et al.,* 1999), whereas TLR 5 recognizes flagellin, a major component of bacterial flagella (Hayashi *et al.,* 2001). TLR 9 has been demonstrated to recognize unmethylated CpG-motifs of bacterial DNA and is a potent stimulator of immune responses (Hemmi *et al.,* 2000; Bauer *et al.,* 2001). TLR 11 is not expressed in humans due to the presence of a stop codon, but has been shown in the murine model to convey protection from uropathogenic bacteria in kidney and bladder (Zhang *et al.,* 2004). TLR 13 is also only expressed in the murine context and has been shown to recognize bacterial 23S rRNA (Oldenburg *et al.,* 2012).

1.3.2.2 Scavenger receptors

Scavenger receptors were first described as capable of mediating the uptake of modified lipoproteins (Brown *et al.,* 1980). They comprise a large number of receptors with a broad variety of binding specificities (Gough and Gordon, 2000; Platt and Gordon, 2001). Six different classes of scavenger receptors, termed A-F, have been distinguished. What all scavenger receptor classes have in common is that they are transmembrane proteins that typically bind polyanionic ligands (Gough and Gordon, 2000).

Class A scavenger receptors (SRA) have been shown to play a role in the recognition of LPS of Gram (-) bacteria and LTA of Gram (+) bacteria and have thus been given a role as PRRs (Hampton *et al.,* 1991; Dunne *et al.,* 1994). They are comprised of a collagen-like domain and an α-helical coiled-coil domain. The N-terminus can either contain a cysteine-rich domain (type I) or not (type II) (Gough and Gordon, 2000).

Macrophages lacking SRA have a significantly decreased capacity of taking up Bacillus Calmette-Guérin, an attenuated strain of *Mycobacterium bovis* used to vaccinate against tuberculosis (Peiser *et al.,* 2000) and are also more susceptible to infection by the clinically relevant strains *Staphylococcus aureus* and *Neisseria meningitides* (Thomas *et al.,* 2000; Peiser *et al.,* 2002a). Mice lacking SRA have also been reported to have a higher susceptibility to *Listeria monocytogenes*, displaying a higher bacterial replication in the liver (Ishiguro *et al.,* 2001). Additionally, SRA have been shown to play a role in the protection against infection with *L.m.* and herpes simplex virus (Suzuki *et al.,* 1997). Interestingly, transgenic expression of SRA on non-phagocytic cells has been shown to allow for binding of bacteria, but fails to promote significant internalization, displaying the need for the expression of other cellular factors specific for phagocytes to accomplish phagocytosis (Elomaa *et al.,* 1995; van der Laan, L J *et al.,* 1999).

1.3.2.3 C-type lectin receptors

C-type lectin receptors recognize carbohydrates, predominantly located on pathogen surfaces, in a calcium-dependent manner and are expressed on various different cell populations including platelets, macrophages and dendritic cells (Weis *et al.,* 1998). They are grouped into two types depending on their carbohydrate recognition domains (CRD).

Type I C-type lectin receptors comprise the mannose receptors, which are expressed by a variety of professional phagocytes, including tissue macrophages and dendritic cells (Geijtenbeek and Gringhuis, 2009). They are type I transmembrane glycoproteins and their binding site consists of an array of eight tandem lectin-like CRDs, which primarily recognize the carbohydrates L-fucose, D-mannose and N-acetylglucosamine (GlcNac) (Schlesinger *et al.,*

1978; Stahl *et al.,* 1978). Mannose receptors have been shown to recognize and internalize *Klebsiella pneumoniae*, *Mycobacterium tuberculosis* and *Pseudomonas aeruginosa* (Kabha *et al.,* 1995; Astarie-Dequeker *et al.,* 1999).

Type II C-type lectin receptors comprise the asialoglycoprotein receptors and all only contain a single CRD (Taylor *et al.,* 2005). Dectin-1, a member of this superfamily, has been shown to not only bind simple carbohydrates, but can also recognize complex polysaccharides, such as β(1-3)-linked glucan present in cell walls of fungi and some bacteria (Brown and Gordon, 2001). It was initially thought to be exclusively expressed on dendritic cells, but is now known to be present on macrophages, monocytes, neutrophils and T-cells in the mouse (Taylor *et al.,* 2002). Other members of this superfamily, like Dectin-2 or CD209, recognize not only galactose as their name would suggest, but also high mannose carbohydrates (Robinson *et al.,* 2009).

1.4 Phagocytes

Phagocytic cell populations play a central role in the initial defence of host organisms against invading pathogens. When a pathogen invades a host, it is normally detected by tissue resident macrophages via the above described pattern recognition receptors. After recognition of infection, macrophages signal for assistance via the secretion of inflammatory molecules, such as cytokines and lipids (Stark *et al.,* 2005). As a consequence, neutrophil granulocytes arrive on the scene as first responders to combat infection (Hayashi *et al.,* 2003).

1.4.1 Neutrophil Granulocytes

Neutrophil granulocytes are the largest subset of polymorphonuclear leukocytes, which also comprise basophil and eosinophil granulocytes (Murphy *et al.,* 2014). Neutrophil granulocytes were first described by Ehrlich in 1880 and reported to aid host defence during infection by Metchnikoff in 1893 (Ehrlich, 1880; Metchnikoff, 1893). They are generated continuously from myeloid progenitors in the bone marrow at a rate of up to $2x10^{11}$ cells per day (Borregaard, 2010). After reaching the bloodstream, neutrophil granulocytes have a short half-life remaining in the circulating for approximately 1.5 h in mice and 8 h in humans (Pillay *et al.,* 2010; Galli *et al.,* 2011). It is of note that while neutrophil granulocytes are the largest leukocyte population in human blood, comprising 50-70% of all circulating leukocytes, murine blood contains substantially less, with only 10-25% of all circulating leukocytes being neutrophil granulocytes (Doeing *et al.,* 2003; Mestas and Hughes, 2004).

When circulating neutrophil granulocytes reach a site of infection, they are known to adhere to the endothelium and become activated dependent on the presence of inflammatory mediators and P- and E-selectin (Ley *et al.,* 2007; Phillipson and Kubes, 2011). After adhering they transmigrate through the endothelia to reach the site of infection and encounter the pathogen. After pathogen encounter, neutrophil granulocytes engage in what they are most proficient in: the killing of pathogens by multiple means. These means by which pathogens are killed are I) phagocytosis, after which neutrophil granulocytes produce reactive oxygen species and antibacterial proteins (Häger *et al.,* 2010), II) degranulation and thus expulsion of antibacterial peptides and proteases, which can either directly degrade bacterial proteins or remove bacterial substrates from the environment in an effort to starve the invading pathogen (Rodriguez *et al.,* 2009; Youn and Gabrilovich, 2010), and III) the release of neutrophil extracellular traps, composed of core DNA element to which antibacterial proteins from neutrophil granules can be attached (Brinkmann *et al.,* 2004).

The recruitment of neutrophil granulocytes to liver sinusoids has been reported to be an exception to the normal process of granulocyte recruitment (Wisse *et al.,* 1985; Wong *et al.,* 1997). During infection of the liver, neutrophil granulocytes directly adhere to liver sinusoid endothelial cells, from where they can migrate to the pathogen, a process termed “crawling”, and kill the pathogen via the described processes. Apart from the highly efficient killing of invading pathogens, neutrophil granulocytes have been reported to play a role in pathogen transport to lymph nodes (Maletto *et al.,* 2006), antigen presentation (Beauvillain *et al.,* 2008) and the induction of T-cell responses (Tacchini-Cottier *et al.,* 2000). Neutrophil granulocytes may also play a role in the resolution of inflammation, as removing them from inflamed tissue often leads to an increase in tissue pathology (Fournier and Parkos, 2012), although this has yet to be investigated in more detail.

1.4.2 Kupffer cells

Kupffer cells are professional phagocytic cells of the liver, whose main function is the clearance of metabolites and foreign materials from portal vein blood. It has been reported that Kupffer cells can clear over 80% of intravenously injected *E. coli* and staphylococci (Benacerraf *et al.,* 1959). Kupffer cells were first described by Karl Wilhelm von Kupffer in 1899 as a cell population located inside the liver sinusoids with the capability to take up intravenously injected erythrocytes, which he believed to be endothelial cells (Kupffer, 1899). 70 years later, this cell population was differentiated from sinusoidal endothelial cells by their phagocytic properties and also their endogenous peroxidase activity (Singer *et al.,* 1969; Fahimi, 1970; Wisse, 1970, 1974). They are seen as part of the mononuclear phagocyte system (van Furth *et al.,* 1972; van Furth, 1980, 1989) and account for approximately 20% of all nonparenchymal

cells in the liver (Naito *et al.,* 2004). Furthermore, they account for approximately 80-90% of all tissue resident macrophages in the body (Dong *et al.,* 2007). They are amoeboid in shape with microvilli and lamellipodia extruding in every direction and adhere to the surface of fenestrated endothelial cells in the liver sinusoids (Naito *et al.,* 2004).

Kupffer cells first form in the foetus, when primitive macrophages migrate to the foetal liver, where they mature (Widmann *et al.,* 1972; Naito *et al.,* 1997; Gomez Perdiguero *et al.,* 2015). The life span of Kupffer cells has been shown to be extensive, being over 6 weeks in mice (Yamada *et al.,* 1990; Naito and Takahashi, 1991). Two subsets of Kupffer cells have been described, discernible by the expression of either CD68 or CD11b (Klein *et al.,* 2007; Kinoshita *et al.,* 2010; Movita *et al.,* 2012). While the $CD11b^+$ fraction has been shown to be derived from circulating monocytes originating from the bone marrow, $CD68^+$ Kupffer cells have been described as descendants of $CD32^+$ c-kit^+ hepatic precursor Kupffer cells with some stem cell-like qualities (Klein *et al.,* 2007; Ikarashi *et al.,* 2013). Furthermore it has been shown that $CD68^+$ Kupffer cells of hepatic origins are highly efficient at phagocytosing bacteria and subsequently producing reactive oxygen species, whereas $CD11b^+$ Kupffer cells have very potent cytokine-producing activity (Kinoshita *et al.,* 2010; Ikarashi *et al.,* 2013).

To facilitate clearance of pathogens from the bloodstream Kupffer cells express a wide array of phagocytic receptors such as the complement receptors CR1, CR3 (only in a subset), CR4 and CRIg (Hinglais *et al.,* 1989; Yan *et al.,* 2000; Helmy *et al.,* 2006), scavenger receptors such as SRA-I, SRA-II and MARCO (Peiser and Gordon, 2001; Peiser *et al.,* 2002b; Yuasa and Watanabe, 2003; Willekens *et al.,* 2005; Movita *et al.,* 2012), c-type lectin receptors such as the mannose receptor CD206 and asialogycoprotein receptors ASGR1 and ASGR2 (Haltiwanger *et al.,* 1986; Zhu *et al.,* 2004; Coombs *et al.,* 2006) and also the Toll-like receptors 1, 2, 3 , 4, 6, 7, 8, and 9 (Wu *et al.,* 2010). Depletion of Kupffer cells prior to infection with sublethal doses of *L.m.* leads to death of the mice and a lack of neutrophil granulocyte infiltration, implying a role for Kupffer cells in the recruitment of neutrophil granulocytes (Gregory and Wing, 1998; Ebe *et al.,* 1999). Kupffer cells have also been reported to be essential for the clearance of *Borrelia burgdorferi*, *Bacillus cereus* and methicillin-resistant *Staphylococcus aureus* (Lee *et al.,* 2010; Wong *et al.,* 2013a). Furthermore, infection with *B. cereus* was reported to lead to platelet nucleation on the surface of Kupffer cells, where platelets encase immobilized bacteria on the surface of Kupffer cells (Wong *et al.,* 2013a).

1.5 Platelets

Platelets are small, anuclear cell fragments that play an important role in haemostasis, thrombosis and inflammation and derive from bone marrow megakaryocytes (Michelson, 2012). Human and murine platelets are morphologically similar, with murine platelets being smaller in size (2-4 µm diameter in humans vs. 0.5 µm in mice (Schmitt *et al.,* 2001; Michelson, 2012)) and more numerous (2-4x10^5 platelets/µl blood in humans vs. 1-1.5x10^6 platelets/µl blood in mice (Corash and Levin, 1990; Jackson *et al.,* 1990; Daly, 2011)). Murine platelets have a comparably short lifespan of 3-4 days, whereas human platelets have a lifespan of 8-12 days (Schmitt *et al.,* 2001).

Platelets are primarily known for their role in haemostasis (Michelson, 2012). Platelets scour the vasculature and upon recognition of an injury are activated. Activation can be induced by soluble agonists such as thrombin, adenosine 5'-diphosphate (ADP), thromboxane A2 (T_xA_2) or fibrinogen (Clemetson and Clemetson, 2004) or by membrane bound agonists that become exposed after damage to the vascular endothelium, for example collagen, vWF or tissue factor (Jackson *et al.,* 2003; Li *et al.,* 2010). These activated platelets aggregate at the site of injury by binding exposed vWF via the glycoprotein receptor (GP) Ib, which is part of the surface expressed receptor complex GPIb/IX/V (Ruggeri *et al.,* 1983; Savage *et al.,* 1996). This receptor-binding induces an increase in intracellular Ca^{2+}, which in turn causes exocytosis of further platelet activating agents from granules present in the platelet, such as ADP, thrombin or T_XA_2 (Holmsen, 1989; Brass, 2003). ADP and T_xA_2 then mediate a conformational change of the platelet surface receptor GPIIb/IIIa and thus heightening the receptors affinity for fibrinogen (Shattil and Newman, 2004). Fibrinogen is then converted to fibrin by thrombin, which in turn was produced by the coagulation cascade and a clot is formed (Leslie, 2010).

In addition to interactions with haemostatic and coagulation proteins, platelets are known to interact with factors of the complement system in several different ways. It has been hypothesized that platelets play the role of a sentinel for infections thus aid in the process of innate and adaptive immunity. Human platelets have been demonstrated to express the complement receptors CR2, CR3 and CR4 and also C1q-specific receptors (Wautier *et al.,* 1977; Cosgrove *et al.,* 1987; Nunez *et al.,* 1987; Vik and Fearon, 1987; Peerschke and Ghebrehiwet, 1997, 2001). Murine platelets have been described to express two C3d binding receptors termed C3dR-125 and C3dR-150 for their binding preference and their molecular weight (Quigg *et al.,* 1997). Additionally, experiments in our laboratory recently supported C3-binding capacity of the murine platelet glycoprotein Ib (GPIb), complexing platelets to opsonized pathogens in the bloodstream (Verschoor *et al.,* 2011). It has been reported that a lack of complement regulatory proteins, leading to a hyper-reactive complement system, increases the risk of thrombosis (Richards *et al.,* 2003; Fremeaux-Bacchi *et al.,* 2004). The anaphylatoxin

C3a has been reported to promote activation of platelets (Polley and Nachman, 1983) and it has furthermore been shown that C1q can bind to exposed phosphatidylserine on activated platelets and induce the expression of GPIIb/IIIa (Peerschke *et al.,* 1993). This increased the binding of activated platelets to fibrinogen and stabilized clot formation. On the other hand, the secretion of ATP and Ca^{2+} by activated platelets leads to a phosphorylation of C3b, inhibiting inhibition of C3b by fI (Ekdahl and Nilsson, 1995). Thus, interaction between complement and platelets leads to mutual activation and to a favourable outcome for the host (Markiewski *et al.,* 2007). Complement activation during thrombus formation induces immune responses to any pathogens infiltrating through on open wound and platelet activation via complement leads to thrombus-formation in close proximity to pathogens.

Additionally, numerous interactions between platelets and bacteria have been described (Fitzgerald *et al.,* 2006). Platelets are known to express TLRs that can recognize bacterial antigen and induce platelet activation (Andonegui *et al.,* 2005) and also have been shown to contain platelet microbicidal proteins (PMPs) to directly act on the bound pathogen (Semple *et al.,* 2011). To further contribute to host defence against infection, platelets present CD154 on their surface after activation, contributing to chemotactic recruitment and inducing pathogen killing mechanisms by phagocytic cells (Li *et al.,* 2008; Jin *et al.,* 2013). Platelet are furthermore capable of inducing the formation of neutrophil extracellular traps (NETs) by neutrophil granulocytes, which are known to capture bacteria and yeast within the bloodstream (Brinkmann *et al.,* 2004; Urban *et al.,* 2006; Clark *et al.,* 2007). They furthermore have been shown to encase pathogens, which have been immobilized on the surface of Kupffer cells in the liver (Wong *et al.,* 2013a). To aid the induction of adaptive immunity, platelets can also recruit dendritic cells via JAM-C/CR3 interaction and modulate their function (Langer *et al.,* 2007) and have also been shown to bind circulating C3-opsonized pathogens and shuttle them to $CD8\alpha^{+}$ dendritic cells within the spleen, which in turn lead to strong $CD8^{+}$ T-cell immune responses (Neuenhahn *et al.,* 2006; Verschoor *et al.,* 2011).

1.6 *Listeria monocytogenes*

Listeria monocytogenes (*L.m*.), the causative agent of listeriosis in humans, is a gram positive, bacillary, non-sporulating, facultative anaerobic bacteria. It is phylo-genetically closely related to the species *Bacillus*, *Clostridium*, *Enterococcus*, *Streptococcus* and *Staphylococcus* (Ludwig *et al.,* 1985). It is an opportunistic pathogen and can infect both human and animals. Though case numbers of food-related infections with *L.m.* are low, with only 355 reported cases in Germany for the year of 2013 (Gesundheitsberichterstattung des Bundes), the rate of mortality is exceptionally high at approximately 30% even after early treatment with

antibiotics (Schuchat *et al.,* 1991). Especially young, old, immunocompromised and pregnant patients have a high risk of succumbing to Listeriosis (Farber and Peterkin, 1991).

Infection with *L.m.* generally takes place via the gastrointestinal tract after the consumption of contaminated foods, such as dairy products, raw vegetables or meats (Dalton *et al.,* 1997; Gombas *et al.,* 2003). Ingested *L.m.* then adhere to epithelial cells of the lower small intestine. Bacterial virulence factors internalin A, which binds basolaterally expressed E-cadherin (Dussurget *et al.,* 2004), internalin B, which binds the hepatocyte growth factor receptor c-Met (Shen *et al.,* 2000), and also the surface molecule Actin assembly-inducing protein (ActA), which binds proteoglycans (Suarez *et al.,* 2001), facilitate this adhesion. The binding via internalin A and B induces actin rearrangement in the epithelial cell and thus the formation of membrane ruffles. *L.m*. then enters the host cell via the formation of a primary vacuole, a process termed zipper-mechanism (Ireton *et al.,* 1996). The acidification of the formed phagosome then activates the virulence factor Listeriolysin O (LLO), which binds cholesterol and forms pores in the phagosomal membrane, through which the *L.m.* reach the cellular cytosol (Alvarez-Dominguez *et al.,* 1997). After reaching the cytosol, *L.m.* propagates (Joseph *et al.,* 2006) and expresses large amounts of ActA on its surface. ActA is used to recruit actin monomers of the host cell to the *L.m.* surface, which are then rearranged to polymers in a fashion that allows *L.m.* to move throughout the cell (Brundage *et al.,* 1993; Chakraborty, 1996). When *L.m.* reaches the inner side of the host cytoplasmic membrane, a pseudopodium is formed, which then infiltrates the neighbouring cell and is subsequently phagocytosed. It can then again escape the resulting phagosome and thus spread from cell to cell without having to leave the intracellular environment (Tilney and Portnoy, 1989). This protects *L.m.* not only from a large part of the host's immune system by circumventing the bloodstream, where antibody recognition, complement activation and phagocytosis occur, but also from the action of most standard antibiotics, which it is normally sensitive to (Hof *et al.,* 1997; Poros-Gluchowska and Markiewicz, 2003). After spreading from cell to cell and finally crossing the epithelial barrier, *L.m.* can enter the bloodstream and spread throughout the host body. Infection of the brain is particularly dangerous, since *L.m.* can cross the blood-brain barrier and cause meningitis and encephalitis (Schuchat *et al.,* 1991; Disson and Lecuit, 2012). *L.m.* is also capable of traversing the placental barrier in pregnant women, generally leading to the death of the unborn child (Abram *et al.,* 2003).

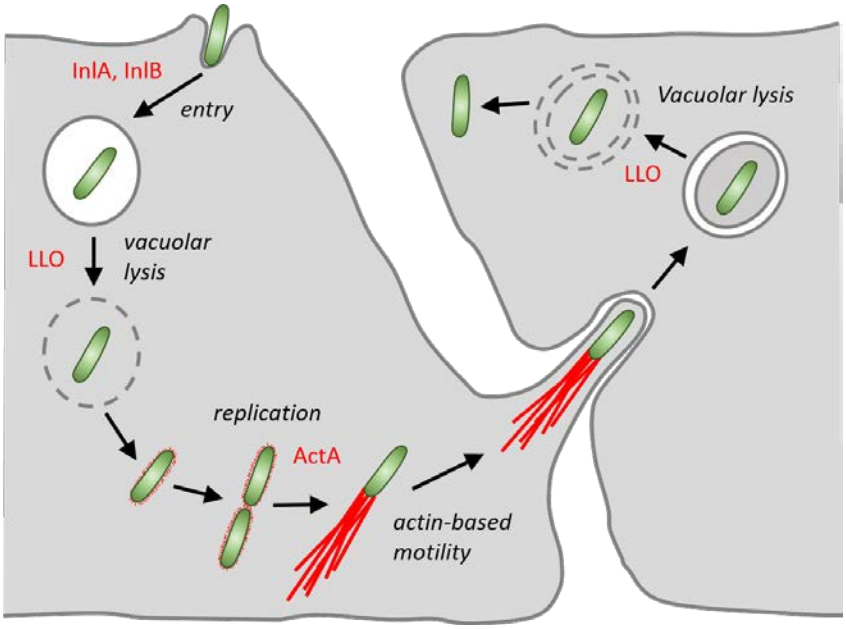

Illustration 1-5 Intracellular life cycle of *L.m.*
L.m. binds epithelial cells via its surface expressed virulence factors InlA and InlB. This binding induces actin rearrangement in the epithelial cell and leads to *L.m.* entry into the cell via the Zipper-mechanism. Expression of the pore-forming toxin LLO leads to lysis of the vacuole and bacterial entry into the cell cytoplasm. Here *L.m.* replicates efficiently and expresses the virulence factor ActA on its surface. This allows *L.m.* to polymerize host cell actin and thus become motile within the host cell. This motility leads to the formation of pseudopodia reaching into neighbouring host cells, which are again phagocytosed. Here LLO can again facilitate the escape from the vacuole and thus facilitate cell-to-cell spread. Adapted from (Pizarro-Cerdá *et al.,* 2012)

L.m. is a widely used tool in immunology to study host-pathogen interactions, especially the induction of cytolytic adaptive immune responses. For laboratory use they are easily culturable and can be genetically modified (Pamer, 2004). Infection of mice has to be performed via intravenous infection though, since wild-type *L.m.* are incapable of binding to E-cadherin in the murine gut due to a point mutation in the gene *Cdh1* (Lecuit *et al.,* 2001).

1.7 Aim of this thesis

Deficiencies of the complement system are generally linked to pathology, for example a lack of C3 results in increased susceptibility to respiratory tract infection (Skattum *et al.,* 2011). Surprisingly, previous studies from our lab revealed that mice lacking C3 are not only more resistant to systemic *L.m.* infection, as seen in the splenic *L.m.* burden at peak infection (Figure 1-1a, published in (Verschoor *et al.,* 2011)), but also that circulating *L.m.* are cleared from the bloodstream faster in absence of C3 (Figure 1-1b). Further studies linked this phenotype to the formation of *L.m.* – platelet complexes in the bloodstream, dependent on C3 and the platelet receptor GPIb (Figure 1-1c, d). This complex formation was essential for the targeting

of circulating *L.m.* to splenic CD8α⁺ DCs and for the formation of robust cytolytic T-cell responses (Verschoor *et al.,* 2011).

The aim of this thesis was to closer investigate the nature of *L.m.* – platelet interaction and to reveal the impact of *L.m.* – platelet complex formation on the fate of systemically circulating *L.m.* in the murine context. To closer examine *L.m.* – platelet interaction a novel method was developed based on light-transmission platelet aggregometry. To investigate, how platelet binding altered the fate of circulating *L.m.*, a combination of established models, such as the *ex vivo* detection of blood clearance kinetics or flow cytometry analysis of infected cell populations, and novel methods developed in the context of this thesis were used. Novel methods developed were the *in vivo* measurement of blood clearance and platelet association via 2-photon intravital microscopy as well as the whole body visualization of early systemic *L.m.* infection using a combination of positron-emission-tomography and radioactively labelled *L.m.*.

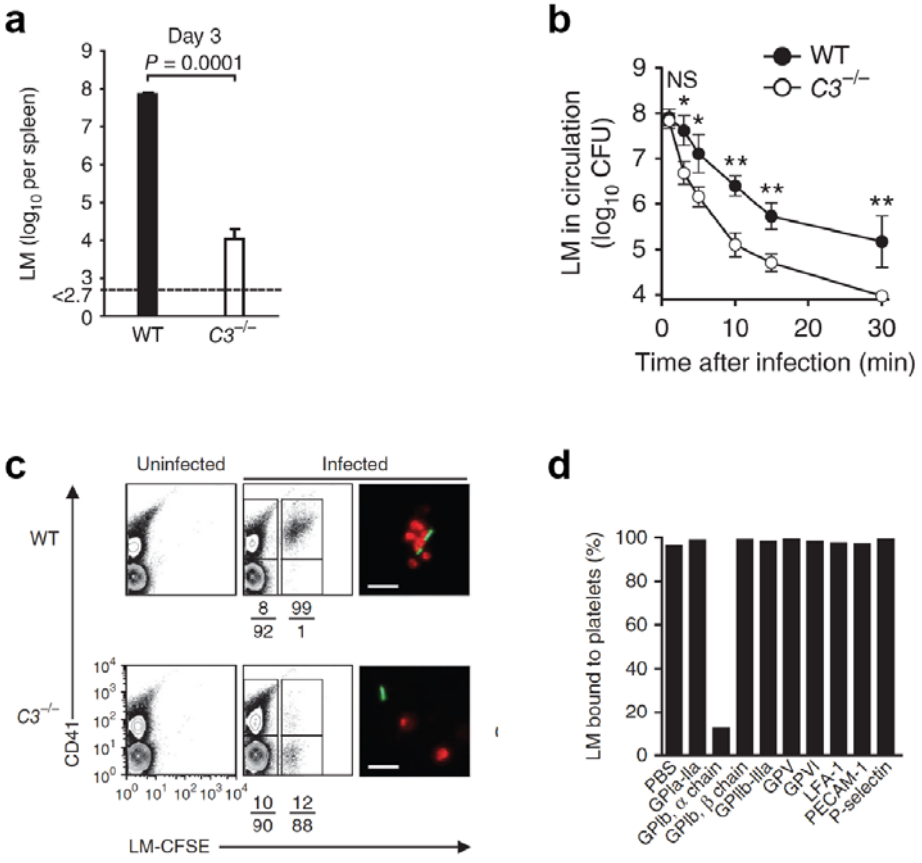

Figure 1-1 C3-mediated association to platelets prolongs splenic localization and circulation time
(a) Splenic burden 3 d after systemic infection with *L.m.* **(b)** Vascular clearance of *L.m.* in min after intravenous injection into wild-type and $C3^{-/-}$ mice **(c)** Flow cytometry (left and middle) and fluorescent microscopy (right) of blood samples of wild-type mice (top) or $C3^{-/-}$ mice (bottom) obtained within 1 min of infection with CFSE-labelled *L.m.* (platelets = red; *L.m.* = green, scale bars = 5µm) **(d)** *In vitro* blocking assay of hirudinated $C4b^{-/-}$ whole blood and monoclonal antibodies to specified platelet surface molecules. Adapted by permission from Macmillan Publishers Ltd: Nature Immunology 12: 1194-1201, © 2011

2 Results

2.1 Intravital microscopy of *L.m.* – platelet complexes in the bloodstream

To investigate the process of *L.m.* – platelet complex formation and its implications on the clearance of *L.m.* from the bloodstream in the complex system of the mouse, a multiphoton intravital imaging model to visualize systemically circulating *L.m.* within the vasculature of the ear was established (Figure 2-1a). Bacterial clearance was quantified by enumeration of circulating *L.m.* during discreet timeframes of 1 minute. The validity of this method was assured by comparing the resulting clearance and circulatory half-live in wild-type animals (Figure 2-1b, Supplementary movie 1) to the observed kinetic of the already established method of plating blood samples drawn at successive time points after infection (Figure 2-1c).

It was previously described that clearance of *L.m.* from the circulation is more rapid when C3 is lacking (Verschoor *et al.,* 2011). This phenotype of faster clearance and thus a shorter circulatory half-life in absence of C3 was confirmed via intravital imaging (Figure 2-2a, Supplementary movie 2). Analysis of $GPIb^{-/-}$ mice, in which *L.m.* are fully opsonized with activated C3 in a speed similar to the wild-type (Figure 2-2c) but cannot bind platelets (Verschoor *et al.,* 2011), resulted in a very similar phenotype compared to $C3^{-/-}$ mice and a significantly shorter circulatory half-life than wild-type mice (Figure 2-2b, Supplementary movie 3). These data confirmed that systemically circulating *L.m.* are cleared from the bloodstream faster when binding to platelets is prevented, be it by a lack of C3 or GPIb.

Wild-type, $C3^{-/-}$ and $GPIb^{-/-}$ mice were furthermore injected with platelet labelling antibodies to visualize platelets and *L.m.* – platelet interactions (Supplementary movies 4-6). Quantification of *L.m.* positive for platelets in wild-type mice revealed that within the first minute after infection, approximately 40% of all detected *L.m.* had bound one or more platelets and by 5 min post infection only *L.m.* that have successfully formed *L.m.* – platelet complexes remain within the circulation (Figure 2-3a). In contrast, both in $C3^{-/-}$ and in $GPIb^{-/-}$ mice no association of *L.m.* and platelets was detectable within 10 min after infection (Figure 2-3b, c), by which time over 99% of *L.m.* had been cleared from the circulation (see Figure 2-2a, b).

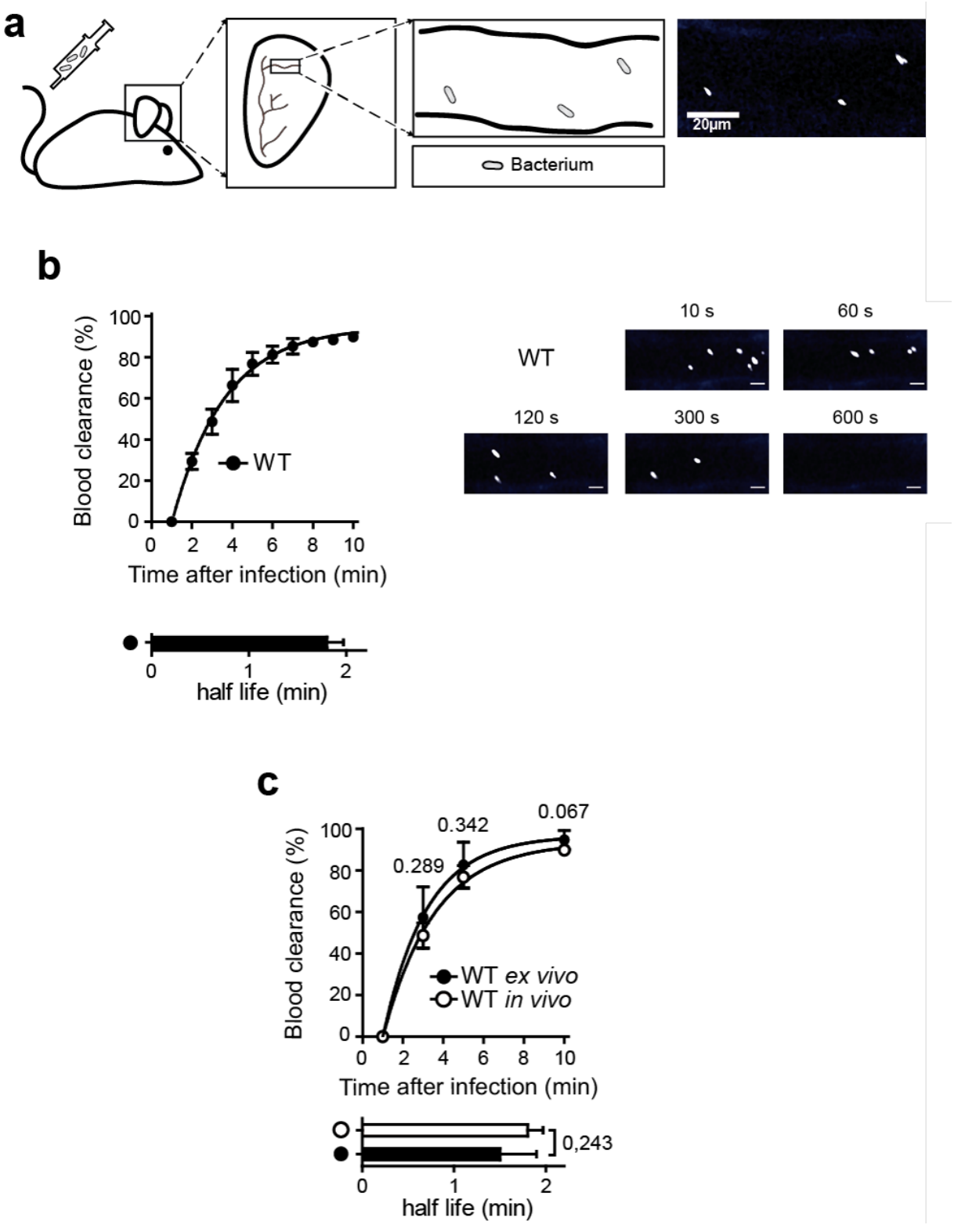

Figure 2-1 Multiphoton intravital imaging of *L.m.* circulation in the vasculature of the ear
(a) Schematic setup of the detection of circulating *L.m.* via multiphoton intravital imaging **(b)** Calculated clearance kinetic and circulatory half-life of *L.m.* in wild-type mice after infection with $1x10^8$ eFluor670-labelled, heat inactivated *L.m.* (mean ± SD of 4 mice) **(c)** Comparison of clearance kinetics acquired via *in vivo* microscopy and *ex vivo* plating of blood samples drawn at 1, 3, 5 and 10 min post infection (mean ± SD for 4 mice via intravital microscopy and 10 mice for ex vivo plating of blood samples, P values indicated, Two-way ANOVA with Bonferroni post-test adjustment and two-tailed Student's t-test). Scheme in **(a)** provided by P. Rämer.

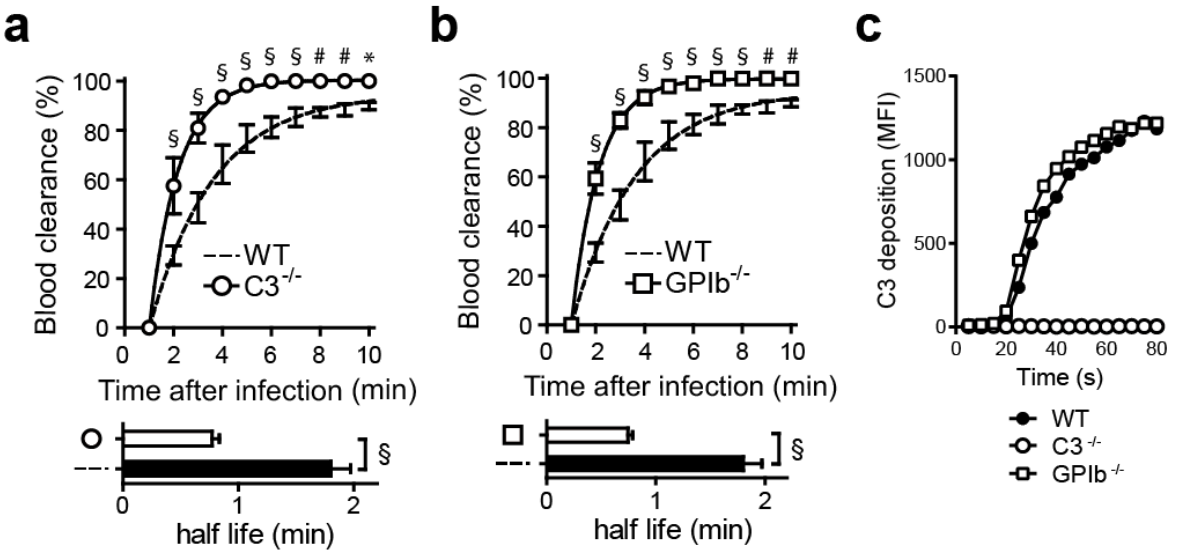

Figure 2-2 *L.m.* are cleared more efficiently when platelet binding is inhibited
(a) $C3^{-/-}$ mice and **(b)** $GPIb^{-/-}$ mice were infected i.v. with $1x10^8$ eFluor670-labelled, heat inactivated *L.m.*. Circulating *L.m.* were imaged during the first 10 min of infection and the clearance kinetic and circulatory half-lives calculated and compared to the wild-type (mean ± SD of 3 mice per strain, * = P < 0.05, # = P < 0.01, § = P < 0.001, Two-way ANOVA with Bonferroni post-test adjustment and two-tailed Student's t-test). **(c)** *L.m.* were incubated in wild-type, $C3^{-/-}$ or $GPIb^{-/-}$ plasma, samples were taken every 5 seconds and subsequently stained for C3 and analysed via flow cytometry.

This observation confirmed the presence of *L.m.* – platelet complexes in the bloodstream *in vivo* and hinted towards an effect of *L.m.* – platelet complex formation on the circulation time of *L.m.* after systemic infection. To closer investigate and also define the process of complex formation between *L.m*. and platelets, a controlled *in vitro* setting using light transmission platelet aggregometry was chosen.

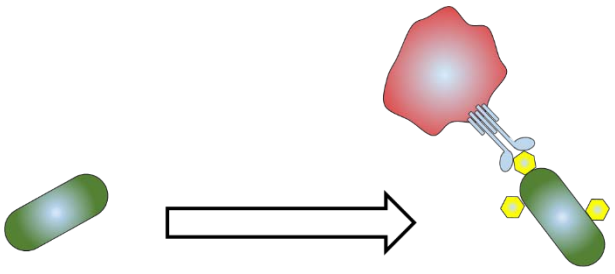

Illustration 2-1 Summary of chapter 2.1
The formation of *L.m.* – platelet in the bloodstream of wild-type mice was confirmed. Formation was not observed in the bloodstream of mice lacking either C3 or GPIb.

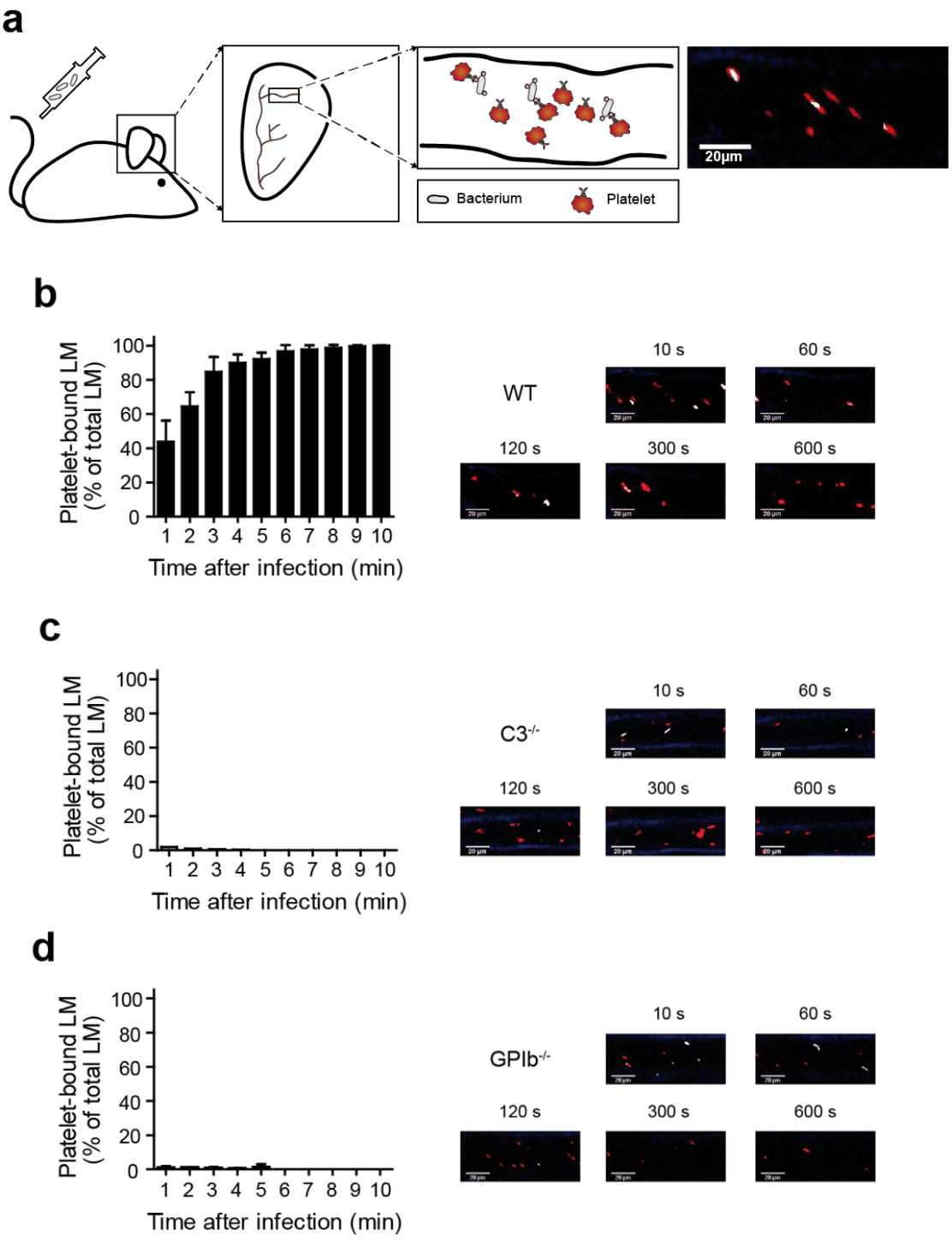

Figure 2-3 Visualization of *L.m.* – platelet complex formation *in vivo*
(a) Schematic setup of the multiphoton intravital imaging procedure to detect circulating *L.m.* and platelets. Wild-type **(b)**, $C3^{-/-}$ **(c)** and $GPIb^{-/-}$ **(d)** mice were administered 4 µg αGPIbβ-antibody and subsequently infected with $1x10^8$ eFLuor670-labelled, heat inactivated *L.m.*. Observed *L.m.* were analysed for platelet binding and percentage of $platelet^+$ *L.m.* of all observed *L.m.* was determined (mean ± SD of 3 mice per strain). Scheme in **(a)** provided by P. Rämer.

2.2 *In vitro* analysis of *L.m.* – platelet interactions

To elucidate the interaction of *L.m.* with circulating platelets, an *in vitro* system to observe *L.m.* – platelet complexes formation under shear conditions in a controlled, isolated setting was established using light transmission platelet aggregometry (Born, 1962). For this, platelet rich plasma (PRP) was isolated from mice and *L.m.* were added at timepoint 0. To prevent coagulation and also the activation of complement components, EDTA was added to blood after bleeding. EDTA complexes all divalent ions in the plasma, especially Ca^{2+} and Mg^{2+} required for the activation of C3 (Mayer *et al.,* 1946). To regain these ions needed for complement activation, Mn^{2+} was added 30 s before timepoint 0. Mn^{2+} has a higher affinity for EDTA and thus displaced Mg^{2+} and Ca^{2+} from the complexing EDTA (Corsello *et al.,* 2009), making Ca^{2+} and Mg^{2+} available for physiological complement activation reactions. Complex formation was analysed by measurement of the increase in light transmission through the optically dense PRP. When *L.m.* were incubated with PRP from wild-type mice a distinct three phase progression of aggregation was observed (Figure 2-4a). Fluorescent microscopy of samples taken during each stage revealed these to predominantly consist of I) *L.m.* not yet or rarely having bound to platelets; II) the formation of small complexes containing 1-2 *L.m.* and 1-5 platelets on average; and III) the formation of highly aggregated complexes (Figure 2-4b).

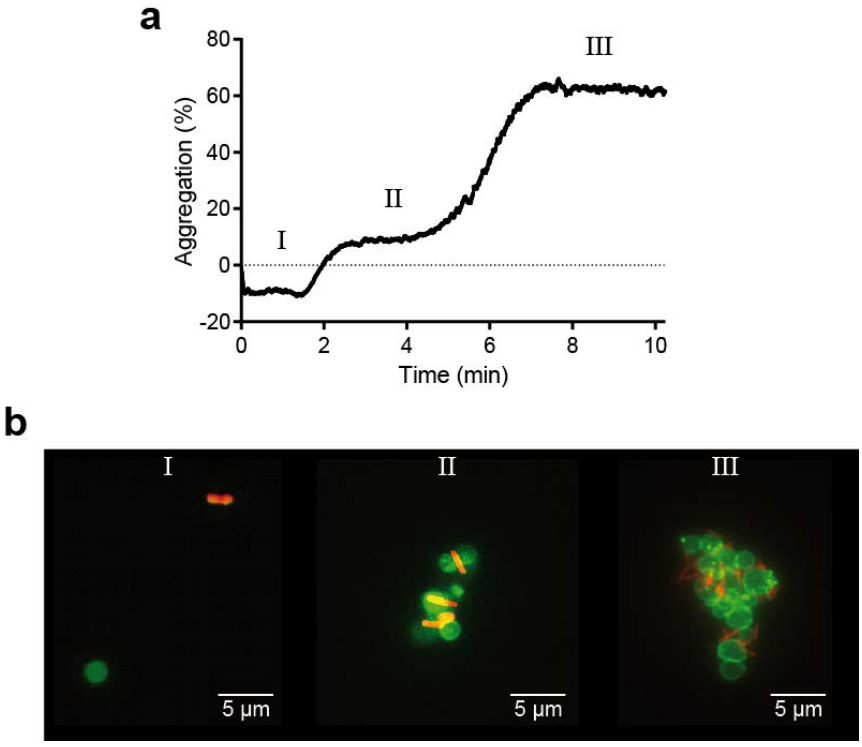

Figure 2-4 Aggregometry reveals three distinct phases of *L.m.* – platelet interaction
(a) 5x10^7 CMTMR-labelled *L.m.* were added to 1x10^8 murine platelets in 200 µl PRP (time = 0) and aggregation was measured over a time of 10 min. Samples were taken 30 s (Phase I), 200 s (Phase II) and 500 s (Phase III) after addition of *L.m.* and added to PBS supplemented with 10 mM EDTA. **(b)** Platelets were labelled with αCD41-FITC antibody and visualized with an Axiovert S100 (100x objective). Experiments performed by Eva Gillmeier under my supervision.

Intravital microscopy of systemically circulating *L.m.* in mice lacking either C3 or the platelet receptor GPIb had shown no formation of *L.m.* – platelet complexes (see Figure 2-3). In contrast to PRP of wild-type mice, the use of PRP from $C3^{-/-}$ or $GPIb^{-/-}$ mice displayed a lack of measurable aggregation after addition of *L.m.* (Figure 2-5a, b). It was hypothesized that phase I occurred in the wild-type setting due to the process of *L.m.* being opsonized by serum factors, especially C3, which in turn was then needed to form the small complexes of phase II. To test this, *L.m.* that had been pre-treated with wild-type plasma and thus already carried activated C3 on their surface (a process termed "preopsonization") were added to $C3^{-/-}$ PRP (Figure 2-5c). Accelerated transition to phase II and the formation of small complexes was observed, confirming this hypothesis. Addition of similarly pre-treated *L.m.* to $GPIb^{-/-}$ PRP on the other hand, in which *L.m.* are unable to bind platelets regardless of opsonisation due to the lacking receptor on platelets, displayed no aggregation as expected (Figure 2-5d).

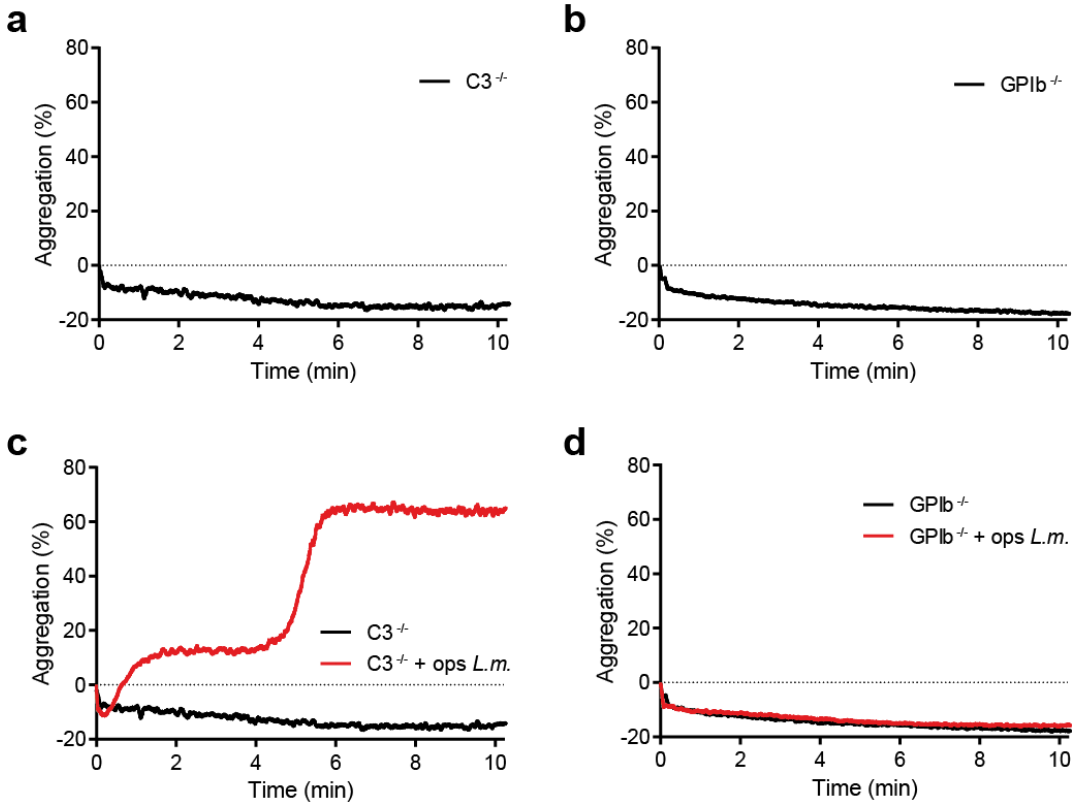

Figure 2-5 Complex formation is absent in $C3^{-/-}$ and $GPIb^{-/-}$ PRP, but can be rescued by preopsonization of *L.m.* in $C3^{-/-}$ PRP
PRP was isolated from $C3^{-/-}$ **(a, c)** or $GPIb^{-/-}$ mice **(b, d)** and platelet count adjusted to $5x10^5$/µl with plasma of the same strain. $5x10^7$ untreated *L.m.* **(a, b)** or *L.m.* preopsonized in wild-type serum **(c, d)** were added at time point 0 and aggregation was measured for the following 10 min. Experiments performed by Eva Gillmeier under my supervision.

It was further investigated, if various opsonins that act within the complement cascade play a role in the observed aggregation. The absence of the soluble opsonins C1q, which is necessary for the classical pathway of complement activation (MacKenzie *et al.,* 1971), and C4, which is needed for both the classical and the lectin pathway (Götze and Müller-Eberhard, 1970; Ikeda *et al.,* 1987), had no effect the formation of *L.m.* – platelet complexes (Figure 2-6a, b). A lack of Bf, an essential part of the alternative pathway of complement activation, in which C3 is spontaneously hydrolysed (Lachmann and Nicol, 1973), led to a prolonged phase I before the formation of *L.m.* – platelet complexes that define phase II were observed (Figure 2-6c). These data indicate that the alternative pathway of complement activation is predominantly responsible for the formation of *L.m.* – platelet complexes in this setting, although when this pathway is abrogated, it can be compensated by the other pathways of complement activation, though in a less efficient manner.

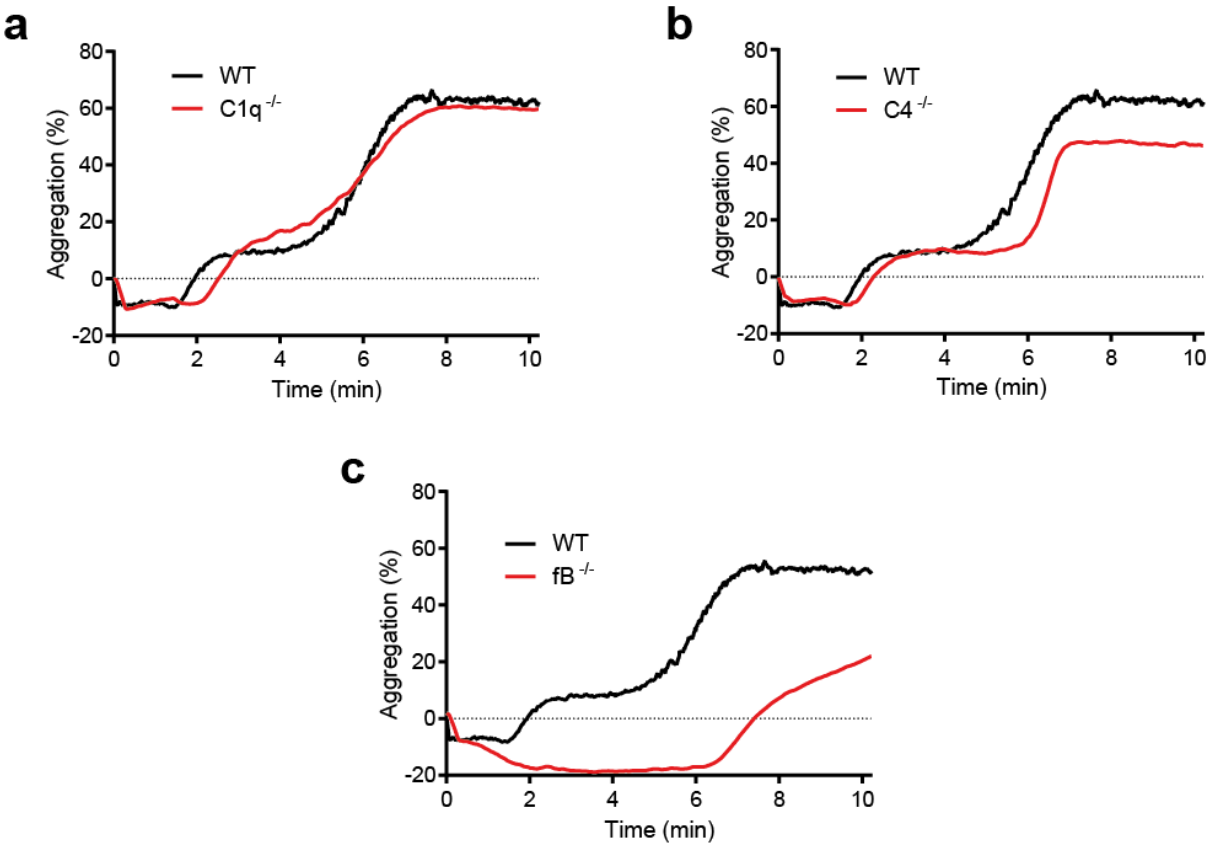

Figure 2-6 Formation of *in vivo* like complexes is not dependent on C1q or C4, but lack of fB extends phase I
PRP was isolated from $C1q^{-/-}$ **(a)**, $C4^{-/-}$ **(b)**, or $Bf^{-/-}$ mice **(c)** and platelet count adjusted to $5x10^5$/µl with plasma of the same strain. $5x10^7$ *L.m.* were added at timepoint 0 and aggregation was measured for 10 min. Experiments performed by Eva Gillmeier under my supervision.

Furthermore the influence of serum antibodies was investigated. Circulating antibodies within the blood of naïve animals are primarily of the IgG or IgM isotypes (Chaplin *et al.,* 1965). When *L.m.* were added to isolated PRP of AID$^{-/-}$sIgM$^{-/-}$ mice, which lack any form of circulating antibodies, the transition from phase I to phase II, representing the formation of small complexes, was comparable to the wild-type reference, but transition to phase III, representing further platelet aggregation, was abrogated (Figure 2-7a). Experiments using PRP of AID$^{-/-}$, which lack all circulating antibodies except IgM, or sIgM$^{-/-}$ mice, which only lack circulating IgM, revealed IgG to be necessary for the formation of large aggregates of phase III, whereas a lack of IgM led to a slight increase of in the speed of aggregate formation (Figure 2-7b, c).

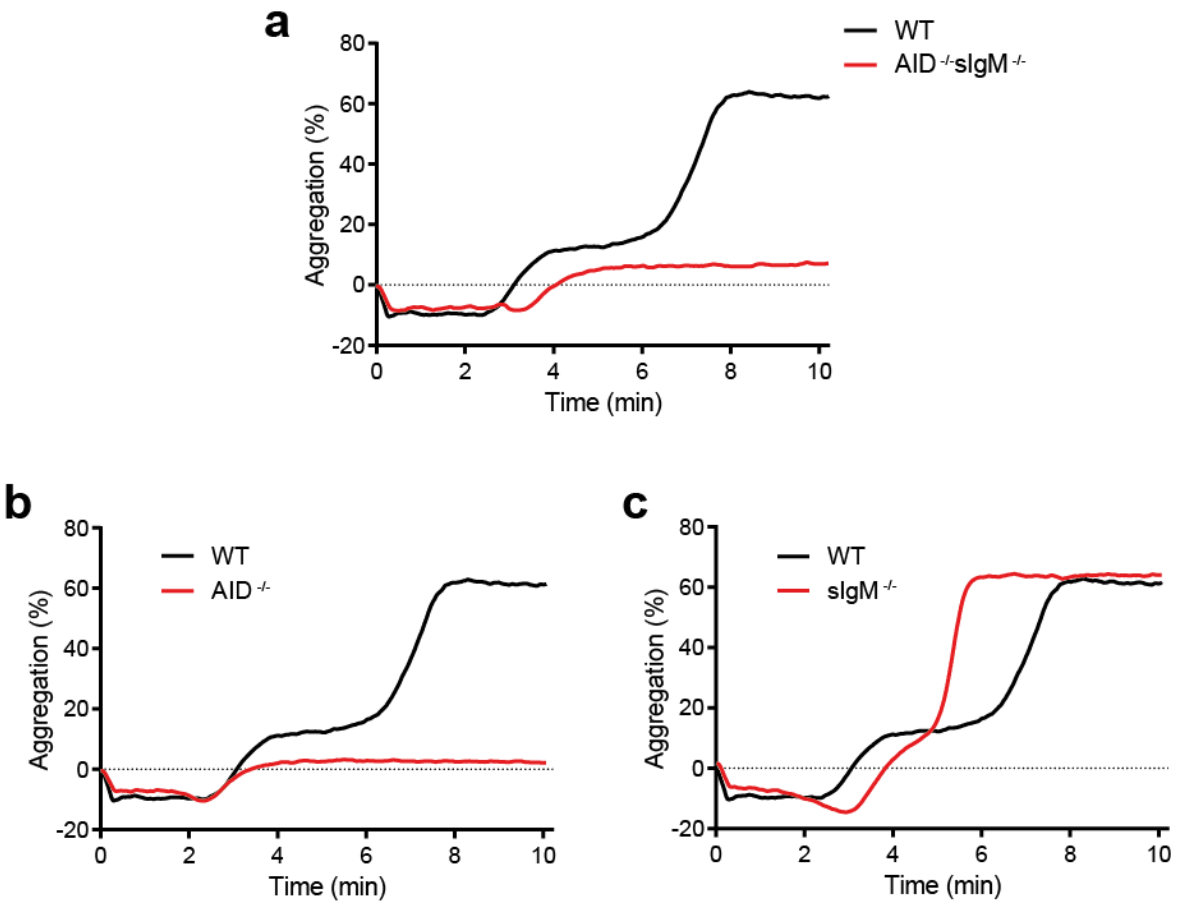

Figure 2-7 Formation of phase III large aggregates is dependent on presence of IgG
PRP was isolated from AID$^{-/-}$sIgM$^{-/-}$ **(a)**, AID$^{-/-}$ **(b)**, or sIgM$^{-/-}$ mice **(c)** and platelet count adjusted to 5x10^5/µl with plasma of the same strain. 5x10^7 *L.m.* were added at timepoint 0 and aggregation was measured for 10 min.

It was hypothesized that the IgG-dependent formation of large aggregates was due to activation of platelets in the small complexes of phase II. Platelets activation can be facilitated in several ways, the most common being thrombin-signalling, T_xA_2-signalling and extracellular ADP which leads to aggregation via fibrinogen-binding via the GPIIb/IIIa receptor (Gross and Weitz, 2009). To test if platelet activation was the cause for the observed platelet aggregation in phase III, wild-type mice were treated with the platelet activation inhibitors aspirin, which inhibits T_xA_2 formation (Schror, 1997) or clopidogrel, which blocks the binding of extracellular ADP to platelet receptors (Mills *et al.,* 1992). Both treatments inhibited the formation of large aggregates, thus proving platelet activation as the main cause of aggregate formation (Figure 2-8a, b), potentially induced by IgG antibodies.

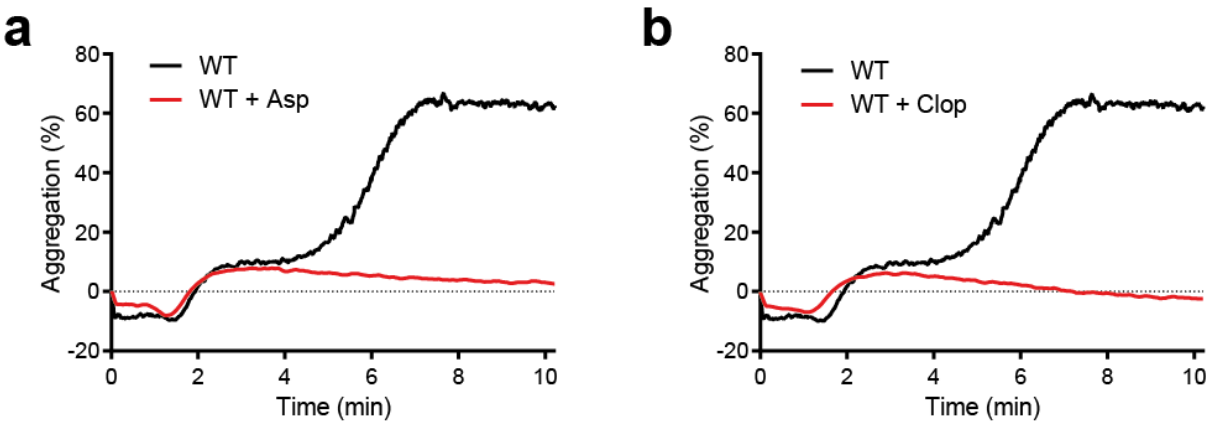

Figure 2-8 Platelet activation inhibitors inhibit the formation of large aggregates of phase III
Wild-type mice were treated with Aspirin (Asp) or clopidogrel (Clop) prior to being bled. PRP was isolated, platelet count was adjusted to $5x10^5$/µl with plasma of the same strain. $5x10^7$ *L.m.* were added at timepoint 0 and aggregation was measured for 10 min.

The complement regulatory protein fH has been described as being present on the surface of murine platelets and mediating interaction with complement opsonized particles (Alexander *et al.,* 2001). It was thus investigated if fH is involved in the interaction of *L.m.* with platelets. Mice lacking fH have a reduced amount of C3 in their circulation due to lacking regulation of C3 activation, leading to reduced complement opsonization of *L.m.* in $fH^{-/-}$ plasma (Pickering *et al.,* 2007). To circumvent the lack of C3, *L.m.* were preincubated in plasma of mice with mutated, inactive fHΔ16-20, which have normal levels of C3 in the plasma (Pickering *et al.,* 2007). Addition of *L.m.* preincubated in fHΔ16-20 plasma to PRP of $fH^{-/-}$ mice led to normal complex formation, comparable to the control wild-type (Figure 2-9), ruling out an involvement of fH in the interaction between *L.m.* and platelets.

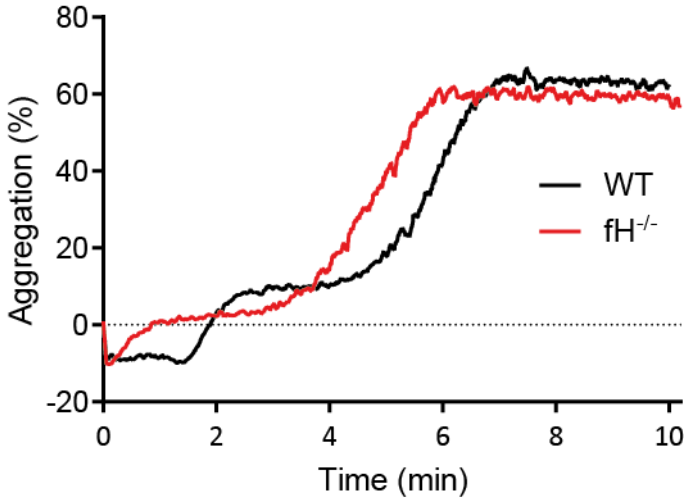

Figure 2-9 *L.m.* – platelet complex formation occurs in absence of fH
1x10^8 *L.m.* were incubated in fHΔ16-20 plasma for 1 min, washed extensively and added to PRP of fH$^{-/-}$ mice. PRP was isolated, platelet count was adjusted to 5x10^5/µl with plasma of the same strain. 5x10^7 *L.m.* were added at timepoint 0 and aggregation was measured for 10 min.

To investigate the role of *L.m.* in this observed platelet aggregation, differently inactivated *L.m.* were added to wild-type PRP and aggregation was observed. Interestingly, addition of heat-inactivated *L.m.* to wild-type PRP fully abolished the transition from phase II to phase III, and thus platelet activation and aggregation, although no variation in the formation of small complexes was observed (Figure 2-10a). This indicated an active role of the bacteria in the induction of platelet aggregation. To further examine the role of *L.m.*, *L.m.* lacking either the virulence factor LLO or ActA were used for aggregometry. While a lack of LLO was found to abrogate platelet aggregation (Figure 2-10b), a lack of ActA had no pronounced effect on platelet aggregation (Supplemental figure 1).

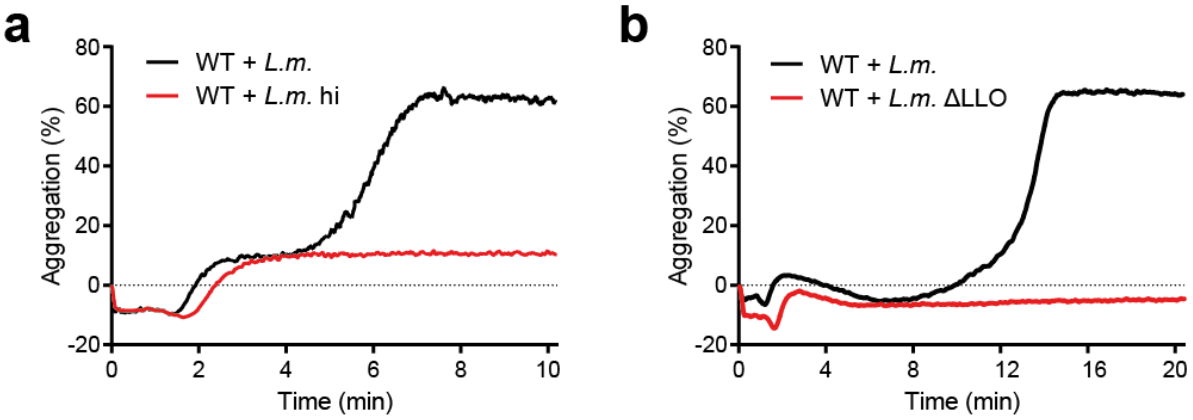

Figure 2-10 Vitality and LLO expression of *L.m.* is not important for the formation of in vivo like complexes, but determines platelet activation and thus transition to phase III
PRP was isolated from wild-type mice and platelet count adjusted to 5x10^5/µl with plasma of the same strain. 5x10^7 heat-inactivated *L.m.* **(a)** or ΔLLO *L.m.* **(b)** were added at time point 0 and aggregation was observed for 10 or 20 min.

In summary, light transmission platelet aggregometry revealed that the formation of *L.m.* – platelet complexes is a robust process that *in vitro* needs approximately 1-2 min to be fully accomplished. It was observed that the time-limiting factor is not the binding of platelets to *L.m.*, which happens rapidly, but the opsonisation of *L.m.* with C3-activation products. This opsonization relies primarily on the alternative pathway of complement activation. Some minutes after these complexes form full aggregation follows due to platelet activation, dependent on the presence of IgG and active LLO-production by *L.m.*.

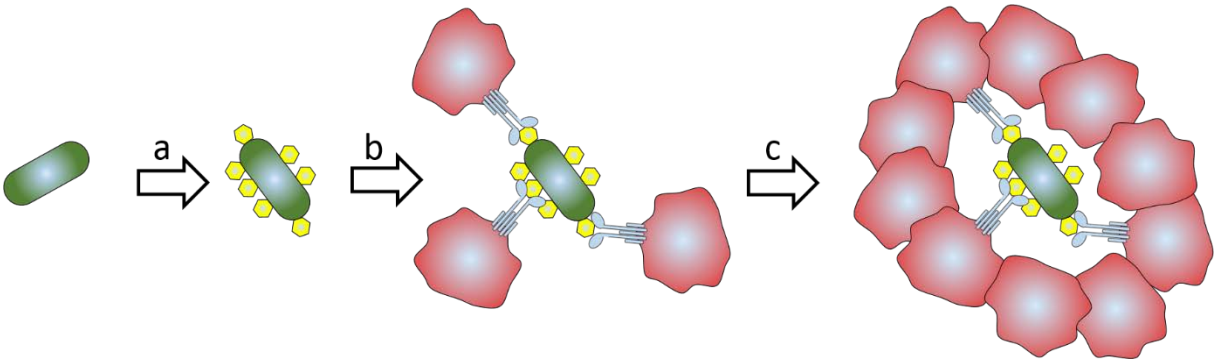

Illustration 2-2 Summary of chapter 2.2
In vitro platelet aggregometry revealed three distinct phases after *L.m.* reaches blood plasma. These phases consist of **(a)** the opsonization of *L.m.* with activated C3 via the alternative pathway of complement activation **(b)** the formation of *L.m.* – platelet complexes dependent on activated C3 on the surface of *L.m.* and GPIb on the surface of platelets and **(c)** platelet activation and aggregation around bound *L.m.*, dependent on the presence of IgG and *L.m.*-LLO.

2.3 Bodily distribution of *L.m.* depends on complex formation

To investigate the consequences of *L.m.* – platelet complex formation beyond blood clearance kinetics and how it influences bacterial organ distribution within the mouse, the location of clearance of systemically circulating *L.m.* from the bloodstream was examined. Clearance of *L.m.* from the bloodstream of wild-type mice has been shown to reach over 99% 15 min after intravenous infection (Verschoor *et al.,* 2011). Thus this time point was selected to screen organs with major phagocytic populations for viable bacteria: liver (Benacerraf *et al.,* 1959), spleen (Altamura *et al.,* 2001) and to a certain degree the lung (Singh *et al.,* 1998)) and known bacterial niches (kidneys (Smith *et al.,* 2010), bone marrow (Das *et al.,* 2013) and brain (Disson and Lecuit, 2012).

When comparing clearance in wild-type mice to mice in which *L.m.* – platelet complex formation has been abrogated ($C3^{-/-}$ and $GPIb^{-/-}$), it became clear that in all strains the majority of clearance was facilitated by the liver, followed by the spleen (Figure 2-11a). All other organs screened contained less than 1% of total *L.m.* found.

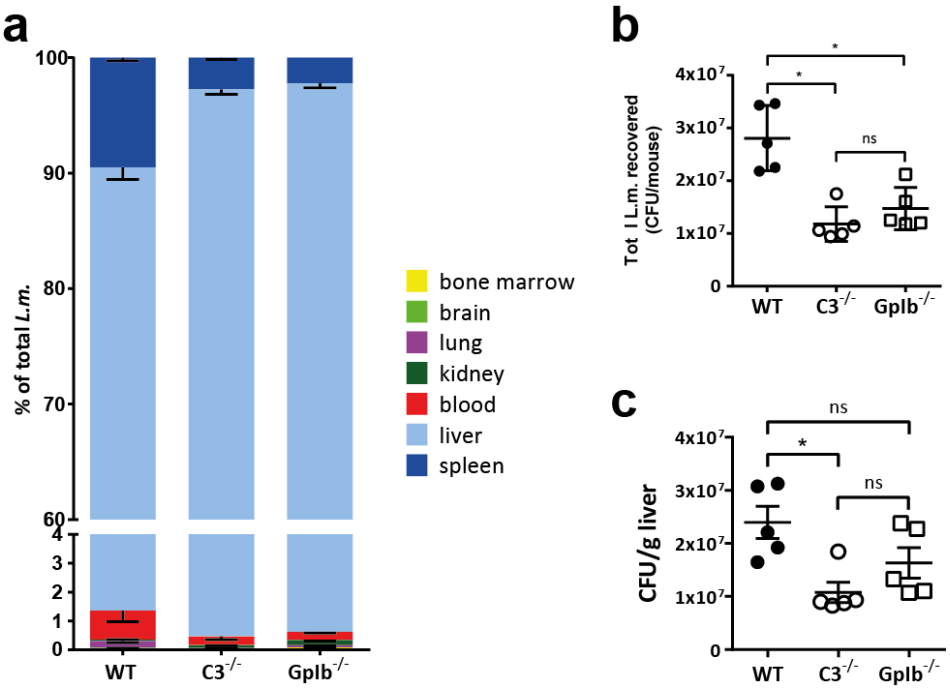

Figure 2-11 Distribution of *L.m.* 15 min after infection
WT, $C3^{-/-}$ and $GPIb^{-/-}$ mice were infected with $1x10^8$ *L.m.* i.v.. 15 min post infection liver, spleen, lung, kidney, brain, bone marrow and blood samples were harvested, homogenized and plated for CFU detection. **(a)** Distribution of recovered *L.m.* throughout screened organs. 100 % represent all recovered CFU (mean ± SEM of 5 mice per strain) **(b)** Total number of recovered *L.m.* and **(c)** number or recovered *L.m.* in the liver per g tissue for WT, $C3^{-/-}$ and $GPIb^{-/-}$ (mean ± SEM of 5 mice per strain, * = $P < 0.05$, # = $P < 0.01$, § = $P < 0.001$, One-way ANOVA with Tukey post-test adjustment) Experiments performed in cooperation with Ann Plaumann.

Compared to the wild-type, the uptake of *L.m.* in the liver was significantly higher in $C3^{-/-}$ mice (96.79% vs. 92.04%, P = 0.002, two-tailed Student's t-test) as well as in $GPIb^{-/-}$ mice (97.15% vs. 92.04%, P = 0.001, two-tailed Student's t-test). In contrast, the uptake of *L.m.* in the spleen was reduced in both $C3^{-/-}$ and $GPIb^{-/-}$ mice in comparison to the wild-type (3.04% vs. 6.26%, P = 0.003 and 2.63% vs. 6.26%, P = 0.001 respectively, two-tailed Student's t-test). *L.m.* uptake in lung, brain and bone marrow were also significantly reduced (Supplemental figure 2). This indicated that when binding to platelets is abrogated, *L.m.* are cleared to a higher degree by the liver and reach other organs to a significantly smaller degree. Moreover, although the percentage of *L.m.* found within the liver was increased in both $C3^{-/-}$ and $GPIb^{-/-}$ mice compared to the wild-type, the actual number of live *L.m.* found in $C3^{-/-}$ and $GPIb^{-/-}$ mice was significantly reduced in the liver as well as in all organs combined (Figure 2-11b, c). It was thus unclear, if the observed heightened liver uptake was actually due to an increase in hepatic uptake or due to increased killing of *L.m.* in other organs in absence of platelet binding.

To investigate this question, a novel method was developed capable of detecting all *L.m.* in a time-course resolution instead of being limited to detecting live *L.m.* at one timepoint as is the case in multi-organ screening. Detection of all *L.m.* throughout the body was accomplished utilizing a PET-CT based full-body imaging technique in combination with radioactively labelled *L.m.*. *L.m.*, which had been starved for nutrients by incubation in PBS for 60 min, were incubated with ^{18}FDG for 90 min before being extensively washed and used as infective inoculum (Figure 2-12a). Control *L.m.*, which had not been starved in PBS, failed to take up any radioactivity for the first 2 h of incubation. Infection of wild-type mice with these radioactively labelled *L.m.* confirmed the targeting of *L.m.* to liver and spleen (Figure 2-12b, c). Signal was also visible in the lung for early timepoints, due to the high vascularization, but decreased over time as *L.m.* were cleared from the bloodstream. At late timepoints, signal was also detected in both kidneys and bladder. Plating of urine from the bladder and homogenized kidneys found few live *L.m.* to have localized to these organs (Supplemental figure 3). It is thus likely that the detected signal within these organs was not due to bacterial uptake or infection, but due to free ^{18}F-Glucose, which had been leaked by *L.m.* killed elsewhere, being filtered from the bloodstream.

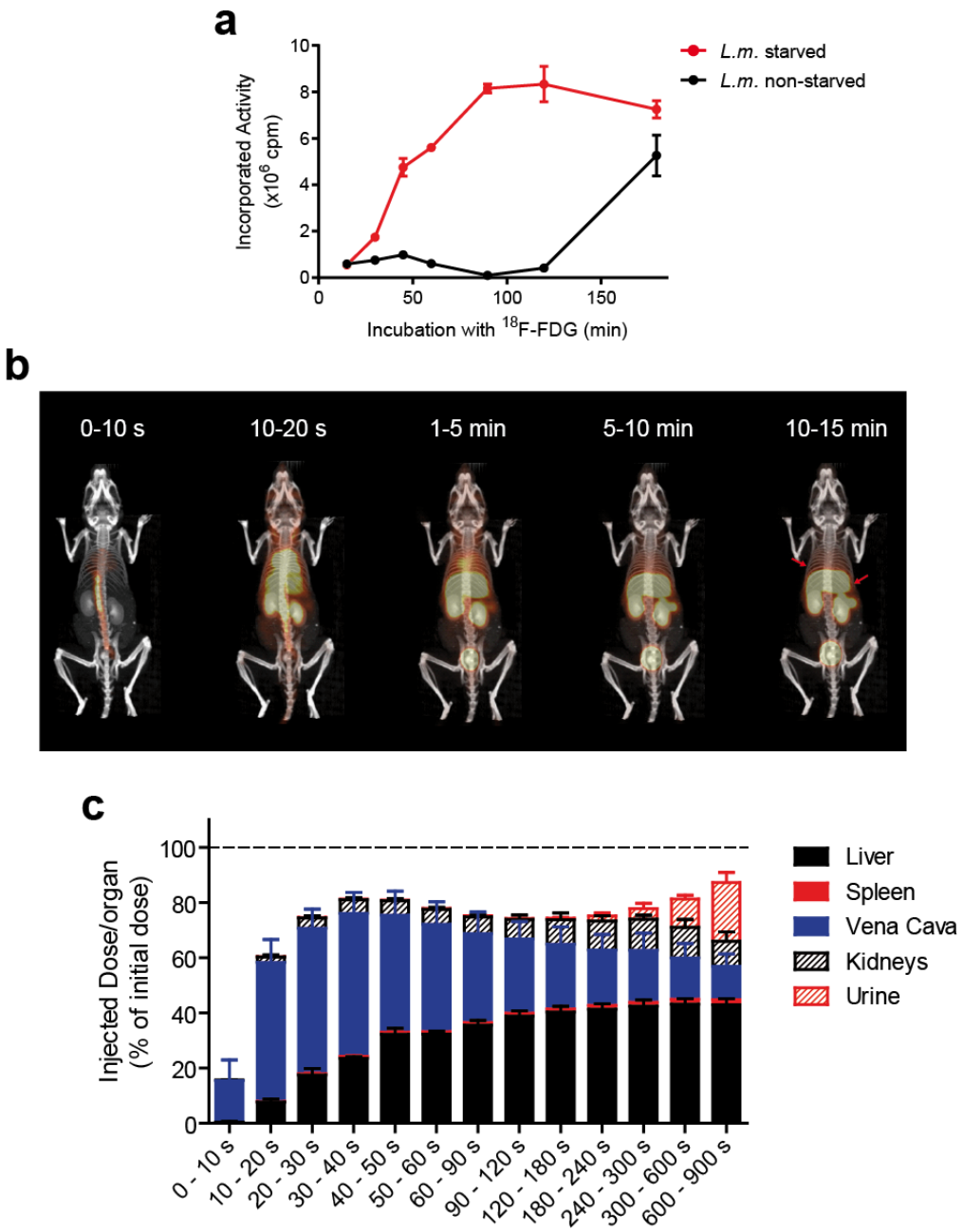

Figure 2-12 PET-CT imaging of systemic *L.m.* infection
(a) Starved or non-starved *L.m.* were incubated with ^{18}FDG for time points of up to 180 min, washed thrice in PBS + 10% BHI media and incorporated radioactivity was measured. **(b)** Time course heat map images from the systemic infection of a wild-type mouse with *L.m.* incubated with ^{18}FDG for 90 min. Arrows indicate splenic and hepatic uptake of *L.m.*. **(c)** Calculated uptake of detected activity per organ per time frame in wild-type mice (mean ± SD of 4 mice).

In C3$^{-/-}$ and GPIb$^{-/-}$ mice, where *L.m.* – platelet complex formation is abrogated, the liver phagocytosed an increased percentage of injected bacteria in comparison to the wild-type (Figure 2-13a, c). This was associated with a lower percentage of bacteria been taken up in the spleen in C3$^{-/-}$ and GPIb$^{-/-}$ mice in comparison to the wild-type (Figure 2-13b, d), resembling the observed phenotype during the multi-organ screen for live *L.m.* (see Figure 2-11).

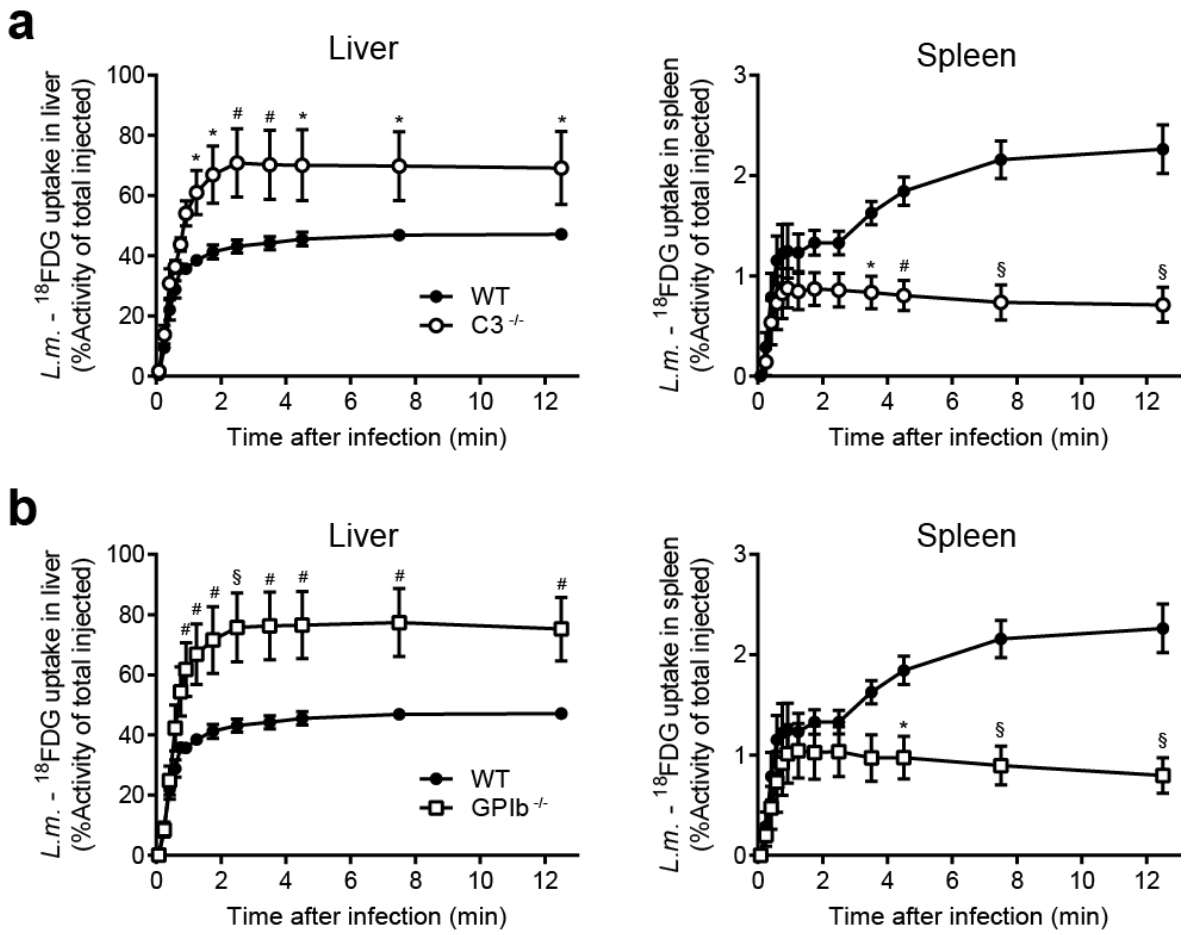

Figure 2-13 *L.m.* uptake in wild-type, C3$^{-/-}$ and GPIb$^{-/-}$ mice
Hepatic (left) and splenic (right) uptake of ^{18}FDG - *L.m.* in wild-type vs. C3$^{-/-}$ mice **(a)** and wild-type vs. GPIb$^{-/-}$ mice. **(c)** Mice were infected with 1x10^{8} *L.m.* labelled with ^{18}FDG for 90 min and distribution was acquired for 15 min post infection via PET-CT (mean ± SD of 3-4 mice per strain, * = P < 0.05, # = P < 0.01, § = P < 0.001, Two-way ANOVA with Bonferroni post-test adjustment).

Interestingly, splenic uptake of systemically circulating *L.m.* was not significantly different between wild-type mice and mice lacking *L.m.* – platelet complex formation until 3-4 min after infection. Intravital microscopy of systemically circulating *L.m.* in wild-type mice had revealed this timepoint of approximately 4 min post infection to be the timepoint from which on all *L.m.* remaining in the circulation had formed *L.m.* – platelet complexes (see Figure 2-3). It can thus be speculated that all *L.m.* uptake after the 4 min mark is due to the formation *L.m.* – platelet complexes.

Taken together these data indicated that the clearance of *L.m.* from the bloodstream is predominantly facilitated by the liver and is in part dependent on the binding of *L.m.* to platelets. In absence of *L.m.* – platelet complex formation the liver took up *L.m.* more efficiently and thus less bacteria reach other organs throughout the system, especially the spleen. Less viable *L.m.* were recovered from mice lacking *L.m.* – platelet complex formation, but full-body visualization of systemic *L.m.* infection confirmed the heightened liver uptake of

L.m. in absence of *L.m.* – platelet complex formation to be true. To further pinpoint *L.m.* clearance and its dependence on *L.m.* – platelet complex formation, it was investigated which hepatic cell population is the main facilitator of clearance of systemically circulating *L.m.* from the bloodstream.

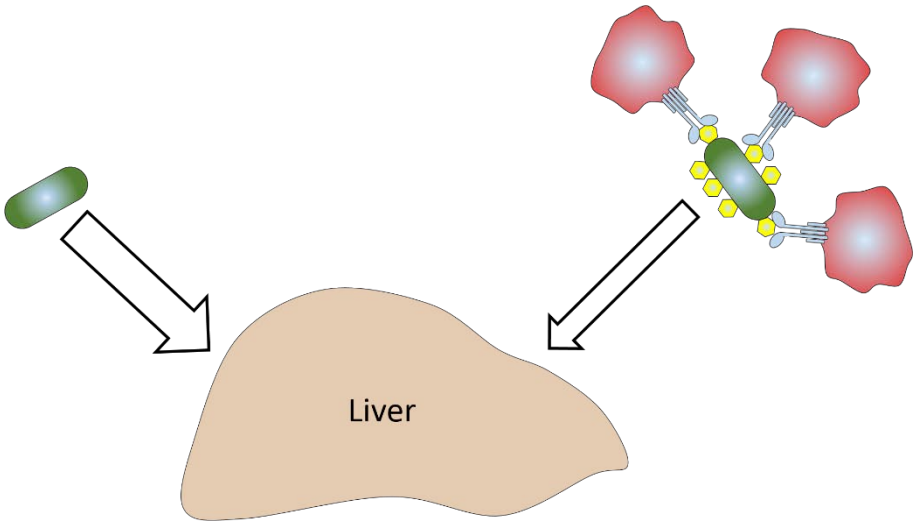

Illustration 2-3 Summary of chapter 2.3
L.m. that have not bound to platelets (left), as is the case in $C3^{-/-}$ mice and $GPIb^{-/-}$ mice, and *L.m.* – platelet complexes (right), which are observed in wild-type mice, are cleared predominantly by the liver, though increased hepatic uptake is visible in mice lacking *L.m.* – platelet complex formation.

2.4 Hepatic uptake of *L.m.* is facilitated predominantly by Kupffer cells

To closer pinpoint the facilitating cell population of increased hepatic *L.m.* uptake in absence of platelet binding, wild-type mice were infected with fluorescently labelled *L.m.* and flow cytometry analysis was performed on hepatic cell isolates at 30 min post intravenous infection (Figure 2-14a, b). Three major cell populations were found to be positive for *L.m.* in large numbers in wild-type mice: F4/80$^+$ Kupffer cells, Ly6G$^+$ neutrophil granulocytes and CD19$^+$ B-cells (Figure 2-14c).

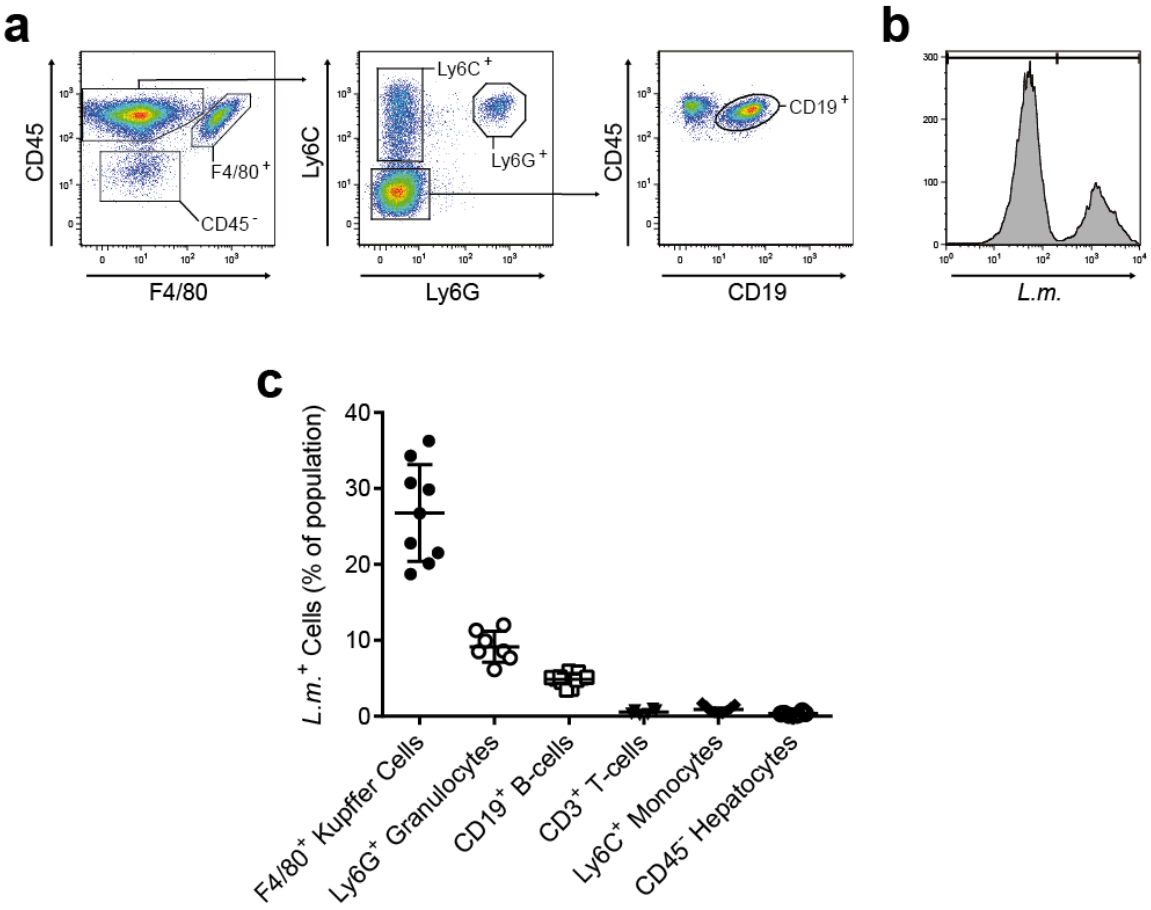

Figure 2-14 Kupffer Cells, neutrophil granulocytes and B-cells capture *L.m.* in the liver
Wild-type mice were infected with 1x10^8 eFluor670-labeled *L.m.*. Livers were removed 30 min after infection, cells isolated, stained and analysed for *L.m.* uptake via flow cytometry. **(a)** Gating schematic of isolated liver cells stained for the cellular markers F4/80 (Kupffer cells), Ly6G (neutrophil granulocytes), Ly6C (monocytes) and CD19 (B-cells) and CD3 (T-cells). Samples were pregated on live singlets. **(b)** Sample diagram of detectable eFluor670-*L.m.* uptake for F4/80$^+$ Kupffer cells in wild-type mice (grey solid) and an uninfected control (black line). **(c)** Percentage of cells positive for eFluor670-*L.m.* within each defined population in wild-type mice (mean ± SD of 9 mice).

CD19^{+} B-cells found within the liver were significantly more frequently associated with fluorescent *L.m.* than their counterparts in the bloodstream (Figure 2-15a), matching a recently described liver-resident B-cells population with bactericidal capacities (Nakashima *et al.,* 2012). Hepatic B-cells in C3$^{-/-}$ mice failed to take up fluorescently labelled *L.m.* after systemic infection though (Figure 2-15b). Interaction between B-cells and *L.m.* was furthermore found to be dependent on CR1/2 (Figure 2-15c). This strict complement dependency ruled out this cell population as cause of the overall increased hepatic uptake observed in C3$^{-/-}$ mice (see Figure 2-11 and Figure 2-13).

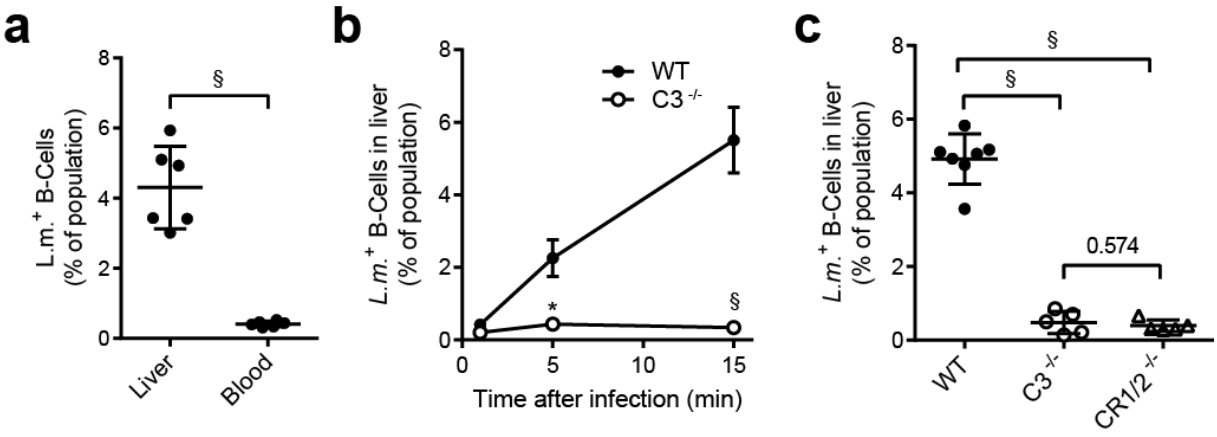

Figure 2-15 *L.m.* uptake via B-cells is C3 and CR1/2-dependent
Wild-type mice were infected with 1x10^{8} eFLuor670-labeled *L.m.*, livers were removed at indicated time points and cell populations analysed for *L.m.* uptake. **(a)** Comparison of frequency of *L.m.*$^{+}$ B-cells in liver isolates and corresponding blood samples taken simultaneously to the removal of the liver (mean ± SD of 6 mice, * = P < 0.05, # = P < 0.01, § = P < 0.001, Two-tailed Student's t-test). **(b)** *L.m.* uptake by hepatic B-cells in wild-type and C3$^{-/-}$ mice at 1, 5 and 15 min post infection (mean ± SD of 3-4 mice per timepoint, * = P < 0.05, # = P < 0.01, § = P < 0.001, Two-way ANOVA with Bonferroni post-test adjustment). **(c)** Comparison of *L.m.* uptake by hepatic B-cells 15 min post infection in wild-type, C3$^{-/-}$ and CR1/2$^{-/-}$ mice (mean ± SD of 5-7 mice, * = P < 0.05, # = P < 0.01, § = P < 0.001, Two-tailed Student's t-test).

Neutrophil granulocytes isolated from the liver had, similarly to B-cells, taken up significantly more fluorescent *L.m.* than neutrophil granulocytes circulating in the bloodstream (Figure 2-16a). As observed in B-cells, uptake of *L.m.* by neutrophil granulocytes also proved to be C3-dependent (Figure 2-16b) again ruling out neutrophil granulocytes as causative cell population of increased hepatic *L.m.* uptake in C3$^{-/-}$ mice.

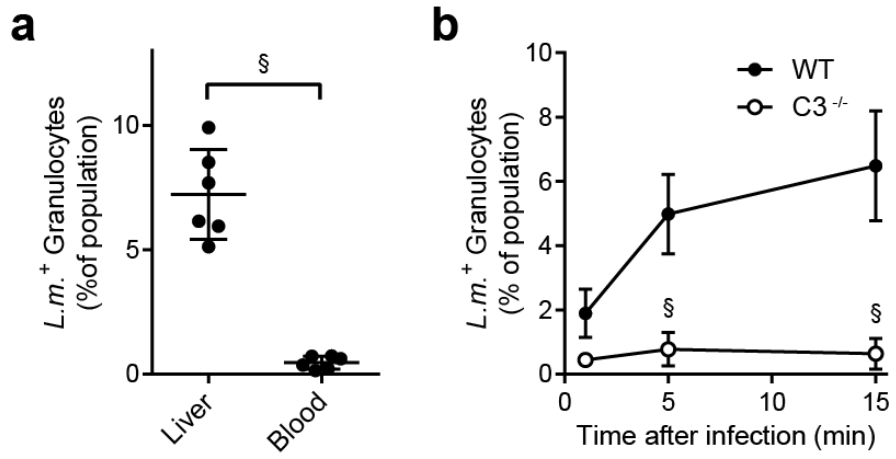

Figure 2-16 *L.m.* uptake via neutrophil granulocytes is C3-dependent
Wild-type mice were infected with 1x10^8 eFLuor670-labeled *L.m.*, livers were removed at indicated time points and cell populations analysed for *L.m.* uptake. **(a)** Comparison of frequency of *L.m.*$^+$ neutrophil granulocytes in liver isolates and corresponding blood samples taken simultaneously to the removal of the liver (mean ± SD of 6 mice, * = P < 0.05, # = P < 0.01, § = P < 0.001, Two-tailed Student's t-test). **(b)** *L.m.* uptake by neutrophil granulocytes in the liver in wild-type and C3$^{-/-}$ mice at 1, 5 and 15 min post infection (mean ± SD of 3-4 mice per timepoint, * = P < 0.05, # = P < 0.01, § = P < 0.001, Two-way ANOVA with Bonferroni post-test adjustment).

In contrast to B-cells and neutrophil granulocytes, uptake of *L.m.* by Kupffer cells was increased in both C3$^{-/-}$ and GPIb$^{-/-}$ mice (Figure 2-17a, b), making this population a likely cause for the observed phenotype of more efficient clearance in lack of platelet binding. Kupffer cells positive for *L.m.* in all strains had a similar mean fluorescent intensity (MFI) for *L.m.*-eFluor670 (Supplemental figure 4), indicating that on average, Kupffer cells in all strains had taken up a comparable number of *L.m.*.

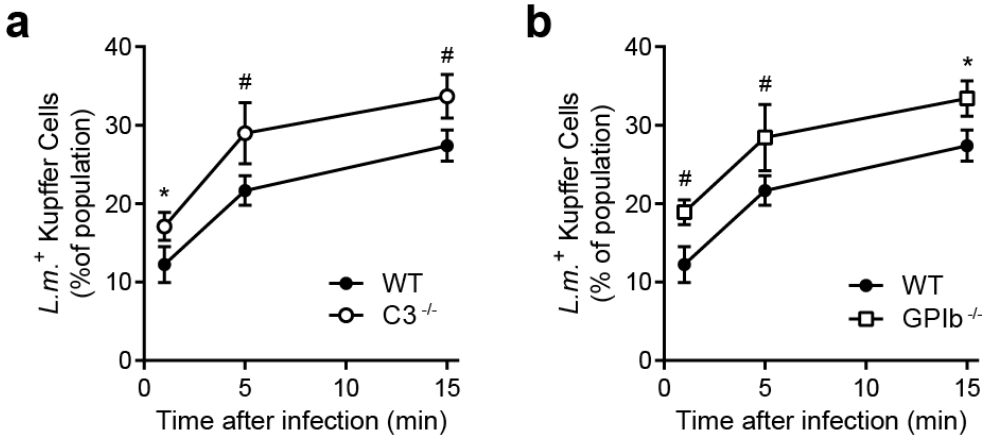

Figure 2-17 *L.m.* uptake by hepatic Kupffer Cells is increased in C3$^{-/-}$ and GPIb$^{-/-}$ mice
Wild-type, C3$^{-/-}$ and GPIb$^{-/-}$ mice were infected with 1x10^8 eFLuor670-labeled *L.m.*, livers were removed at indicated time points and cell populations analysed for *L.m.* uptake. Comparison wild-type mice to C3$^{-/-}$ **(a)** and GPIb$^{-/-}$ **(b)** mice at 1, 5 and 15 min post infection (mean ± SD of 3-4 mice per timepoint, * = P < 0.05, # = P < 0.01, § = P < 0.001, Two-way ANOVA with Bonferroni post-test adjustment).

Since Kupffer cells were hereby implicated in being the main facilitator of clearance of *L.m.* from the circulation, the phenotype of potentially heightened killing of taken up *L.m.* in $C3^{-/-}$ and $GPIb^{-/-}$ mice observed during the multi-organ screening for live *L.m.* was revisited (see Figure 2-11). There it was observed that while a higher percentage of all *L.m.* was retrieved in the liver, indicating more efficient uptake, the actual number of *L.m.* retrieved was significantly reduced. Kupffer cells of infected wild-type, $C3^{-/-}$ and $GPIb^{-/-}$ mice were isolated by cell sorting via flow cytometry, lysed and plated to determine containing live *L.m.* (see Figure 2-18). Although the uptake of stably fluorescently labelled *L.m.* was increased in Kupffer cells of $C3^{-/-}$ and $GPIb^{-/-}$ mice (see Figure 2-17a, b), live *L.m.* were again reduced significantly in both strains in comparison to the wild-type. This indicated a potentially different clearance mechanisms of *L.m.* uptake by Kupffer cells in wild-type mice vs. $C3^{-/-}$ and $GPIb^{-/-}$ mice, where inactivation seemed more efficient.

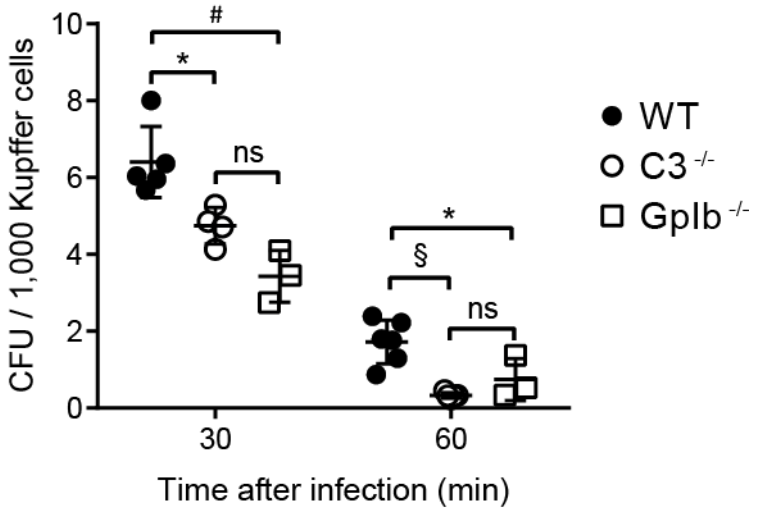

Figure 2-18 Lack of platelet binding leads to less viable *L.m.* recovered from Kupffer cells
Wild-type, $C3^{-/-}$ and $GPIb^{-/-}$ mice were systemically infected with $1x10^7$ *L.m.* and livers were removed at indicated timepoints. Kupffer cells were FACS sorted as $CD45^+$ $F4/80^+$. Cells were subsequently lysed and plated for CFU detection. Each knockout-mouse tested had at least one wild-type control (mean ± SD of 3-5 mice per timepoint, * = $P < 0.05$, # = $P < 0.01$, § = $P < 0.001$, Two-way ANOVA with Bonferroni post-test adjustment). Experiments performed by Ann Plaumann and presented here with her kind permission.

In vitro aggregometry had revealed Bf to be important for the formation of small complexes of *L.m.* and platelets (see Figure 2-6), similar to the observed complexes *in vivo* (see Figure 2-3). Additionally the presence of IgG had been observed to be essential for the formation of larger platelet aggregates after prolonged contact of the platelets with *L.m.* (see Figure 2-7). To investigate the relevance of these factors for the clearance of *L.m. in vivo*, $Bf^{-/-}$ mice lacking Bf, $AID^{-/-}sIgM^{-/-}$ lacking both circulating IgG and IgM, $AID^{-/-}$ mice lacking only circulating IgG, and $sIgM^{-/-}$ mice lacking only circulating IgM were infected with fluorescently labelled *L.m.* and

Kupffer cells were analysed by flow cytometry for *L.m.* uptake 15 min after infection (Figure 2-19). Interestingly, a lack of Bf had no pronounced effect on the uptake of *L.m.* by Kupffer cells in comparison to the wild-type. This indicated a very robust system of *L.m.* – platelet complex formation *in vivo*, in which a lack of Bf can be compensated by the other pathways of complement activation. Also, a lack of antibodies, be it IgG, IgM or both, had no detectable effect on the uptake of *L.m.* by Kupffer cells, indicating that the formation of large platelet aggregates around circulating *L.m.* are not important for the clearance of *L.m.* – platelet complexes from the bloodstream by Kupffer cells.

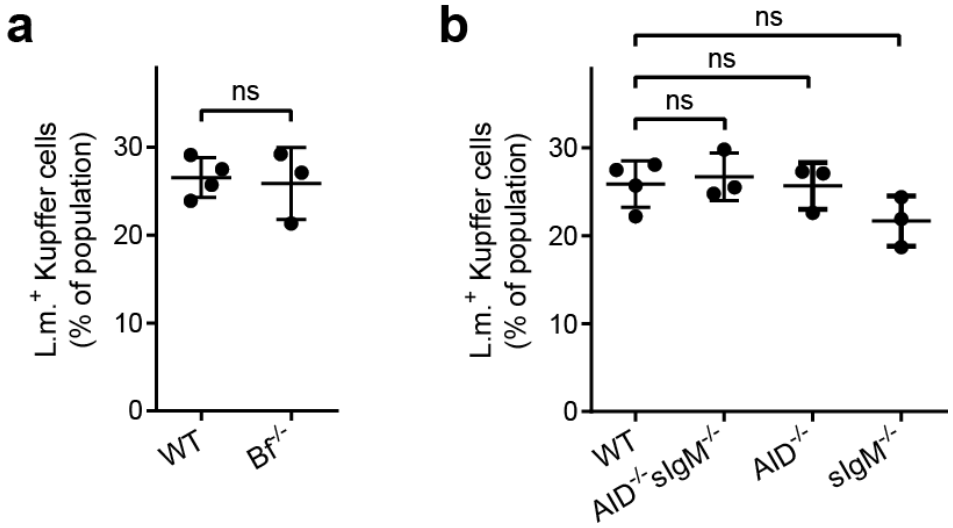

Figure 2-19 Uptake of *L.m.* by hepatic Kupffer cells is unaltered when Bf, IgG or IgM is lacking
(a) Wild-type and $Bf^{-/-}$ mice were infected with $1x10^8$ eFluor670-labelled *L.m.*. Livers were removed 15 min post infection and cells were isolated, stained and analysed for *L.m.* uptake by flow cytometry (mean ± SD of 3-4 mice per strain, Two-tailed Student's t-test). **(a)** Wild-type, $AID^{-/-}sIgM^{-/-}$, $AID^{-/-}$ and $sIgM^{-/-}$ mice were infected with $1x10^8$ eFluor670-labelled *L.m.*. Livers were removed 15 min post infection and cells were isolated, stained and analysed for *L.m.* uptake by flow cytometry (mean ± SD of 3-4 mice per strain, One way ANOVA with Bonferroni post-test adjustment for multiple comparisons).

To directly visualize the clearance of *L.m.* from the bloodstream *in vivo* a liver model for multiphoton intravital imaging was established (Figure 2-20a). Imaging systemic infection with *L.m.* confirmed hepatic Kupffer cells to be the first and major point of immobilization of *L.m.* in the liver (Figure 2-20b). Interestingly, interaction between Kupffer cells and neutrophil granulocytes was observed on multiple occasions: herein *L.m.* were immobilized on Kupffer cells and subsequently phagocytosed by crawling granulocytes (Figure 2-20c). This fits a model of Kupffer cell – neutrophil granulocyte interaction described by Gregory and Wing (Gregory and Wing, 1998).

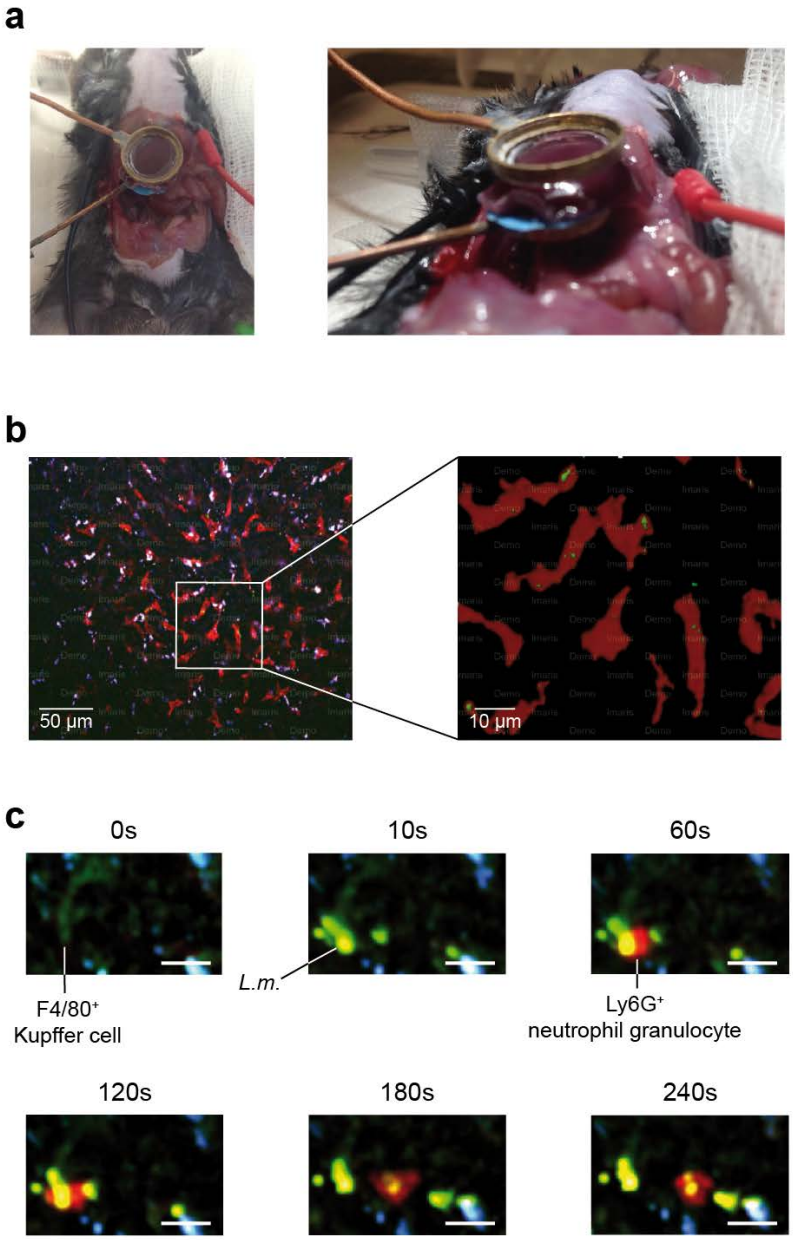

Figure 2-20 Intravital Imaging of the liver revealed Kupffer cell and neutrophil granulocyte uptake of *L.m.*
(a) Intravital imaging setup of the liver (top-view left, side-view right) **(b)** Raw image (left) and 5x magnified surface rendering (right) of Kupffer cell uptake of *L.m.* in livers of wild-type mice 1 minute after infection with $1x10^8$ CFSE-labelled *L.m.* (red = F4/80-PE, green = L.m.-CFSE, white = autofluorescence) **(c)** Still images of a 2D time-lapse video displaying Kupffer cell – neutrophil granulocyte interaction after infection with *L.m.* (green = F4/80-FITC, yellow = L.m. – CFSE, red = Ly6G-PE, scale bar = 10 µm)

Platelets were also observed coating already immobilized *L.m.* on Kupffer cells (Figure 2-21a). Interestingly, this process was also observed in $C3^{-/-}$ mice (Figure 2-21b), where *L.m.* – platelet complex formation within the circulation is not observable (Verschoor *et al.,* 2011). This process has in the meantime been described for *B. cereus*, where it is dependent on interaction of GPIb on the platelet surface and vWF bound on the surface of Kupffer cells (Wong *et al.,* 2013a).

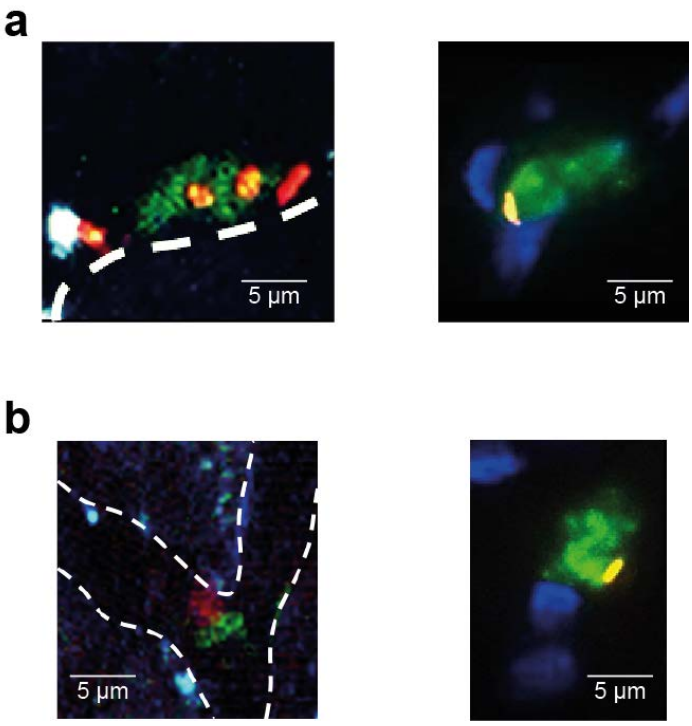

Figure 2-21 Platelet aggregation on immobilized *L.m.* in the liver
(a) Wild-type and **(b)** $C3^{-/-}$ mice were infected with $1x10^8$ CMTMR-labelled *L.m.* and hepatic uptake was visualized via intravital microscopy (left, red = CMTMR-L.m., green = αCD49b-Alexa Fluor488, white = autofluorescence). After imaging, livers were removed and cryo-section of 5µm were cut and stained with αF4/80-eFluor450 to visualize Kupffer cells (right, blue = F4/80-eFluor450, green = αCD49b-Alexa Fluor 488, yellow = CMTMR-*L.m.*)

Kupffer cells have been described to consist of multiple subsets: Kupffer cells derived from the bone marrow uniquely express CD11b and are thus the only Kupffer cell subset with CR3 on their surface. $CD32^+$ Kupffer cells are immature liver resident Kupffer cells which mature to $CD68^+$ Kupffer cells while losing their expression of CD32. Both of these liver derived subsets express CRIg, but not CR3, whereas bone marrow derived Kupffer cells do not express CRIg (Kinoshita *et al.,* 2010; Ikarashi *et al.,* 2013). Since CD68 is expressed intracellularly and is not stainable for flow cytometry without permeabilization of the cells, subsets were defined as $CD11b^+CD32^-$ for bone marrow derived Kupffer cells, $CD11b^-CD32^+$ for immature liver resident Kupffer cells and $CD11b^-CD32^-$ for mature liver resident Kupffer cells (Figure 2-22a). It was observed that $CD32^-$ $CD11b^-$ Kupffer cells handled the bulk of *L.m.* clearance whereas immature liver derived $CD32^+$ $CD11b^-$ Kupffer cells and bone marrow derived $CD32^-$ $CD11b^+$ Kupffer cells contributed little to *L.m.* clearance within the first 10 min of infection (Figure 2-22b). Additionally, *L.m.* uptake was increased in absence of *L.m.* – platelet complex formation in the $CD11b^-CD32^-$ Kupffer cell subset. Distribution of these subtypes was constant in all examined strains with approximately 60% $CD32^+$ $CD11b^-$, 15% $CD32^-$ $CD11b^+$, and 25% $CD32^-$ $CD11b^-$ Kupffer cells on average (Figure 2-22c).

a

Kupffer cell subset	F4/80	CD11b	CD32	CD68	CRIg
immature liver derived	+	-	+	+	+
mature liver derived	+	-	-	-	+
bone marrow derived	+	+	-	-	-

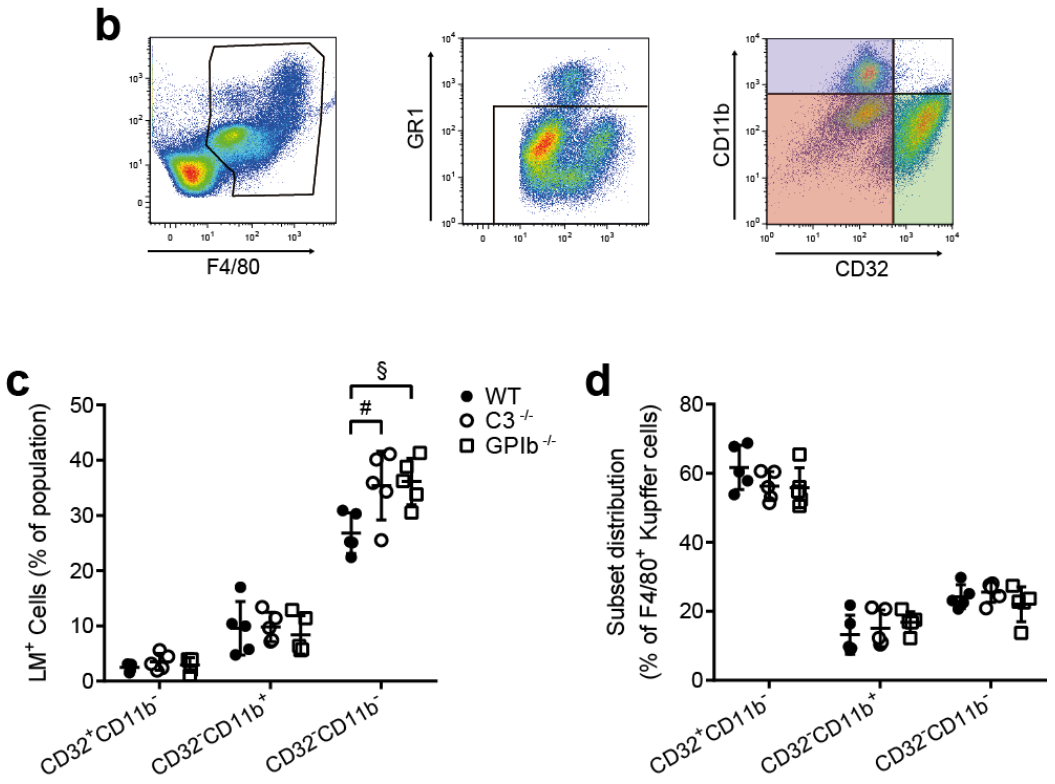

Figure 2-22 CD32$^-$ CD11b$^-$ Kupffer cells handle the majority of *L.m.* uptake
Wild-type, C3$^{-/-}$ and GPIb$^{-/-}$ mice were infected with 1x10^8 eFLuor670-labeled *L.m.*, livers were removed 15 min post infection and cell populations analysed for *L.m.* uptake. **(a)** Classification of known Kupffer cell subsets by Ikarashi et al. 2013. **(b)** Gating schematic to determine Kupffer cell subsets. Cells were gated on F4/80$^+$ and Ly6G$^-$ before discrimination of subsets via the expression of CD32 and CD11b. Subsets are highlighted in the same colour as in (a). **(c)** Comparison of *L.m.* uptake in CD32$^+$ CD11b$^-$, CD32$^-$ CD11b$^+$ and CD32$^-$ CD11b$^-$ Kupffer cells. CD32$^-$ CD11b$^-$ Kupffer cells most frequently took up *L.m.* and uptake by this population was further increased in C3$^{-/-}$ and GPIb$^{-/-}$ mice (mean ± SD of 5 mice, * = P < 0.05, # = P < 0.01, § = P < 0.001, Two-tailed Student's t-test). **(d)** Distribution of all Kupffer cells detected by subpopulation. No significant differences were observed (mean ± SD of 5 mice, * = P < 0.05, # = P < 0.01, § = P < 0.001, Two-tailed Student's t-test).

The examination of hepatic uptake of systemically circulating *L.m.* had revealed Kupffer cells to be the main facilitator of *L.m.* clearance. Uptake in both other cell populations positive for *L.m.* in wild-type mice, B-cells and neutrophil granulocytes, proved to be complement dependent. Thus neither B-cells nor neutrophil granulocytes can be the facilitator or rapid uptake of circulating *L.m.* in absence of *L.m.* – platelet complex formation. Discrimination of Kupffer cells by subsets revealed mature, liver-resident CD11b$^-$CD32$^-$ Kupffer cells to both be

the Kupffer cell population with the highest phagocytic activity and the cell population responsible for rapid clearance of *L.m.* in absence of *L.m.* – platelet complex formation. The next focus of this thesis was to determine which mechanism on these $CD11b^{-}CD32^{-}$ Kupffer cells was responsible for the observed phenotype of rapid uptake in mice lacking *L.m.* – platelet complexes.

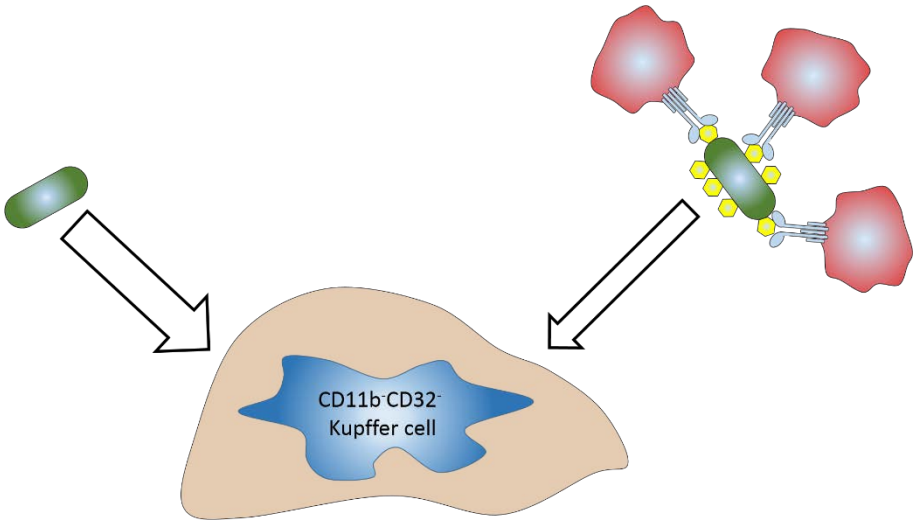

Illustration 2-4 Summary of chapter 2.4
Mature, liver-resident $CD11b^{-}CD32^{-}$ Kupffer cells are the main facilitator of clearance of systemically circulating *L.m.*. Uptake of *L.m.* in $C3^{-/-}$ and $GPIb^{-/-}$ mice, where *L.m.* – platelet complex formation is not possible, was found to be increased in this cell population, indicating $CD11b^{-}CD32^{-}$ Kupffer cells to be responsible for the rapid clearance of systemically circulating *L.m.* observed in $C3^{-/-}$ and $GPIb^{-/-}$ mice.

2.5 Clearance of nonopsonized *L.m.* is facilitated by scavenger receptors

Mice lacking C3, in which systemically circulating *L.m.* are not opsonized with C3 and cannot bind platelets were used to determine how non-platelet bound, nonopsonized *L.m.* are cleared from the circulation. These mice were treated with various blocking agents for phagocytic receptors known to be expressed by hepatic Kupffer cells shortly before systemic infection with *L.m.*, after which clearance of *L.m.* from the bloodstream was measured (Table 2-1).

Table 2-1: Blocking agents used and their respective ligands

Name	Ligand for	reference
GlcNac	Class I and II C-type lectin receptors	(Geijtenbeek and Gringhuis, 2009)
Arabinogalactan	Class II C-type lectin receptors	(Groman *et al.,* 1994)
Mannan	Class I C-type lectin receptors	(Zhang *et al.,* 2005)
Lactoferrin	Low Density Lipoprotein receptors	(Misra and Pizzo, 1998)
Polyinosinic acid	Class A scavenger receptors Toll-like receptors 3, 7, 8, 9	(Terpstra and van Berkel, 2000; Marshall-Clarke *et al.,* 2007)
Polycytidylic acid	Toll-like receptors 3, 7, 8, 9	(Stewart *et al.,* 2012)

Off all tested agents, only polyinosinic acid (Poly(I)) significantly increased the circulatory half-life of *L.m.* (Figure 2-23e, g). Arabinogalactan, GlcNac, lactoferrin, mannan, and polycytidylic acid displayed no measurable effect on the clearance of *L.m.* in $C3^{-/-}$ mice, where *L.m.* – platelet complex formation was inhibited (Figure 2-23a-d, f). Poly(I) has been shown to block the function of class A scavenger receptors and also of toll-like receptors 3, 7, 8 and 9 (Terpstra and van Berkel, 2000; Marshall-Clarke *et al.,* 2007). Polycytidylic acid (Poly(C)), a structurally very similar substance to Poly(I), has been shown to inhibit only the toll-like receptors 3, 7, 8 and 9 (Stewart *et al.,* 2012) and when tested in these experiments showed no significant effect on the clearance of *L.m.* from the bloodstream of $C3^{-/-}$ mice (Figure 2-23f). Therefore, the reduction of clearance during treatment with polyinosinic acid was attributed to the blockade of SRA.

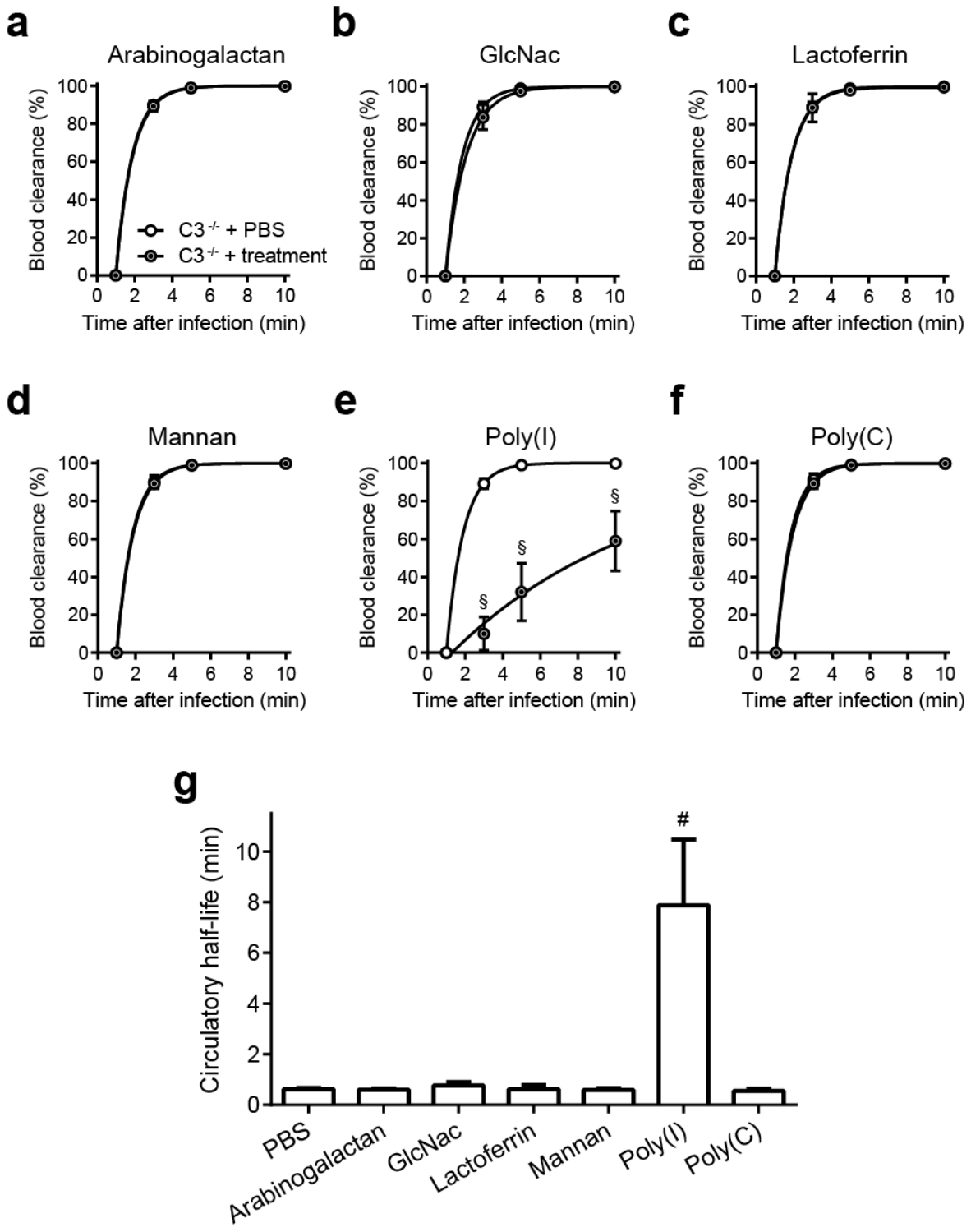

Figure 2-23 Uptake of nonopsonized *L.m.* can be inhibited by treatment with Poly(I)
$C3^{-/-}$ mice were treated with either **(a)** arabinogalactan, **(b)** GlcNac, **(c)** lactoferrin, **(d)** mannan, **(e)** Poly(I) or **(f)** Poly(C) 2 min before systemic infection with $1x10^8$ *L.m.*. Clearance kinetic **(a-f)** and circulatory half-life **(g)** were determined by plating blood samples taken 1, 3, 5 and 10 min after infection and subsequent CFU quantification (mean ± SD of 3-4 mice per strain, * = $P < 0.05$, # = $P < 0.01$, § = $P < 0.001$, Two-way ANOVA with Bonferroni post-test adjustment).

It was observed though that while Poly(I) reduced clearance of *L.m.* from the bloodstream significantly, approximately half of the infective inoculum was still cleared by 10 min post infection. It has been reported that the immunostimulatory compound Poly(I:C), consisting of both Poly(I) and Poly(C), is degraded rapidly in human plasma (Clercq, 1979). Plasma half-life of 1 µg Poly(I:C) was only 6 min in the presence of 50% v/v plasma. It was thus hypothesized that degradation of Poly(I) was the cause of remaining clearance of the infective inoculum. To test this transient blocking phenotype, Poly(I) was given continuously at a dosage of 100 µg per minute during the first 10 min after intravenous infection (Figure 2-24a). Constant treatment with Poly(I) nearly fully abolished clearance of *L.m.* from the bloodstream. Again, flow cytometry analysis confirmed the lack of hepatic clearance of *L.m.* during continuous presence of Poly(I), showing starkly diminished *L.m.* uptake into Kupffer cells 15 min after infection (Figure 2-24b).

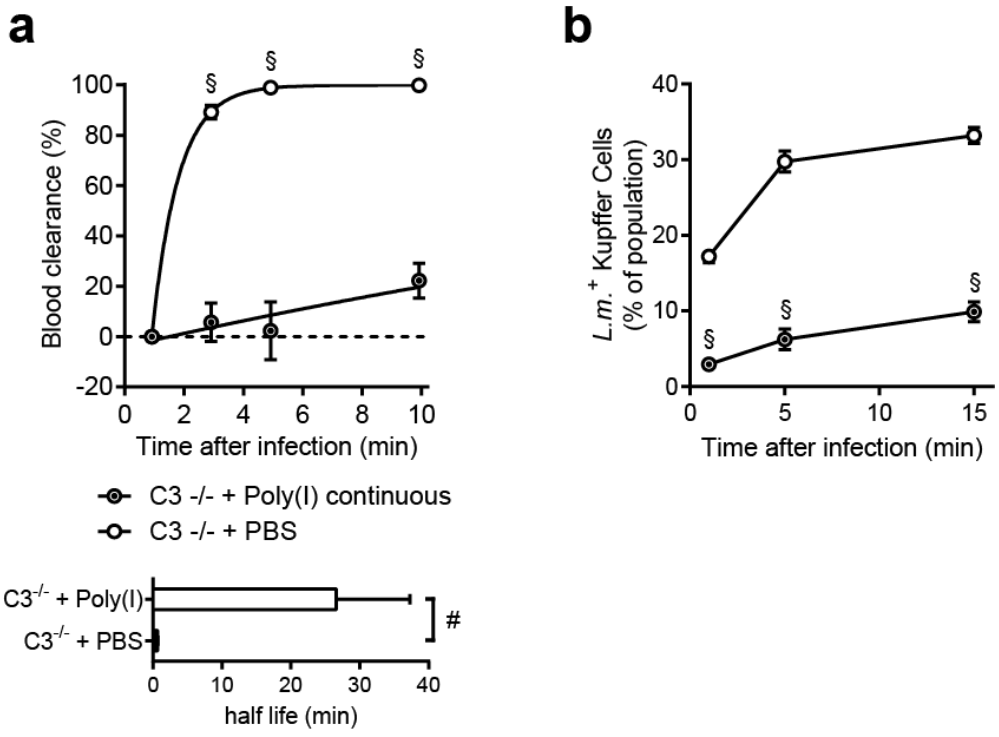

Figure 2-24 Continuous treatment with Polyinosinic acid abolishes clearance of nonopsonized *L.m.*
$C3^{-/-}$ mice were treated with Polyinosinic acid at a dosage of 100 µg/min and systemically infected with $1x10^8$ *L.m.* 2 min after treatment. **(a)** Clearance kinetic and circulatory half-life were determined by plating blood samples taken 1, 3, 5 and 10 min after infection (mean ± SD of 3 mice per treatment, * = P < 0.05, # = P < 0.01, § = P < 0.001, Two-way ANOVA with Bonferroni post-test adjustment and two-tailed Student's t-test). **(b)** Hepatic uptake of *L.m.* by Kupffer cells analysed by flow cytometry at 1, 5 and 15 min after infection (mean ± SD of 3 mice per treatment per timepoint, * = P < 0.05, # = P < 0.01, § = P < 0.001, Two-way ANOVA with Bonferroni post-test adjustment).

This data confirmed that nonopsonized *L.m.* are efficiently cleared from the bloodstream by SRA on hepatic Kupffer cells. Previous experiments had indicated that *L.m.* – platelet complexes may be cleared by a different mechanism than nonopsonized *L.m.* (see Figure 2-13). To test this hypothesis, *L.m.* were preopsonized in wild-type serum and used as infective inoculum in $C3^{-/-}$ mice treated with Poly(I) (Figure 2-25).

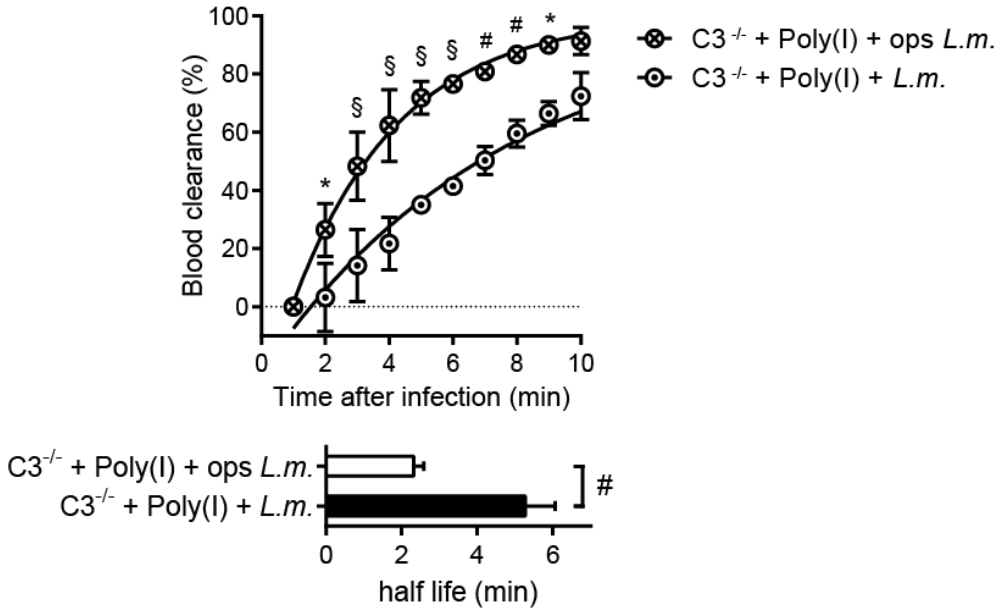

Figure 2-25 Treatment with Poly(I) has no effect on the clearance of preopsonized *L.m.* in $C3^{-/-}$ mice
$C3^{-/-}$ mice were administered 500 µg Poly(I) i.v. and 2 min later infected with either $1x10^8$ nonopsonized *L.m.* or $1x10^8$ preopsonized *L.m.* labelled with eFluor670 and clearance was observed for 10 min post infection via intravital microscopy (mean ± SD of 3 mice per treatment, * = $P < 0.05$, # = $P < 0.01$, § = $P < 0.001$, Two-way ANOVA with Bonferroni post-test adjustment and two-tailed Student's t-test).

Pre-treatment with wild-type serum let *L.m.* regain the capacity to rapidly form *L.m.* – platelet complexes in $C3^{-/-}$ mice (see Figure 2-5), while the treatment with Poly(I) blocked SRA-mediated clearance of *L.m.* (see Figure 2-23e). If *L.m.* – platelet complexes are cleared from the bloodstream via a different mechanism than SRA mediated uptake, the circulatory half-life of preopsonized *L.m.* should be reduced in comparison to nonopsonized *L.m.*. Interestingly, the preopsonized *L.m.* were cleared significantly faster than nonopsonized *L.m.* and the circulatory half-life of preopsonized *L.m.* was similar to the circulatory half-life of *L.m.* in wild-type mice (2.31 ± 0.27 min vs. 2.1 ± 0.18 min). This confirmed a second mechanism that acts in parallel on *L.m.* – platelet complexes in the wild-type situation, which was to be investigated next.

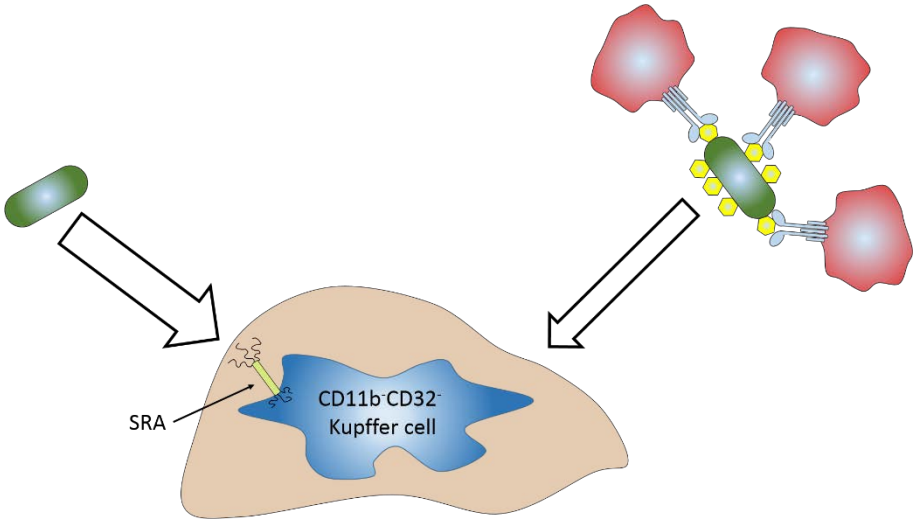

Illustration 2-5 Summary of chapter 2.5
Treatment with Poly(I) revealed rapid uptake of nonopsonized *L.m.* in $C3^{-/-}$ mice to be SRA-mediated. Uptake of *L.m.* – platelet complexes was observed to be independent of SRA.

2.6 Complement receptor CRIg influences clearance of *L.m.* from the bloodstream at later timepoints

To investigate how *L.m.* – platelet complexes are clearance from the bloodstream by Kupffer cells and due to the fact that *L.m.* – platelet complex formation is strictly dependent on C3, it was examined if complement receptors expressed on Kupffer cells play a role in the efficient removal of systemically circulating *L.m.*.

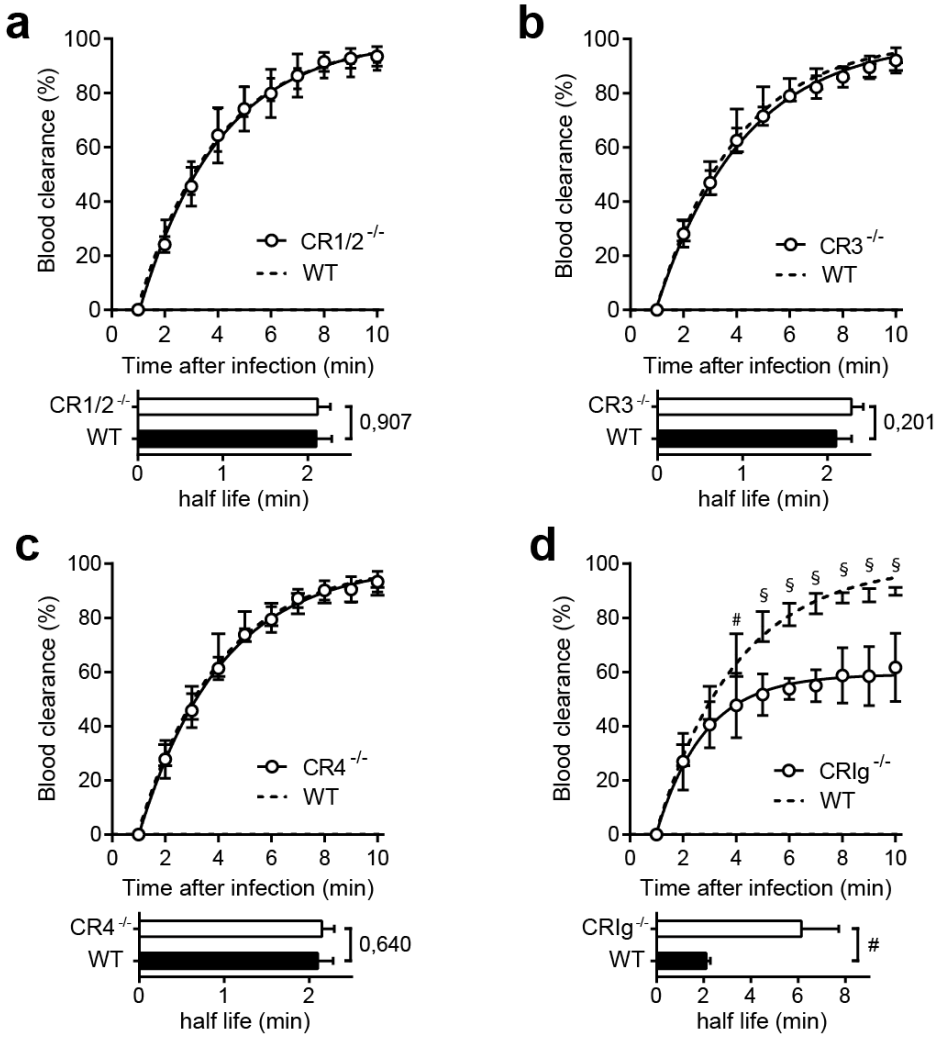

Figure 2-26 CRIg influences *L.m.* clearance from the bloodstream
(a) CR1/2$^{-/-}$, **(b)** CR3$^{-/-}$, **(c)** CR4$^{-/-}$ and **(d)** CRIg$^{-/-}$ mice were infected i.v. with 1x10^{8} eFluor670-labelled, heat inactivated *L.m.* and clearance from the bloodstream was calculated using multiphoton intravital microscopy. Circulating *L.m.* were imaged during the first 10 min of infection and the clearance kinetic and circulatory half-lives calculated and compared to the wild-type (mean ± SD of 3-4 mice per strain, * = P < 0.05, # = P < 0.01, § = P < 0.001, Two-way ANOVA with Bonferroni post-test adjustment and two-tailed Student's t-test).

Kupffer cells have long been known to express the complement receptors CR1, CR3 and CR4 (Hinglais *et al.,* 1989; Yan *et al.,* 2000) and have recently been shown to also express the complement receptor CRIg (Helmy *et al.,* 2006). A lack of CR1/2, CR3 or CR4 had no significant influence on the circulatory half-life of *L.m.* in the murine bloodstream (Figure 2-26a-c). Lack of CRIg though had a marked influence on the clearance of *L.m.*, slowing clearance especially from 3 min post infection onwards (Figure 2-26d). The abrogation of clearance after 3-4 min coincided with the observed timepoint after which in wild-type animals all *L.m.* remaining in the circulation have successfully formed *L.m.* – platelet complexes (see Figure 2-3b). Additionally, 3-4 min is also the first timepoint in which splenic uptake of radioactively labelled *L.m.* as determined by PET in wild-type animals was significantly increased in comparison to $C3^{-/-}$ and $GPIb^{-/-}$ mice (see Figure 2-13). All these data taken together indicated a potential role for CRIg in the uptake of *L.m.* – platelet complexes.

To investigate the effect of a lack of CRIg on the global distribution of *L.m.* after systemic infection, multi-organ screening 15 min post infection as well as PET-CT imaging of early systemic infection with radioactively labelled *L.m.* was performed. Mice lacking CRIg exhibited a phenotype of *L.m.*- uptake disparate from wild-type mice when organs were screened for live *L.m.* 15 min after systemic infection (Figure 2-27a). Total recovery of *L.m.* in both strains was similar (Figure 2-27b). Hepatic uptake was reduced significantly in comparison to the wild-type (53.11% vs. 92.04%, P = 4E-06, two-tailed Student's t-test), whereas splenic uptake of *L.m.* was increased 6-fold (37.57% vs. 6.26%, P = 0.0002, two-tailed Student's t-test) (Figure 2-27c, d). Uptake of *L.m.* in other screened organs, especially in the lung (2.97% vs. 0.31%, P = 0.0004, two-tailed Student's t-test), was also significantly increased 15 min after systemic infection (Figure 2-27e, Supplemental figure 5).

A shift of *L.m.* distribution from liver to spleen was also observed using radioactively labelled *L.m.* in PET to visualize early systemic infection distribution (Figure 2-28a, b). Similar to what was observed in the clearance kinetic of systemically circulating *L.m.* visualized by intravital microscopy (Figure 2-26d), early time points in $CRIg^{-/-}$ mice closely resembled the wild-type control. Uptake in the liver was abrogated from timepoints of 2-3 min after infection, again indicating a role of CRIg in the uptake of formed *L.m.* – platelet complexes in the liver. In contrast, uptake of radioactively labelled *L.m.* in the spleen was increased in mice lacking CRIg only from 7 min onwards. This timepoint interestingly coincides with the *in vitro* observation of platelet aggregation around bound *L.m.* (see Figure 2-4a), which began approximately 5 min after addition of *L.m.* to PRP and was complete after approximately 8 min.

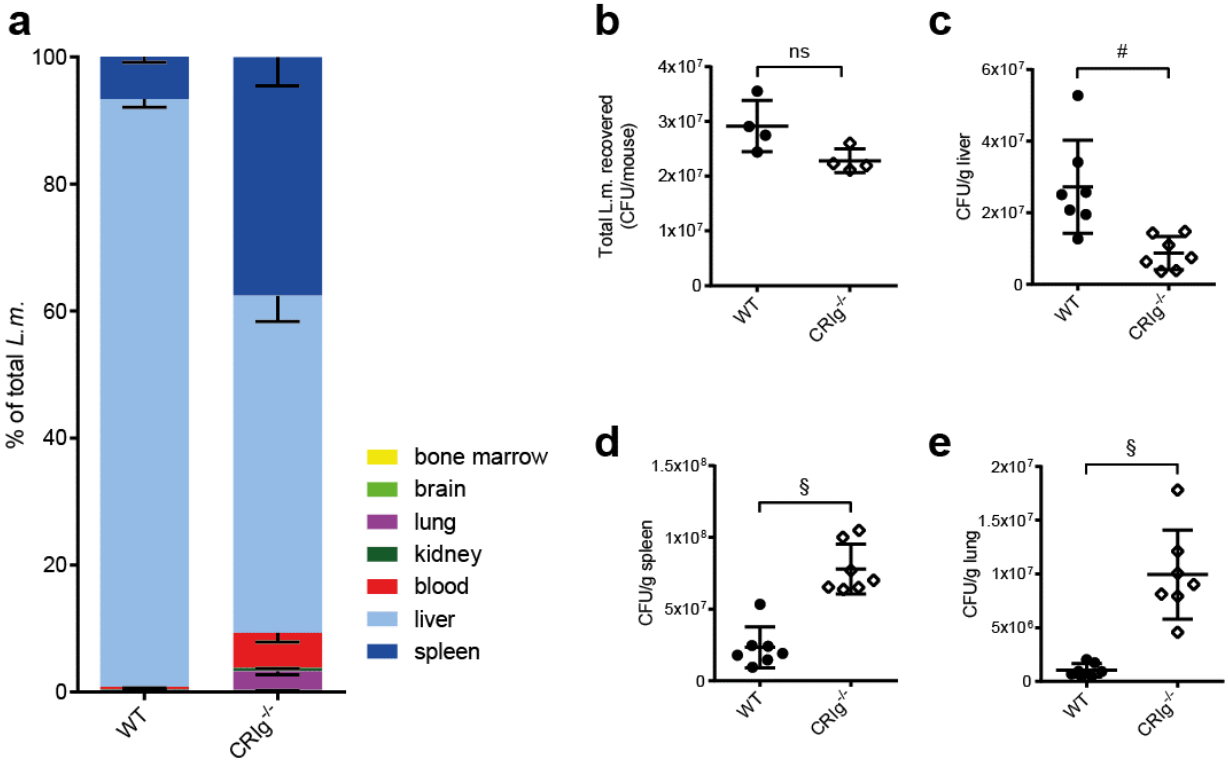

Figure 2-27 Lack of CRIg shifts bacterial distribution from liver to spleen
Wild-type and CRIg$^{-/-}$ mice were systemically infected with 1x10^8 *L.m.*. Organs were harvested 15 min post infection, homogenized and serial dilutions plated to detect live CFU. **(a)** Distribution of detected *L.m.* throughout screened organs. 100% represents all *L.m.* found (mean ± SEM of 5 mice per strain) **(b-d)** *L.m.* found in **(b)** liver, **(c)** spleen and **(d)** lung per gram organ in wild-type and CRIg$^{-/-}$ mice (mean ± SD of 6 mice, * = P < 0.05, # = P < 0.01, § = P < 0.001, Two-tailed Student's t-test). Experiments performed in cooperation with Ann Plaumann.

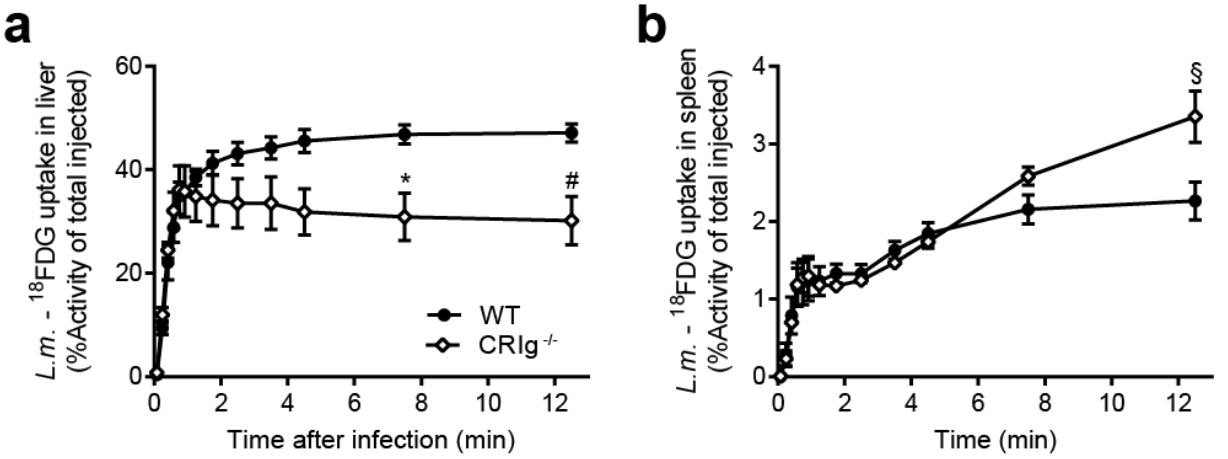

Figure 2-28 Hepatic *L.m.* uptake abrogates in CRIg$^{-/-}$ mice in comparison to wild-type mice
(a) Hepatic and **(b)** splenic uptake of ^{18}FDG-*L.m.* as detected via PET-CT. Mice were infected with 1x10^8 *L.m.* labelled with ^{18}FDG for 90 min and distribution was acquired for 15 min post infection via PET-CT (mean ± SD of 3-4 mice per strain, * = P < 0.05, # = P < 0.01, § = P < 0.001, Two-way ANOVA with Bonferroni post-test adjustment).

Blood kinetic measurement and global visualization had confirmed an important role of CRIg in the liver for the clearance of *L.m.* at timepoints after 2-3 min. To confirm that Kupffer cells were the main facilitator of CRIg-mediated clearance of *L.m.* from the bloodstream, flow cytometry analysis of livers of $CRIg^{-/-}$ mice systemically infected with fluorescently labelled *L.m.* was performed. Uptake of fluorescent *L.m.* was decreased in Kupffer cells at 5 and 15 min after infection, while the earliest time point of 1 minute exhibited no statistically significant difference to uptake in control wild-type mice (Figure 2-29a). The similar clearance in clearance between wild-type and $CRIg^{-/-}$ mice for timepoints under 3 min again reflected previously observed clearance kinetics and PET visualization of infection, which displayed no significant difference between these strains for the first minutes after systemic infection (see Figure 2-26d and Figure 2-28a). Congruent with the wild-type, mature liver resident $CD32^{-}$ $CD11b^{-}$ Kupffer cells were found facilitated the majority of clearance, although the overall percentage of cells positive for phagocytosed bacteria was significantly reduced in comparison to the wild-type (Figure 2-29b), indicating that CRIg-mediated uptake of *L.m.* from the bloodstream is facilitated by this cell population. Distribution of Kupffer cell subtypes was again consistent with the wild-type control (Figure 2-29c).

It could thus be concluded that the same cell population, mature liver resident $CD11b^{-}CD32^{-}$ Kupffer cells, is responsible for the clearance of *L.m.* via SRA (see Figure 2-24b) and CRIg (see Figure 2-29b). While SRA mediated clearance of *L.m.* from the bloodstream was determined to be the source of rapid uptake of nonopsonized *L.m.* (see Figure 2-23), a lack of CRIg was observed to be essential for clearance of *L.m.* from the bloodstream at timepoints later than 3 min post infection (see Figure 2-26d). The observations that formation of *L.m.* – platelet complexes was a process consisting first of opsonization of *L.m.* (see Figure 2-2c and Figure 2-4a) and then the binding to platelets (see Figure 2-4) and that approximately 4 min after systemic infection only *L.m.* – platelet complexes could be detected in the bloodstream of wild-type mice (see Figure 2-3b) suggested that CRIg-mediated clearance is targeted towards formed *L.m.* – platelet complexes. To determine if CRIg really is responsible for the clearance of *L.m.* – platelet complexes, it was decided to create an experimental model, in which *L.m.* can bind to platelets from the moment of entry into the bloodstream.

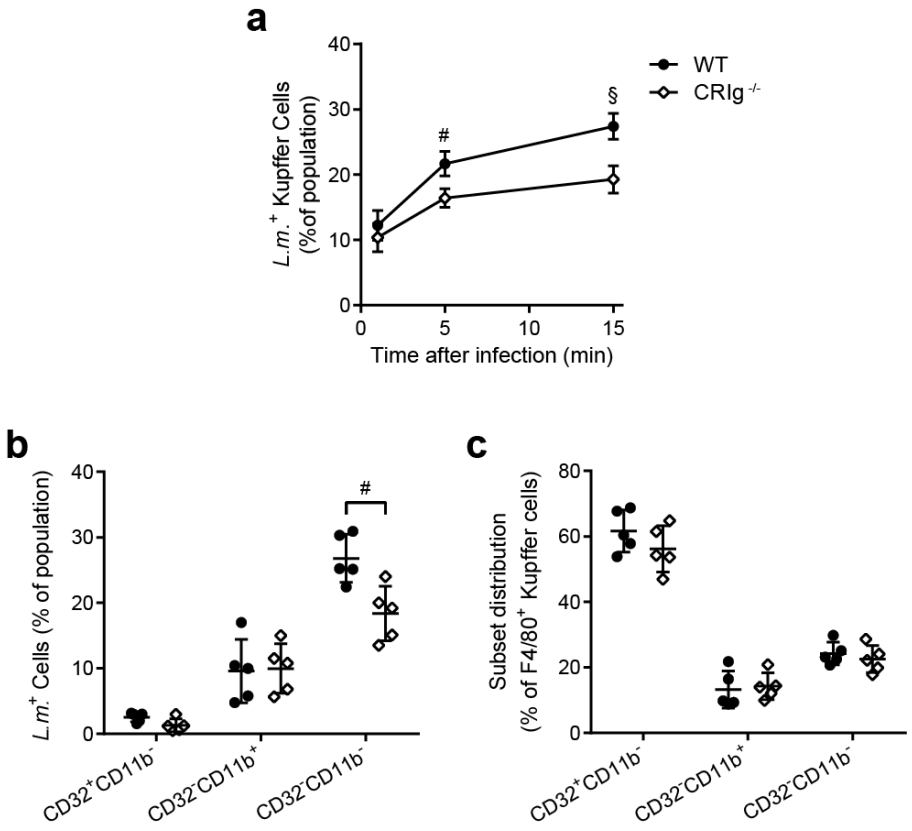

Figure 2-29 *L.m.* uptake via hepatic Kupffer Cells is decreased in CRIg$^{-/-}$ mice
Wild-type and CRIg$^{-/-}$ mice were infected with 1x10^{8} eFLuor670-labeled *L.m.*, livers were removed at indicated time points and cell populations analysed for *L.m.* uptake. Cells were gated on F4/80^{+} and Ly6G^{-} before subsets were discriminated via the expression of CD32 and CD11b. **(a)** Comparison of *L.m.* uptake by all F4/80^{+} Kupffer cells in wild-type and CRIg$^{-/-}$ mice at 1, 5 and 15 min post infection (mean ± SD of 3-4 mice per strain, * = P < 0.05, # = P < 0.01, § = P < 0.001, Two-way ANOVA with Bonferroni post-test adjustment). **(b)** Comparison of *L.m.* uptake in CD32^{+} CD11b^{-}, CD32^{-} CD11b^{+} and CD32^{-} CD11b^{-} Kupffer cells (mean ± SD of 5 mice per strain, * = P < 0.05, # = P < 0.01, § = P < 0.001, two-tailed Student's t-test). **(c)** Distribution of all Kupffer cells detected by subpopulation (mean ± SD of 5 mice per strain, * = P < 0.05, # = P < 0.01, § = P < 0.001, two-tailed Student's t-test).

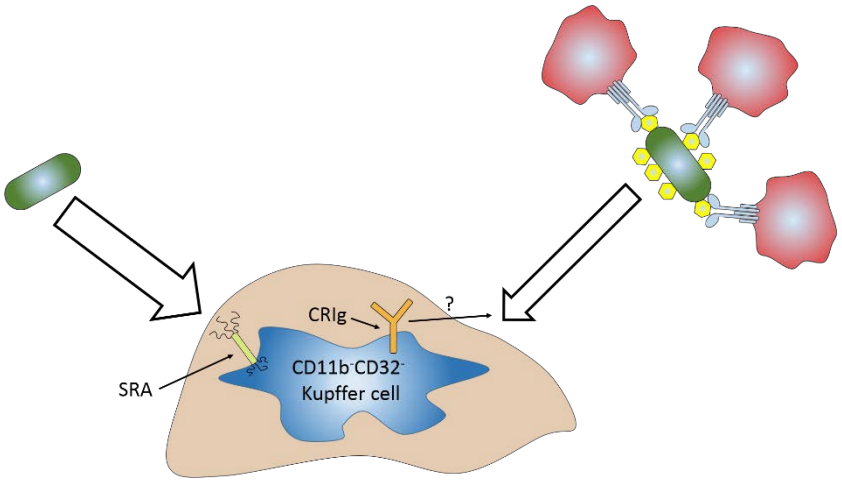

Illustration 2-6 Summary of chapter 2.6
Complement receptor CRIg expressed on CD11b^{-}CD32^{-} Kupffer cells was revealed to be involved in the clearance of systemically circulating *L.m.* at timepoints of 3 min post infection an onwards. The coinciding timeframe of *L.m.* – platelet complex formation and CRIg-mediated uptake led to the hypothesis that CRIg facilitates clearance of systemically circulating *L.m.* – platelet complexes.

2.7 Clearance of *L.m.* – platelet complexes is abrogated in absence of CRIg

In vitro aggregometry had revealed that after *L.m.* come into contact with blood it takes approximately 1-2 min before all *L.m.* have the capacity to bind platelets (see Figure 2-4). This was also observed using intravital microscopy, where within the first minute less than half of observed *L.m.* were bound to one or more platelets (see Figure 2-3b). To circumvent the delay caused by opsonisation *in vivo* and reduce the time until *L.m.* are capable of binding platelets, *L.m.* were incubated in wild-type plasma prior to systemic infection, allowing for activated C3 to already be deposited on the surface of *L.m.*. *In vitro* platelet aggregometry had revealed that preopsonization of *L.m.* reduced the time until all *L.m.* had bound to platelets to nearly 0 (see Figure 2-5c). Subsequently the clearance of these preopsonized *L.m.* from the bloodstream was visualized via intravital microscopy. As control, non-treated nonopsonized *L.m.*, fluorescently labelled in a different colour, were added to the inoculum and quantified simultaneously (Figure 2-30).

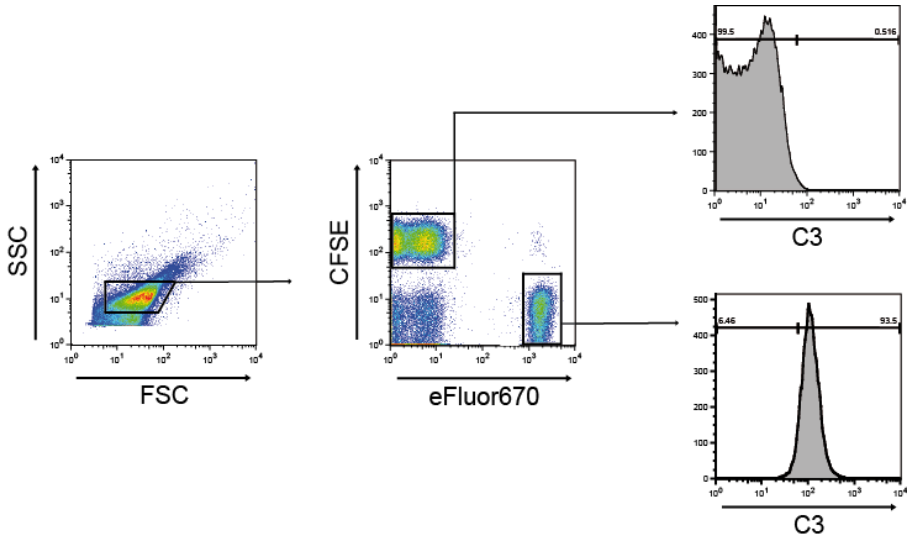

Figure 2-30 Schematic setup oft two population intravital imaging
L.m. inoculum was split into two equal populations. Population A was labelled with CFSE, Population B was labelled with eFluor670 and subsequently incubated in wild-type plasma for 10 min. This led to C3-deposition on the *L.m.* surface. After heat inactivation and extensive washing, population A and B were combined again and used as inoculum. Clearance and circulatory half-life of both populations was observed and determined via intravital microscopy.

To test this experimental setup, wild-type, $C3^{-/-}$ and $GPIb^{-/-}$ mice were infected with preopsonized and nonopsonized *L.m.* simultaneously (Figure 2-31). Interestingly, when these two differently treated *L.m.* populations were injected into wild-type mice, no significant difference in the circulatory half-life was observed (Figure 2-31a, Supplementary movie 7), indicating that preopsonized *L.m.* can be cleared as efficiently as nonopsonized *L.m.* in the wild-type situation. Clearance of preopsonized *L.m.* in $C3^{-/-}$ mice on the other hand was significantly slowed in comparison to nonopsonized *L.m.* (Figure 2-31b, Supplementary movie 8). The increased circulatory half-life of preopsonized *L.m.* in $C3^{-/-}$ mice indicated that SRA mediated uptake, shown to be responsible for the clearance of nonopsonized *L.m.* from the bloodstream (see Figure 2-23e, g), was not capable of efficiently clearing formed *L.m.* – platelet complexes. Control $GPIb^{-/-}$ mice, where *L.m.* are not capable of binding platelets regardless of opsonization due to the lacking platelet receptor, displayed no difference in clearance kinetics of nonopsonized and preopsonized *L.m.* (Figure 2-31c, Supplementary movie 9).

To confirm that the observed reduction of clearance of preopsonized *L.m.* in mice lacking C3 was due to *L.m.* – platelet complex formation and not due to the opsonization of *L.m.*, $C3^{-/-}$ mice depleted for platelets were systemically infected with preopsonized and nonopsonized *L.m.* simultaneously and clearance kinetics were measured via intravital microscopy (Figure 2-32). Clearance of both preopsonized and nonopsonized *L.m.* was rapid in absence of platelets, with circulatory half-lives similar of under 1 min, confirming the presence of platelets and the formation of *L.m.* – platelet complexes to be the defining factor for the slowed clearance of preopsonized *L.m.* in $C3^{-/-}$ mice (see Figure 2-31b).

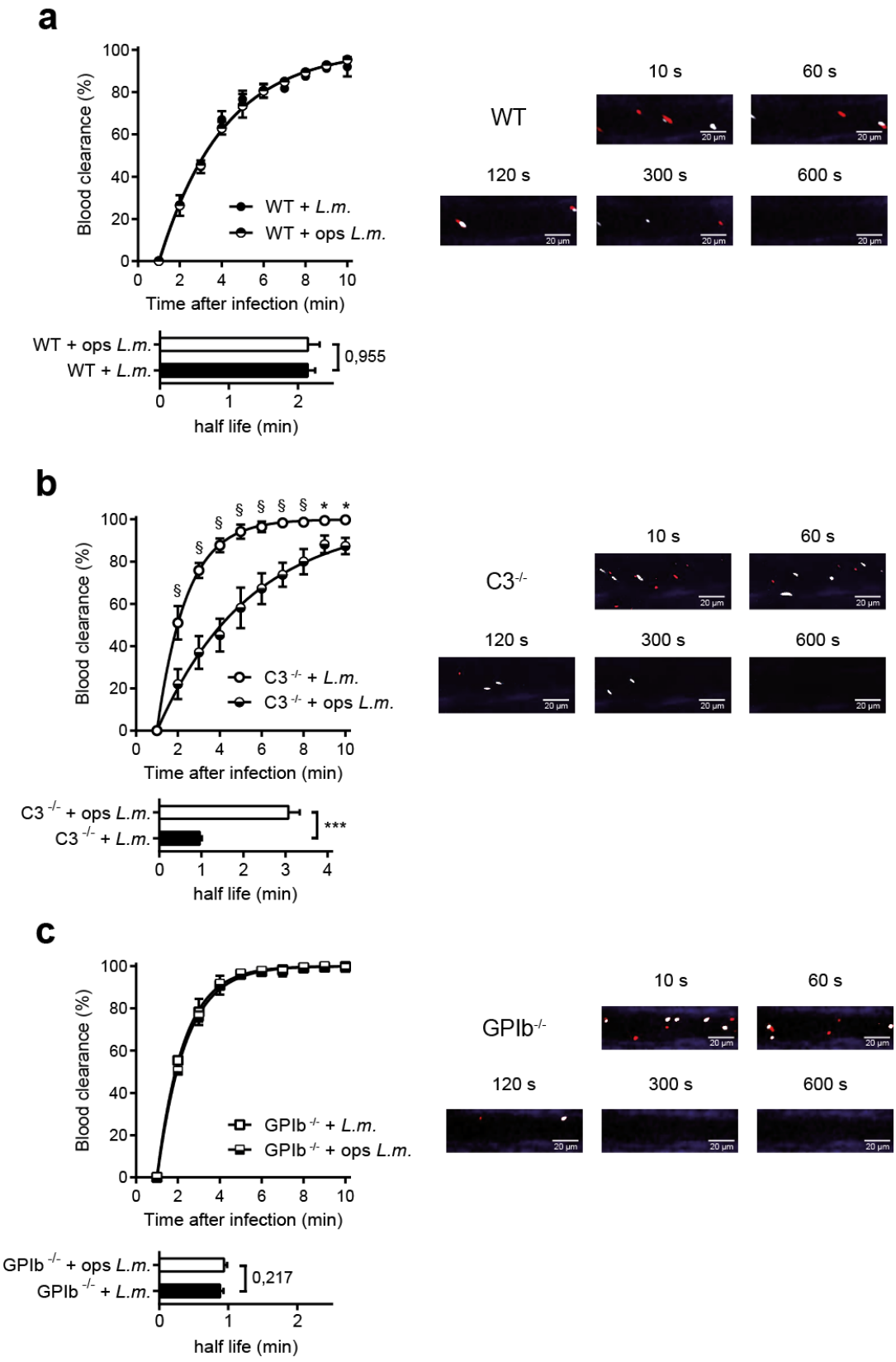

Figure 2-31 Preopsonization of *L.m.* reduces clearance speed in C3$^{-/-}$ mice
(a) Wild-type, **(b)** C3$^{-/-}$ and **(c)** GPIb$^{-/-}$ mice were infected with 5x10^7 nonopsonized CFSE-labelled *L.m.* and 5x10^7 preopsonized eFluor670-labeled *L.m.* and clearance speed and circulatory half-life were determined via intravital microscopy (mean ± SD of 3-4 mice per treatment, * = P < 0.05, # = P < 0.01, § = P < 0.001, Two-way ANOVA with Bonferroni post-test adjustment and two-tailed Student's t-test).

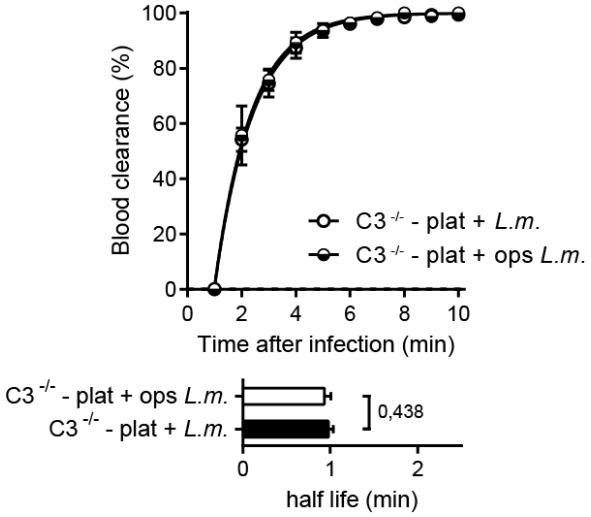

Figure 2-32 Platelet depletion increases clearance speed of preopsonized *L.m.* in C3$^{-/-}$ mice
C3$^{-/-}$ mice were depleted of platelets 24h before being infected with 5x10^7 nonopsonized CFSE-labelled *L.m.* and 5x10^7 preopsonized eFluor670-labelled *L.m.*. Clearance speed and circulatory half-life were determined via intravital microscopy. Depletion efficiency was confirmed by flow cytometry analysis of whole blood (Data not shown). (mean ± SD of 3-4 mice per treatment, * = P < 0.05, # = P < 0.01, § = P < 0.001, Two-way ANOVA with Bonferroni post-test adjustment and two-tailed Student's t-test)

It was observed that a lack of CRIg significantly reduced clearance of systemically circulating *L.m.* from 3-4 min post infection on (see Figure 2-26d). Additionally, intravital microscopy of circulating *L.m.* and platelets in wild-type mice had revealed that of 3-4 min almost all *L.m.* remaining in the bloodstream had successfully bound to platelets (see Figure 2-3b). These two observations led to the hypothesis that CRIg plays a role in the clearance of *L.m.* – platelet complexes. Thus CRIg$^{-/-}$ mice were infected with both preopsonized and nonopsonized *L.m.* simultaneously to observe if clearance of preopsonized *L.m.*, which are able to rapidly bind platelets, was abrogated (Figure 2-33, Supplementary movie 10). While the non-treated *L.m.* population displayed a similar clearance to what had already been observed using intravital microscopy in CRIg$^{-/-}$ mice (see Figure 2-26d), clearance of preopsonized *L.m.* was drastically abrogated from the first minute on, confirming the hypothesis that CRIg is of immense importance for the clearance of *L.m.* – platelet complexes from the bloodstream.

To confirm that the observed abrogated clearance of *L.m.* – platelet complexes from the bloodstream when CRIg is lacking was in fact due to a lack of in hepatic uptake, blood and livers of CRIg$^{-/-}$ mice infected with preopsonized *L.m.* were screened for live *L.m.* 15 min after systemic infection (Figure 2-34a, b).

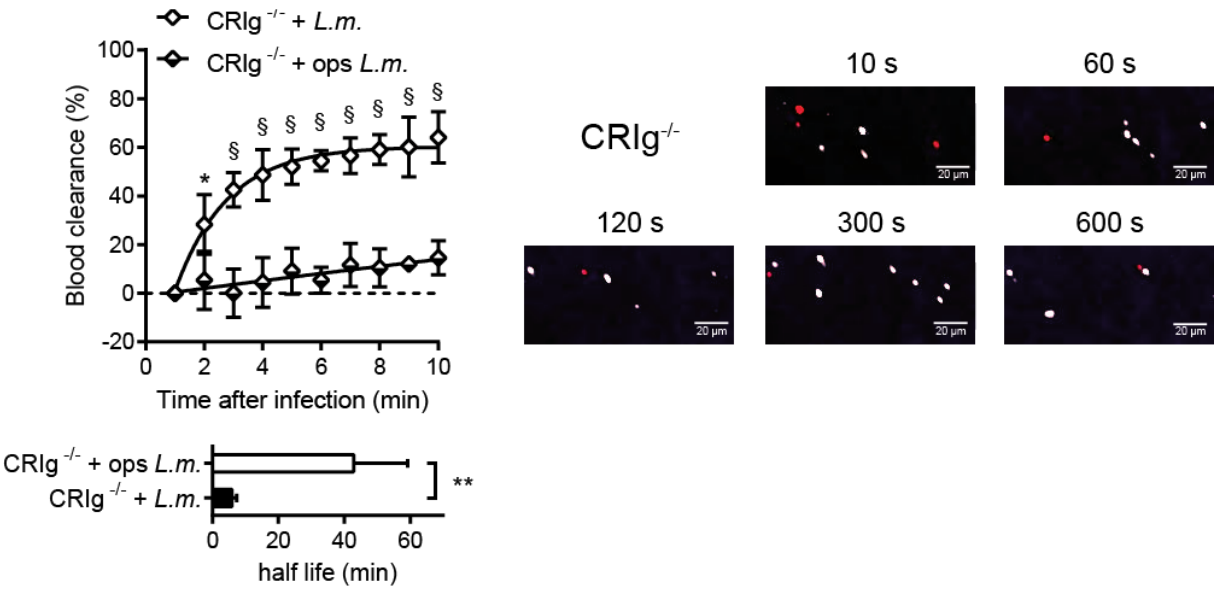

Figure 2-33 Clearance of preopsonized *L.m.* is drastically impaired in CRIg$^{-/-}$ mice
CRIg$^{-/-}$ mice were infected with 5x10^7 nonopsonized CFSE-labelled *L.m.* (red) and 5x10^7 preopsonized eFluor670-labelled *L.m.* (white) and clearance kinetic and circulatory half-life were determined via intravital microscopy (mean ± SD of 3-4 mice, * = P < 0.05, # = P < 0.01, § = P < 0.001, Two-way ANOVA with Bonferroni post-test adjustment and two-tailed Student's t-test).

In comparison to CRIg$^{-/-}$ mice infected with nonopsonized *L.m.*, the number of live preopsonized *L.m.* found in the bloodstream was significantly increased (Figure 2-34a), mirroring the observed abrogated clearance of preopsonized *L.m.* in mice lacking CRIg (see Figure 2-33). Live *L.m.* retrieved from the liver on the other hand were significantly reduced when CRIg$^{-/-}$ mice were infected with preopsonized *L.m.* in comparison to nonopsonized *L.m.*, confirming a lack of hepatic uptake of *L.m.* – platelet complexes in mice lacking CRIg (Figure 2-34b). Wild-type mice, in which no difference in clearance for preopsonized *L.m.* and nonopsonized *L.m.* had been observed (see Figure 2-31a), were used as control. No significant differences in the number of live *L.m.* recovered from both blood and liver were observed in wild-type mice (Figure 2-34a, b), ruling out any possible adverse effects of the preopsonization process on the vitality of *L.m.*. To further pinpoint the lacking hepatic uptake of *L.m.* – platelet complexes in absence of CRIg to Kupffer cells, flow cytometry analysis of CRIg$^{-/-}$ mice infected with preopsonized *L.m.* was performed (Figure 2-34c). In all examined timepoints, CRIg$^{-/-}$ mice infected with preopsonized *L.m.* had taken up significantly less Kupffer cells positive for *L.m.* than CRIg$^{-/-}$ mice infected with nonopsonized *L.m.*, confirming that in absence of CRIg, Kupffer cells are impaired in their capacity to clear *L.m.* – platelet complexes from the bloodstream.

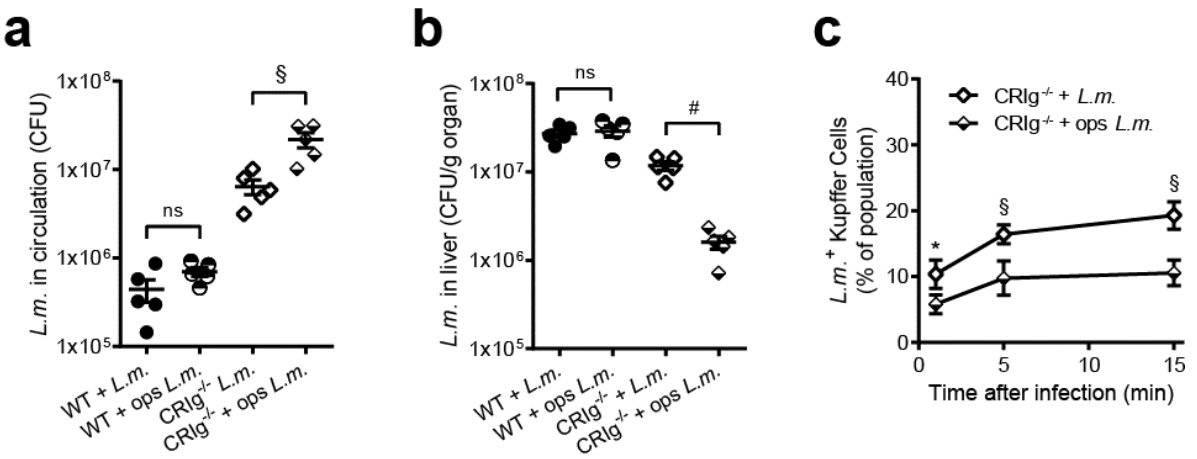

Figure 2-34 Uptake of platelet bound *L.m.* is abrogated in absence of CRIg
Wild-type and CRIg$^{-/-}$ mice were infected with 1x10^8 preopsonized *L.m.*. 15 min post infection **(a)** blood samples and **(b)** livers were removed and plated to screen for live *L.m.* (mean ± SEM of 5 mice per strain, * = P < 0.05, # = P < 0.01, § = P < 0.001, two-tailed Student's t-test). **(c)** Wild-type and CRIg$^{-/-}$ mice were infected with 1x10^8 preopsonized, eFLuor670-labelled *L.m.* and livers were removed 1, 5 and 15 min after infection. Hepatic cells were isolated and F4/80$^+$ Kupffer cells were analysed for *L.m.* uptake via flow cytometry (mean ± SD of 3 mice per timepoint, * = P < 0.05, # = P < 0.01, § = P < 0.001, Two-way ANOVA with Bonferroni post-test adjustment).

Concluding, the data confirmed the notion that while clearance of nonopsonized *L.m.* and *L.m.* – platelet complexes from the bloodstream is facilitated by the same cell population, CD11b$^-$ CD32$^-$ hepatic Kupffer cells, the action of binding to platelets within the circulation changes the mechanism by which the *L.m.* are cleared. While clearance of nonopsonized *L.m.* had already been observed to rely on SRA, *L.m.* – platelet complexes were found to remain in the bloodstream in absence of CRIg. It was further investigated, if the receptor necessary for the one pathway also plays a role in the uptake via the other pathway, meaning if SRA also has a role in the CRIg-mediated uptake of *L.m.* – platelet complexes or vice versa.

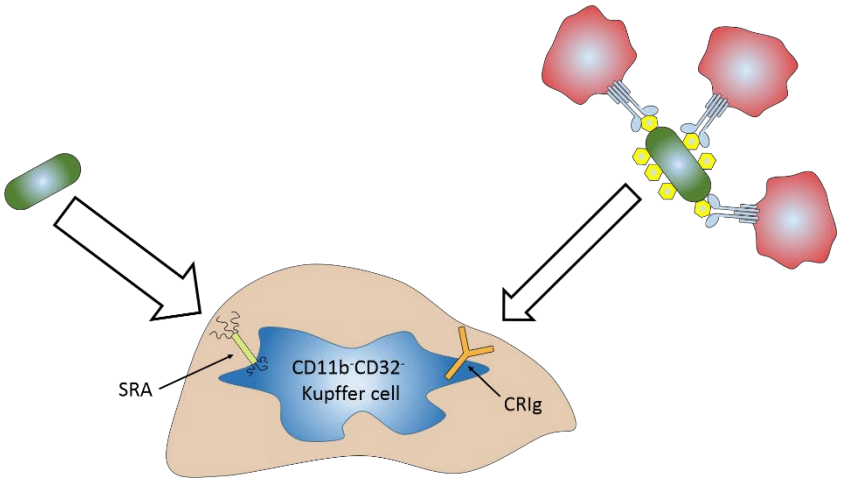

Illustration 2-7 Summary of chapter 2.7
Uptake of circulating *L.m.* – platelet complexes by CD11b$^-$CD32$^-$ Kupffer cells was found to be dependent on the presence of CRIg.

2.8 SRA- and CRIg-mediated uptake are independent processes

Treatment of $C3^{-/-}$ mice with Poly(I) had determined SRA to be the main facilitator of hepatic clearance of nonopsonized *L.m.* (see Figure 2-23), whereas infection of $CRIg^{-/-}$ mice with preopsonized *L.m.* and nonopsonized *L.m.* confirmed the hypothesis that CRIg is essential for the clearance of *L.m.* – platelet complexes from the bloodstream (see Figure 2-33).

In order to investigate if these two uptake mechanisms are independent of each other and to utilize the full capacity of the established experimental model of simultaneous infection with preopsonized *L.m.* and nonopsonized *L.m.*, mice lacking both C3 and CRIg were bred. In these $C3^{-/-}CRIg^{-/-}$ mice, nonopsonized *L.m.* will remain nonopsonized with activated C3 and thus have no capacity to bind platelets, whereas preopsonized *L.m.* have the exclusive ability to bind to platelets and rapidly form *L.m.* – platelet complexes. Thus, using $C3^{-/-}CRIg^{-/-}$ mice and the infection with preopsonized *L.m.* and nonopsonized *L.m.*, the disparate clearance kinetics of both extremes, all *L.m.* not bound to platelets vs. all *L.m.* present in *L.m.* – platelet complexes, was visualized (Figure 2-35a, Supplementary movie 11). Nonopsonized *L.m.* without any capacity to bind to platelets, were cleared rapidly from the bloodstream, mirroring the SRA-dependent uptake observed in $C3^{-/-}$ mice (see Figure 2-23e, g). In contrast, preopsonized *L.m*. capable of rapidly forming *L.m.* – platelet complexes (see Figure 2-5c), remained selectively in the bloodstream due to the lack of CRIg. The selective clearance of nonopsonized *L.m.* in $C3^{-/-}CRIg^{-/-}$ mice confirmed that SRA-mediated clearance of nonopsonized *L.m.* acts independently of CRIg. Additionally, the lacking clearance of preopsonized *L.m.* confirmed that SRA cannot mediate clearance of *L.m.* – platelet complexes.

Similar results were obtained with other experimental models: $C3^{-/-}CRIg^{-/-}$ mice were screened for live *L.m.* in the bloodstream 15 min post infection (Figure 2-35b). Blood samples of $C3^{-/-}CRIg^{-/-}$ mice infected with preopsonized *L.m.* were found to contain approximately 200-fold more viable *L.m.* than $C3^{-/-}CRIg^{-/-}$ mice infected with nonopsonized *L.m.* ($3.31x10^7$ vs. $1.68x10^5$ CFU per mouse). Flow cytometry analysis of Kupffer cells of $C3^{-/-}CRIg^{-/-}$ mice for *L.m.* uptake displayed a matching phenotype (Figure 2-35c). Infection of $C3^{-/-}CRIg^{-/-}$ mice with nonopsonized *L.m.* unable to bind platelets led to uptake of fluorescent *L.m.* in significantly more Kupffer cells than infection of $C3^{-/-}CRIg^{-/-}$ mice with preopsonized *L.m.*, which rapidly form *L.m.* – platelet complexes. The results obtained by both plating of blood samples and flow cytometry analysis of Kupffer cells confirmed the observed blood clearance kinetic. Nonopsonized *L.m.* were cleared rapidly from the circulation of $C3^{-/-}CRIg^{-/-}$ by Kupffer cells, mirroring the SRA-dependent uptake in $C3^{-/-}$ mice, whereas preopsonized *L.m.* formed *L.m.* – platelet complexes and selectively remained in the circulation due to a lack of CRIg.

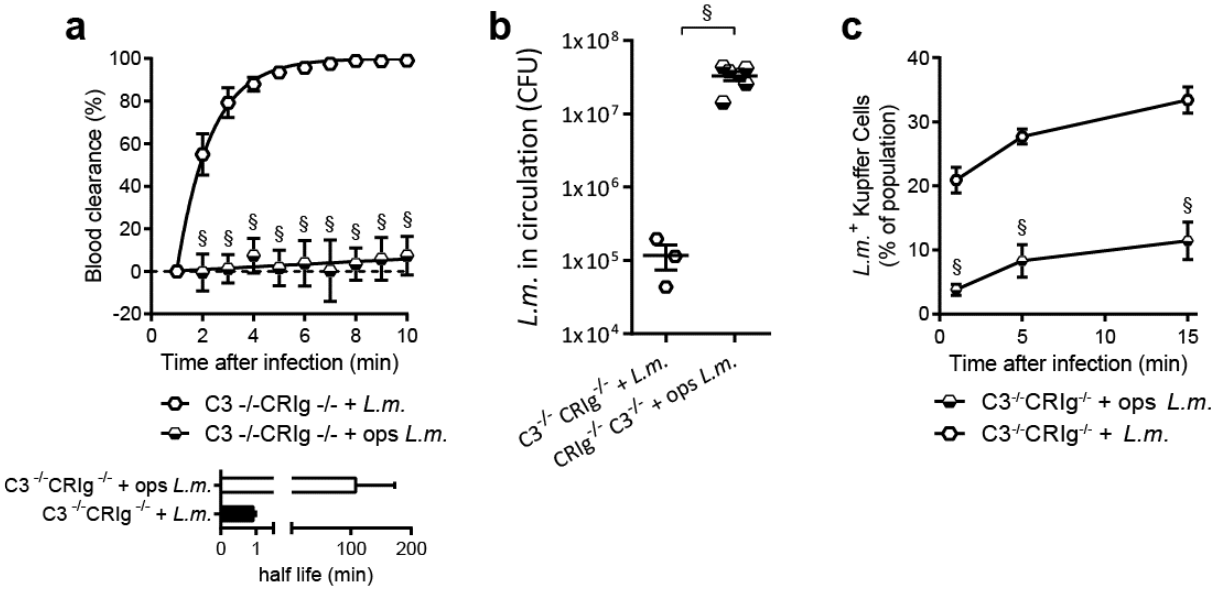

Figure 2-35 Preopsonized *L.m.* cannot be efficiently cleared by SRA in C3$^{-/-}$CRIg$^{-/-}$ mice
(a) C3$^{-/-}$CRIg$^{-/-}$ were infected with 5x10^7 nonopsonized CFSE-labelled *L.m.* and 5x10^7 preopsonized eFluor670-labelled *L.m.*. Clearance kinetic and circulatory half-life were calculated using intravital microscopy of the ear vasculature (mean ± SD of 4 mice, * = P < 0.05, # = P < 0.01, § = P < 0.001, Two-way ANOVA with Bonferroni post-test adjustment and two-tailed Student's t-test). **(b)** C3$^{-/-}$CRIg$^{-/-}$ mice were systemically infected with 7x10^7 *L.m.*. Blood samples taken 15 min after infection were plated on BHI agar and circulating *L.m.* quantified (mean ± SEM of 3-5 mice per strain, * = P < 0.05, # = P < 0.01, § = P < 0.001, two-tailed Student's t-test). **(c)** C3$^{-/-}$CRIg$^{-/-}$ mice were systemically infected with 1x10^8 eFLuor670-labelled *L.m.*. Livers were removed at indicated timepoints post infection and F4/80$^+$ Kupffer cells were analysed via flow cytometry for *L.m.* uptake (mean ± SD of 4 mice per timepoint, * = P < 0.05, # = P < 0.01, § = P < 0.001, Two-way ANOVA with Bonferroni post-test adjustment and two-tailed Student's t-test).

To confirm that the act of *L.m.* – platelet complex formation was the defining switch that pushed clearance of *L.m.* from SRA-dependent uptake to CRIg-dependent uptake by Kupffer cells, C3$^{-/-}$CRIg$^{-/-}$ mice were depleted of platelets before simultaneous infection with preopsonized *L.m.* and nonopsonized *L.m.* and subsequent measurement of blood clearance kinetics via intravital microscopy (Figure 2-36). In platelet depleted C3$^{-/-}$CRIg$^{-/-}$ mice both nonopsonized *L.m.* and preopsonized *L.m.* were cleared rapidly, with circulatory half-lives of under 1 min, mirroring SRA-mediated uptake in C3$^{-/-}$ mice (see Figure 2-23e). This rapid clearance of the preopsonized *L.m.* population highlighted that in non-platelet depleted C3$^{-/-}$ CRIg$^{-/-}$ mice (see Figure 2-35a) it was the binding of *L.m.* to blood platelets that shielded preopsonized *L.m.* from the uptake by SRA.

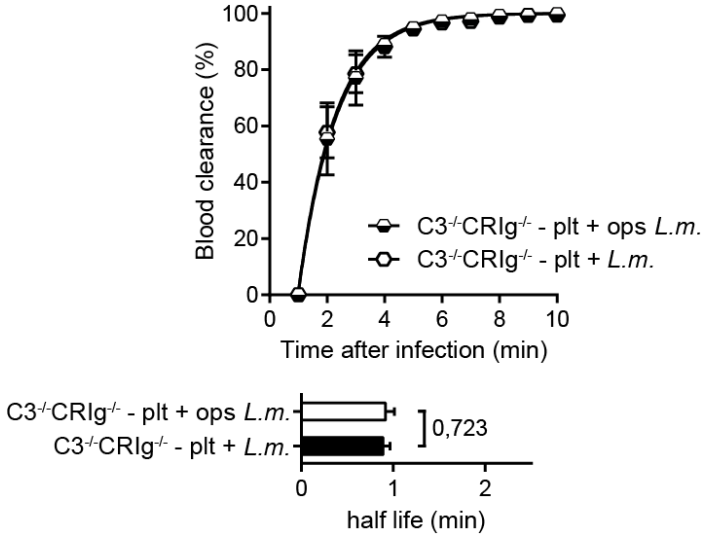

Figure 2-36 Depletion of platelets in C3$^{-/-}$CRIg$^{-/-}$ mice leads to efficient clearance of preopsonized *L.m.*
C3$^{-/-}$CRIg$^{-/-}$ mice were infected with 5x10^7 nonopsonized CFSE-labelled *L.m.* and 5x10^7 preopsonized eFluor670-labelled *L.m.* and clearance kinetic and circulatory half-life were determined via intravital microscopy (mean ± SD of 4 mice/strain, * = P < 0.05, # = P < 0.01, § = P < 0.001, Two-way ANOVA with Bonferroni post-test adjustment and two-tailed Student's t-test).

Using the experimental model of infecting C3$^{-/-}$CRIg$^{-/-}$ mice with preopsonized *L.m.* and/or nonopsonized *L.m.* clarified that SRA-mediated uptake and CRIg-mediated uptake are two independent processes. Although the facilitating cell population remains the same, CD11b$^-$ CD32$^-$ Kupffer cells (see Figure 2-22b and Figure 2-29b), the mechanism of clearance of *L.m.* from the bloodstream by Kupffer cells depends on if *L.m.* – platelet complexes have formed or not. *L.m.* not bound to platelets are cleared rapidly in an SRA dependent manner, but when *L.m.* – platelet complexes have formed these complexes cannot be taken up by Kupffer cells in absence of CRIg.

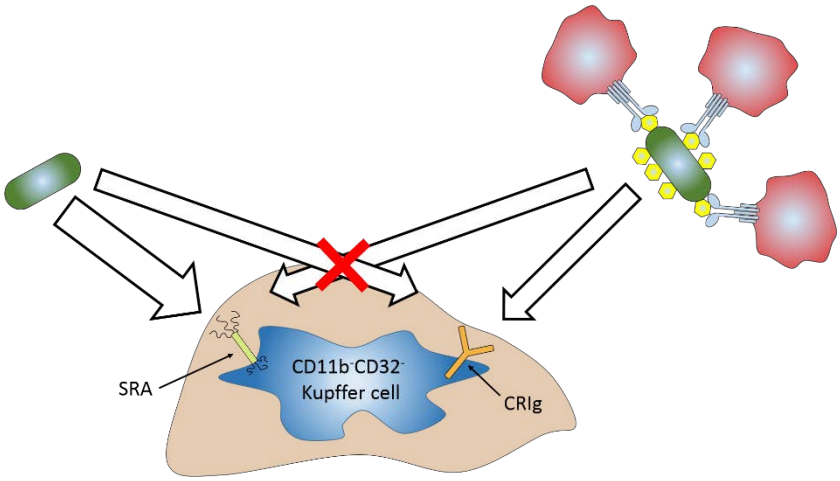

Illustration 2-8 Summary of chapter 2.8
Analysing the blood clearance kinetics in mice lacking both C3 and CRIg, it was observed that clearance of circulating *L.m.* by SRA and CRIg are two independent mechanisms with no overlap. Nonopsonized *L.m.* are efficiently removed by SRA in absence of CRIg, while *L.m.* – platelet complexes remain selectively in the bloodstream.

2.9 CRIg mediated clearance of platelet-complexes is found in other bacterial strains

Although *L.m.* is often used for systemic infections in immunology due to intracellular survival and resulting induction of cytolytic $CD8^+$ T-Cell response (Pamer, 2004), the number of clinical cases diagnosed to be Listeriosis are consistently low (Gesundheitsberichterstattung des Bundes, 2015). It had already been reported that other Gram (+) and Gram (-) bacterial pathogens have the capacity to bind platelets when incubated in murine whole blood (Verschoor *et al.,* 2011). It was thus tested if the here described process of CRIg dependent clearance of pathogen – platelet complexes held true for other bacteria also.

The most frequently found Gram (+) bacteria in bloodstream infection are coagulase-negative *staphylococci*, *Staph. aureus* and *Enterococci spp,* in descending order (Orsini *et al.,* 2012). It was thus decided to test *Staph. epidermidis* (ATCC 12228), belonging to the coagulase-negative *staphylococci*, *Staph. aureus* (ATCC 25923) and *Ent. faecalis* (ATCC 29212) for CRIg mediated clearance of bacteria – platelet complexes from the bloodstream. Initial flow cytometry analysis of livers of wild-type mice infected with these Gram (+) bacteria confirmed an uptake pattern of fluorescently labelled Gram (+) bacteria similar to what had been observed for infection with *L.m.* (see Figure 2-14c). Again, Kupffer cells facilitated the majority of clearance from the bloodstream, indicating the potential of a similar SRA/CRIg dual track clearance process mediated by Kupffer cells (Figure 2-37).

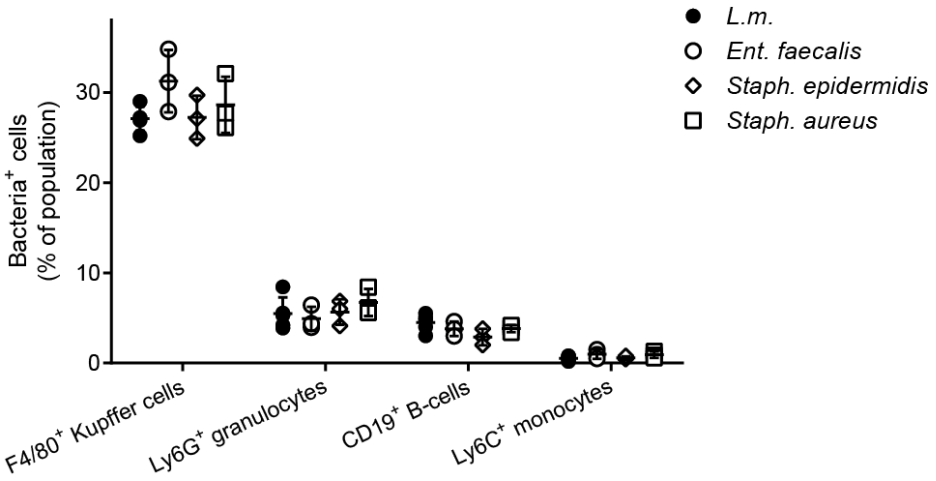

Figure 2-37 *Ent. faecalis*, *Staph. epidermidis* and *Staph. aureus* are cleared by the same hepatic cell populations as *L.m.*
Wild-type mice were systemically infected with $1x10^8$ eFLuor670-labelled bacteria. Livers were removed 30 min after infection and cells were isolated, stained and analysed for bacteria uptake via flow cytometry (mean ± SD of 3-4 mice per group, * = $P < 0.05$, # = $P < 0.01$, § = $P < 0.001$, Two-way ANOVA with Bonferroni post-test adjustment).

To investigate if the discovered dual-track clearance of complement nonopsonized bacteria and bacteria-platelet complexes held true as well, $C3^{-/-}CRIg^{-/-}$ mice were infected simultaneously with preopsonized bacteria and nonopsonized bacteria, as had been done for

L.m. (see Figure 2-35a). This setup allowed for the observation of bloodstream-clearance of bacteria – platelet complexes and its dependence on CRIg as well as the rapid clearance of nonopsonized *L.m.* from the bloodstream. *Ent. faecalis*, *Staph. epidermidis, Staph. aureus* and *B. subtilis* were labelled fluorescently, prepared as described for *L.m.* (see Figure 2-30) and clearance kinetic and circulatory half-lives were measured via intravital microscopy (Figure 2-38). Clearance of preopsonized *B. subtilis*, *Ent. faecalis*, *Staph. epidermidis* and *Staph. aureus* and the resulting bacteria – platelet complexes from the bloodstream was found to be drastically reduced in absence of CRIg, as had been the case of *L.m.* (see Figure 2-35a). In contrast, nonopsonized bacteria were cleared rapidly from the bloodstream with circulatory half-lives of approximately 1 min, mirroring the observed kinetic of SRA-mediated clearance of *L.m.* from the bloodstream (see Figure 2-23e).

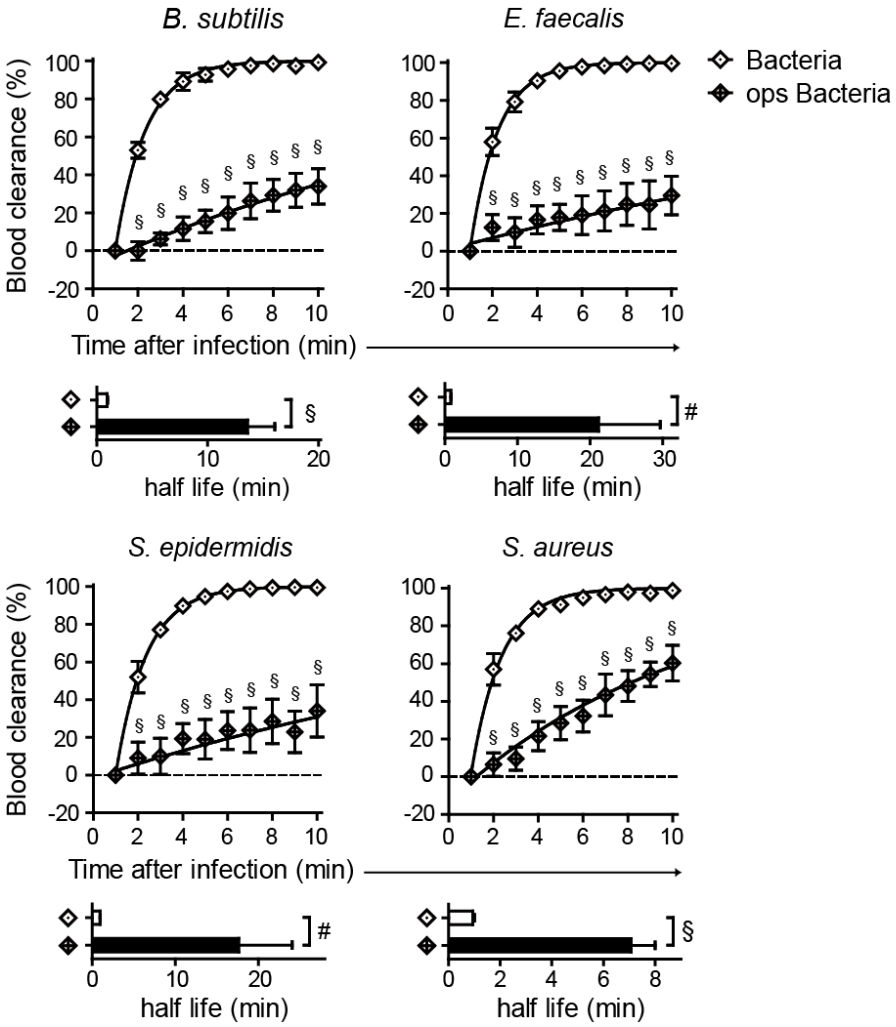

Figure 2-38 *Ent. faecalis*, *Staph. epidermidis* and *Staph. aureus* are all cleared from the murine bloodstream in a CRIg-dependent manner after having bound to platelets

$C3^{-/-}CRIg^{-/-}$ mice were infected with $5x10^7$ non-treated CFSE-labelled bacteria and $5x10^7$ preopsonized eFluor670-labelled bacteria and clearance kinetic and circulatory half-life were determined using intravital microscopy (mean ± SD of 3-4 mice, * = P < 0.05, # = P < 0.01, § = P < 0.001, Two-way ANOVA with Bonferroni post-test adjustment and two-tailed Student's t-test).

Gram (-) bacteria frequently found in bloodstream infections are *Klebsiella spp*, *Pseudomonas spp* and *E. coli,* among others (Decousser *et al.,* 2003). The species *K. pneumoniae* (ATCC 13883), *P. aeruginosa* (ATCC 27853) and *E. coli* (ATCC 29522) were selected to determine, if Gram (-) bacteria that have bound to platelets are also cleared in a CRIg dependent manner from the bloodstream. Additionally, it was decided to test *S. typhimurium* since it, like *L.m.*, is a facultative intracellular bacteria. All tested Gram (-) strains were not fluorescently label-able to a degree in which detection of systemically circulating bacteria via intravital microscopy or detection of bacterial uptake via flow cytometry was possible (data not shown). Thus, clearance kinetics and circulatory half-lives were determined *ex vivo* by plating obtained blood samples 1, 3, 5 and 10 min after systemic infection of $C3^{-/-}CRIg^{-/-}$ mice (Figure 2-39). Additionally, all Gram (-) strains were preopsonized in blood plasma lacking C5 in order to minimize lysis of the bacteria due to the formation of membrane attack complexes. Similar to the tested Gram (+) bacteria, preopsonized *E. coli*, *S. typhimurium*, *K. pneumoniae* and *P. aeruginosa* all exhibited a significant reduction in clearance from the bloodstream when CRIg was lacking, indicating a similar dependency on CRIg to clear complexes formed between Gram (-) bacteria and platelets. In contrast, nonopsonized *E. coli*, *S. typhimurium*, *K. pneumoniae* and *P. aeruginosa* were all cleared significantly faster from the bloodstream than their preopsonized counterparts.

In summary, a reduction of clearance from the bloodstream was observed for all tested strains, no matter if Gram (+) or Gram (-), when platelet binding was possible and CRIg was absent. This indicates a general role for CRIg in the clearance of bacteria – platelet complexes that form after the pathogen has reached the bloodstream. The drastic phenotype also implies that CRIg is specialized on and thus is the main facilitator of the clearance of these formed bacteria – platelet complexes.

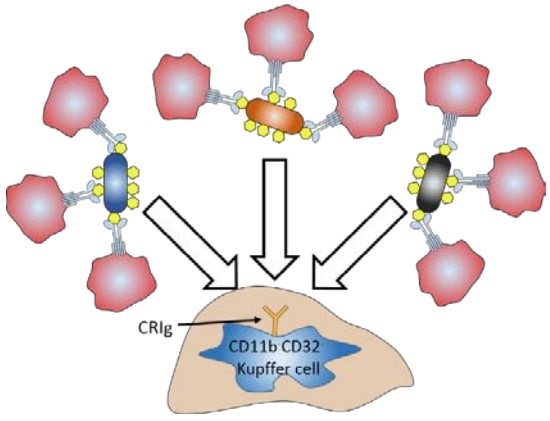

Illustration 2-9 Summary of chapter 2.9
Infection of $C3^{-/-}CRIg^{-/-}$ mice revealed that preopsonization of the Gram (+) bacteria *Ent. faecalis*, *Staph. epidermidis* and *Staph. aureus* and the Gram (-) bacteria *K. pneumoniae*, *E. coli* and *P. aeruginosa* led to an abrogation of clearance of these bacteria from the bloodstream. This data strongly indicated that clearance of bacteria – platelet complexes from the bloodstream in general is CRIg-dependent and not only specific of infection with *L.m.*.

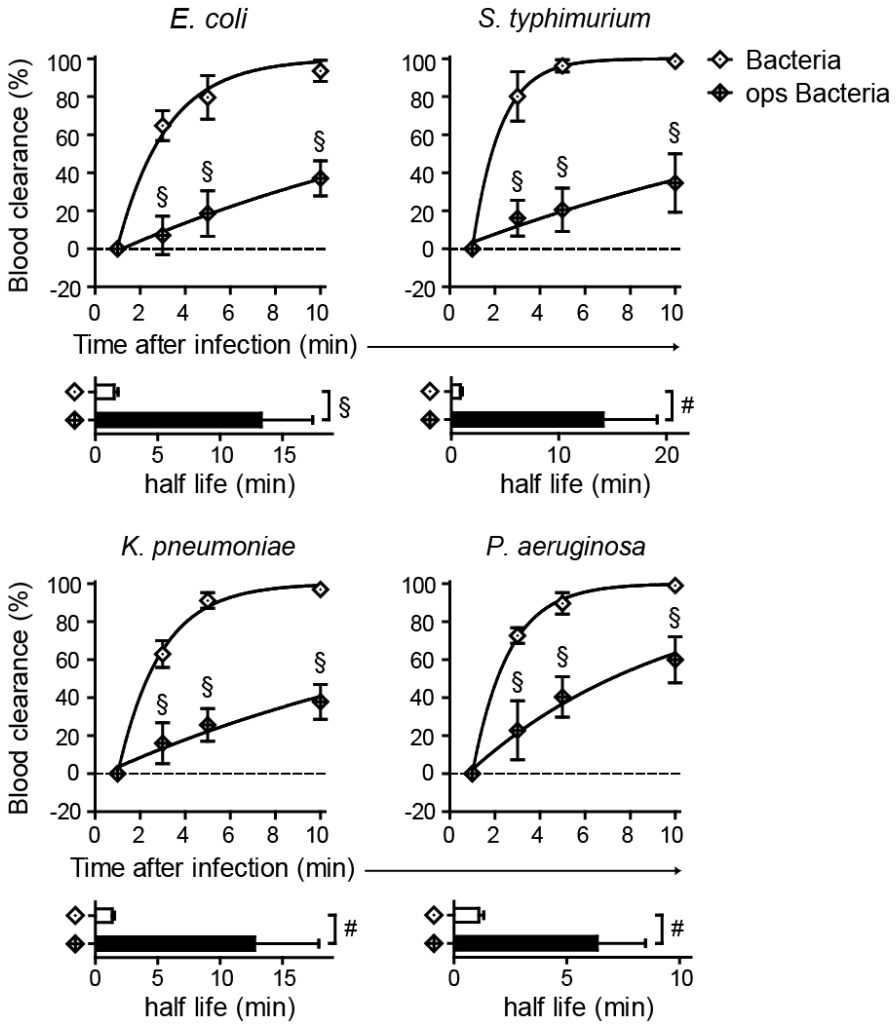

Figure 2-39 Preopsonized *E.coli*, *K. pneumoniae* and *P. aeruginosa* are cleared from the murine bloodstream highly inefficiently in absence of CRIg

$C3^{-/-}CRIg^{-/-}$ mice were infected with either $1x10^8$ nonopsonized bacteria or $1x10^8$ preopsonized bacteria. Circulating bacteria were quantified by plating blood samples on BHI-Agar taken 1, 3, 5 and 10 min post infection. (mean ± SD of 3-4 mice, * = $P < 0.05$, # = $P < 0.01$, § = $P < 0.001$, Two-way ANOVA with Bonferroni post-test adjustment and two-tailed Student's t-test)

2.10 Clearance of opsonized, non – platelet bound *L.m.*

It was found in this thesis that blocking of SRA drastically diminishes *L.m.* hepatic clearance of nonopsonized *L.m.* (see Figure 2-23e), whereas a lack of CRIg strictly impaired uptake of *L.m.* – platelet complexes by Kupffer cells (see Figure 2-33). These two states, nonopsonized and *L.m.* – platelet complexes, represent two extremes of how *L.m.* can be present in the bloodstream. These two states do not transition directly from one to another, but via an intermediate state, in which *L.m.* is opsonized by complement but has not yet bound to platelets. To further elucidate the capacity of Kupffer cells to clear *L.m*., it was investigated if either SRA of CRIg have the capacity to mediate uptake of bacteria present in this complement opsonized but non-platelet bound intermediate state.

Mice lacking GPIb were used to investigate the clearance of opsonized *L.m.* from the bloodstream. It had been observed that opsonization of *L.m.* with C3 in mice lacking GPIb was similar to control wild-type mice (see Figure 2-2c) but no *L.m.* – platelet complex formation had been observed using intravital microscopy (see Figure 2-3d) due to the fact that binding to platelets is strictly GPIb-dependent (Verschoor *et al.,* 2011). This lack of platelet binding independent of opsonization allowed for the investigation of uptake of C3 opsonized, non-platelet bound *L.m.*.

2.10.1 SRA can efficiently clear opsonized *L.m.*

To investigate the capacity of SRA to clear opsonized, non-platelet bound *L.m.* from the bloodstream, mice lacking both GPIb and CRIg were used to ensure that only SRA-mediated uptake by Kupffer cells would be observed. When $GPIb^{-/-}CRIg^{-/-}$ mice were infected with nonopsonized *L.m.* (Figure 2-40a), rapid clearance mirroring observed SRA-dependent uptake in $C3^{-/-}$ mice was detected. To ensure that only fully opsonized *L.m.* are present in the bloodstream from timepoint 0, $GPIb^{-/-}CRIg^{-/-}$ mice were additionally infected with preopsonized *L.m.*, already carrying activated C3 on their surface (Figure 2-40b). Again, rapid clearance with a circulatory half-life of under 1 min was measured. This rapid clearance revealed that SRA can clear fully opsonized *L.m.* with a similar efficiency than it can clear nonopsonized *L.m.* (see Figure 2-23e).

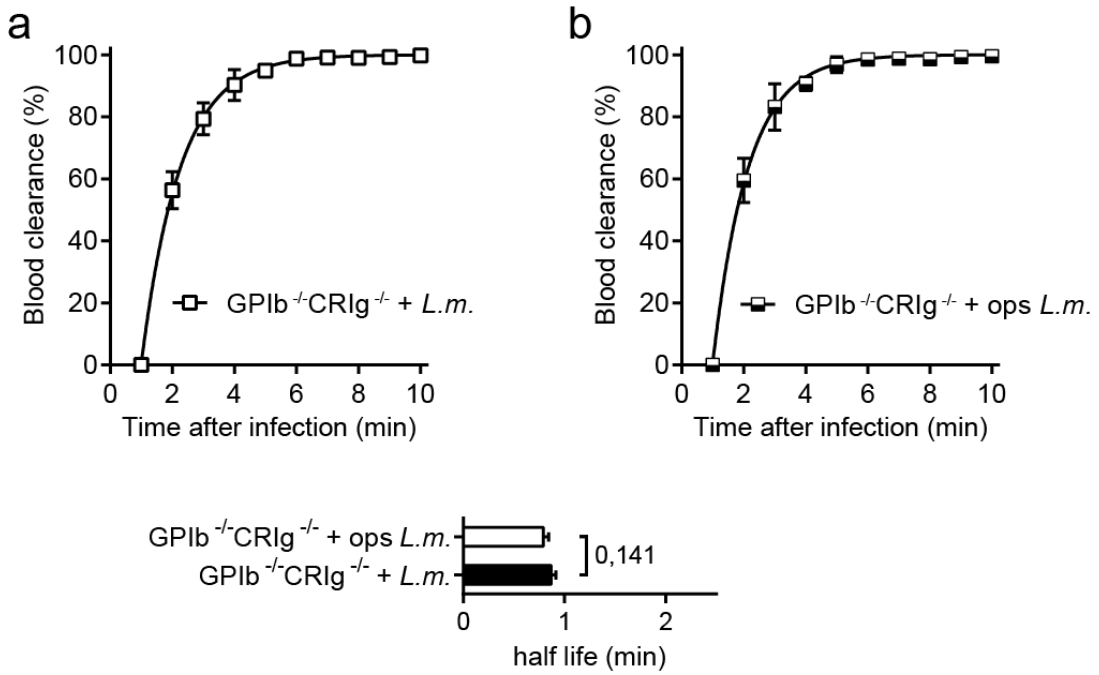

Figure 2-40 Preopsonized *L.m.* are efficiently cleared in GPIb$^{-/-}$CRIg$^{-/-}$ mice
GPIb$^{-/-}$CRIg$^{-/-}$ mice were infected with 5x10^7 nonopsonized CFSE-labelled *L.m.* and 5x10^7 preopsonized eFluor670-labelled *L.m.* and clearance kinetic and circulatory half-life were determined via intravital microscopy (mean ± SD of 3 mice, * = P < 0.05, # = P < 0.01, § = P < 0.001, Two-way ANOVA with Bonferroni post-test adjustment and two-tailed Student's t-test).

2.10.2 CRIg can clear opsonized *L.m.*

To investigate if clearance of opsonized *L.m.* can be facilitated by CRIg, GPIb$^{-/-}$ mice treated with Poly(I), which had been observed to block SRA-mediated clearance of *L.m.* from the bloodstream (see Figure 2-23e), were infected with *L.m.* and clearance kinetic as well as circulatory half-life were determined. In comparison to C3$^{-/-}$ mice treated with Poly(I), in which *L.m.* are not opsonized with C3 and thus SRA-mediated uptake by Kupffer cells is inhibited, *L.m.* were cleared significantly faster from the bloodstream of GPIb$^{-/-}$ mice treated with Poly(I) (Figure 2-41a). To determine if this increase in uptake was CRIg-mediated uptake of opsonized *L.m.*, mice lacking both GPIb and CRIg were treated with Poly(I) shortly before systemic infection with *L.m.* (Figure 2-41b). The resulting clearance kinetic of systemic *L.m.* in GPIb$^{-/-}$ CRIg$^{-/-}$ mice treated with Poly(I) was significantly slower than in GPIb$^{-/-}$ mice treated with Poly(I) and similar to the observed clearance kinetic in C3$^{-/-}$ mice treated with Poly(I) (Figure 2-41a). Since the only difference between GPIb$^{-/-}$ and GPIb$^{-/-}$CRIg$^{-/-}$ mice was the absence of CRIg, the faster clearance of systemic *L.m.* from the bloodstream in GPIb$^{-/-}$ mice was attributed to CRIg-mediated uptake of *L.m.* by hepatic Kupffer cells.

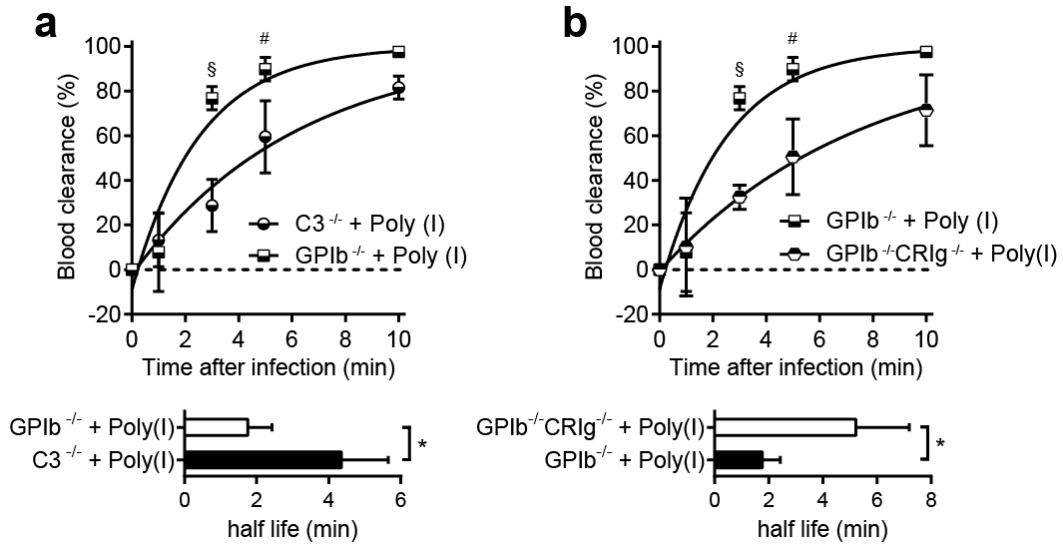

Figure 2-41 CRIg can facilitate clearance of opsonized *L.m.* from the bloodstream
(a) GPIb$^{-/-}$ and **(b)** GPIb$^{-/-}$CRIg$^{-/-}$ mice were treated with 500 µg polyinosinic acid 2 min prior to infection with 1x10^8 *L.m.* and clearance kinetic and circulatory half-life was determined by plating of blood samples taken 1, 3, 5 and 10 min post infection (mean ± SD of 3-4 mice, * = P < 0.05, # = P < 0.01, § = P < 0.001, Two-way ANOVA with Bonferroni post-test adjustment and two-tailed Student's t-test).

Summed up, mice lacking GPIb were used to investigate if either SRA or CRIg were capable of clearing systemically circulating opsonized, non-platelet bound *L.m.* from the bloodstream. Rapid clearance of preopsonized *L.m.* from the circulation in GPIb$^{-/-}$CRIg$^{-/-}$ mice confirmed that SRA could efficiently facilitate the uptake of opsonized, non-platelet bound *L.m.*. Heightened clearance of *L.m.* from the circulation of GPIb$^{-/-}$ mice treated with Poly(I) in comparison to GPIb$^{-/-}$CRIg$^{-/-}$ mice treated with Poly(I) also indicated that CRIg has the capacity to facilitate clearance of opsonized, non-platelet bound *L.m.* from the bloodstream.

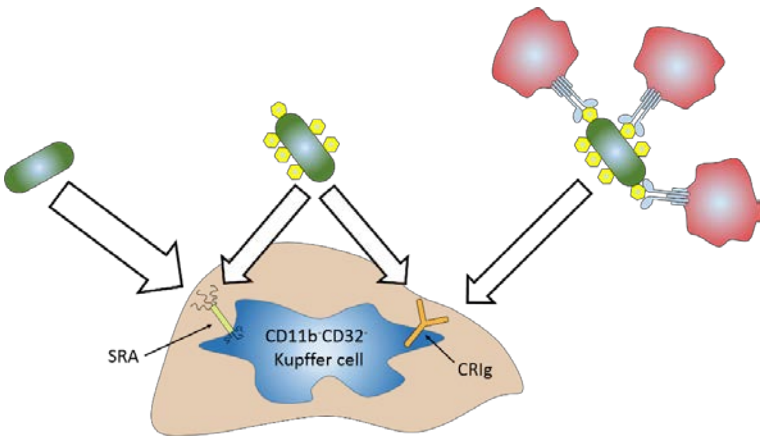

Illustration 2-10 Summary of chapter 2.10
Opsonized, non-platelet bound *L.m.* were found to be taken up by both SRA- and CRIg- mediated mechanisms.

2.11 Lack of Kupffer cell clearance leads to potential pathology

Clearance of *L.m.* from the bloodstream by hepatic Kupffer cells was in this thesis discovered to be a dual track system: nonopsonized *L.m.* are cleared dependent on SRA, *L.m.* – platelet complexes clearance was found to be dependent on CRIg (see Figure 2-23e and Figure 2-34). *In vitro* analysis of *L.m.* – platelet complex formation had additionally revealed that platelets are activated after prolonged close proximity to *L.m.* (see Figure 2-8) dependent on the presence of IgG (see Figure 2-7) which in turn led to the formation of platelet aggregates around bound *L.m.* (see Figure 2-4). It was hypothesized that such platelet activation should also occur in the bloodstream of systemically infected mice. Should the removal of *L.m.* – platelet complexes by CRIg be abrogated and *L.m.* – platelet complexes thus remain in the bloodstream for a prolonged time, platelets in the *L.m.* – platelet complexes could be activated and subsequently larger platelet aggregates could be formed, leading to the formation of microthrombi.

To investigate if this hypothesis held true and thus elucidate an important biological role of the here described CRIg-mediated clearance of *L.m.* – platelet complexes from the bloodstream, the consequences of a lack of CRIg-mediated clearance of *L.m.* – platelet complexes for the host were investigated. To this end, mice were depleted of Kupffer cells by i.v. administration of clodronate liposomes (Figure 2-42a) (van Rooijen and van Nieuwmegen, 1984). This treatment depleted Kupffer cells in the liver, thus reducing the capacity for hepatic uptake of formed *L.m.* – platelet complexes (Figure 2-42b). Systemic infection with *L.m.* of wild-type mice depleted of Kupffer cells showed a strong reduction of clearance of *L.m.* from the bloodstream (Figure 2-42c), confirming a drastic reduction in hepatic uptake of circulating *L.m.*. Treatment of $C3^{-/-}$ mice and $GPIb^{-/-}$ mice, in which no *L.m.* – platelet complexes are formed (see Figure 2-3c, d), resulted in similar impaired clearance of *L.m.* from the bloodstream (Supplemental figure 6). Thus, although hepatic clearance is lacking in all three strains, *L.m.* circulating in wild-type animals are present in *L.m.* – platelet complexes, while in both $C3^{-/-}$ mice and $GPIb^{-/-}$ mice, *L.m.* circulate unbound from platelets.

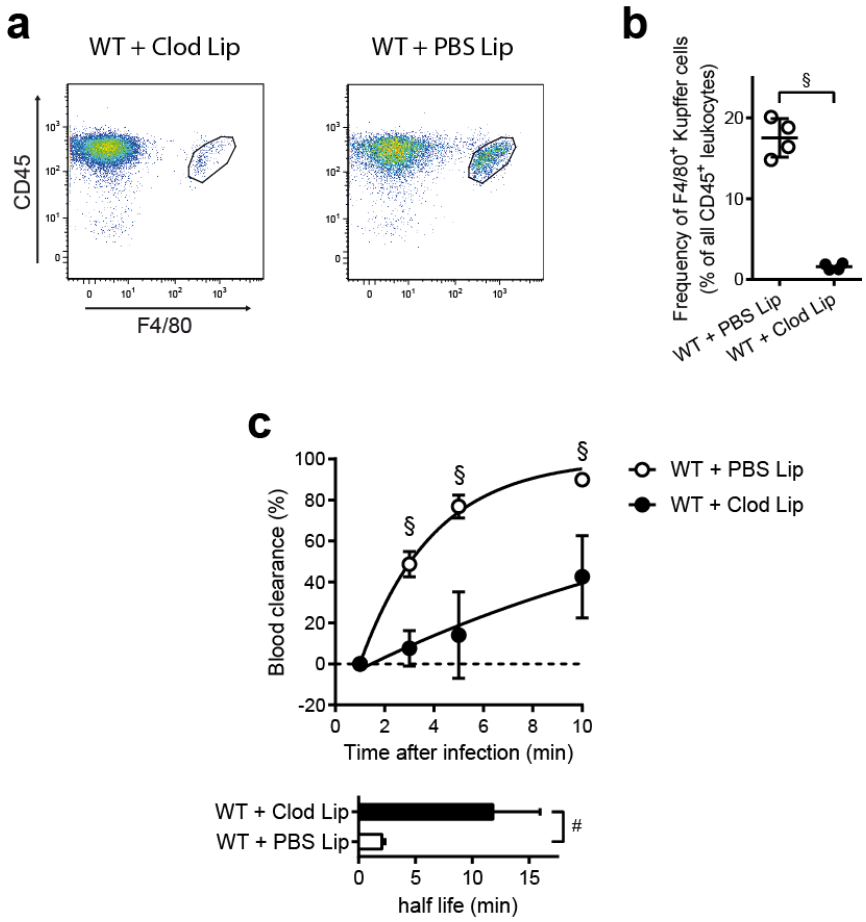

Figure 2-42 Depletion of Kupffer cells strongly reduces clearance of systemically circulating *L.m.* in wild-type mice
(a) Flow cytometry analysis of hepatic cell isolates (pregated on FCS/SSC and live cells) and **(b)** pooled data of Kupffer cell frequency in wild-type mice 48 h after i.v. injection of 200 µl either clodronate liposomes or control PBS liposomes (mean ± SD of 4 mice per treatment, * = P < 0.05, # = P < 0.01, § = P < 0.001, two-tailed Student's t-test). **(c)** Clearance kinetic and circulatory half-life of systemic *L.m.* in wild-type mice depleted of Kupffer cells 48 h prior to infection (mean ± SD of 4 mice per treatment, * = P < 0.05, # = P < 0.01, § = P < 0.001, Two-way ANOVA with Bonferroni post-test adjustment and two-tailed Student's t-test).

To visualize the consequences of impaired clearance of *L.m.* – platelet complexes, PET-CT was performed on wild-type mice treated with clodronate liposomes to deplete hepatic Kupffer cells, where *L.m.* – platelet complexes are formed (see Figure 2-3b), and $C3^{-/-}$ and $GPIb^{-/-}$ mice also treated with clodronate liposomes to deplete Kupffer cells, where no *L.m.* – platelet complex formation had been observed (see Figure 2-3c, d). Interestingly it was observed that in wild-type mice treated with clodronate liposomes, where *L.m.* – platelet complexes are formed but are failed to be cleared in a CRIg-mediated timely manner, an accumulation of radioactively labelled *L.m.* in the lung occurred (Figure 2-43a, b). In both $C3^{-/-}$ mice treated with clodronate liposomes and $GPIb^{-/-}$ mice treated with clodronate liposomes no such accumulation of *L.m.* in the lung was observed (Figure 2-43a, b). The observed accumulation in wild-type mice treated with clodronate liposomes occurred in hot-spots, sometimes only appearing in one lung and not in the other (Figure 2-43c), further indicating that the observed localization to the lung is due to microthrombi formation.

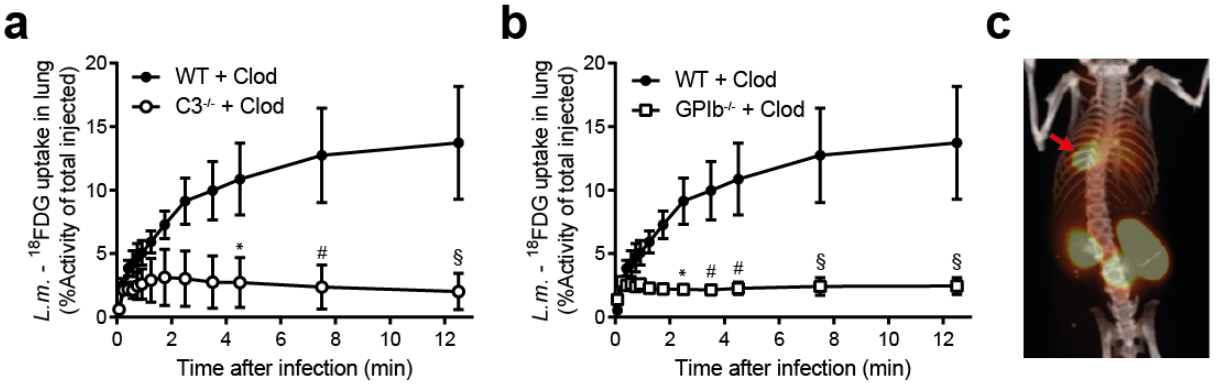

Figure 2-43 Lack of CRIg leads to accumulation of *L.m.* in the lung of wild-type mice
Wild-type, $C3^{-/-}$ and $GPIb^{-/-}$ mice were treated with 200 µl clodronate liposomes 48 h before infection with $1x10^8$ *L.m.* labelled with ^{18}FDG. **(a-b)** Uptake of *L.m.* – ^{18}FDG in the lung as acquired via PET-CT (mean ± SD of 3 mice, * = P < 0.05, # = P < 0.01, § = P < 0.001, Two-way ANOVA with Bonferroni post-test adjustment). **(c)** Heat-map image of *L.m.* – ^{18}FDG hot spot in the lung of a wild-type mouse.

To closer investigate the localization of circulating *L.m.* to the lung in wild-type mice depleted of Kupffer cells, wild-type mice treated either with clodronate liposomes or control PBS-liposomes, which do not deplete any cells (van Rooijen and van Nieuwmegen, 1984) were infected systemically with fluorescently labelled *L.m.*. 15 min post infection lungs were removed and lung leukocytes were analysed for uptake of *L.m.* via flow cytometry (Figure 2-44a, b). It was observed that in wild-type mice treated with clodronate liposomes, the circulating populations of neutrophil granulocytes and monocytes had taken up large numbers of *L.m.* (Figure 2-44b). In contrast, lung resident populations of alveolar and interstitial macrophages exhibited no increased uptake of *L.m.* after treatment with clodronate liposomes. It was furthermore analysed how i.v. treatment with clodronate liposomes altered existing cell populations within the lung (Figure 2-44c). It was observed that lung resident interstitial macrophages were also depleted by i.v. application of clodronate liposomes, while an influx of both neutrophil granulocytes and monocytes was evident. The population of $CD11c^{hi}$ $CD11b^{lo}$ alveolar macrophages, which are not in contact with the bloodstream, was used as a control for comparability of wild-type animals treated with clodronate liposomes and PBS liposomes.

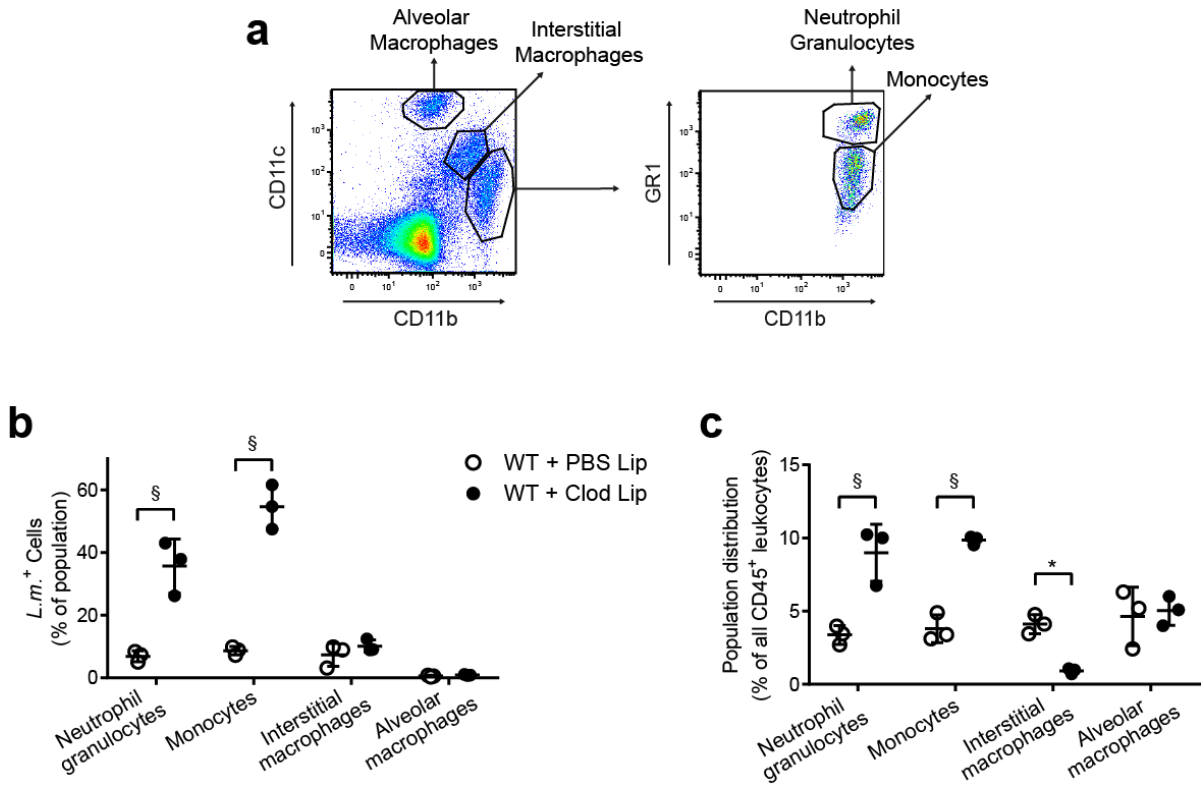

Figure 2-44 *L.m.* are taken up by neutrophil granulocytes and monocytes in absence of hepatic Kupffer cells
(a) Schematic flow cytometry analysis of lung leukocytes. **(b)** Uptake of eFLuor670-labelled *L.m.* into phagocytic populations of the lung in wild-type animals treated with either 200 µl clodronate liposomes or 200 µl PBS liposomes 48 h prior to infection. **(c)** Distribution of phagocytic populations in wild-type mice 48 h after treatment either with clodronate liposomes or PBS liposomes. (mean ± SD of 3 mice per group, * = P < 0.05, # = P < 0.01, § = P < 0.001, Two-way ANOVA with Bonferroni post-test adjustment and two-tailed Student's t-test)

These data indicated that in wild-type mice treated with clodronate liposomes *L.m.* remain within the circulation and passively get stuck in the lung microvasculature before being phagocytosed by circulating neutrophil granulocytes and monocytes. This process of accumulation in microvasculature hints towards an active role of platelet aggregation around the bound *L.m.*, similar as to what was observed in an isolated *in vitro* setting using platelet aggregometry (see Figure 2-4). Taken together, there is strong evidence that the binding of *L.m.* to platelets is a double edged sword for the host: The prolongation of *L.m.* circulation ensures delivery of enough antigen to other organs, especially the spleen, to induce strong responses and the formation of adaptive immunity (Verschoor *et al.,* 2011), but if these complexes are not cleared in a timely manner, the presence of *L.m.* can cause platelets to aggregate around the bacteria and thus induce pathologies, especially in the microvasculature of the lung. To minimize this risk, CRIg facilitates the clearance of these complexes from the bloodstream, so that a middle ground is reached between prolonged circulation time and danger of platelet aggregation.

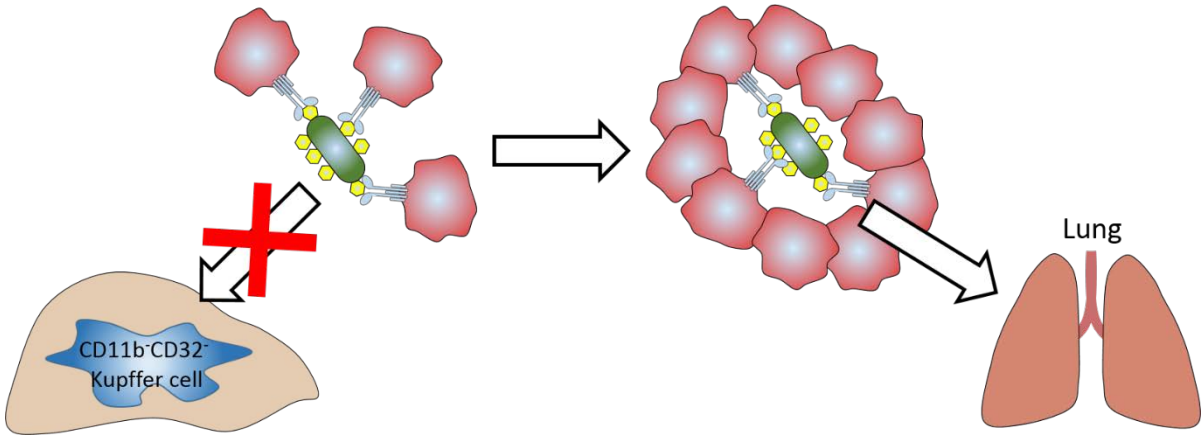

Illustration 2-11 Summary of chapter 2.11
It was observed that in wild-type mice treated with clodronate liposomes, known to deplete Kupffer cells, *L.m.* localised to the lung. This localisation of *L.m.* to the lung was absent in $C3^{-/-}$ mice and $GPIb^{-/-}$ mice treated with clodronate liposomes, where *L.m.* – platelet complex formation was inhibited. *L.m.* uptake in lungs of wild-type mice treated with clodronate was almost exclusively facilitated by circulating neutrophil granulocytes and monocytes. The data thus indicates that a lack of CRIg-mediated clearance of *L.m.* – platelet complexes by Kupffer cells leads to *L.m.* getting stuck in the microvasculature of the lung, possibly due to the activation of surrounding platelets, as had been observed in platelet aggregometry.

3 Discussion

Bacteraemia, defined as the presence of viable bacteria in the bloodstream can occur in many ways, be it by a disseminating infection or something as mundane as brushing ones teeth (Bone, 1991). While generally transient due to the efficient clearance by the hosts immune system, when uncontrolled bacteraemia can lead to systemic infection and sepsis. It was previously observed, that a lack of C3 had a surprising protective effect on the splenic infection of mice systemically infected with *L.m.* (Verschoor *et al.,* 2011). Further investigation linked this reduction in splenic infection to a reduced targeting of *L.m.* to splenic $CD8\alpha^+$ DCs in absence of C3, a situation in which *L.m.* were also cleared significantly faster from the bloodstream. It was found that in wild-type mice, platelets formed complexes with the circulating pathogen in a C3 and GPIb dependent manner and thus targeted small quantities of *L.m.* to a splenic survival niche. The aim of this thesis was to investigate how this complex formation between platelets and bacteria altered the fate of the circulating pathogen.

This thesis found the system of *L.m.* – platelet complex formation to be a fine tuned mechanism, resulting in prolonged circulation time of complexed *L.m.* by shifting clearance from rapid uptake by a pattern recognition receptor to a slower, complement-mediated uptake. Initial uptake of non-platelet bound bacteria was facilitated by the pattern recognition receptor SRA, whereas the uptake of formed bacteria-platelet complexes was dependent on the complement receptor CRIg. Both clearance mechanisms, SRA- and CRIg-dependent, were facilitated by $CD11b^-CD32^-$ Kupffer cells, described as mature liver derived Kupffer cells in the literature (Klein *et al.,* 2007). Lack of Kupffer cell mediated clearance led to the formation of thrombi only when *L.m.* – platelet complex formation was possible, indicating a protective function of CRIg-mediated removal of formed *L.m.* – platelet complexes. The described handover of responsibility from SRA-mediated hepatic uptake to CRIg-mediated hepatic uptake slowed total clearance of systemically circulating *L.m.* from the bloodstream while remained sufficiently efficient to prevent pathology due to platelet activation by the pathogen.

3.1 Newly established techniques to trace bacteria *in situ*

Two novel methods were established during the course of this thesis, both with marked advantages in investigating early clearance of systemic bacteria from the bloodstream, but also with inherent limitations. In the following both the advantages and limitations will be described briefly and also how the limitations were compensated for by other methods.

This thesis used multiphoton intravital laser scanning microscopy of the ear vasculature to obtain detailed clearance kinetics and to directly observe platelet binding of systemically circulating bacteria with a high temporal resolution (see Figure 2-1). To our knowledge, this is the first time this technology has been used in this setup to this end. In comparison to classical methods, such as plating of drawn blood samples to detect live *L.m.*, using intravital microscopy to track bacterial removal from the circulation offers several advantages, for example the discrimination of bacteria bound to certain blood cells, such as platelets (see Figure 2-3), vs. bacteria circulating on their own. This novel distinction is not detectable using classical methods, such as the quantification of live bacteria in acquired blood samples, and was integral to the discovery that two distinct mechanisms facilitate bacterial clearance simultaneously. Investigating clearance kinetics of two different bacterial populations simultaneously was also only achievable with this novel method (see Figure 2-30). Tracking the removal of two bacterial populations simultaneously allows for the use of an internal control, as demonstrated in the experiment using preopsonized and nonopsonized bacteria in $C3^{-/-}CRIg^{-/-}$ mice (see Figure 2-35 and Figure 2-37). In this experimental setup, nonopsonized bacteria acted as internal control populations, being cleared rapidly via SRA, whereas the experimental population, carrying activated C3 on its surface selectively remained in the circulation for a prolonged period of time. It is thus possible to distinguish single clearance patterns from each other in a single experiment and so control for unknown factors when comparing *in vivo* data between individual mice, such as fluctuations of the infectious dose or age, weight or gender of the animal (Løvik and North, 1985; Pasche *et al.,* 2005). To ensure that the presence of one population had no influence on the removal of the other population from the bloodstream, control experiments were performed in selected mouse strains, such as $C3^{-/-}CRIg^{-/-}$ mice, using only one bacterial population, either nonopsonized or preopsonized (Supplemental figure 7). Removal of single bacterial populations from the bloodstream displayed no statistically significant variance in presence or absence of a second bacterial population.

A further advantage of using multiphoton intravital laser scanning microscopy to track bacterial removal from the bloodstream is the comparatively non-invasiveness of the technique. In contrast to detection of live, systemically circulating bacteria by repeated acquisition of blood samples and plating, no blood needs to be drawn during visualization of

bacterial removal from the bloodstream. Blood loss of as low as 15% total blood volume has been described to potentially lead to tachycardia and intense arteriolar constriction, leading to a redirection of blood flow away from the gut and skin (McGuill and Rowan, 1989), thus potentially skewing experimental data. Therefore, the non-invasive setup of the established technique circumvents the potential effect of blood loss for the host.

Lastly, the use of multiphoton intravital laser scanning microscopy allowed for an unprecedented temporal resolution of bacterial removal from the circulation (see Figure 2-1). By quantifying circulating bacteria visualized during discrete timeframes of 1 min each, removal could be followed near continuously. This in turn enables the detection of transient effects, such as single dose treatment with Poly(I) to block SRA-mediated uptake of circulating *L.m.* by hepatic Kupffer cells (see Figure 2-23), as well as more detailed and exact visualization of different phases during clearance processes, such as the abrogated clearance of *L.m.* from the bloodstream after initial wild-type like clearance in $CRIg^{-/-}$ mice (see Figure 2-26).

As with other techniques relying on fluorescence labelling of cells, one general limitation of intravital microscopy is the so called “black box”: Apart from some exceptions, such as the visualization of collagen via second harmonics generation (Campagnola and Loew, 2003), one only detects what has been fluorescently labelled. Thus any interaction with non-labelled cell populations of *L.m.* in the bloodstream will not be detectable. This limitation was addressed by intravital imaging of mice that had been administered rhodamine 6G (Supplementary movie 12), shown to label white blood cells non-selectively (Baatz *et al.,* 1995). This method confirmed blood platelets to be the only murine blood cell population to bind a large number of *L.m.*. It is furthermore important to note that all experiments using multiphoton intravital laser scanning microscopy were performed using heat-inactivated bacteria due to a lack of biosafety level 2 clearance. As *in vitro* light transmission platelet aggregometry revealed significant differences in the interaction between live *L.m.* and heat-inactivated *L.m.*, in that live *L.m.* activated platelets after a lag phase of approx. 2.5 min whereas heat-inactivated *L.m.* did not activate platelets during the first 10 min of incubation with PRP, it was of utmost importance to compare clearance of *L.m.* between *in vivo* imaging and *ex vivo* plating of blood samples. Comparison of the two methods for wild-type, $C3^{-/-}$ and $GPIb^{-/-}$ (see Figure 2-1c and Supplemental figure 8) displayed no significant variation from one another. Additionally, flow cytometry analysis of hepatic single cell suspensions of wild-type mice infected with heat-inactivated *L.m.* was performed, which displayed a similar pattern of uptake as measured in wild-type mice infected with live *L.m.* (Supplemental figure 9). Thus it was concluded that possible influence of live *L.m.* on surrounding platelets was neglectable for the evaluation of early clearance kinetics. It would still be desirable to obtain clearance kinetics with live *L.m.* and other bacteria in a setup for intravital microscopy allowing for the use of biosafety level 2 bacteria.

Another technique used in this thesis was the detection of *L.m.* infection by PET/CT (see Figure 2-12). Labelling bacteria with a radioactive compound to detect bacterial clearance *in vivo* is not a new concept, though used sparsely. Studies can be found were ^{99m}Technetium, ^{111}Indium or ^{67}Gallium, compounds, which are also used in humans for diagnostic purposes, are used as radioactive labels (Johanson *et al.,* 1973; Zundel and Bernard, 2006; Petrik *et al.,* 2012). In this thesis, ^{18}Fluor was used as radioactive label, incorporated into a deoxy-Glucose molecule (Fukuda *et al.,* 1982), allowing for bacterial uptake and partial metabolism. ^{18}Fluor has the advantage of being highly instable, with a decay half-life of under 110 min, allowing for a large amount of detectable radioactivity in short timeframes and thus increasing the possible temporal resolution at which bacterial localization can be visualized. Though ^{18}FDG has been used to label leukocytes such as mesenchymal stem cells and multipotent adult progenitor cells to track biodistribution and cell migration *in vivo* (Elhami *et al.,* 2013; Wolfs *et al.,* 2013), to the best of our knowledge no previous use of this label to selectively mark and follow systemic bacterial infection has been made. The established model gave unparalleled insight into the stages of early clearance of systemic *L.m.* from the bloodstream on a whole body scale (see Figure 2-12, Figure 2-13 and Figure 2-28).

Still, one limitation remained: Although ^{18}FDG is taken up by glucose transporter proteins by *L.m.* and subsequently metabolized to ^{18}FDG-6-phosphate, a state in which it cannot be secreted from the live cell (Fukuda *et al.,* 1982), radioactive signal appeared to be filtered from the blood by the kidneys into the bladder in every experiment (for example, see Figure 2-12). Plating of urine and kidney samples confirmed no *L.m.* to be present in the bladder and low numbers of live *L.m.* to be located in the kidney (less than 0.01% of initial inoculum) (see Supplemental figure 3). Additionally, control experiments in which either non-metabolized ^{18}FDG or supernatant of radioactively labelled *L.m*. presumably containing ^{18}FDG-6-phosphate were used as inoculum displayed a similar phenotype of significant uptake in kidneys and bladder (Supplemental figure 10a-b). These data indicate that the detected radioactive signal in kidneys and bladder do not originate from bacterial uptake in the locations, but from the filtration of circulating free ^{18}FDG. The cardiac muscle, as a highly metabolically active muscle, is known to take up significant amounts of non-metabolized ^{18}FDG, whereas metabolized ^{18}FDG-6-phosphate is not taken up (Fukuda *et al.,* 1982). This observation was confirmed comparing the uptake of radioactive signal by the cardiac muscle when either non-metabolized ^{18}FDG or supernatant of washed, radioactively labelled *L.m*. (Supplemental figure 10c-d) were used. The uptake of radioactive signal by the cardiac muscle using radioactively labelled *L.m.* as inoculum was comparable to the use of supernatant containing metabolized ^{18}FDG-6-phosphate (Supplemental figure 10e). It is thus likely that the observed signal in both kidneys and bladder do not stem from non-metabolized FDG, but from ^{18}FDG-6-phosphate, which has leaked from the radioactively labelled *L.m.*. The question how this leakage occurs, be it by active destruction of circulating or immobilized *L.m.* by partial complement lysis or

immune cells such as neutrophil granulocytes, or by passive escape from the bacterium itself, remains to be answered. The fact, that radioactive signal is measurable in the supernatant of washed radioactively labelled *L.m.* gives a first hint that the latter may be the case.

3.2 Characterization of *L.m.* – platelet complex formation

An aims of this thesis was to closer characterize the formation of *L.m.* – platelet complexes. *In vitro* investigation of complex formation in wild-type PRP revealed three phases consisting of *L.m.* opsonisation, *L.m.* – platelet complex formation depending on the presence of C3 and GPIb, and platelet aggregation around *L.m.* (see Figure 2-4, Figure 2-5). Complement opsonization *in vitro* was found to be predominantly facilitated via the alternative pathway of complement activation, since PRP of mice lacking Bf displayed a visible delay in the formation of *L.m.* – platelet complexes, prolonging the opsonization phase from approx. 1.5 min to over 6 min (see Figure 2-6). On the other hand, PRP lacking either C1q or C4, which are integral for the classical pathway of complement activation and the mannose-binding lectin pathway, displayed wild-type like kinetics of complex formation (see Figure 2-6). This is consistent with studies also concluding that complement opsonization of *L.m.* in mouse serum is predominantly due to alternative complement activation (van Kessel *et al.,* 1981; Drevets and Campbell, 1991). It is of note though that even in absence of Bf, complex formation was observable, albeit delayed, indicating the capacity of the other complement activation pathways to compensate for a lack of C3-activation via the alternative pathway *in vitro* (see Figure 2-6).

The binding of *L.m.* to platelets has been shown to be dependent on both C3 and GPIb (Verschoor *et al.,* 2011), but it was not revealed if they directly interact. It can be hypothesized that complex formation is due to a mediator protein and not direct interaction between C3 and GPIb. Alexander *et al.* described a membrane bound protein with the characteristics of fH as an integral part of the binding of C3b and thus complexing complement opsonized particles to platelets (Alexander *et al.,* 2001). Mice lacking fH have a strongly reduced plasma levels of C3 due to lacking regulation of the alternative complement convertase, in turn resulting in a hyper activation of C3 (Pickering *et al.,* 2007). Thus complement opsonization of *L.m.* in $fH^{-/-}$ plasma is inefficient and incomplete. To circumvent the lacking complement opsonization, plasma of mice expressing a mutated form of fH (fHΔ16-20), which lacks a binding site for C3b and thus displays impaired adhesion and complement regulatory functions while retaining plasma C3 levels (Pickering *et al.,* 2007), was used opsonize *L.m.* for one minute, a timeframe comparable to the time needed for complete opsonization with activated C3 in wild-type plasma (see Figure 2-2c). The opsonized *L.m.* were then used to examine *L.m.* – platelet

complex formation using light transmission platelet aggregometry (see Figure 2-9). It was observed that a lack of functional fH had no effect on the kinetics and quantity of *L.m.* – platelet binding, indicating that fH plays no essential role in the interaction between *L.m.* and platelets. Another candidate is vWF, a natural ligand of GPIb, which has been described to mediate platelet nucleation around *Bacillus cereus* on the surface of Kupffer cells (Wong *et al.,* 2013b). Incubation of *L.m.* in whole blood of mice lacking vWF led to formation of *L.m.* – platelet complexes (Supplemental figure 11), while intravital microscopy furthermore revealed wild-type like clearance kinetics in $vWF^{-/-}$ mice as well as the presence of *L.m.* – platelet complexes in the circulation seconds after systemic infection (Supplemental figure 12), indicating vWF to be dispensable for the interaction between *L.m.* and platelets in the bloodstream. Taken together, the data presented in this thesis could not confirm the necessity for a mediator between C3 and GPIb during the formation of *L.m.* – platelet complexes. Both described candidates, fH and vWF, were observed to be dispensable in the process of *L.m.* – platelet interaction. It may thus be that the interaction between C3 and GPIb is direct, which would potentially be in line with the findings of Quigg *et al*., who described a membrane protein on murine platelets with a size of 150 kDa, the size of GPIb, with an affinity to bind C3d (Quigg *et al.,* 1997). Experiments from our laboratory in mice lacking complement factor I, in which C3b is not degraded and thus no C3d is formed, revealed wild-type like *L.m.* – platelet complex formation (data not shown). This is a first hint that GPIb-C3d interaction is likely not the defining interaction during *L.m.* – platelet complex formation. To clarify if binding between C3 and GPIb happens directly and thus classify GPIb as a complement receptor in the murine system, ectopic expression of recombinant GPIb on the surface of cultured cells is an option. The addition of C3-coated particles could then reveal if binding is possible only in the presence of these two proteins.

Bacteria-platelet interaction, as observed in this thesis (see Figure 2-4) has been reported for a range of bacteria with platelets of various species. Clawson and White were the first to show that *Strep. pyogenes*, *Staph. aureus*, *Ent. faecalis* and *E. coli* were capable of adhering to rabbit platelets and induced aggregation (Clawson and White, 1971b, 1971a; Clawson, 1973; Clawson *et al.,* 1975). Others showed similar results for *Pseudomonas* (Kessler *et al.,* 1987) and *Salmonella* (Timmons *et al.,* 1986). These interactions can lead to a variety of outcomes: Interaction with platelets can induce phagocytosis of bacteria by other cell populations (Semple *et al.,* 2007), direct destruction of the pathogen by the platelet (Krijgsveld *et al.,* 2000) or the formation of neutrophil extracellular traps (NETs), in which neutrophil granulocytes disgorge DNA from their nucleus to form nets capable of capturing bacteria in flow (Brinkmann *et al.,* 2004). Interestingly, two bacteria species that have been observed to actively activate platelets rapidly and strongly are *Staph. aureus* and *P. aeruginosa*, both of which are known to induce thrombus formation *in vivo* after infection (Hawiger *et al.,* 1979; Coutinho *et al.,* 1988; Machado *et al.,* 2010). *Staph. aureus* and *P. aeruginosa* were also the two bacteria

species that, when preopsonized and used as inoculum in $C3^{-/-}CRIg^{-/-}$ mice, exhibited the shortest circulatory half-lives (see Figure 2-38 and Figure 2-39). While all other tested bacteria majorly remained in the bloodstream, over 50% of both *Staph. aureus* and *P. aeruginosa* stopped circulating within the first 10 min of infection. Thus there is a possibility that what was interpreted as removal of the bacteria from the bloodstream by hepatic Kupffer cells and other phagocytosing cell populations is partly due to a rapid formation of platelet aggregates resulting in thrombi, which then become lodged in the microvasculature. The use of PET-CT with *Staph. aureus* or *P. aeruginosa* could clarify if thrombi formation occurs on a large scale and is the cause of observed clearance from the bloodstream.

Interestingly, *L.m.* was also found to have a capacity to induce aggregation of rat platelets (Czuprynski and Balish, 1981). It was found that aggregation was dependent on plasma-mediated contact between *L.m.* and platelets. Also an approximately 2 min lag-time before aggregation started was described. These results fit the observations of this thesis very well. The plasma-mediated contact is interaction between C3 and GPIb (Verschoor *et al.,* 2011), the lag-time is similar as found in this thesis and due to the complement opsonization of *L.m.* (see Figure 2-4 and Figure 2-2c). The differentiation of *L.m.* – platelet interaction and platelet aggregation however was not described by Czuprynski and Balish. As to why can only be hypothesized. One explanation may be that the use of a 1:1 *L.m.* to platelet ratio, which in our hands led to a rapid induction of platelet aggregation after *L.m.* – platelet interaction, making the differentiation between complex formation and platelet aggregation nearly impossible (Supplemental figure 13). These data imply that the number of *L.m.* within an *L.m.* – platelet complex has a significant impact on the time it takes for surrounding platelets to become activated and form aggregates. This aggregative potential of *L.m.* is likely also a source of possible pathology in absence of Kupffer cell-mediated clearance of formed *L.m.* – platelet complexes. Similar as is described for *Staph. aureus* and *P. aeruginosa* (Hawiger *et al*., 1979; Coutinho *et al*., 1988; Machado *et al*., 2010), *L.m.* infection in mice depleted of Kupffer cells led to bacterial localization to the lung, occurring in hot-spot fashion consistent with embolism (see Figure 2-43). It can thus be speculated that all bacteria entering the bloodstream that can induce platelet aggregation will lead to the formation of thrombi in the microvasculature if Kupffer cell-mediated clearance of bacteria – platelet complexes is unable to clear formed complexes before true thrombi can form and lodge in the microvasculature.

Heat-inactivated *L.m.* failed to induce platelet aggregation as measured by aggregometry, just as *L.m.* lacking the expression of the virulence factor LLO (see Figure 2-10), while *L.m.* lacking the virulence factor ActA showed no variation from the wild-type control (see Supplemental figure 1). Since the process of heat inactivation is known to destroy conformational epitopes present on the bacterial surface, it is reasonable to assume the presence of LLO on *L.m.* is a facilitator of platelet aggregation. Additionally, it was observed in this thesis that the induction

of platelet aggregation is dependent on the presence of IgG (see Figure 2-7). It has been published that *L.m.* localization is different between μMT$^{-/-}$ mice, lacking all antibodies but also having vast alteration in splenic architecture, and naïve wild-type mice (Ochsenbein *et al.,* 1999), indicating the presence of natural antibodies capable of recognizing *L.m.*. It can be speculated that natural antibodies recognize a conformational epitope of surface expressed LLO on *L.m.* and thus activate surrounding platelets. Similar mechanisms of antibody-dependent platelet activation have been described for other bacteria: It has been reported that presence of IgG is necessary for *Strep. sanguinis* to induce aggregation of human platelets (McNicol *et al.,* 2006) and that the platelet Fc-receptor FcγRIIa is phosphorylated during this aggregation (Pampolina and McNicol, 2005). Further studies have revealed, that blocking antibodies targeted at FcγRIIa could inhibit platelet aggregation not only mediated by *Strep. sanguinis* (Ford *et al.,* 1997; Kerrigan *et al.,* 2002), but also by other bacteria such as *H. pylori* (Byrne *et al.,* 2003) and *Strep. pyogenes* (Kerrigan *et al.,* 2002). Interestingly, in the case of *Staph. aureus* it has been reported that activation of FcγRIIa via IgG is not enough to induce platelet aggregation, but that a secondary signal, such as the interaction of complement with a complement receptor, is needed (Miajlovic *et al.,* 2007). Since mice do not have Fc-receptors on platelets, this additionally could give the bacteria – platelet complex formation via C3-GPIb a potential role in previously described activation of binding platelets around the pathogen. Interestingly, heat-inactivated *L.m.* and *L.m.* lacking LLO-expression, which here were observed not to induce platelet aggregation, have been shown to induce little to no protective adaptive immune response when used for systemic infection in comparison to wild-type *L.m.* (Xiong *et al.,* 1998; Tanabe *et al.,* 1999). It was concluded that not the presence of LLO as an epitope for T-cell generation was important, but that a lack of LLO lead to a distinct lack of cytokine production in early stages of infection. Activated platelets have been described to present and secrete various chemokines and cytokines, including IL-1β, IL-8 and MIP-1α (Weyrich and Zimmerman, 2004) and upon binding to endothelial cells can induce the production of a broad array of proinflammatory molecules (Boehlen and Clemetson, 2001). Furthermore, it has been reported that platelets express CD40L upon activation (Henn *et al.,* 1998). Elzey *et al.* described that platelet-derived CD40L alone was sufficient to induce maturation of dendritic cells and augment CD8^{+} T-cell responses to infection with adenovirus (Elzey *et al.,* 2003). It is thus reasonable to hypothesize that LLO mediates platelet activation, which in turn helps shape the milieu for the induction of efficient T-cell immunity. These findings could give the process of platelet aggregation around circulating *L.m.* an important role in the shuttling of antigen to and the creation of niches of adaptive immunity induction.

3.3 Hepatic clearance of systemically circulating *L.m.*

This thesis found Kupffer cells to be the main facilitator of hepatic uptake of systemically circulating *L.m.* (see Figure 2-14). Depletion of Kupffer cells led to an abrogation in clearance of systemically circulating *L.m.* (see Figure 2-42). It has been described that depletion of Kupffer cells significantly reduced natural resistance of the host to bacterial infection, highlighting the importance of this cell population for control of circulating pathogens (Pinto *et al.,* 1991). In this thesis, two distinct mechanisms of Kupffer cell-mediated clearance of *L.m.* from the bloodstream were found: SRA-mediated uptake of nonopsonized *L.m.* and CRIg-mediated uptake of *L.m.* – platelet complexes. Kupffer cells have been described to consist of distinct subsets, depending on their origin: Kupffer cells, which derive from the bone marrow and migrate to the liver are discernible by their expression of CD11b and thus CR3, whereas Kupffer cells derived from primitive macrophages which infiltrated the foetal liver (and thus termed "liver-derived") do not express CD11b. Immature liver derived Kupffer cells have been reported to express CD32, which is lost during maturation. Both of these liver derived subsets express CRIg, but not CR3, whereas bone marrow derived Kupffer cells do not express CRIg (Kinoshita *et al.,* 2010; Ikarashi *et al.,* 2013). Both SRA-mediated and CRIg-mediated uptake of *L.m.* from the bloodstream was found to be facilitated the mature liver-derived $CD11b^{-}CD32^{-}$ Kupffer cells (see Figure 2-22 and Figure 2-29). While these two uptake mechanisms showed no overlap in function for nonopsonized *L.m.* and *L.m.* – platelet complexes (see Figure 2-35), opsonized bacteria could be cleared by both pathways (see Figure 2-40 and Figure 2-41).

The uptake of *L.m.* via SRA and CRIg on Kupffer cells is in line with the literature. It has been described, that SRA plays an important role in the clearance of *Staph. aureus* and *E. coli* from the bloodstream (Ono *et al.,* 2006) and also the importance of SRA for bloodstream clearance of *L.m.* has been described (Suzuki *et al.,* 1997; Ishiguro *et al.,* 2001), while the phagocytic capacity of CRIg on Kupffer cells was first described by Helmy *et al.,* 2006. The family of Class A Scavenger receptors consists of four members: SRA-1, SRA-2, SRA-3 and MARCO. SRA-1, SRA-2 and MARCO are functional PAMP recognizing receptors, while SRA-3 is an inert splice variant that is trapped in the endoplasmatic reticulum (Elomaa *et al.,* 1998). While SRA-1 and SRA-2 are expressed by Kupffer cells under resting conditions and thus are readily available to facilitate the clearance of circulating bacteria upon systemic infection (Naito *et al.,* 1992; Hughes *et al.,* 1995), expression of MARCO is not present in Kupffer cells under noninflamed conditions, but is upregulated upon recognition of bacterial infection (van der Laan *et al.,* 1999). It thus seems unlikely that MARCO contributes to the observed efficient SRA-mediated removal of circulating *L.m.* from the bloodstream and that this is accomplished by SRA-1 and SRA-2. In our hands, blocking of C-type lectins, be it type I, type II or both simultaneously, had no visible effect on circulation time of nonopsonized *L.m.* (see Figure 2-23). Although both classes have been described to be able of facilitating phagocytosis (Kerrigan and Brown, 2009),

this data indicates no dominant role for these PRRs in the early clearance of circulating *L.m.* from the bloodstream. Also, a pronounced role of TLRs, especially TLR2 and TLR4, which have been described as integral survival during bacterial infection (Flo *et al.,* 2000; Su *et al.,* 2000; Deng *et al.,* 2013), was not observed in terms of early clearance of pathogens from the bloodstream and restoration of sterile conditions in the blood. A mechanism in which TLRs could possibly become involved would be via a cooperative interaction with SRA, as has been described for the recognition of Hepatitis C virus via SRA-1 and TLR2 (Beauvillain *et al.,* 2010).

Furthermore, it was observed in this thesis that a lack of CRIg led to a reduction in hepatic uptake of *L.m.*, whereas bacterial numbers were increased in other screened organs, such as lung and spleen (see Figure 2-27). This finding is supported by the findings of Helmy *et al.*, where a similar phenotype was observed (Helmy *et al.,* 2006). This shift in bodily distribution was linked to the formation of *L.m.* – platelet complexes as underlying cause for the reduction in hepatic clearance of *L.m.* from the bloodstream (see Figure 2-33). Interestingly, it was found in this thesis that if complex formation is disrupted, a higher percentage of *L.m.* is found in the liver, but absolute numbers of retrieved *L.m.* are significantly decreased (See Figure 2-18). This may be due to different efficiencies of bactericidal activity of the SRA- or CRIg-dependent pathways. The collected data implies that SRA-mediated uptake in Kupffer cells leads to a faster destruction or inactivation of *L.m.* than CRIg-mediated uptake. Supporting literature can be found: Both of these surface receptors have been described as phagocytic and capable of inducing bacterial destruction (Haworth *et al.,* 1997; Helmy *et al.,* 2006; Gorgani *et al.,* 2008; Pluddemann *et al.,* 2009; Kim *et al.,* 2013), but interestingly a lack of SRA was reported to lead to increased numbers of *L.m.* in the liver even though initial clearance was similar to the wild-type (Suzuki *et al.,* 1997). Further investigation also revealed that *L.m.* phagocytosed by $SRA^{-/-}$ Kupffer cells were significantly more likely to escape the phagosome both *in vitro* and *in vivo* (Ishiguro *et al.,* 2001). So while it can be speculated that uptake of nonopsonized *L.m.* via SRAs mediates direct and efficient destruction of the circulating pathogen, the function of CRIg may be somewhat more complex: While absence of CRIg is detrimental to the host during systemic infection, as shown by Helmy *et al.* who observed a significant increase of lethality in $CRIg^{-/-}$ mice after systemic *L.m.* infection (Helmy *et al.,* 2006), the findings of Ishiguro *et al.* (Ishiguro *et al.,* 2001) and also of this thesis (see Figure 2-18) imply that *L.m.* removed from the circulation via CRIg survive longer after clearance from the bloodstream than *L.m.* cleared by SRA. As to why this is can only be speculated: One recent finding is that Kupffer cells undergo necroptosis after uptake of *L.m.* and thus induce the recruitment of monocytes (Bleriot *et al.,* 2015). It would be easy to hypothesize that this trade off of Kupffer cells for an enhanced innate immune response is due to CRIg mediated uptake and intracellular survival of *L.m.*. It has also been described that CRIg on a local level has the capacity to dampen adaptive immune responses, as it can act as a negative regulator of T-cell activation (Vogt *et al.,* 2006). Furthermore, a recent publication by Heymann *et al.* described that under

noninflammatory conditions, Kupffer cells-associated antigen presentation leads to expansion of Foxp3^{+} CD25^{+} regulatory T-cells and thus induction of tolerogenic immunity (Heymann *et al.,* 2015). It can thus be hypothesized that CRIg-mediated uptake of *L.m.* by CD11b^{-}CD32^{-} Kupffer cells initially directs the hepatic immune response towards innate immunity, inducing monocyte recruitment on the one hand and preventing hepatic T-cell activation on the other. A further indicator towards the induction of innate immunity by Kupffer cells is the well documented interaction between Kupffer cells and neutrophil granulocytes (Gregory and Wing, 1998; Gregory *et al.,* 2002), which was also observed *in vivo* in this thesis (see Figure 2-20) and will be discussed separately below.

How CRIg is capable of recognizing platelet-encased *L.m*., whereas SRA seemingly cannot reach the pathogen surface after *L.m.* have complexed to platelets, remains unclear. Interesting findings possibly pertaining to this are that complement is deposited on activated platelets (Del Conde *et al.,* 2005) and furthermore that platelets lacking expression of complement regulatory proteins DAF and Crry are opsonized with C3 and cleared in a CRIg-mediated mechanism by Kupffer cells (Kim *et al.,* 2008). Following these findings, it could be speculated that platelets in close contact with *L.m.* are also opsonized by complement due to the close proximity to the pathogen's surface and their eventual activation. However, the observed phenotype of efficient clearance of preopsonized *L.m.* from C3$^{-/-}$ mice (see Figure 2-25), where no endogenous C3 is present to additionally opsonize platelets, making this hypothesis unlikely. This data indicates that CRIg is still able to recognize the opsonized surface of the pathogen, even after the pathogen is covered by platelets. It thus remains speculation how CRIg gains access to the pathogens surface. One hypothesis would be that platelets indirectly enable the detection of C3 on the bacterial surface: P-selectin is a cell adhesion molecule presented on the surface of activated endothelial cells and platelets, and has been reported to lead to platelet sequestration in the liver upon presentation, i.e. during ischemia-reperfusion injury (Khandoga *et al.,* 2002). It has furthermore been described that activated Kupffer cells can modulate the expression of P-selectin in the liver (Shi *et al.,* 1998). It could thus be speculated that Kupffer cells induce P-selectin expression in the liver, which in turn arrests *L.m.* – platelet complexes in the liver sinusoids and enables Kupffer cells to probe the bacterial surface for C3. Another factor could simply be the size of resulting complexes: Along the lines of P-selectin interaction, the size on *L.m.* – platelet complexes alone could slow the speed during traverse of the hepatic sinusoids, allowing for CRIg to probe inside the complex to reach the bacterial surface covered with activated C3.

Intravital microscopy of hepatic *L.m.* uptake observed neutrophil granulocytes interacting with Kupffer cells after these had cleared *L.m.* from the circulation (see Figure 2-20), but *L.m.*$^{+}$ neutrophil granulocytes were only observed in presence of C3 (see Figure 2-16). Interaction between Kupffer cells and neutrophil granulocytes was first characterized by Gregory *et al.,*

2002. It was described as being CR3 dependent on the side of the Kupffer cell, though the influence of C3, which was observed as essential in this thesis, was not examined. Interestingly, CD11b, which is an integral part of CR3, is only expressed on the subset of $CD11b^{+}CD32^{-}$ Kupffer cells. Flow cytometry analysis revealed that while less cells of this population bound bacteria than $CD11b^{-}CD32^{-}$ Kupffer cells, still substantially more bound *L.m.* than the third population of $CD11b^{-}CD32^{+}$ Kupffer cells (see Figure 2-22). Surprisingly, binding of *L.m.* to these Kupffer cells was independent of platelet binding and complement opsonization, as there were no detectable differences in $GPIb^{-/-}$ or $C3^{-/-}$ mice compared to the wild-type. On the other hand, the uptake of *L.m.* by neutrophil granulocytes was strictly dependent on opsonization of *L.m.* with C3 (see Figure 2-16), confirming reported data that effective phagocytosis of bacteria by neutrophil granulocytes depends on C3b opsonization and CR3 expression (Xia *et al.,* 1999). It can be speculated, that the independence of C3 for uptake of *L.m.* by $CD11b^{+}CD32^{-}$ Kupffer cells is due to CR3 acting as a pattern recognition receptor and not as a complement receptor, recognizing parts of the bacterial cell wall directly, as has been described (Ross and Vetvicka, 1993).

$CD11b^{+}CD32^{-}$ Kupffer cells have been described as the primary hepatic source of the proinflammatory cytokines IL-1β, IL-6, IL-12 and TNF-α (Salkowski *et al.,* 1995; Gregory and Wing, 1998), all of which have been reported to play important roles in the recruitment and activation of neutrophil granulocytes (Moreno *et al.,* 2006; Miller *et al.,* 2007; Fielding *et al.,* 2008; Vieira *et al.,* 2009). The presence of CR3 and thus neutrophil granulocyte recruitment to the liver has been demonstrated to be negligible for early bacterial clearance, supporting the observed transient reduction on bacterial removal from the bloodstream in intravital microscopy observed in $CR3^{-/-}$ mice (Supplemental figure 14), but of major importance to combat hepatic infection at later timepoints (Rosen *et al.,* 1989). It can thus be speculated that the uptake of *L.m.* by $CD11b^{+}CD32^{-}$ Kupffer cells initiates another route of innate immune defence important for the clearance of hepatic infection. This could hypothetically make the liver-internal innate immune response a three-pronged approach: direct destruction of pathogens via SRA-mediated uptake by $CD11b^{-}CD32^{-}$ Kupffer cells, monocyte-recruitment via CRIg-mediated uptake by $CD11b^{-}CD32^{-}$ Kupffer cells and additionally the induction of an inflammatory milieu and recruitment of neutrophil granulocytes by $CD11b^{+}CD32^{-}$ Kupffer cells.

One aspect of neutrophil granulocyte induced immune response that was not examined in this thesis is the formation of NETs, composed of core DNA element to which antibacterial proteins from neutrophil granules can be attached (Brinkmann *et al.,* 2004). NETs have been linked to hepatic clearance of *E. coli* (Massberg *et al.,* 2010; McDonald *et al.,* 2012) and *Staph. aureus* (Kolaczkowska *et al.,* 2015) though in both cases, NET formation was observed after the bulk of removal of bacteria from the bloodstream had already occurred. These findings are

supported by the observation that depletion of neutrophil granulocytes via administration of α-GR1 antibody had no measurable effect on the overall clearance kinetics of systemically circulating *L.m.* (Supplemental figure 15). It thus seems likely that NET formation plays no major role in the initial clearance of *L.m.* from the bloodstream. Interestingly though, the formation of NETs is known to rely on interaction of activated platelets with neutrophil granulocytes (Zawrotniak and Rapala-Kozik, 2013). One such interaction relies on the presentation of HMGB1 on activated platelets, reported to induce NET formation in thrombosis (Maugeri *et al.,* 2014). Recognition of extracellular HMGB1 led to further recruitment of neutrophil granulocytes in dependence of CR3 (Orlova *et al.,* 2007). It could thus be speculated, that the observed CR3 dependent association of neutrophil granulocytes in the liver is associated with NET formation. To test this, the recognition of extracellular HMGB1 could be blocked *in vivo* by antibody administration (Scaffidi *et al.,* 2002). Another recently identified pathway of interaction relies on P-selectin presented on the platelet surface and PSGL-1 on neutrophils (Sreeramkumar *et al.,* 2014). The influence NETosis induced by P-selectin could also be investigated *in vivo* by use of α-PSGL-1 antibodies that block P-selectin induced signalling (Sreeramkumar *et al.,* 2014). Additionally to the specific blocking of one interaction leading to NET formation, NET formation as a whole can be disrupted by *in vivo* administration of DNase, which has been reported to dissolve NETs rapidly (McDonald *et al.,* 2012). Additionally, fluorescent detection of NETs during intravital microscopy can be obtained by the i.v. administration of antibodies targeting the histone protein H2Ax (McDonald *et al.,* 2012). Thus, given the multiple links of the induction of NET formation to observed (CR3) and potential (P-selectin) factors influencing bacterial clearance in the liver and the multiple avenues of approach, further investigation would be of interest.

Flow cytometry analysis performed in this thesis revealed B-cells in the liver to bind *L.m.* in wild-type animals (see Figure 2-15), which was found to be dependent on C3 deposition on the bacterial surface and the presence of CR2 on the B-cells. Recently, a hepatic population of B-cells was discovered by Nakashima *et al.* with the capacity of phagocytosing and lysing *E. coli* (Nakashima *et al.,* 2012). This phagocytosis was described as enhanced in the presence of fresh serum, in line with the C3 dependency of association found in this thesis, though no interacting receptor on the B-cell was described. Hepatic B-cells were also found to produce substantial amounts of the proinflammatory cytokines IFN-γ and IL-12 and only small quantities of IgM after stimulation with LPS (Matsumoto *et al.,* 2006). These findings, should they hold true for the model of systemic *L.m.* infection, would also give this population of hepatic B-cells a role in early development of an immune response to circulating pathogens. This could be investigated by measuring blood cytokine levels in presence and absence of hepatic B-cell – *L.m*. interaction, i.e. wild-type mice vs. CR1/2$^{-/-}$ mice.

L.m. immobilized on the surface of Kupffer cells were also observed to be encased by platelets from the circulation after immobilization, independent of the presence of C3 (see Figure 2-21). This phenotype has been described also for *B. cereus* (Wong *et al.,* 2013a). Platelet aggregation on the surface of Kupffer cells was shown to be dependent on surface presentation of vWF by the Kupffer cells, which interacted with GPIb on the platelet surface. Wong *et al.* further hypothesized that these encased bacteria could be removed from the Kupffer cell surface by shear forces and thus be the reason for circulating bacteria – platelet complexes. While the absence of platelet aggregate formation on the surface of Kupffer cells in $GPIb^{-/-}$ mice was also observed in this thesis (Supplemental figure 16), no budding of *L.m.* with encasing platelets into the circulation in wild-type or $C3^{-/-}$ mice was observed. Additionally, circulating *L.m.* – platelet complexes was observed in mice lacking vWF (see Supplemental figure 12) and *L.m.* – platelet complex formation was observed in the isolated *in vitro* setting of light transmission platelet aggregometry (see Figure 2-4). The results in this thesis thus indicate that complex formation between *L.m.* and platelets happens rapidly in the bloodstream and is independent of Kupffer cells.

The capacity of other pathogenic bacteria to form bacteria – platelet complexes dependent on C3 had been described by our lab previous to the start of this thesis (Verschoor *et al.,* 2011). In this thesis it was additionally revealed that the clearance of these bacteria – platelet complexes was facilitated by the same cell population as was the case for *L.m.* (see Figure 2-37) and that it was dependent on the presence of CRIg (see Figure 2-38 and Figure 2-39). Since $C3^{-/-}CRIg^{-/-}$ mice lacking C3 were used for the investigation of clearance kinetics, complement nonopsonized bacteria injected remained as such during circulation. While the clearance of bacteria – platelet complexes was abrogated due to an absence of CRIg, no statement can be made if SRA is the main facilitator of clearance of all nonopsonized bacteria from the bloodstream. It is of note that while the circulatory half-lives of all tested Gram (+) bacteria varied less than 0.1-fold from the half-life of nonopsonized *L.m.* in $C3^{-/-}CRIg^{-/-}$ mice, indicating a similar clearance mechanism, the half-lives of all tested Gram (-) bacteria, except *S. typhimurium*, were strikingly longer than the *L.m.* reference (see Table 3-1). This could be an indication for a mechanism other than SRA-mediated uptake by $CD11b^{-}CD32^{-}$ Kupffer cells by which these circulating Gram (-) bacteria are cleared when platelet binding does not occur, although it has been reported that SRA also play a role in the uptake of circulating *E. coli* by Kupffer cells (Ono *et al.,* 2006).

Table 3-1: Comparison of half-lives of nonopsonized bacteria vs. nonopsonized *L.m.* reference

Bacteria	Half-life (fold change vs. *L.m.*)	Bacteria	Half-life (fold change vs. *L.m.*)
L.m.	1 ± 0.08	*L.m.*	1 ± 0.08
B. subtilis	0.95 ± 0.06	*E. coli*	1.65 ± 0.32
Ent. faecalis	0.93 ± 0.06	*S. typhimurium*	0.91 ± 0.29
Staph. epidermidis	1.02 ± 0.05	*K. pneumoniae*	1.47 ± 0.21
Staph. aureus	1.02 ± 0.08	*P. aeruginosa*	1.21 ± 0.21

3.4 Biological significance

Intravital microscopy confirmed the previously observed phenotype of faster *L.m.* clearance from the bloodstream in absence of complex formation (see Figure 2-2 and Verschoor *et al.,* 2011). Faster clearance was found to be due to an increased uptake in the liver, reaching approx. 97% of the total inoculum and in turn reduced the number of bacteria capable of reaching all other investigated niches, such as spleen, lung and brain (see Figure 2-11). The efficient clearance and the liver's enormous capacity to take up bacteria via Kupffer cells displays that the liver alone is principally capable of completely removing systemically circulating bacteria from the bloodstream. This is supported by reports that splenectomised mice clear systemically circulating *L.m.* from the bloodstream as efficiently as non-splenectomised mice (Skamene and Chayasirisobhon, 1977). On the other hand, if hepatic clearance was reduced, here exemplified by clodronate treatment or a lack of the complement receptor CRIg, then a sharp increase in bacterial localization to other organs, especially the spleen and lung was observed (see Figure 2-27). The question comes up why the wild-type mouse would allow sub-optimal clearance, with hepatic clearance of circulating *L.m.* moderately reduced to approx. 90%, but splenic localization increased 2-3-fold when comparing wild-type clearance vs. clearance in $C3^{-/-}$ or $GPIb^{-/-}$ mice (see Figure 2-2). It is known that for the generation of protective adaptive immunity, in case of *L.m.* $CD8^+$ T-cells (Baldridge *et al.,* 1990), infection of $CD8\alpha^+$ DCs in the splenic marginal zone is essential (Belz *et al.,* 2005; Neuenhahn *et al.,* 2006; Edelson *et al.,* 2011). This impact of bacterial clearance speed in the liver on the targeting of *L.m.* to their splenic survival niche and the resulting induction of $CD8^+$ T-cell responses was investigated by Ann Plaumann in her dissertation titled "Factors influencing cellular targeting of Listeria monocytogenes in the mouse". It was observed that in absence of *L.m.* – platelet complex formation, i.e. $C3^{-/-}$ and $GPIb^{-/-}$ mice, less *L.m.* were capable of infecting $CD8\alpha^+$ DCs in the splenic marginal zone (Figure 3-1a, b). On the other hand, if hepatic clearance of circulating *L.m.* – platelet complexes was abrogated due to a lack of CRIg, a 5-10-fold increase in *L.m.* capable of infecting $CD8\alpha^+$ DCs was observed (Figure 3-1c).

This dependency of *L.m.* circulation time also directly translated to the induction of adaptive CD8$^+$ T-cell immune responses: Abrogation of *L.m.* – platelet complex formation and thus shortening the circulatory half-life of *L.m.* significantly reduced the number of recovered CD8$^+$ T-cells specific for the infection, while disrupting hepatic uptake of formed *L.m.* – platelet complexes significantly increased the number of infection-specific CD8$^+$ T-cells recovered (Figure 3-2).

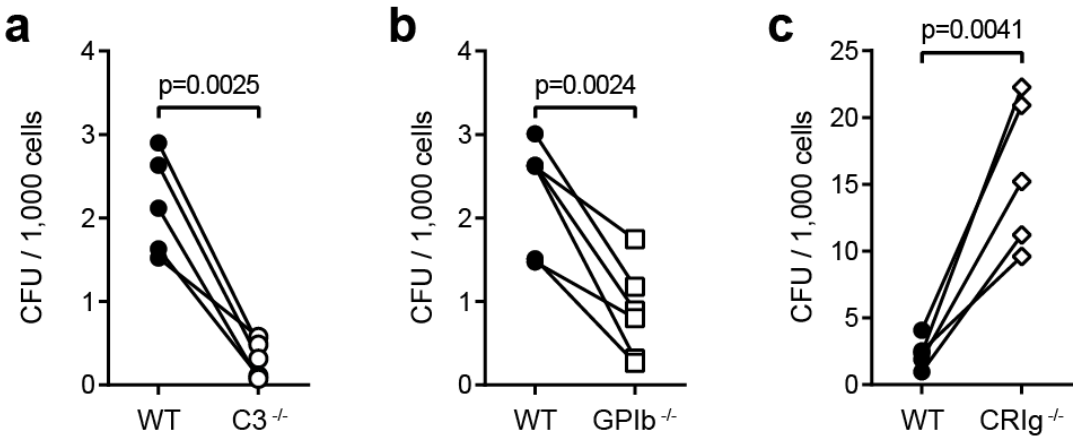

Figure 3-1 *L.m.* uptake in splenic CD8α$^+$ DCs is linked to circulation time of *L.m.* – platelet complexes
Mice were inoculated with 1x10^6 *L.m.* and spleens were harvested 1 h post infection. CD11c$^+$CD8a$^+$ DCs were FACS sorted, lysed and platelet for CFU detection. For each knock-out mouse one wild-type mouse of the same experiment was paired as control (5-6 mice per strain, P values indicated, Student's t-test). Experiments performed by Ann Plaumann and presented here with her kind permission.

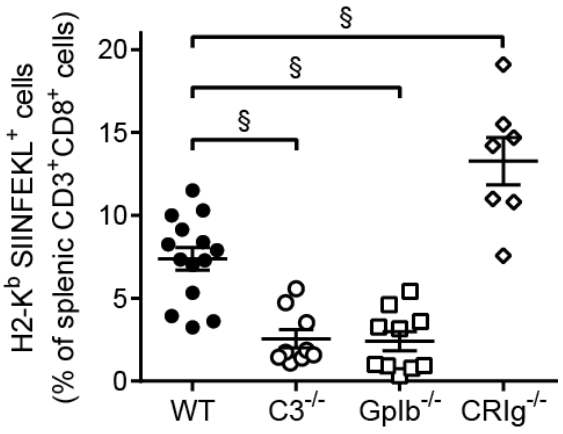

Figure 3-2 CD8$^+$ T-cell response depends on circulation time of *L.m.*
Mice were infected i.v. with the spreading-deficient ΔActA *L.m.*-OVA strain and sacrificed after 7 days. Spleen were removed, splenocytes isolated and the frequency of H2-Kb–SIINFEKL multimer$^+$ (OVA-specific) CD8$^+$ T-cells quantified by flow cytometry. Data represent at least 3 independent experiments per genotype. For statistical significance the groups of C3$^{-/-}$, GpIb$^{-/-}$ and CRIg$^{-/-}$ mice were compared with the corresponding wild-type control group (mean ± SD of 7-14 mice per strain, * = P < 0.05, # = P < 0.01, § = P < 0.001, One-way ANOVA with Bonferroni post-test adjustment). Experiments performed by Ann Plaumann and presented here with her very kind permission.

It thus seems as though liver and spleen compete for circulating antigen, on the one hand for immediate control of infection by efficient destruction in the liver and on the other hand for the induction of adaptive immunity by the generation of an adaptive immune response in the spleen. With this competition in mind, the separation of hepatic removal of circulating *L.m.* into two mechanism becomes reasonable: Initially, when higher numbers of pathogen are present in the circulation, SRA-mediated removal is highly efficient to reduce the number of circulating *L.m.*. With time hepatic clearance then shifts to a less efficient CRIg-mediated mechanism that allows for bacterial antigen to reach the splenic niche and thus the induction of adaptive immunity to the infection. This hypothesis is additionally supported by a study by Balmer *et al.*, in which the development of adaptive immunity against gut commensal bacteria during liver disease was investigated (Balmer *et al.,* 2014). During intestinal inflammation, breakdown products of gut commensal bacteria were detected in hepatic Kupffer cells, but no induction of systemic adaptive immunity was detected. But if intestinal inflammation was induced in mice suffering from non-alcoholic steatohepatitis, during which liver filtration of venous blood from the gut is impaired, both systemic circulation of commensal gut bacteria and the development of specific IgG targeted against these bacteria was detected. But the question remains that if induction of adaptive immunity in the spleen is improved in absence of CRIg-mediated hepatic clearance of circulating *L.m*., why does CRIg-mediated clearance exist at all? It has been reported that mice lacking CRIg succumb to doses as low as $5x10^4$ systemically circulating *L.m.*, while wild-type mice can control such inocula (Helmy *et al.,* 2006), indicating a tightly regulated balance between liver and spleen in the clearance of systemic *L.m.*. Additionally, it was observed in this thesis that lacking clearance of bacteria – platelet complexes may potentially lead to the formation of thrombi in the microvasculature of the lung (see Figure 2-43). Taking all data into account, it would seem as though the antigen-uptake in the spleen is purely determined by the efficiency of hepatic clearance or non-clearance. But one further factor potentially influencing bacterial localization has not yet been investigated: the size of the circulating bacteria vs. bacteria – platelet complex. It has been reported for rodents that the spleen is more efficient in the uptake of particles larger than 2 µm, while the liver preferentially removes smaller particles from the bloodstream (Moghimi *et al.,* 1993; Wiegand *et al.,* 2009). It is thus imaginable that the size alone of bacteria – platelet complexes, consisting of a bacterium of 1-2 µm and one or multiple platelets of approx. 0.5 µm, could shift uptake from liver to spleen. To test this, artificial “bacteria” – platelet complexes in different sizes could be administered, after which organ distribution would be examined. The complexes would consist of C3-opsonized polystyrene beads in different sizes, which readily bind blood platelets in dependence of GPIb (Supplemental figure 17). Fluorescent labelling of the beads would allow for flow cytometry analysis of organs and detection of distribution of the beads by cell population.

To sum up, the tightly regulated balance between liver clearance and splenic uptake allows enough bacterial antigen to reach the spleen to induce efficient T-cell priming and a robust adaptive immune response but at the same time limits bacterial localization to other compartments by efficiently capturing and destroying the majority of circulating *L.m.* in the liver. The division of labour between the bacteria killing liver and the immunity inducing spleen seems to ensure the best of both worlds: robust immunity with minimum risk.

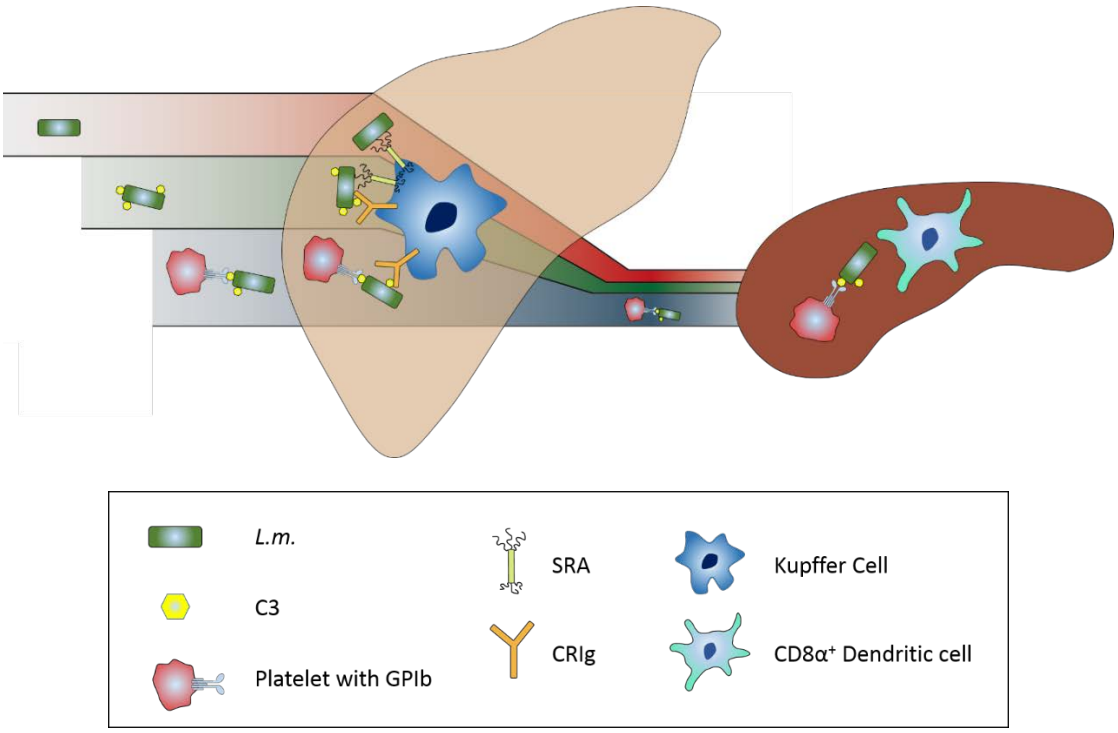

Illustration 3-1 Schematic representation of *L.m.* - clearance after systemic infection
After reaching the circulation, *L.m.* is opsonized and binds platelets via GPIb. The majority of circulating *L.m.* are cleared in the liver. Nonopsonized *L.m.* are cleared via SRA, platelet complexed *L.m.* are cleared via CRIg and opsonized *L.m.* are cleared by both phagocytic receptors. *L.m.* – platelet complexes are cleared slower than nonopsonized or opsonized *L.m.* and reach other organs, such as the spleen, to a higher degree. After reaching the spleen, *L.m.* – platelet complexes enter their survival niche of CD8α⁺ dendritic cells, propagate and are ultimately used to prime a robust adaptive immune response. Adapted from a schematic made by P. Rämer.

4 Material

4.1 Mouse strains

Table 4-1: Mouse strains used in this thesis

Strain	Background	Genotype	Reference	Source
wild-type	C57Bl/6	wild-type		In-house facility
$C3^{-/-}$	C57Bl/6	$C3^{-/-}$	(Wessels *et al.,* 1995)	In-house facility
$GPIb^{-/-}$	C57Bl/6	$GPIb\alpha^{-/-}hIL4R^{+}$	(Kanaji *et al.,* 2002)	In-house facility
$C1q^{-/-}$	C57Bl/6	$C1qa^{-/-}$	(Mitchell *et al.,* 2002)	In-house facility
$C4^{-/-}$	C57Bl/6	$C4^{-/-}$	(Wessels *et al.,* 1995)	In-house facility
$Bf^{-/-}$	C57Bl/6	$Bf^{-/-}$	(Matsumoto *et al.,* 1997)	In-house facility
$AID^{-/-}$	C57Bl/6	$AID^{-/-}$	(Muramatsu *et al.,* 2000)	In-house facility
$sIgM^{-/-}$	C57Bl/6	$sIgM^{-/-}$	(Boes *et al.,* 1998)	In-house facility
$AID^{-/-}sIgM^{-/-}$	C57Bl/6	$AID^{-/-}sIgM^{-/-}$	In-house breeding	In-house facility
$CR1/2^{-/-}$	C57Bl/6	$Cr2^{-/-}$	(Molina *et al.,* 1996)	In-house facility
$CR3^{-/-}$	C57Bl/6	$CD11b^{-/-}$	(Melo *et al.,* 2000)	In-house facility
$CR4^{-/-}$	C57Bl/6	$CD11c^{-/-}$	(Wu *et al.,* 2009)	In-house facility
$CRIg^{-/-}$	C57Bl/6	$CRIg^{-/-}$	(Helmy *et al.,* 2006)	In-house facility
$C3^{-/-}CRIg^{-/-}$	C57Bl/6	$C3^{-/-}CRIg^{-/-}$	In-house breeding	In-house facility
$GPIb^{-/-}CRIg^{-/-}$	C57Bl/6	$GPIb^{-/-}CRIg^{-/-}$	In-house breeding	In-house facility

4.2 Bacteria strains

Table 4-2: Bacteria strains used in this thesis

Species	Strain	Genotype	Source
Listeria monocytogenes	10403S	wild-type	In-house
Listeria monocytogenes	10403S	Δhly	(Bahjat *et al.,* 2006)
Listeria monocytogenes	10403S	ΔactA	(Bahjat *et al.,* 2006)
Bacillus subtilis	ATCC 6051	wild-type	In-house
Enterococcus faecalis	ATCC 29212	wild-type	In-house
Staphylococcus epidermidis	ATCC 12228	wild-type	In-house
Staphylococcus aureus	ATCC 25923	wild-type	In-house
Escherichia coli	ATCC 25922	wild-type	In-house
Salmonella enterica ssp. enterica sr. typhimurium	ATCC 13311	wild-type	In-house

Klebsiella pneumoniae	ATCC 13883	wild-type	In-house
Pseudomonas aeruginosa	ATCC 27853	wild-type	In-house

4.3 Chemicals

Arabinogalactan, >99 % purity	Sigma Aldrich
BHI (brain heart infusion) CM225	Oxoid
BSA (bovine serum albumin)	PAA Laboratories
Citric acid	Roth
CFSE cell proliferation dye	Sigma Aldrich
Cell tracker orange CMTMR dye	Life Technologies
Collagenase Type IV, 713 U/mg	Sigma Aldrich
DMEM, high glucose	PAA
DMSO, Hybri-Max, ≥99.7%	Sigma Aldrich
DNase Type I, 761 U/mg	Sigma Aldrich
EDTA	Sigma Aldrich
eFluor670 cell proliferation dye	eBioscience
FCS (fetal calf serum), heat-inactivated	PAA Laboratories
Fentanyl	CuraMed
FITC-Dextran (MW 20,000)	Sigma Aldrich
Gentamicin	PAA Laboratories
D(+)glucose	Sigma Aldrich
L-Glutamin	Roth
Glycerol	Roth
Heparin-Natrium-25000	Ratiopharm

HEPES, PUFFERAN® ≥99,5 %, CELLPURE®	Roth
Hoechst 33258	Sigma Aldrich
Ionomycin	Sigma Aldrich
KCl	Sigma Aldrich
KH_2PO_4	Sigma Aldrich
Lactoferrin	Sigma Aldrich
Mannan	Sigma Aldrich
Medetomidine	Pfizer
Microspheres, Flouresbrite YT carboxylate, 1 µm, excitation: 441nm, emission:486 nm	Polysciences
Midazolame	Ratiopharm
NaCl	Sigma Aldrich
$NaHCO_3$	Roth
Na_2HPO_4	Roth
N-Acetyl-D-glucosamine (GlcNAc)	Sigma Aldrich
NH_4Cl	Sigma Aldrich
Polycytidylic acid	Sigma Aldrich
Polyinosinic acid	Sigma Aldrich
Phorbol 12-myristate 13-acetate (PMA)	Sigma Aldrich
Propidium iodide (PI)	eBioscience
Refludan	Schering
RPMI 1640	PAA Laboratories
Sodium citrate	Sigma Aldrich
Tris	Sigma Aldrich
TRITC-Dextran	Sigma Aldrich

Triton X-100	Sigma Aldrich
Tryptophan Blue stain 0.4 %	Gibco
Tween20	AppliChem

4.4 Buffers and solutions

ACD Buffer	25 g/l Na-citrate; 13,64 g/l citric acid; 20 g/l D(+)glucose; pH adjusted to 4.69 with NaOH; sterile
Arabinogalactan stock solution	2 mg/ml in PBS; sterile
BHI medium	3.7 % (w/v) BHI in ddH_2O
Cell culture medium	500 ml RPMI supplemented with 25 ml SC^-, 50 ml heat-inactivated FCS
Collagenase stock solution	400 U/ml in cell culture medium
Collagenase-DNase-Mix	1 % (v/v) DNase stock solution, 2.5 % (v/v) Collagenase stock solution, 5 µg/ml Gentamicin in cell culture medium
DNase stock solution	0.01 % (w/v) DNase in cell culture medium; frozen in 200 µl single-use aliquots at -20 °C
EDTA buffer	0.5 M in ddH_2O, pH 7.2
Erythrocyte lysis buffer	0.15 M NH_4Cl, 17 mM Tris in ddH_2O, pH 7.2; stored at 4 °C
FACS buffer	0.5 % (w/v) BSA, 2mM EDTA in PBS
GlcNac stock solution	2 mg/ml in PBS; sterile
PI stock solution	0.2 % (w/v) in PBS; 2.5 ml aliquots stored at -20 °C
Polyinosinic/-cytidylic acid stock solution	4 mg/ml in PBS; sterile
Mannan stock solution	2 mg/ml in PBS; sterile
Narcotic MMF	5 mg/kg Midazolame; 0.5 mg/kg Medetomidine; 0.05 mg/kg Fentanyl

Narcotic Ketamin/Xylazin	100 mg/ml Ketamin; 125 mg/ml Xylazin
SC^-	100 mM HEPES, 27.4 mM L-Glutamine, 14.3 mM β-Mercaptoethanol in 1 l RPMI 1640, stored at -20 °C
Tyrodes-Buffer	1 g/l BSA; 1 g/l D(+)glucose; 100 ml 10x Tyrodes salts; 10 mM HEPES; ad 1 l with ddH_2O; pH adjusted to 7.4 with HCl
Tyrodes salts (10x)	80 g/l NaCl; 10.15 g/l NaHCO3; 1.95 g/l KCl; sterile

4.5 Antibodies

Table 4-3: Fluorescently labelled antibodies used for flow cytometry analysis of liver cells

Target	Host	Anti	Dye	Dilution	Source	Clone
Ly6C	Rat	Mouse	FITC	1:1000	BioLegend	HK1.4
F4/80	Rat	Mouse	PE	1:200	BioLegend	BM8
CD45	Rat	Mouse	PerCP-Cy5.5	1:200	BioLegend	30-F11
CD11b	Rat	Mouse	PE-Cy7	1:300	BioLegend	M1/70
CD19	Rat	Mouse	Brilliant Violet 570	1:300	BioLegend	6D5
Ly6G	Rat	Mouse	VioletFluor 450	1:300	Tonbo	1A8
CD16/32	Rat	Mouse	Alexa Fluor 647	1:500	BioLegend	93
CD3	Hamster	Mouse	PE-Cy7	1:200	BioLegend	145-2C11

Table 4-4: Fluorescently labelled antibodies used for flow cytometry analysis of lung cells

Target	Host	Anti	Dye	Dilution	Source	Clone
GR1	Rat	Mouse	FITC	1:1000	BioLegend	RB6-8C5
CD11c	Hamster	Mouse	PE	1:250	BioLegend	N418
CD45	Rat	Mouse	PerCP-Cy5.5	1:200	BioLegend	30-F11
CD11b	Rat	Mouse	PE-Cy7	1:300	BioLegend	M1/70
F4/80	Rat	Mouse	eFluor450	1:200	eBioscience	BM8

Table 4-5: Fluorescently labelled antibodies for intravital imaging

Target	Host	Anti	Dye/Conjugation	Dose	Source	Clone
F4/80	Rat	Mouse	eFluor450	5 µg	BioLegend	BM8
F4/80	Rat	Mouse	Alexa Fluor 488	5 µg	BioLegend	BM8

F4/80	Rat	Mouse	PE	5 µg	BioLegend	BM8
Ly6G	Rat	Mouse	Alexa Fluor 488	4 µg	BioLegend	1A8
Ly6G	Rat	Mouse	PE	4 µg	BioLegend	1A8
CD49b	Hamster	Mouse	Alexa Fluor 488	5 µg	BioLegend	HMa2
GPIbβ	Rat	Mouse	DyLight649	7 µg	Emfret	polyclonal

Table 4-6: Miscellaneous antibodies and fluorescent reagents used in this thesis

Target	Host	Anti	Dye/Conjugation	Dilution	Source	Clone
Fc Block	Rat	Mouse	-	1:200	Becton Dickinson	2.4G2
C3	Chicken	Human	Biotin	1:500	Cedarlane	polyclonal
Biotin	-	-	Streptavidin PE	1:500	Life technologies	-
CD41	Rat	Mouse	Alexa Fluor 488	1:400	BioLegend	MWReg30

4.6 Treatments

Depletion of	Depleting Agent	Source	Clone	Reference
Platelets	Rabbit anti-mouse Thrombocyte serum	Cedarlane	polyclonal	
Kupffer cells	Clodronate liposomes	ClodronateLiposomes.org	-	(van Rooijen and van Nieuwmegen, 1984)
Granulocytes	Rat anti mouse GR1	BioLegend	RB6-8C5	(Tepper *et al.,* 1992)

4.7 Equipment

Centrifuge Biofuge fresco	Heraeus
Centrifuge Multifuge 3 S-R	Heraeus
Counting chamber, depth 0.1 mm, 0.0025 m^2	Neubauer
Cryostat CM3050 S	Leica
CyAn ADP Lx	DakoCytomation
FACSCalibur	Becton Dickinson
Homogenisator ULTRA Turrax	IBA
Incubator Shaker Certomat IS	Sartorius
Incubator BB 6220	Heraeus
Inveon small-animal PET/CT scanner	Siemens Medical Solutions
Microscope Axiovert S100	Zeiss
MoFlo XDP cell sorter	Beckman Coulter
pH Meter MultiCal	WTW
BioPhotometer Plus	Eppendorf
Pipettes:	
2-1000 µl Lambda Plus single channel	Corning
100/300 µl Research plus multi channel	Eppendorf
Scale XB120A	Precisa
Vortexer	VWR International

4.8 Consumptive materials

Cell strainer 70 µm, 100 µm	Falcon
Glass pipette	

6-Well plate	Falcon
24-Well plate	Falcon
96-Well plate	Falcon
96-Well plate black	Thermo Scientific
Nylon net (FACS filter)	
Petri dish	Nunc
Syringe, 1 ml Sub-Q	Becton Dickinson
Tube 15 ml	Greiner bio-one
Tube 50 ml	Greiner bio-one

4.9 Software

Cell Quest Pro 5.2.1	Becton Dickinson
Flowjo 9.3.2	Flowjo Enterprise
ImageJ	National Institute of Health
Imaris	Bitplane
Imspector 4.7.1	LaVision Biotech
Prism 5.0.4	Graphpad
Summit 4.3	DakoCytomation

5 Methods

5.1 Bacterial cultivation and infection

5.1.1 Bacterial culture

I) *Listeria monocytogenes*

L.m. 10403S glycerol stock solutions were thawed and 5 µl were added to 10 ml BHI medium. Bacteria were then incubated at 37 °C and 90 rpm. *L.m.* were grown until an optical density at 600 nm (OD_{600}) of 0.05-0.2 had been reached, indicating logarithmic growth. For overnight cultures, *L.m.* were grown with a timer that changed the incubation temperature from 4 °C to 37 °C at a predetermined time point. OD was measured photometrical as light absorbance at 600 nm wavelength. In order to quantify the concentration of bacteria corresponding to the OD, standard curves had been established for the photometer. CFU per ml were calculated as: OD x 11 x 10^8.

II) *Bacillus subtilis*

B. subtilis ATCC 6051 was obtained from the Diagnostic Department of the Institute for Medical Microbiology, Immunology and Hygiene. Single colonies were used to inoculate an overnight culture grown at 30 °C and 180 rpm. The next morning, cells were diluted 1:100 and grown to an OD_{600} of 0.1-0.2. CFU per ml were calculated as: OD x 8 x 10^8.

III) *Enterococcus faecalis*

Ent. faecalis glycerol stock solution was thawed and 5 µl were added to 10 ml BHI media. Bacteria were incubated at 37 °C and 90 rpm until an OD_{600} of 0.05-0.2 was reached. For overnight cultures bacteria were grown with a timer that changed the incubation temperature from 4 °C to 37 °C to a given time point. CFU per ml were calculated as: OD x 5.2 x 10^8.

IV) *Staphylococcus aureus* and *Staphylococcus epidermidis*

Staph. aureus and *Staph. epidermidis* glycerol stock solutions were thawed and 5 µl were added to 10 ml BHI media. Bacteria were incubated at 37 °C and 90 rpm until an OD_{600} of 0.05-0.2 was reached. For overnight cultures bacteria were grown with a timer that changed the incubation temperature from 4 °C to 37 °C to a given time point. CFU per ml were calculated as: OD x 8.5 x 10^8.

V) *Escherichia coli*

E. coli ATCC 29522 was obtained from the Diagnostic Department of the Institute for Medical Microbiology, Immunology and Hygiene. Single colonies were used to inoculate an overnight culture grown at 37 °C and 180 rpm. The next morning, cells were diluted 1:100 and grown to an OD_{600} of 0.1-0.2. CFU per ml were calculated as: OD x 8 x 10^8.

VI) *Salmonella enterica* ssp*. enterica sr. typhimurium*

Salmonella enterica ssp*. enterica sr. typhimurium* ATCC 13311 was obtained from the Diagnostic Department of the Institute for Medical Microbiology, Immunology and Hygiene. Single colonies were used to inoculate an overnight culture grown at 37 °C and 180 rpm. The next morning, cells were diluted 1:100 and grown to an OD_{600} of 0.1-0.2. CFU per ml were calculated as: OD x 8 x 10^8.

VII) *Klebsiella pneumoniae*

K. pneumoniae ATCC 13883 was obtained from the Diagnostic Department of the Institute for Medical Microbiology, Immunology and Hygiene. Single colonies were used to inoculate an overnight culture grown at 37 °C and 180 rpm. The next morning, cells were diluted 1:100 and grown to an OD_{600} of 0.1-0.2. CFU per ml were calculated as: OD x 4 x 10^8.

VIII) *Pseudomonas aeruginosa*

P. aeruginosa ATCC 27853 was obtained from the Diagnostic Department of the Institute for Medical Microbiology, Immunology and Hygiene. Single colonies were used to inoculate an overnight culture grown at 37 °C and 180 rpm. The next morning, cells were diluted 1:100 and grown to an OD_{600} of 0.1-0.2. CFU per ml were calculated as: OD x 8 x 10^8.

5.1.2 Fluorescent labelling of Bacteria

Bacteria were grown as described in 5.1.1 and washed twice in 10 ml PBS by centrifugation at 4 °C and 13,000 x g for 5 min. Bacteria were then resuspended in PBS supplemented with 10% BHI medium at a concentration of 5x10^7 per ml and 5 µM cell proliferation dye (CFSE, CMTMR or eFluor670) was added. Bacteria were then incubated at 37 °C for 30 min and subsequently washed thrice in 10 ml PBS.

5.1.3 Heat inactivation of bacteria

Bacteria used for intravital imaging (*L.m.*, *Ent. faecalis*, *Staph. aureus* and *Staph. epidermidis*) were heat-inactivated before experiments. Bacteria were grown as described in 5.1.1 and washed twice in 10 ml PBS by centrifugation at 4 °C and 13,000 x g for 5 min and labelled with fluorescent dyes. Bacteria were then resuspended at a concentration of 1 x 10^{10} per ml and heat inactivated according to published protocols. *L.m.* was inactivated by shaken incubation for 90 min at 70 °C (Muraille *et al.,* 2005), *Ent. faecalis* was inactivated by shaken incubation at 90 °C for 60 min (Karygianni *et al.,* 2012), while both *Staph. aureus* and *epidermidis* were inactivated by shaken incubation at 90°C for 60 min (Ko *et al.,* 2013). Inactivation was confirmed by plating 1x10^8 bacteria on BHI-agar and incubation at 37 °C overnight.

5.1.4 Opsonization of bacteria

Wild-type mice were anaesthetized, treated with Refludan i.p. and blood was obtained from the retrobulbar venous plexus as described in 5.2.1. Blood plasma was isolated by centrifugation of the whole blood at 4 °C and 6,000 x g for 5 min. Pelleted, washed bacteria were resuspended in blood plasma (50µl plasma per 1x10^8 bacteria) and incubated at 37 °C for 10 min. Bacteria were subsequently washed thrice in 2 ml PBS at 4 °C and 13,000 x g for 3 min.

5.1.5 Preparation of infectious inoculum

Bacteria were grown and quantified as described in 5.1.1 and resuspended at a concentration of 5x10^8 per ml. Systemic infection was established by injection of 200 µl bacteria solution in the lateral tail vein with a 1-ml subcutaneous syringe in case of flow cytometry analysis of *ex vivo* clearance kinetic determination. In this case mice were pre-warmed by exposure to infrared light for 2 min to dilate the tail vein. When intravital multiphoton microscopy or PET/CT imaging was performed, a catheter was placed in the lateral tail vein and bacteria were injected at timepoint zero. Infectious dose was determined by plating serial dilutions of the inoculum on BHI agar. All dilution steps were performed on ice after repeated vortexing.

5.2 Platelet aggregometry

5.2.1 Bleeding of mice

Mice were anaesthetized by i.p. application of 200 µl Ketamine/Xylazin. Coagulation was inhibited by i.p. application of 100 µg Refludan in 100 µl sterile NaCl 10 min before blood was collected. After 3 min below an infrared lamp, mice were bled from the retrobulbar venous plexus using Pasteur pipettes coated with 0.5% bovine serum albumin (BSA) in PBS to prevent platelet activation. Blood was collected into 5 ml polystyrene tubes with 200µl Tyrode's buffer (pH 7.4) supplemented with 100 µg Refludan and 3 mM EDTA. After a total volume of 1 ml blood had been collected, mice were sacrificed by cervical dislocation.

5.2.2 Preparation of platelet rich plasma (PRP) and platelet poor plasma (PPP)

Isolated whole blood was centrifuged at room temperature and 60 x g for 20 min without brakes. The upper phase, consisting of platelets and plasma was isolated as PRP and the lower phase was again centrifuged at 3000 x g for 5 min. The upper phase consisting of plasma was isolated and used as PPP.

Platelet counts within PRP and PPP were determined by addition of 1 µl of PRP or PPP to 400 µl Tyrode's buffer (pH 7.4) containing $1x10^5$ YG-fluorescent polystyrene beads per µl. The ratio of platelets to beads was determined by flow cytometry and platelet concentration was calculated with the formula:

$$c(platelets) = 1x10^5 * \frac{n\,(platelets)}{n\,(YG\ beads)}$$

PPP was defined as containing less than $1x10^4$ platelets per µl, whereas PRP was adjusted to $5x10^5$ platelets per µl with PPP to ensure comparable platelet numbers between experiments and to retain physiological concentrations of plasma proteins.

5.2.3 Platelet aggregometry

Platelet aggregation was examined by an APACT 4S Plus from Diasys Greiner by measuring the turbidity of the sample. The formation of complexes or aggregates was determined by a reduction in optical density at 740 nm. PPP was used to calibrate the system to 100% aggregation. 200 µl PRP were used as experimental sample and placed in the light transmission aggregometer at 37 °C and 300 rpm. After equilibrium of optical density was reached (approx. 1 min), 3 mM manganese (Mn^{2+}) was added to the sample to free divalent

Ca^{2+} and Mg^{2+} complexed by EDTA and restore physiological platelet aggregation capacity. Mn^{2+} has an association constant K_a of $10^{13.8}$ in comparison to 10^{11} for Ca^{2+} and $10^{8.64}$ for Mg^{2+} and thus displaces both Ca^{2+} and Mg^{2+} from EDTA (Hart, 2000). At timepoint zero, $5x10^7$ *L.m.* were added to the sample and aggregation was observed for the following 20 min.

5.2.4 Fluorescence microscopy of aggregometry samples

To directly observe aggregation phases, fluorescence microscopy was use. At indicated timepoints, 3 µl samples were removed from the light transmission aggregometry samples containing $5x10^7$ CMTMR-labelled *L.m.* and diluted 1:150 into Tyrode's buffer supplemented with 10 mM EDTA to inhibit further formation of *L.m.* – platelet complexes or platelet activation and subsequent aggregation. Samples were vortexed briefly and α-CD41-Alexa Fluor 488 was added at a dilution of 1:400 to label platelets. After 30 min incubation at room temperature, 5 µl sample were transferred onto a slide and both labelled platelets and *L.m.* were visualized using a DMBR microscope (Leica) equipped with an AxioCam MRc with Axiovision software (Zeiss).

5.3 Intravital multiphoton laser scanning microscopy

Intravital microscopy was accomplished using a TrimScope II (LaVision Biotech) connected to an upright microscope (Olympus) equipped with a 10 W Chameleon Ultra II Ti:Sapphire laser (Coherent) and a 16× 0.80 NA water immersion objective (Nikon). Images were acquired at 800 nm excitation wavelength in a 200 x 200 µm (ear vasculature) or 300 x 300 µm (liver) frame with 512 x 512 pixels and detected by PMTs (G6780-20, Hamamatsu). ImSpector Pro (LaVision Biotech) was used as acquisition software. Additionally an environmental box was used to maintain a stable 37 °C environment throughout the imaging process.

5.3.1 Imaging of ear vasculature

Mice were anaesthetized with MMF and fixed on a custom-built stage to visualize the vasculature of the ear. The lateral tail vein was catheterized and blood flow visualization was achieved by administration of 100 µg TRITC-Dextran. To visualize circulating platelets, 4 µg αGPIbβ-Alexa Fluor 647 was given via the tail vein catheter 30 min before image acquisition. Image acquisition was started and mice were infected with either $1x10^8$ eFluor670- or CFSE-

labelled, heat-inactivated *L.m.* or a mixture of $5x10^7$ CFSE labelled-bacteria and $5x10^7$ eFLuor670-labelled, C3 coated bacteria. Image acquisition was performed as 2D time-lapse for a timeframe of 10 min post infection at a frame rate of 40 images per minute with a laser intensity of 3-5%. After image acquisition was finished, mice were sacrificed by cervical dislocation and livers were harvested for immunohistochemical analysis.

5.3.2 Calculation of clearance kinetic and circulatory half-life of bacteria

Acquired 2D time-lapse videos of the ear vasculature were imported into ImageJ (National Institute of Health) and discreet timeframes of 1 minute were defined from the timepoint of infection. Fluorescent bacteria in the circulation were quantified over 100 µm length of vessel for each timeframe and bacterial clearance for each timeframe was defined as:

$$L.m.clearance\ (\min X) = \ 100\% - (\frac{L.m.\ count\ (\min X)}{L.m.count\ (\min 1)} * 100\%\ )$$

Bacterial clearance kinetics were then imported into Prism 5.0.4 software (GraphPad) and nonlinearly fit to an exponential decay with the constraint Plateau = 100% Clearance. Circulatory half-lives were noted as half-life ± 95% confidence interval as calculated by the software.

5.3.3 Imaging of liver

Mice were anaesthetized with MMF narcotic and the lateral tail vein was catheterized. The mouse was fixed onto a custom built stage and body temperature was controlled with the help of a rectal probe. Physiological body temperature was ensured via the use of a heating plate. The abdomen was depilated using Asid-med depilatory cream (Asid-Bonz) and cotton buds. The peritoneal cavity was opened and the intestines were moved from the abdomen to adjacent moistened gauze. The left lateral lobe of the liver was fixed onto the lower stage using Histoacryl topical skin adhesive (B. Braun Melsungen) and gently moved approximately 5 mm into the now empty peritoneal cavity to reduce movement artefacts caused by breathing. A second stage, consisting of a small metal ring and an attached cover glass was placed gently onto the centre of the immobilized lobe and was used to image hepatic infection. If needed, fluorescently labelled antibodies were injected via the tail vein catheter 30 min before imaging. Used antibodies and dosage were: αF4/80-PE (5 µg), αF4/80-FITC (5 µg), αCD49b-Alexa Fluor 488 (5 µg) and αLy6G-PE (4 µg). Infectious inoculum, consisting of $1x10^8$ fluorescently labelled *L.m.*, was given during image acquisition via the tail vein catheter.

Images were acquired as 2D time-lapse for 20 min after infection. After image acquisition mice were sacrificed by cervical dislocation and livers were removed for immunohistochemical analysis. Single images were exported into Imaris 7.1.1 software (Bitplane) to construct computer renderings and surface projection images.

5.3.4 Immunohistochemical analysis of livers

Harvested livers were immediately embedded in Jung Tissue Freezing Medium (Leica) and snap-frozen. Samples were subsequently stored at -80 °C and shifted to -20 °C 12 h before cryosectioning. Organs were mounted on a cryostat holder, after which 10 µm sections were cut with a CM3050 S cryostat (Leica) and transferred to glass slides. Sections were air-dried at room temperature, acetone fixed at -20 °C for 2 min and stored at -80 °C. Sections were rehydrated for 15 min in PBS and incubated for another 15 min in blocking buffer containing 4 % BSA in PBS to mask unspecific binding epitopes. Slides were mounted on an immunostaining chamber and washed twice with 500 µl PBS supplemented with 0.5% BSA and 0.5% Tween. After washing, 150 µl Fc-Block (α-CD16/32) diluted 1:200 in washing buffer was added onto the sections and incubated for 15 min. Subsequently fluorescent labelling antibodies were added and incubated for 30 min at room temperature. Sections were washed repeatedly with washing buffer and incubated with nuclear counterstain Hoechst 33258 (1:500) for 2 min if required. Finally, sections were mounted with Roti-Mount FluorCare (Roth) and examined using a DMBR microscope (Leica) equipped with an AxioCam MRc with Axiovision software (Zeiss).

5.4 Detection of live *L.m.*

Mice were infected with $1x10^8$ *L.m.* prepared as described in 5.1.5 via direct injection into the tail vein using a 1 ml SubQ syringe (BD Medical). For the acquisition of clearance kinetics 50 µl blood samples were drawn from the retrobulbar plexus of the infected mouse 1, 3, 5 and 10 min post infection, diluted 1:10 in PBS supplemented with 10 mM EDTA and serial dilutions were plated on BHI agar. To detect live L.m. in various organs of the mouse, infected mice were sacrificed via cervical dislocation 15 min post infection and 10 µl blood were removed from the heart and diluted 1:10 into PBS supplemented with 10 mM EDTA. Brain, liver, spleen, both lungs and the right kidney were removed and weighed. Bone marrow cells were flushed from both femurs into 1 ml PBS. Whole organs and the left liver lobe were placed in a 2 ml tube filled with 0.7-1 ml of cold PBS. Tissue was minced with a homogenizer until no further organ pieces were visible. The homogenizer was cleaned between each sample in H_2O, 70%

ethanol and H_2O again to avoid contamination between the samples. Tubes were filled up with 0.1% Triton X in H_2O to 2 ml and vortexed for 1 min. A 1:10 dilution series was prepared for all homogenates in a 96-well plate as duplicates. 50 µl of each dilution step were plated for CFU detection and incubated overnight at 37 °C. For quantification, CFU per organ and CFU per g of organ were calculated. CFU per g organ of the liver were calculated for the weight of the whole organ. Additionally, the distribution of CFU in the organs was determined by dividing the sum of all recovered CFU by the number of CFU per organ.

5.5 PET-CT imaging of early *L.m.* infection

5.5.1 Preparation of infectious inoculum

L.m. were grown to logarithmic growth phase (OD_{600} = 0.1-0.2), pelleted at 13,000 x g for 5 min, resuspended in 10 ml PBS and incubated for 30 min. This procedure of washing, resuspension and incubation was repeated twice more. *L.m.* were then pelleted at 13,000 x g for 5 min and resuspended in 1 ml saline containing approximately 1 GBq/ml ^{18}FDG, provided by the Department of nuclear medicine of the Klinikum Rechts der Isar. *L.m.* were incubated for 90 min at 37 °C and 300 rpm in a table top incubator to allow for ^{18}FDG uptake. 400 µl BHI medium was added to the *L.m.* 10 min before end of the incubation. *L.m.* were washed four times with 1 ml BHI medium and finally resuspended in sterile saline at a concentration of $1x10^8$ *L.m.* per 200 µl. Incorporated radioactivity was measured before infection and generally was 4-6 MBq per $1x10^8$ *L.m.*.

5.5.2 PET imaging

Animals were imaged using an Inveon small-animal PET/CT scanner (Siemens Medical Solutions). Mice were anaesthetized using 1.5% isoflurane and breathing was monitored. Body temperature was maintained using a heating pad throughout the imaging procedure. Mice were infected with $1x10^8$ *L.m.* via a tail vein catheter. Dynamic PET images were acquired for 15 min starting at the time of infection. Image data were reconstructed using a 3D-filtered back-projection algorithm. The resulting matrix was 128 x 128 pixels with 159 transverse slices (voxel size of 0.78 x 0.78 x 0.80 mm^3). Data were normalised and corrected for randoms, dead time and decay. No corrections were made for attenuation or scatter.

5.5.3 CT imaging

CT angiography was performed in direct succession to PET imaging to determine anatomical locations. To obtain vascular contrast, 200 µl of iodinated intravascular contrast agent Imeron (Bracco Imaging) was injected. CT acquisition consisted of 270 projections acquired with an exposure time of 400 ms, X-ray voltage of 80 kVp and anode current of 400 µA for 360° rotation. Images were reconstructed using a modified Feldkamp algorithm and the resulting matrix was 256 x 256 pixels with 384 transverse slices (pixel size 0.17 x 0.17 x 0.17 mm). After CT acquisition was complete, mice were sacrificed by cervical dislocation, total body weight was weighed and liver, spleen, lung and kidneys were harvested and individually weighed.

5.5.4 Image analysis

PET and CT images were fused and analysed using an Inveon Research Workplace (Siemens). Image registration was done using an automatic weighted mutual information algorithm and confirmed visually on basis of anatomical landmarks showing physical accumulation of ^{18}FDG, such as liver, spleen, kidneys or bladder. For measurement of *L.m*. uptake, ROIs were manually drawn in the liver (3 separate ROIs), spleen, lung, vena cava, heart, kidneys, bladder, brain, intestine, and in the gluteus maximus. Activities were corrected for injected dose to calculate the percentage of injected dose per gram organ (%ID/g). In the case of the liver, the mean of all 3 ROIs was used to calculate %ID/g. This data was then again multiplied with the actual weight of the organs (or in case of blood with 10% of total body weight) to calculate the percent of injected dose per organ (%ID).

5.6 Flow cytometry

5.6.1 Isolation of liver cells

Mice were sacrificed by cervical dislocation and the abdominal cavity was opened. Livers were perfused by injection of 2 ml pre-warmed DNase-Collagenase-solution into the hepatic vein. The left lateral lobes were removed and digested in 6-well plates in 100 µm cell strainers and 6 ml DNase-Collagenase-solution supplemented with Gentamicin to prevent further spread of *L.m.* infection. Livers were mechanically disrupted by passing through the cell strainers after 10 min of incubation at 37 °C to obtain single cell suspensions. Following further 20 min of incubation cell suspensions were harvested into 15 ml tubes. Cell suspensions were centrifuged at 30 x g for 3 min and the supernatant was transferred to a fresh 15 ml tube. This removed hepatocytes from the cell suspension, leaving only non-parenchymal cells. Cells were

subsequently pelleted by centrifugation at 300 x g for 5 min and resuspended in 5 ml hypotonic buffer to lyse contained erythrocytes. After 7 min of incubation at room temperature 5 ml of chilled cell culture medium was added. Cells were subsequently pelleted at 300 x g for 5 min, cell pellet dry weights were weighed and resuspended to 0.1 g/ml in FACS Buffer.

5.6.2 Isolation of lung cells

Mice were sacrificed by cervical dislocation and the thoracic cavity was opened. Lungs were perfused by injection of 10 ml pre-warmed DNase-Collagenase-solution into the left ventricle of the heart. Lungs were removed and digested in 6-well plates in 100 µm cell strainers and 6 ml DNase-Collagenase-solution supplemented with Gentamicin to prevent further spread of *L.m.* infection. Lungs were mechanically disrupted by passing through the cell strainers after 30 min of incubation at 37 °C to obtain single cell suspensions. Following further 30 min of incubation cell suspensions were harvested into 15 ml tubes. Cells were pelleted by centrifugation at 300 x g for 5 min and resuspended in 5 ml hypotonic buffer to lyse contained erythrocytes. After 7 min of incubation at room temperature 5ml of chilled cell culture medium was added. Cells were subsequently pelleted at 300 x g for 5 min, resuspended in 10 ml cell culture medium and cells were quantified using a counting chamber and trypan blue to identify dead cells. Cell number was subsequently calculated as:

$$Cell\ number = cells\ per\ quadrant * 10^4 * dilution\ factor * volume$$

Cell concentration was adjusted to $1x10^8$ cells/ml with FACS buffer.

5.6.3 Surface staining of cells for flow cytometry analysis

Isolated cell suspensions were aliquoted into 96-well plates and pelleted at 300 x g for 2 min. Samples were resuspended in FACS buffer supplemented with 1:500 α-CD16/32 antibody (Fc block) and incubated for 15 min on ice. Fluorescent-conjugated antibodies were added and samples were incubated for another 30 min on ice in the dark. Liver samples were stained for the surface markers CD45, F4/80, Ly6C, Ly6G, CD19, CD3 and CD11c to detect $F4/80^+$ Kupffer cells, $Ly6C^+Ly6G^+$ neutrophil granulocytes, $Ly6G^-Ly6C^+$ monocytes, $CD19^+$ B-cells, $CD3^+$ T-cells and $CD11c^+$ dendritic cells. Lung samples were stained for the markers CD45, CD11b, CD11c and GR1 to detect $CD11c^{hi}CD11b^{lo}$ alveolar macrophages, $CD11c^{int}CD11b^{int}$ interstitial macrophages, $CD11b^{hi}GR1^{hi}$ neutrophil granulocytes and $CD11b^{hi}GR1^{int}$ monocytes as described in the literature (Vermaelen and Pauwels, 2004). Fluorescent-conjugated antibodies

were prepared in a master mix, which was further diluted 1:10 by addition to the cell suspensions. In order to adjust flow cytometer parameters, single-colour samples for each antibody as well as unstained samples were treated the same as multi-colour samples. After antibody incubation, FACS buffer was added to a volume of 200 µl. Cells were pelleted at 300 x g for 2 min and subsequently washed twice with 200 µl FACS buffer. To exclude dead cells from flow cytometry analysis, samples were resuspended in 50 µl FACS buffer with 1:500 PI and incubated for 2 min. This fluorescent dye visualizes the difference between intact DNA of living cells and partially fragmented DNA of dead or dying cells by binding to DNA proportional to its fragmentation (Nicoletti *et al.,* 1991). After incubation, cells were washed thrice with 200 µl FACS buffer, transferred to FACS tubes and analysed on a Cyan ADP Lx. Prior to analysis of the multi-colour sample the unstained and single-color samples were used to compensate for wavelength overlap of different fluorophores. Acquired data was analysed with FlowJo 9.3.2 software.

5.6.4 Fluorescent assisted cell sorting

Mice were infected with $1x10^7$ *L.m.* and sacrificed at indicated timepoints of 30 min or 1 h. Liver cells were isolated as described in 5.6.1. The staining procedure prior to cell sorting was identical to the preparation of samples for conventional flow cytometry analysis. Fluorescently labelled antibodies used were αCD45-PerCP Cy5.5, αLy6G-VioletFluor450, αCD19-Brilliant Violet 570 and αF4/80-PE to identify $Ly6G^+$ neutrophil granulocytes, $CD19^+$ B-cells and $F4/80^+$ Kupffer cells (see Table 4-3). Before the multi-colour sample was injected to the cell sorter, unstained and single-stained controls were used for automatic compensation. The cell sorter MoFlo was used. The gating strategy to sort liver populations is summarized in Figure 2-14. Sorted cells were collected in 5 ml tubes that contained 1 ml heat-inactivated FCS, and were filled up to 3.5 -4 ml with FACS buffer to coat the inner surface of the tube in order to avoid cell rupture during the sorting procedure.

FACS-sorted cell suspensions were centrifuged at 300 x g and 4 °C for 10 min, after which the supernatant was removed carefully. Cells were resuspended in exactly 100 µl PBS and lysed by addition of 100 µl 0.1% Triton X in H_2O solution and intensive vortexing for 1 min. The cell lysate was plated as triplet of 50 µl each on BHI Agar plates. Collected supernatants were centrifuged for 10 min at 13.000 rpm in order to obtain bacteria from cells disrupted after sorting, and resuspended in 30 µl 0.1% Triton X in H_2O. Resuspended supernatants of each sample were pooled and completely plated on one BHI plate. To determine CFU, the plates were incubated over night at 37 °C. Grown colonies were counted and the mean value of a plated triplet was quantified by division of the CFU number per subpopulation through the

number of cells of that population counted during cell sorting. CFU from the plated supernatants were divided by 4 and added to the corresponding triplet of cell lysate CFU.

5.7 Data analysis and statistical significance

Data was analysed using the software Prism 5.0.4 (Graphpad). Data are presented as mean ± standard deviation (SD) unless stated otherwise. Significance levels were determined using an appropriate statistical test for each experimental setup and are stated in the figure legends.

6 Supplement

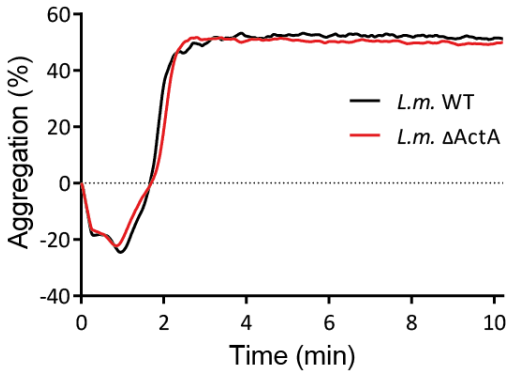

Supplemental figure 1 Expression of ActA has no effect on the formation of *in vivo* like *L.m.* – platelet complexes or platelet activation
PRP was isolated from wild-type mice and platelet count adjusted to $5x10^5$/µl with plasma of the same strain. $5x10^7$ ΔActA *L.m.* were added at time point 0 and aggregation was observed for 10 min.

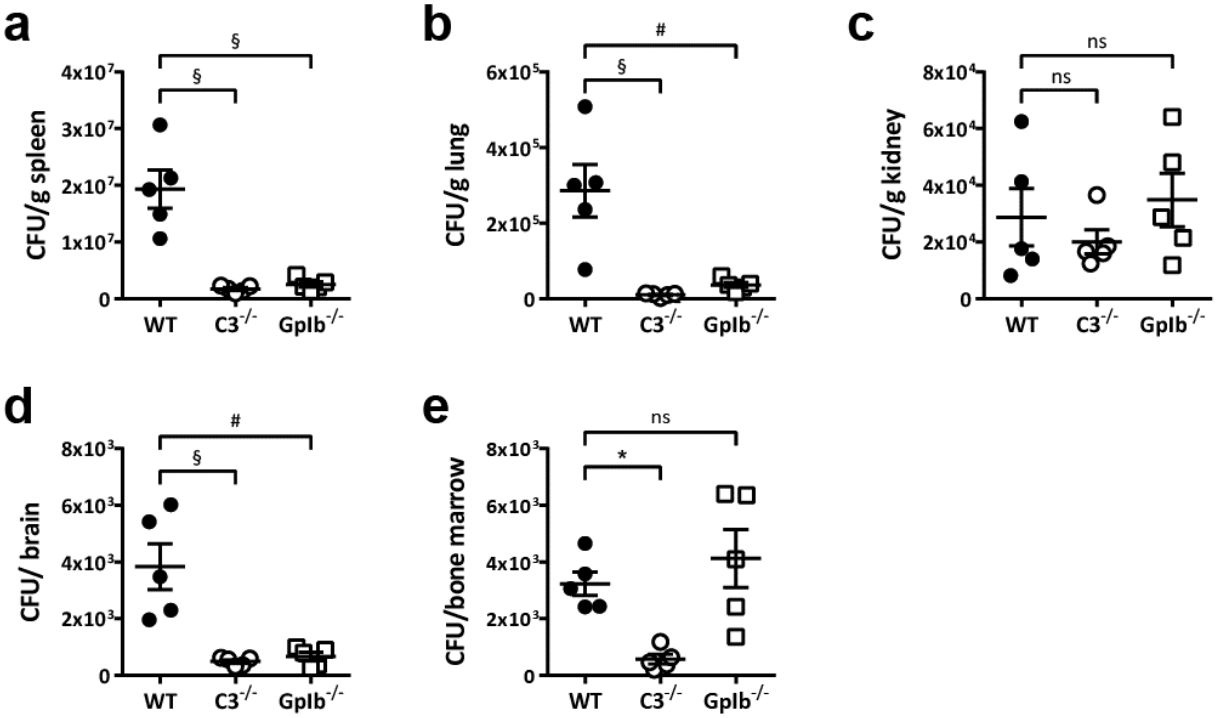

Supplemental figure 2 Distribution of *L.m.* 15 min after infection
WT, $C3^{-/-}$ and $GPIb^{-/-}$ mice were infected with $1x10^8$ *L.m.* i.v.. 15 min post infection liver, spleen, lung, kidney, brain, bone marrow and blood samples were harvested, homogenized and plated for CFU detection. Number of *L.m.* recovered from **(a)** spleen **(b)** lung **(c)** kidney **(d)** brain and **(e)** bone marrow (mean ± SEM of 5 mice per strain, * = $P < 0.05$, # = $P < 0.01$, § = $P < 0.001$, One-way ANOVA with Tukey post-test adjustment). Experiments performed in cooperation with Ann Plaumann.

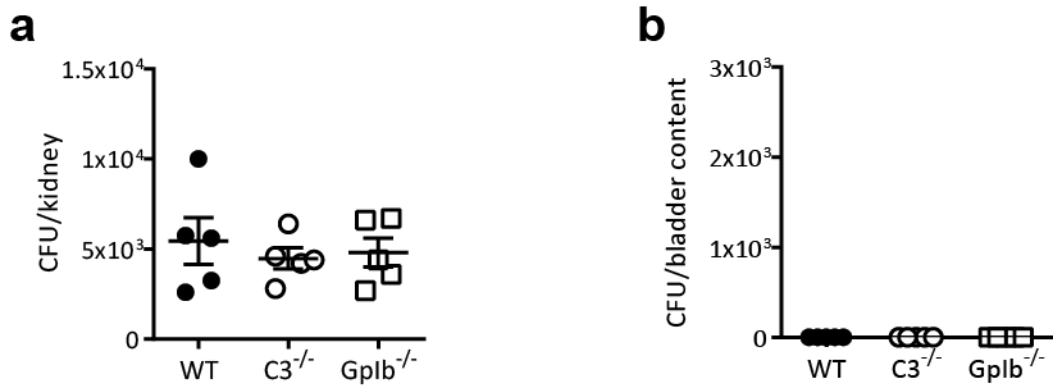

Supplemental figure 3 Control plating of homogenized kidneys or bladder content
Serial dilution of kidney homogenates and bladder content of mice infected with 1x10^8 radioactively labelled *L.m.* were plated on BHI agar, incubated overnight and enumerated.

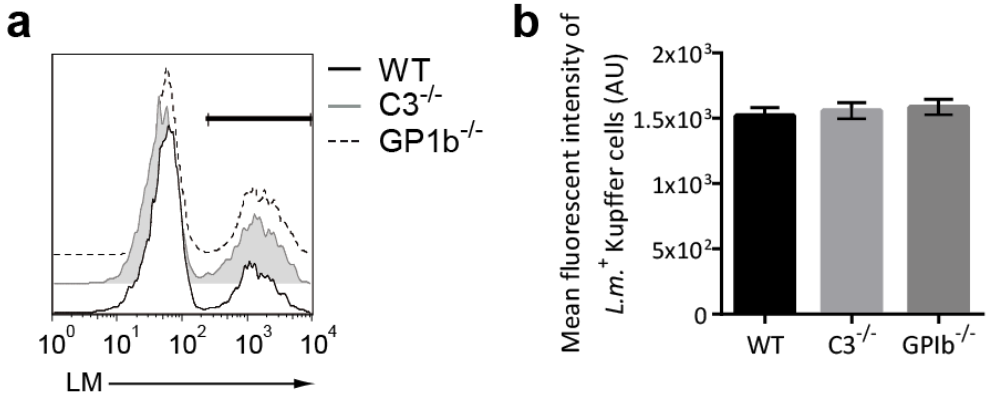

Supplemental figure 4 Flow cytometry analysis of hepatic Kupffer cells
Wild-type, C3$^{-/-}$ and GPIb$^{-/-}$ mice were infected with 1x10^8 eFLuor670-labelled *L.m.*. 15 min post infection, hepatic non-parenchymal cells were isolated and analysed for *L.m.* uptake via flow cytometry **(a)** Histogram of *L.m.* uptake in F4/80$^+$ Kupffer cells after infection **(b)** Quantification of mean fluorescence intensity of *L.m.* uptake in wild-type, C3$^{-/-}$ and GPIb$^{-/-}$ Kupffer cells (mean ± SD of 4 mice per strain).

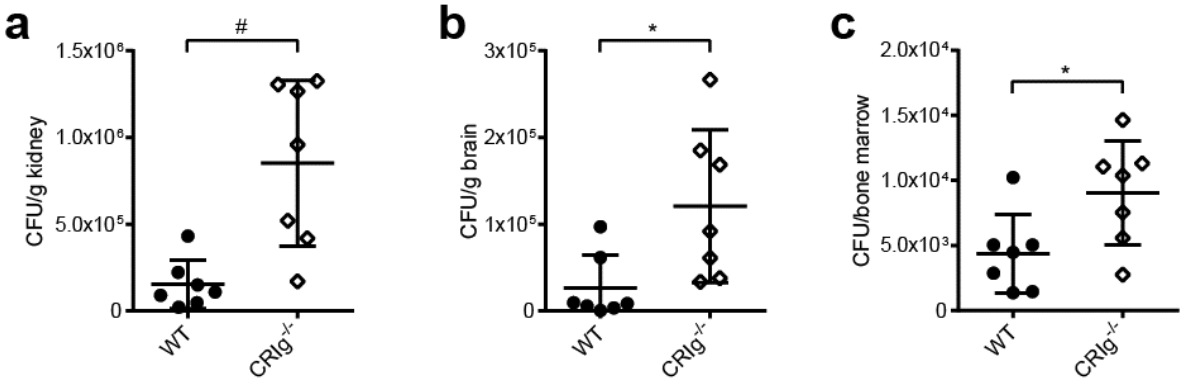

Supplemental figure 5 Distribution of *L.m.* 15 min after infection in CRIg$^{-/-}$ mice
WT and CRIg$^{-/-}$ mice were infected with 1x10^8 *L.m.* i.v.. 15 min post infection liver, spleen, lung, kidney, brain, bone marrow and blood samples were harvested, homogenized and plated for CFU detection. Number of *L.m.* recovered from **(a)** kidney **(d)** brain and **(e)** bone marrow (mean ± SEM of 7 mice per strain, * = P < 0.05, # = P < 0.01, § = P < 0.001, One-way ANOVA with Tukey post-test adjustment). Experiments performed in cooperation with Ann Plaumann.

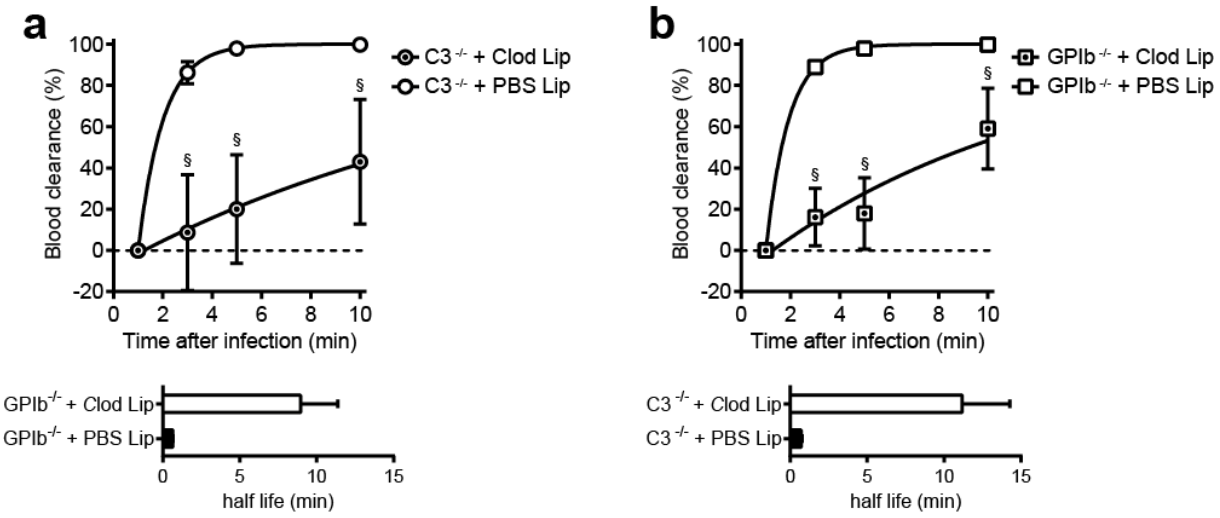

Supplemental figure 6 Depletion of Kupffer cells strongly reduces clearance of systemically circulating *L.m.* in both C3$^{-/-}$ and GPIb$^{-/-}$ mice

Clearance kinetic and circulatory half-life of systemic *L.m.* in **(a)** C3$^{-/-}$ and **(b)** GPIb$^{-/-}$ mice depleted of Kupffer cells 48 h prior to infection (mean ± SD of 4 mice per treatment, * = P < 0.05, # = P < 0.01, § = P < 0.001, Two-way ANOVA with Bonferroni post-test adjustment and two-tailed Student's t-test).

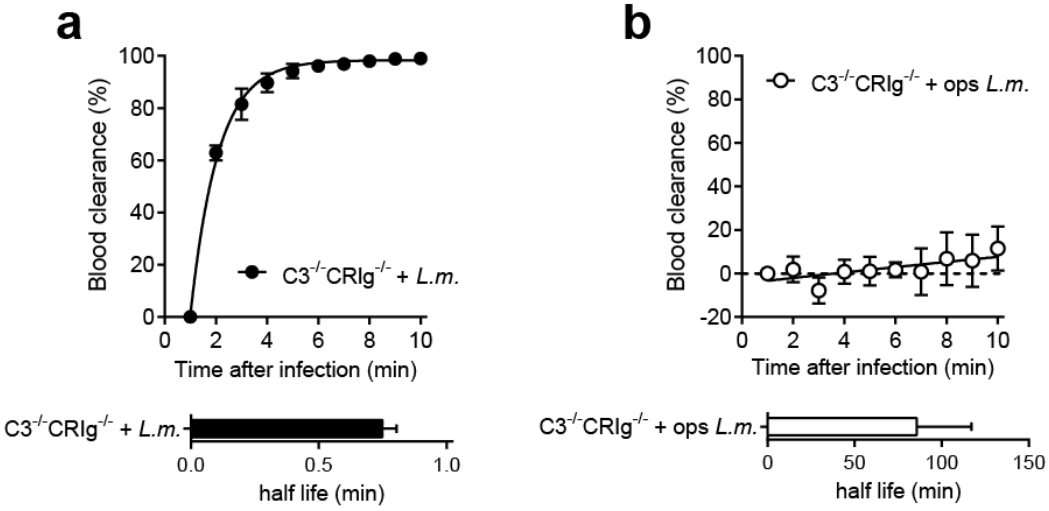

Supplemental figure 7 Bacterial populations do not influence clearance of each other

C3$^{-/-}$CRIg$^{-/-}$ were infected with either **(a)** 5x10^7 nonopsonized *L.m.* or **(b)** 5x10^7 preopsonized *L.m.*. Clearance kinetic and circulatory half-life were calculated using intravital microscopy of the ear vasculature (mean ± SD of 4 mice, * = P < 0.05, # = P < 0.01, § = P < 0.001, Two-way ANOVA with Bonferroni post-test adjustment and two-tailed Student's t-test).

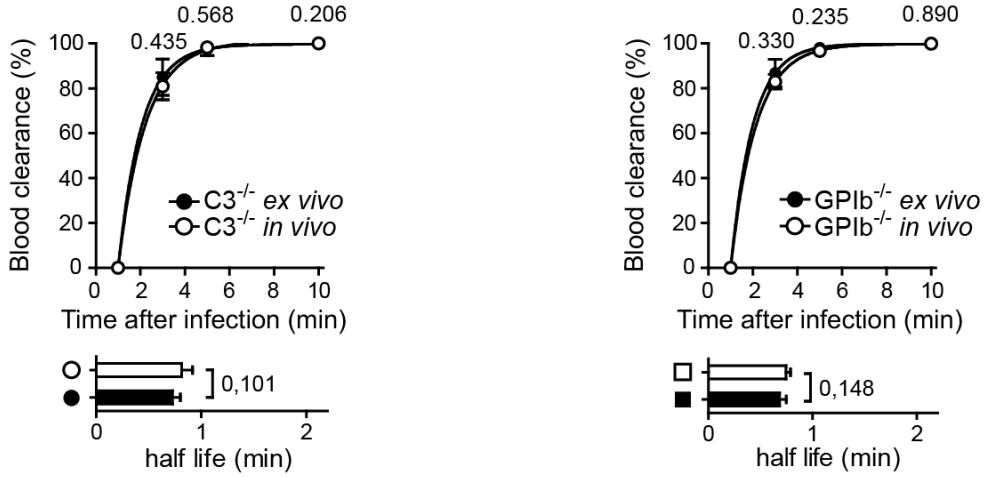

Supplemental figure 8 Comparison of clearance kinetics as quantified by *in vivo* vs. *ex vivo* methods for C3$^{-/-}$ and GPIb$^{-/-}$
Comparison of clearance kinetics acquired via *in vivo* microscopy and *ex vivo* plating of blood samples drawn at 1, 3, 5 and 10 min post infection (mean ± SD for 4 mice via intravital microscopy and 10 mice for *ex vivo* plating of blood samples, P values indicated, Two-way ANOVA with Bonferroni post-test adjustment and two-tailed Student's t-test).

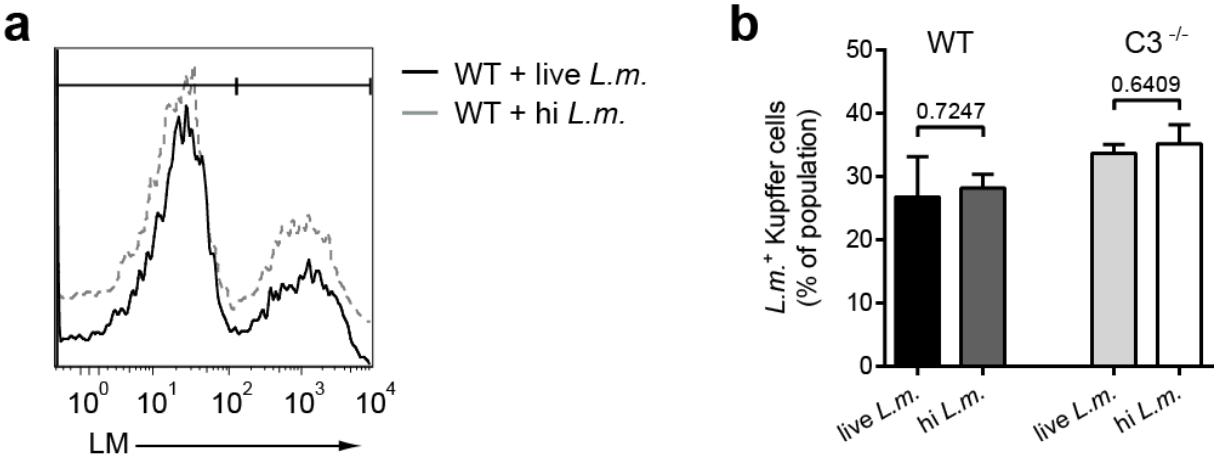

Supplemental figure 9 Hepatic uptake of live and heat-inactivated *L.m.* by Kupffer cells
Wild-type and C3$^{-/-}$ mice were infected with either 1x10^8 live, eFluor670-labelled *L.m.* or 1x10^8 heat-inactivated (hi), eFluor670-labelled *L.m.*. Livers were removed 15 min post infection, hepatic nonparenchymal cells were isolated and analysed via flow cytometry. **(a)** Representative histogram, pregated on CD45$^+$ F4/80$^+$ cells, displaying Kupffer cell uptake of live and hi *L.m.* in wild-type mice. **(b)** Quantification of *L.m.* uptake by Kupffer cells in wild-type and C3$^{-/-}$ mice (mean ± SD for 4-10 mice per strain and *L.m.* state, P values indicated, two-tailed Student's t-test).

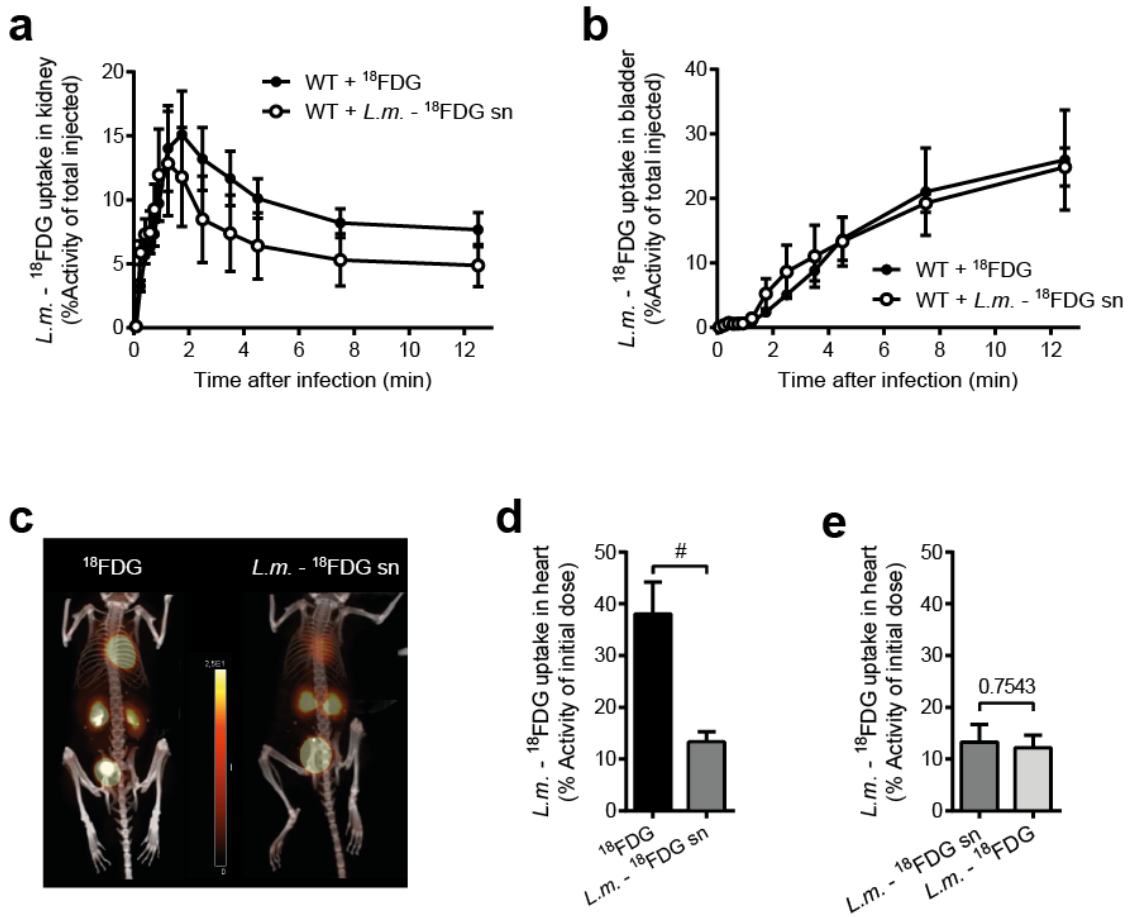

Supplemental figure 10 PET-CT imaging of ^{18}FDG and *L.m.* – ^{18}FDG supernatant uptake
Wild-type mice were injected with either 5 MBq of ^{18}FDG or supernatant (sn) of washed *L.m.* – ^{18}FDG and uptake of radioactive signal in **(a)** kidneys and **(b)** bladder was measured. **(c)** Detected radioactive uptake 15 min post infection. **(d,e)** Uptake of radioactive signal in the cardiac muscle for ^{18}FDG, *L.m.* – ^{18}FDG supernatant and *L.m.* – ^{18}FDG (mean ± SD of 3-4 animals per inoculum, P values indicated, two-tailed Student's t-test).

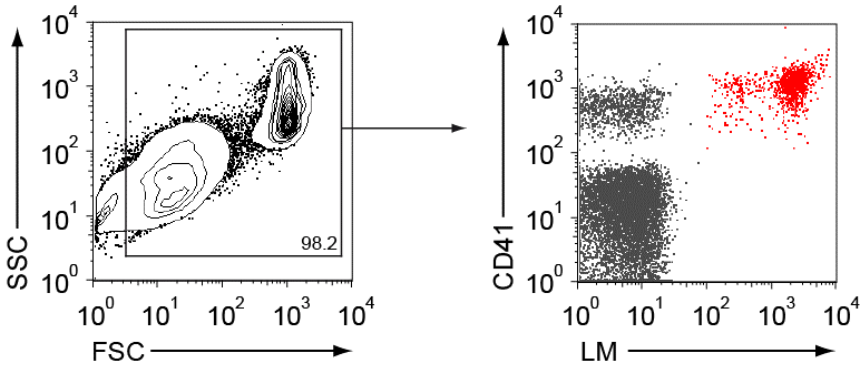

Supplemental figure 11 Formation of *L.m.* – platelet complexes in vWF$^{-/-}$ blood
1x10^6 CFSE-labelled *L.m.* were added to 500 µl whole blood isolated from vWF$^{-/-}$ mice and incubated for 1 min. Blood was diluted 1:500, αCD41-PECy7 was added to label platelets and staining was performed for 15 min at RT after which the sample was analysed by flow cytometry (*L.m.* indicated in red).

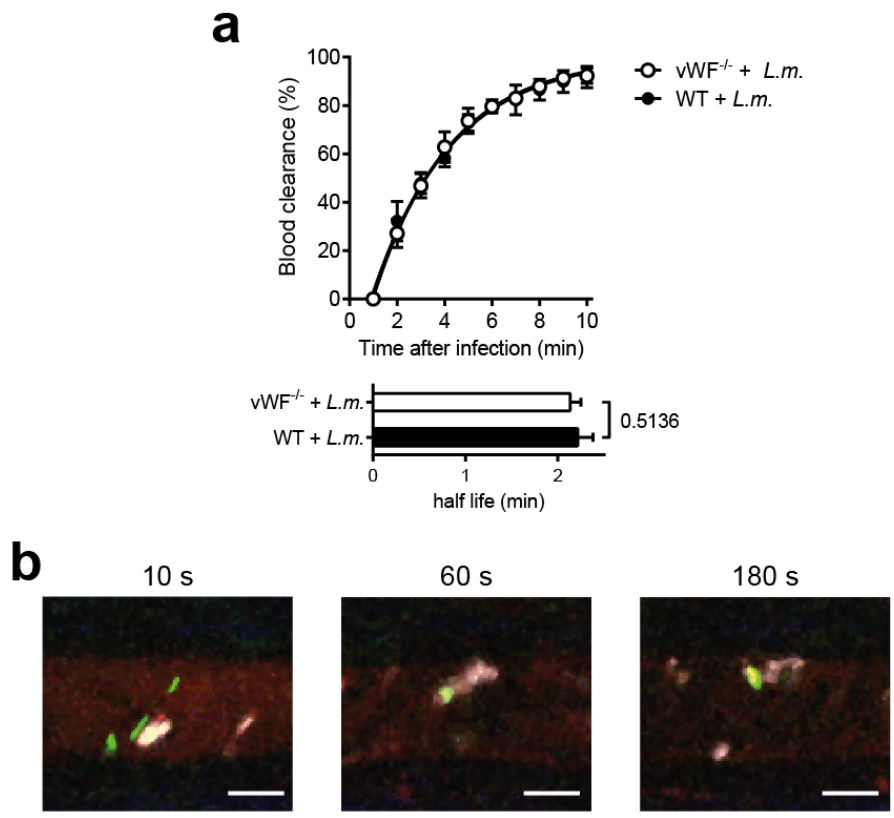

Supplemental figure 12 Lack of von-Willebrand factor does not influence systemic clearance or *L.m.* – platelet complex formation *in vivo*

(a) Wild-type and vWF$^{-/-}$ mice were infected with 1x10^{8} CFSE-labelled *L.m.*, where after systemic clearance kinetics were recorded via intravital microscopy (mean ± SD of 3 mice, * = P < 0.05, # = P < 0.01, § = P < 0.001, Two-way ANOVA with Bonferroni post-test adjustment and two-tailed Student's t-test). **(b)** Representative still images depicting formed *L.m.* – platelet complexes in the circulation of vWF$^{-/-}$ mice at various timepoints after infection (green = CFSE-*L.m.*, red = TRITC-dextran, white = platelets, scale bar = 5 µm).

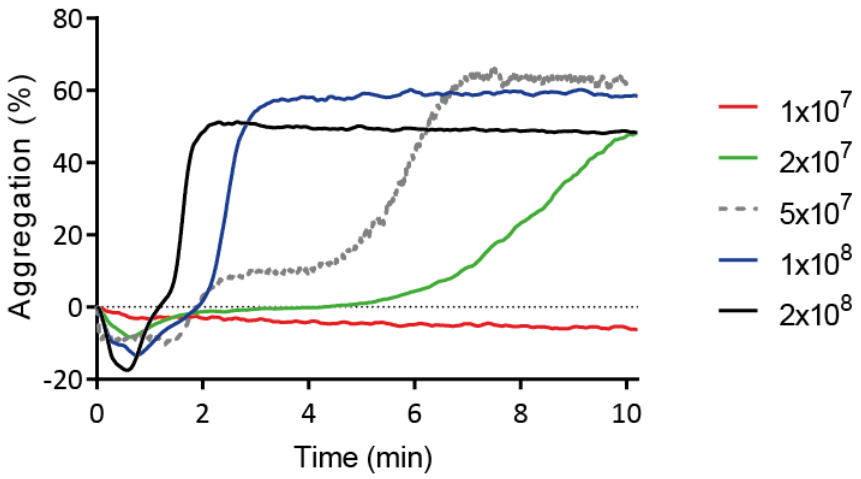

Supplemental figure 13 Titration of *L.m.* for light transmission platelet aggregometry

L.m. numbers of 1x10^{7} to 2x10^{8} were added to 1x10^{8} murine platelets in 200 µl PRP (time = 0), resulting in platelet : *L.m.* ratios of 10:1 to 1:2, and aggregation was measured over a time of 10 min.

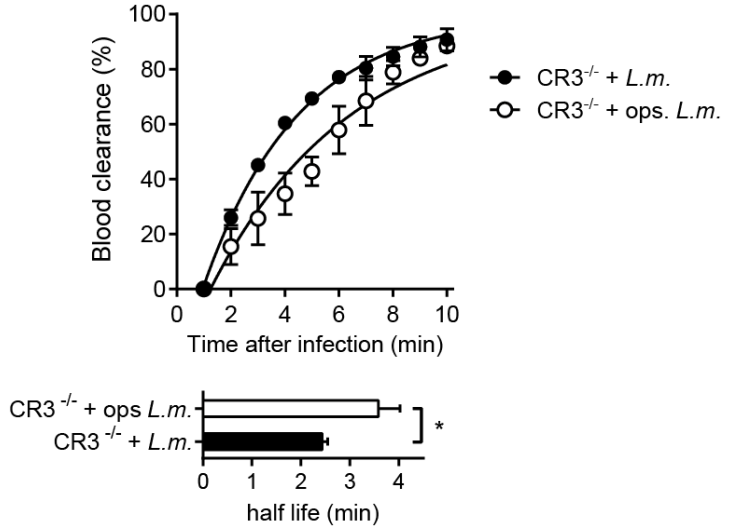

Supplemental figure 14 Clearance of preopsonized *L.m.* is slightly impaired in CR3$^{-/-}$ mice
CR3$^{-/-}$ mice were infected with 5x10^7 nonopsonized CFSE-labelled *L.m.* and 5x10^7 preopsonized eFluor670-labelled *L.m.* and clearance kinetic and circulatory half-life were determined via intravital microscopy (mean ± SD of 3 mice, * = P < 0.05, # = P < 0.01, § = P < 0.001, Two-way ANOVA with Bonferroni post-test adjustment and two-tailed Student's t-test).

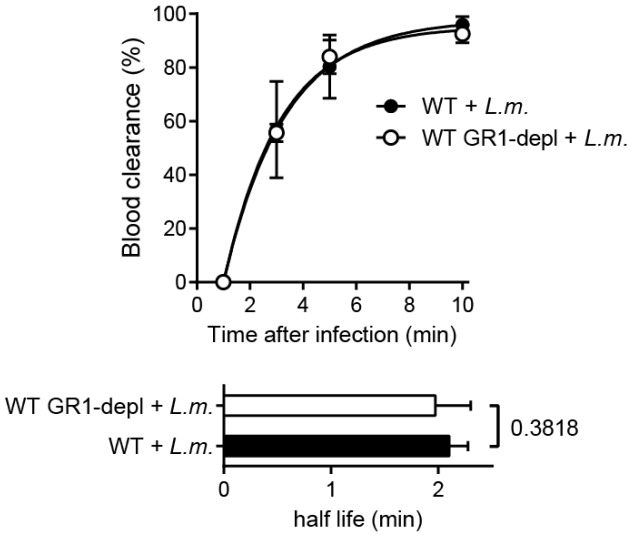

Supplemental figure 15 Clearance of systemic *L.m.* from the bloodstream is not influenced by an absence of neutrophil granulocytes
Wild-type mice were depleted of neutrophil granulocytes by treatment with αGR1-antibody 24 h prior to infection with 1x10^8 *L.m.*. Blood samples were drawn at 1, 3, 5 and 10 min post infection and serial dilutions were plated on BHI agar (mean ± SD of 4 mice, * = P < 0.05, # = P < 0.01, § = P < 0.001, Two-way ANOVA with Bonferroni post-test adjustment and two-tailed Student's t-test).

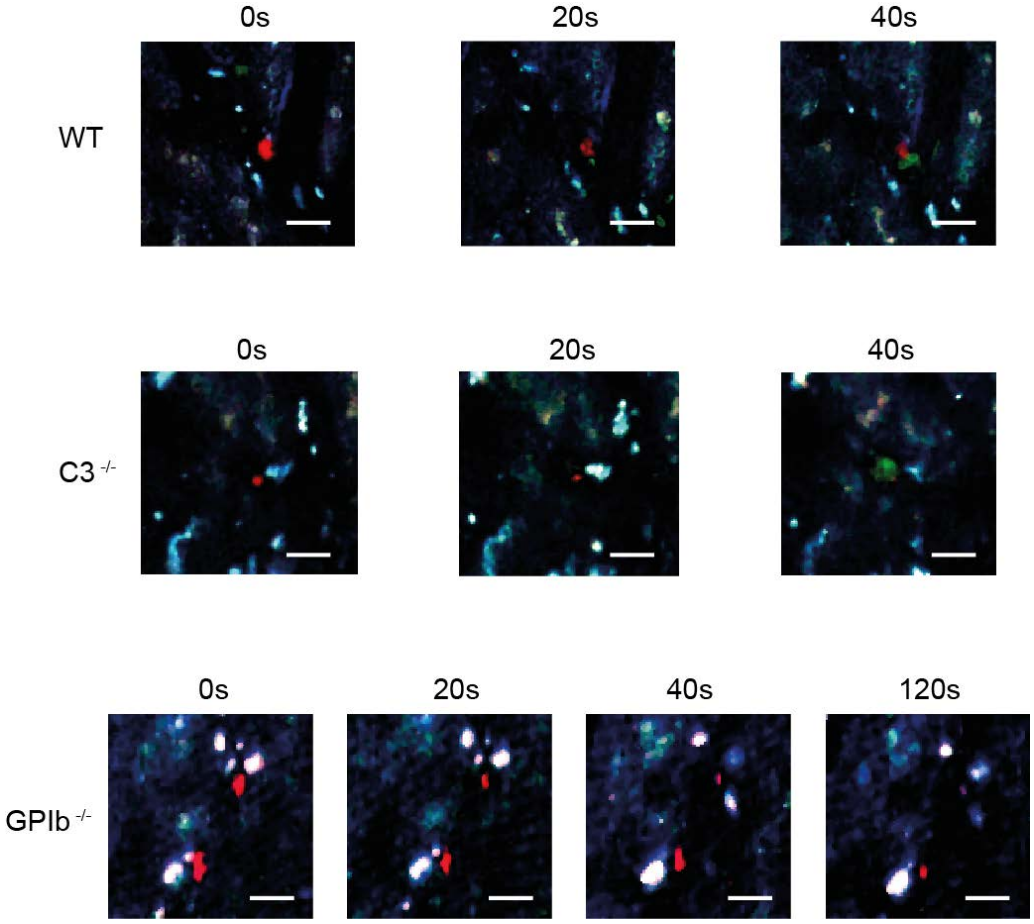

Supplemental figure 16 Platelet clustering around immobilized *L.m.* in the liver is observed in wild-type and C3$^{-/-}$ mice, but not in GPIb$^{-/-}$ mice
Wild-type, C3$^{-/-}$ and GPIb$^{-/-}$ mice were infected with 1x10^{8} *L.m.* i.v. and hepatic uptake was examined via intravital microscopy (red = *L.m.*, green = αCD49b-AF488 platelets, white = autofluorescence indicating hepatic Kupffer cells, scale bar = 5 µm).

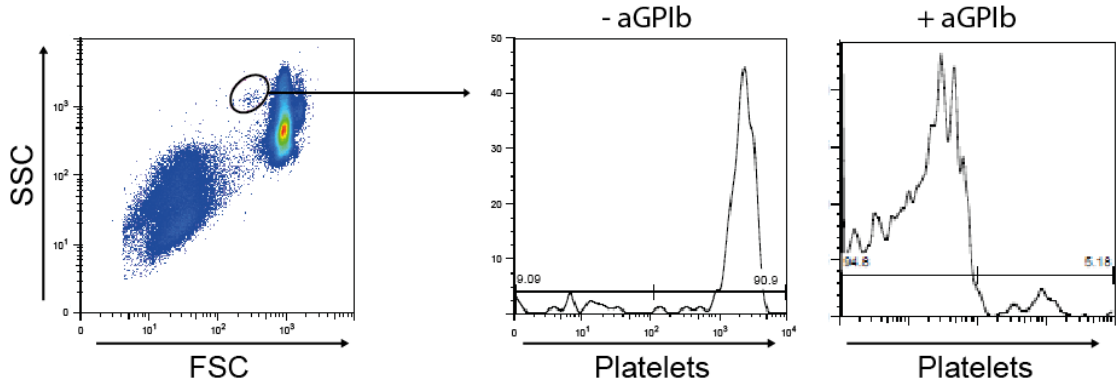

Supplemental figure 17 Microspheres bind platelets in whole blood in a GPIb-dependent manner
Hydroxyl-functionalised polystyrene microspheres were incubated in wild-type plasma for 10 min to ensure deposition of activated C3 and subsequently added to wild-type whole blood in absence (left) or presence (right) of αGPIb-antibody. After incubation for 1 min, flow cytometry analysis was performed to examine platelet association of the microspheres.

7 Video Supplement

This thesis includes supplementary videos showing dynamic data discussed quantitatively in the text. All movie files are included on a CD-ROM attached to the thesis. A short description of the dynamic data is given below.

Supplementary Movie 1: 2D time course movie of *L.m.* clearance in the vasculature of the ear of a wild-type mouse. Images were acquired at 40 frames per second (white = *L.m.*, blue = collagen)

Supplementary Movie 2: 2D time course movie of *L.m.* clearance in the vasculature of the ear of a $C3^{-/-}$ mouse. Images were acquired at 40 frames per second (white = *L.m.*, blue = collagen)

Supplementary Movie 3: 2D time course movie of *L.m.* clearance in the vasculature of the ear of a $GPIb^{-/-}$ mouse. Images were acquired at 40 frames per second (white = *L.m.*, blue = collagen)

Supplementary Movie 4: 2D time course movie of *L.m.* –platelet association in the vasculature of the ear of a wild-type mouse. Images were acquired at 40 frames per second (white = *L.m.*, red = platelets, blue = collagen)

Supplementary Movie 5: 2D time course movie of *L.m.* –platelet association in the vasculature of the ear of a $C3^{-/-}$ mouse. Images were acquired at 40 frames per second (white = *L.m.*, red = platelets, blue = collagen)

Supplementary Movie 6: 2D time course movie of *L.m.* –platelet association in the vasculature of the ear of a $GPIb^{-/-}$ mouse. Images were acquired at 40 frames per second (white = *L.m.*, red = platelets, blue = collagen)

Supplementary Movie 7: 2D time course movie of clearance of preopsonized and nonopsonized *L.m.* in the vasculature of the ear of a wild-type mouse. Images were acquired at 40 frames per second (white = preopsonized *L.m.*, red = nonopsonized *L.m.*, blue = collagen)

Supplementary Movie 8: 2D time course movie of clearance of preopsonized and nonopsonized *L.m.* in the vasculature of the ear of a $C3^{-/-}$ mouse. Images were acquired at 40 frames per second (white = preopsonized *L.m.*, red = nonopsonized *L.m.*, blue = collagen)

Supplementary Movie 9: 2D time course movie of clearance of preopsonized and nonopsonized *L.m.* in the vasculature of the ear of a $GPIb^{-/-}$ mouse. Images were acquired at 40 frames per second (white = preopsonized *L.m.*, red = nonopsonized *L.m.*, blue = collagen)

Supplementary Movie 10: 2D time course movie of clearance of preopsonized and nonopsonized *L.m.* in the vasculature of the ear of a $CRIg^{-/-}$ mouse. Images were acquired at 40 frames per second (white = preopsonized *L.m*., red = nonopsonized *L.m.*, blue = collagen)

Supplementary Movie 11: 2D time course movie of clearance of preopsonized and nonopsonized *L.m.* in the vasculature of the ear of a $C3^{-/-}CRIg^{-/-}$ mouse. Images were acquired at 40 frames per second (white = preopsonized *L.m*., red = nonopsonized *L.m.*, blue = collagen)

Supplementary Movie 12: 2D time course movie of *L.m.* association of blood leukocytes in the vasculature of the ear of a wild-type mouse. Images were acquired at 40 frames per second (white = *L.m*., red = rhodamine 6G, blue = collagen)

8 References

Abram, M., Schluter, D., Vuckovic, D., Wraber, B., Doric, M., and Deckert, M. (2003). Murine model of pregnancy-associated Listeria monocytogenes infection. FEMS Immunol Med Microbiol *35*, 177-182.

Aderem, A., and Underhill, D. M. (1999). Mechanisms of phagocytosis in macrophages. Annu. Rev. Immunol. *17*, 593-623.

Akira, S. (2004). Toll receptor families: structure and function. Semin Immunol *16*, 1-2.

Akira, S. (2006). TLR signaling. Curr. Top. Microbiol. Immunol. *311*, 1-16.

Alexander, J. J., Hack, B. K., Cunningham, P. N., and Quigg, R. J. (2001). A protein with characteristics of factor H is present on rodent platelets and functions as the immune adherence receptor. J Biol Chem *276*, 32129-32135.

Alper, C. A., Johnson, A. M., Birtch, A. G., and Moore, F. D. (1969). Human C'3: evidence for the liver as the primary site of synthesis. Science *163*, 286-288.

Altamura, M., Caradonna, L., Amati, L., Pellegrino, N. M., Urgesi, G., and Miniello, S. (2001). Splenectomy and sepsis: the role of the spleen in the immune-mediated bacterial clearance. Immunopharmacol Immunotoxicol *23*, 153-161.

Alvarez-Dominguez, C., Roberts, R., and Stahl, P. D. (1997). Internalized Listeria monocytogenes modulates intracellular trafficking and delays maturation of the phagosome. J Cell Sci *110 (Pt 6)*, 731-743.

Andonegui, G., Kerfoot, S. M., McNagny, K., Ebbert, K. V. J., Patel, K. D., and Kubes, P. (2005). Platelets express functional Toll-like receptor-4. Blood *106*, 2417-2423.

Astarie-Dequeker, C., N'Diaye, E. N., Le Cabec, V., Rittig, M. G., Prandi, J., and Maridonneau-Parini, I. (1999). The mannose receptor mediates uptake of pathogenic and nonpathogenic mycobacteria and bypasses bactericidal responses in human macrophages. Infect Immun *67*, 469-477.

Baatz, H., Steinbauer, M., Harris, A. G., and Krombach, F. (1995). Kinetics of white blood cell staining by intravascular administration of rhodamine 6G. Int J Microcirc Clin Exp *15*, 85-91.

Bahjat, K. S., Liu, W., Lemmens, E. E., Schoenberger, S. P., Portnoy, D. A., Dubensky, T. W., and Brockstedt, D. G. (2006). Cytosolic entry controls CD8+-T-cell potency during bacterial infection. Infect. Immun. *74*, 6387-6397.

Baldridge, J. R., Barry, R. A., and Hinrichs, D. J. (1990). Expression of systemic protection and delayed-type hypersensitivity to Listeria monocytogenes is mediated by different T-cell subsets. Infection and immunity *58*, 654-658.

Balmer, M. L., Slack, E., Gottardi, A. de, **Lawson, M. A. E., Hapfelmeier, S., Miele, L., Grieco, A., van Vlierberghe, H., Fahrner, R., and Patuto, N.***, et al.* (2014). The liver may act as a firewall mediating mutualism between the host and its gut commensal microbiota. Science translational medicine *6*, 237ra66.

Banchereau, J., and Steinman, R. M. (1998). Dendritic cells and the control of immunity. Nature *392*, 245-252.

Bauer, S., Kirschning, C. J., Hacker, H., Redecke, V., Hausmann, S., Akira, S., Wagner, H., and Lipford, G. B. (2001). Human TLR9 confers responsiveness to bacterial DNA via species-specific CpG motif recognition. Proc Natl Acad Sci USA (Proceedings of the National Academy of Sciences of the United States of America) *98*, 9237-9242.

Beauvillain, C., Donnou, S., Jarry, U., Scotet, M., Gascan, H., Delneste, Y., Guermonprez, P., Jeannin, P., and Couez, D. (2008). Neonatal and adult microglia cross-present exogenous antigens. Glia *56*, 69-77.

Beauvillain, C., Meloni, F., Sirard, J.-C., Blanchard, S., Jarry, U., Scotet, M., Magistrelli, G., Delneste, Y., Barnaba, V., and Jeannin, P. (2010). The scavenger receptors SRA-1 and SREC-I cooperate with TLR2 in the recognition of the hepatitis C virus non-structural protein 3 by dendritic cells. J Hepatol *52*, 644-651.

Belz, G. T., Shortman, K., Bevan, M. J., and Heath, W. R. (2005). CD8alpha+ dendritic cells selectively present MHC class I-restricted noncytolytic viral and intracellular bacterial antigens in vivo. Journal of immunology (Baltimore, Md. : 1950) *175*, 196-200.

Benacerraf, B., Sebestyen, M. M., and Schlossman, S. (1959). A quantitative study of the kinetics of blood clearance of P32-labelled Escherichia coli and Staphylococci by the reticuloendothelial system. J Exp Med *110*, 27-48.

Bleriot, C., Dupuis, T., Jouvion, G., Eberl, G., Disson, O., and Lecuit, M. (2015). Liver-resident macrophage necroptosis orchestrates type 1 microbicidal inflammation and type-2-mediated tissue repair during bacterial infection. Immunity *42*, 145-158.

Boehlen, F., and Clemetson, K. J. (2001). Platelet chemokines and their receptors: what is their relevance to platelet storage and transfusion practice? Transfusion medicine (Oxford, England) *11*, 403-417.

Boes, M., Esau, C., Fischer, M. B., Schmidt, T., Carroll, M., and Chen, J. (1998). Enhanced B-1 cell development, but impaired IgG antibody responses in mice deficient in secreted IgM. J. Immunol. *160*, 4776-4787.

Bokisch, V. A., Dierich, M. P., and Mūller-Eberhard, H. J. (1975). Third component of complement (C3): structural properties in relation to functions. Proc Natl Acad Sci U S A *72*, 1989-1993.

Bokisch, V. A., Muller-Eberhard, H. J., and Cochrane, C. G. (1969). Isolation of a fragment (C3a) of the third component of human complement containing anaphylatoxin and chemotactic activity and description of an anaphylatoxin inactivator of human serum. J Exp Med *129*, 1109-1130.

Bone, R. C. (1991). Sepsis, the sepsis syndrome, multi-organ failure: a plea for comparable definitions. Ann. Intern. Med. *114*, 332-333.

Bordet, J. (1895). Les leucocytes et les proprietes actives du serum chez les vaccines. Annales de L'Institut Pasteur *9*, 462-506.

Born, G. V. (1962). Aggregation of blood platelets by adenosine diphosphate and its reversal. Nature *194*, 927-929.

Borregaard, N. (2010). Neutrophils, from marrow to microbes. Immunity *33*, 657-670.

Bouwens, L., Bleser, P. de, **Vanderkerken, K., Geerts, B., and Wisse, E.** (1992). Liver cell heterogeneity: functions of non-parenchymal cells. Enzyme *46*, 155-168.

Brass, L. F. (2003). Thrombin and platelet activation. Chest *124*, 18S-25S.

Brinkmann, V., Reichard, U., Goosmann, C., Fauler, B., Uhlemann, Y., Weiss, D. S., Weinrauch, Y., and Zychlinsky, A. (2004). Neutrophil extracellular traps kill bacteria. Science *303*, 1532-1535.

Brown, G. D., and Gordon, S. (2001). Immune recognition. A new receptor for beta-glucans. Nature *413*, 36-37.

Brown, M. S., Basu, S. K., Falck, J. R., Ho, Y. K., and Goldstein, J. L. (1980). The scavenger cell pathway for lipoprotein degradation: specificity of the binding site that mediates the uptake of negatively-charged LDL by macrophages. J Supramol Struct *13*, 67-81.

Brundage, R. A., Smith, G. A., Camilli, A., Theriot, J. A., and Portnoy, D. A. (1993). Expression and phosphorylation of the Listeria monocytogenes ActA protein in mammalian cells. Proc Natl Acad Sci U S A *90*, 11890-11894.

Buchner, H. (1894). Neuere Fortschritte in der Immunitätsfrage. Münchener medizinische Wochenschrift *41*, 497-500.

Burge, J., Nicholson-Weller, A., and Austen, K. F. (1981). Isolation of C4-binding protein from guinea pig plasma and demonstration of its function as a control protein of the classical complement pathway C3 convertase. J Immunol *126*, 232-235.

Burton, D. R., Boyd, J., Brampton, A. D., Easterbrook-Smith, S. B., Emanuel, E. J., Novotny, J., Rademacher, T. W., van Schravendijk, M. R., Sternberg, M. J., and Dwek, R. A. (1980). The Clq receptor site on immunoglobulin G. Nature *288*, 338-344.

Byrne, M. F., Kerrigan, S. W., Corcoran, P. A., Atherton, J. C., Murray, F. E., Fitzgerald, D. J., and Cox, D. M. (2003). Helicobacter pylori binds von Willebrand factor and interacts with GPIb to induce platelet aggregation. Gastroenterology *124*, 1846-1854.

Campagnola, P. J., and Loew, L. M. (2003). Second-harmonic imaging microscopy for visualizing biomolecular arrays in cells, tissues and organisms. Nature biotechnology *21*, 1356-1360.

Chakraborty, T. (1996). The molecular mechanisms of actin-based intracellular motility by Listeria monocytogenes. Microbiologia *12*, 237-244.

Chaplin, H., Cohen, S., and Press, E. M. (1965). PREPARATION AND PROPERTIES OF THE PEPTIDE CHAINS OF NORMAL HUMAN 19 S GAMMA-GLOBULIN (IGM). Biochem. J. *95*, 256-261.

Clark, S. R., Ma, A. C., Tavener, S. A., McDonald, B., Goodarzi, Z., Kelly, M. M., Patel, K. D., Chakrabarti, S., McAvoy, E., and Sinclair, G. D.*, et al.* (2007). Platelet TLR4 activates neutrophil extracellular traps to ensnare bacteria in septic blood. Nat Med *13*, 463-469.

Clawson, C. C. (1973). Platelet interaction with bacteria. 3. Ultrastructure. Am J Pathol *70*, 449-471.

Clawson, C. C., Rao, G. H., and White, J. G. (1975). Platelet interaction with bacteria. IV. Stimulation of the release reaction. Am J Pathol *81*, 411-420.

Clawson, C. C., and White, J. G. (1971a). Platelet interaction with bacteria. I. Reaction phases and effects of inhibitors. Am J Pathol *65*, 367-380.

Clawson, C. C., and White, J. G. (1971b). Platelet interaction with bacteria. II. Fate of the bacteria. Am J Pathol *65*, 381-397.

Clemetson, K. J., and Clemetson, J. M. (2004). Platelet receptor signalling. Hematol. J. *5 Suppl 3*, S159-63.

Cohen, J. (2002). The immunopathogenesis of sepsis. Nature *420*, 885-891.

Coombs, P. J., Taylor, M. E., and Drickamer, K. (2006). Two categories of mammalian galactose-binding receptors distinguished by glycan array profiling. Glycobiology *16*, 1C-7C.

Corash, L., and Levin, J. (1990). The relationship between megakaryocyte ploidy and platelet volume in normal and thrombocytopenic C3H mice. Exp. Hematol. *18*, 985-989.

Corsello, S., Fulgenzi, A., Vietti, D., and Ferrero, M. E. (2009). The usefulness of chelation therapy for the remission of symptoms caused by previous treatment with mercury-containing pharmaceuticals: a case report. Cases J *2*, 199.

Cosgrove, L. J., d'Apice, A. J., Haddad, A., Pedersen, J., and McKenzie, I. F. (1987). CR3 receptor on platelets and its role in the prostaglandin metabolic pathway. Immunol Cell Biol *65 (Pt 6)*, 453-460.

Coutinho, I. R., Berk, R. S., and Mammen, E. (1988). Platelet aggregation by a phospholipase C from Pseudomonas aeruginosa. Thromb Res *51*, 495-505.

Czuprynski, C. J., and Balish, E. (1981). Interaction of rat platelets with Listeria monocytogenes. Infect Immun *33*, 103-108.

Dalton, C. B., Austin, C. C., Sobel, J., Hayes, P. S., Bibb, W. F., Graves, L. M., Swaminathan, B., Proctor, M. E., and Griffin, P. M. (1997). An outbreak of gastroenteritis and fever due to Listeria monocytogenes in milk. N Engl J Med *336*, 100-105.

Daly, M. E. (2011). Determinants of platelet count in humans. Haematologica *96*, 10-13.

Das, B., Kashino, S. S., Pulu, I., Kalita, D., Swami, V., Yeger, H., Felsher, D. W., and Campos-Neto, A. (2013). CD271(+) bone marrow mesenchymal stem cells may provide a niche for dormant Mycobacterium tuberculosis. Sci Transl Med *5*, 170ra13.

Decousser, J.-W., Pina, P., Picot, F., Delalande, C., Pangon, B., Courvalin, P., and Allouch, P. (2003). Frequency of isolation and antimicrobial susceptibility of bacterial pathogens isolated from patients with bloodstream infections: a French prospective national survey. J. Antimicrob. Chemother. *51*, 1213-1222.

Del Conde, I., Crúz, M. A., Zhang, H., López, J. A., and Afshar-Kharghan, V. (2005). Platelet activation leads to activation and propagation of the complement system. The Journal of experimental medicine *201*, 871-879.

Dempsey, P. W., Allison, M. E., Akkaraju, S., Goodnow, C. C., and Fearon, D. T. (1996). C3d of complement as a molecular adjuvant: bridging innate and acquired immunity. Science *271*, 348-350.

Deng, M., Scott, M. J., Loughran, P., Gibson, G., Sodhi, C., Watkins, S., Hackam, D., and Billiar, T. R. (2013). Lipopolysaccharide clearance, bacterial clearance, and systemic inflammatory responses are regulated by cell type-specific functions of TLR4 during sepsis. J Immunol *190*, 5152-5160.

Dierich, M. P., Bitter-Suermann, D., König, W., Hadding, U., Galanos, C., and Rietschel, E. T. (1973). Analysis of bypass activation of C3 by endotoxic LPS and loss of this potency. Immunology *24*, 721-733.

Disson, O., and Lecuit, M. (2012). Targeting of the central nervous system by Listeria monocytogenes. Virulence *3*, 213-221.

Doeing, D. C., Borowicz, J. L., and Crockett, E. T. (2003). Gender dimorphism in differential peripheral blood leukocyte counts in mice using cardiac, tail, foot, and saphenous vein puncture methods. BMC Clin Pathol *3*, 3.

Dong, Z., Wei, H., Sun, R., and Tian, Z. (2007). The roles of innate immune cells in liver injury and regeneration. Cell Mol Immunol *4*, 241-252.

Drevets, D. A., and Campbell, P. A. (1991). Roles of complement and complement receptor type 3 in phagocytosis of Listeria monocytogenes by inflammatory mouse peritoneal macrophages. Infect Immun *59*, 2645-2652.

Dunne, D. W., Resnick, D., Greenberg, J., Krieger, M., and Joiner, K. A. (1994). The type I macrophage scavenger receptor binds to gram-positive bacteria and recognizes lipoteichoic acid. Proc Natl Acad Sci U S A *91*, 1863-1867.

Dussurget, O., Pizarro-Cerda, J., and Cossart, P. (2004). Molecular determinants of Listeria monocytogenes virulence. Annu Rev Microbiol *58*, 587-610.

Ebe, Y., Hasegawa, G., Takatsuka, H., Umezu, H., Mitsuyama, M., Arakawa, M., Mukaida, N., and Naito, M. (1999). The role of Kupffer cells and regulation of neutrophil migration into the liver by macrophage inflammatory protein-2 in primary listeriosis in mice. Pathol Int *49*, 519-532.

Edelson, B. T., Bradstreet, T. R., Hildner, K., Carrero, J. A., Frederick, K. E., KC, W., Belizaire, R., Aoshi, T., Schreiber, R. D., and Miller, M. J.*, et al.* (2011). CD8α(+) dendritic cells are an obligate cellular entry point for productive infection by Listeria monocytogenes. Immunity *35*, 236-248.

Ehrlich, P. (1880). Methodologische Beiträge zur Physiologie und Pathologie der verschiedenen Formen der Leukocyten. Zeitschrift fuer klinische Medizin *1*, 553-560.

Ehrlich, P. (1904). Gesammelte Arbeiten zur Immunitätsforschung (Berlin: Verlag von August Hirschwald).

Ekdahl, K. N., and Nilsson, B. (1995). Phosphorylation of complement component C3 and C3 fragments by a human platelet protein kinase. Inhibition of factor I-mediated cleavage of C3b. J. Immunol. *154*, 6502-6510.

Elhami, E., Dietz, B., Xiang, B., Deng, J., Wang, F., Chi, C., Goertzen, A. L., Mzengeza, S., Freed, D., and Arora, R. C.*, et al.* (2013). Assessment of three techniques for delivering stem cells to the heart using PET and MR imaging. EJNMMI research *3*, 72.

Elomaa, O., Kangas, M., Sahlberg, C., Tuukkanen, J., Sormunen, R., Liakka, A., Thesleff, I., Kraal, G., and Tryggvason, K. (1995). Cloning of a novel bacteria-binding receptor structurally related to scavenger receptors and expressed in a subset of macrophages. Cell *80*, 603-609.

Elomaa, O., Sankala, M., Pikkarainen, T., Bergmann, U., Tuuttila, A., Raatikainen-Ahokas, A., Sariola, H., and Tryggvason, K. (1998). Structure of the human macrophage MARCO receptor and characterization of its bacteria-binding region. The Journal of biological chemistry *273*, 4530-4538.

Elzey, B. D., Tian, J., Jensen, R. J., Swanson, A. K., Lees, J. R., Lentz, S. R., Stein, C. S., Nieswandt, B., Wang, Y., and Davidson, B. L.*, et al.* (2003). Platelet-mediated modulation of adaptive immunity. A communication link between innate and adaptive immune compartments. Immunity *19*, 9-19.

Emanuel, E. J., Brampton, A. D., Burton, D. R., and Dwek, R. A. (1982). Formation of complement subcomponent C1q-immunoglobulin G complex. Thermodynamic and chemical-modification studies. Biochem J *205*, 361-372.

Emlen, W., Carl, V., and Burdick, G. (1992). Mechanism of transfer of immune complexes from red blood cell CR1 to monocytes. Clin Exp Immunol *89*, 8-17.

Fahimi, H. D. (1970). The fine structural localization of endogenous and exogenous peroxidase activity in Kupffer cells of rat liver. J Cell Biol *47*, 247-262.

Farber, J. M., and Peterkin, P. I. (1991). Listeria monocytogenes, a food-borne pathogen. Microbiol Rev *55*, 476-511.

Farries, T. C., Seya, T., Harrison, R. A., and Atkinson, J. P. (1990). Competition for binding sites on C3b by CR1, CR2, MCP, factor B and factor H. Complement Inflamm *7*, 30-41.

Feng, S., Liang, X., Kroll, M. H., Chung, D. W., and Afshar-Kharghan, V. (2015). von Willebrand factor is a cofactor in complement regulation. Blood *125*, 1034-1037.

Fielding, C. A., McLoughlin, R. M., McLeod, L., Colmont, C. S., Najdovska, M., Grail, D., Ernst, M., Jones, S. A., Topley, N., and Jenkins, B. J. (2008). IL-6 regulates neutrophil trafficking during acute inflammation via STAT3. J Immunol *181*, 2189-2195.

Fitzgerald, J. R., Foster, T. J., and Cox, D. (2006). The interaction of bacterial pathogens with platelets. Nat. Rev. Microbiol. *4*, 445-457.

Flo, T. H., Halaas, O., Lien, E., Ryan, L., Teti, G., Golenbock, D. T., Sundan, A., and Espevik, T. (2000). Human toll-like receptor 2 mediates monocyte activation by Listeria monocytogenes, but not by group B streptococci or lipopolysaccharide. J Immunol *164*, 2064-2069.

Ford, I., Douglas, C. W., Cox, D., Rees, D. G., Heath, J., and Preston, F. E. (1997). The role of immunoglobulin G and fibrinogen in platelet aggregation by Streptococcus sanguis. Br J Haematol *97*, 737-746.

Fournier, B. M., and Parkos, C. A. (2012). The role of neutrophils during intestinal inflammation. Mucosal Immunol *5*, 354-366.

Fremeaux-Bacchi, V., Dragon-Durey, M.-A., Blouin, J., Vigneau, C., Kuypers, D., Boudailliez, B., Loirat, C., Rondeau, E., and Fridman, W. H. (2004). Complement factor I: a susceptibility gene for atypical haemolytic uraemic syndrome. J. Med. Genet. *41*, e84.

Frevert, U. (2004). Sneaking in through the back entrance: the biology of malaria liver stages. Trends Parasitol. *20*, 417-424.

Fujita, T. (2002). Evolution of the lectin-complement pathway and its role in innate immunity. Nat Rev Immunol *2*, 346-353.

Fukuda, H., Matsuzawa, T., Abe, Y., Endo, S., Yamada, K., Kubota, K., Hatazawa, J., Sato, T., Ito, M., and Takahashi, T.*, et al.* (1982). Experimental study for cancer diagnosis with positron-labeled fluorinated glucose analogs: [18F]-2-fluoro-2-deoxy-D-mannose: a new tracer for cancer detection. Eur J Nucl Med *7*, 294-297.

Galli, S. J., Borregaard, N., and Wynn, T. A. (2011). Phenotypic and functional plasticity of cells of innate immunity: macrophages, mast cells and neutrophils. Nat. Immunol. *12*, 1035-1044.

Gasque, P. (2004). Complement: a unique innate immune sensor for danger signals. Mol Immunol *41*, 1089-1098.

Geijtenbeek, T. B. H., and Gringhuis, S. I. (2009). Signalling through C-type lectin receptors: shaping immune responses. Nat Rev Immunol *9*, 465-479.

Gesundheitsberichterstattung des Bundes. Diagnosedaten der Krankenhäuser ab 2000. https://www.gbe-bund.de/oowa921-install/servlet/oowa/aw92/dboowasys921.xwdevkit/xwd_init?gbe.isgbetol/xs_start_neu/&p_aid=i&p_aid=21828279&nummer=550&p_sprache=D&p_indsp=99999999&p_aid=491153. 05.05.2015.

Gombas, D. E., Chen, Y., Clavero, R. S., and Scott, V. N. (2003). Survey of Listeria monocytogenes in ready-to-eat foods. J Food Prot *66*, 559-569.

Gomez Perdiguero, E., Klapproth, K., Schulz, C., Busch, K., Azzoni, E., Crozet, L., Garner, H., Trouillet, C., Bruijn, M. F. de, and **Geissmann, F.***, et al.* (2015). Tissue-resident macrophages originate from yolk-sac-derived erythro-myeloid progenitors. Nature *518*, 547-551.

Gordon, S., Lawson, L., Rabinowitz, S., Crocker, P. R., Morris, L., and Perry, V. H. (1992). Antigen markers of macrophage differentiation in murine tissues. Curr Top Microbiol Immunol *181*, 1-37.

Gorgani, N. N., He, J. Q., Katschke, K. J., JR, Helmy, K. Y., Xi, H., Steffek, M., Hass, P. E., and van Lookeren Campagne, M. (2008). Complement receptor of the Ig superfamily enhances complement-mediated phagocytosis in a subpopulation of tissue resident macrophages. J Immunol *181*, 7902-7908.

Götze, O., and Müller-Eberhard, H. J. (1970). Lysis of erythrocytes by complement in the absence of antibody. J. Exp. Med. *132*, 898-915.

Gough, P. J., and Gordon, S. (2000). The role of scavenger receptors in the innate immune system. Microbes Infect *2*, 305-311.

Gregory, S. H., Cousens, L. P., van Rooijen, N., Dopp, E. A., Carlos, T. M., and Wing, E. J. (2002). Complementary adhesion molecules promote neutrophil-Kupffer cell interaction and the elimination of bacteria taken up by the liver. J Immunol *168*, 308-315.

Gregory, S. H., and Wing, E. J. (1998). Neutrophil-Kupffer-cell interaction in host defenses to systemic infections. Immunol Today *19*, 507-510.

Gregory, S. H., and Wing, E. J. (2002). Neutrophil-Kupffer cell interaction: a critical component of host defenses to systemic bacterial infections. J Leukoc Biol *72*, 239-248.

Groman, E. V., Enriquez, P. M., Jung, C., and Josephson, L. (1994). Arabinogalactan for hepatic drug delivery. Bioconjug. Chem. *5*, 547-556.

Gross, P. L., and Weitz, J. I. (2009). New antithrombotic drugs. Clin. Pharmacol. Ther. *86*, 139-146.

Gumucio, J. J., Bilir, B. M., Moseley, R. H., and Berkowitz, C. M. (1994). The biology of the liver cell plate. In The Liver: Biology and Pathobiology, I.M. Arias, J.L. Boyer, N. Fausto, W.B. Jakoby, D.A. Schachter and D.A. Shafritz, eds. (New York: Raven Press), pp. 1143–1163.

Häger, M., Cowland, J. B., and Borregaard, N. (2010). Neutrophil granules in health and disease. J. Intern. Med. *268*, 25-34.

Haltiwanger, R. S., Lehrman, M. A., Eckhardt, A. E., and Hill, R. L. (1986). The distribution and localization of the fucose-binding lectin in rat tissues and the identification of a high affinity form of the mannose/N-acetylglucosamine-binding lectin in rat liver. J Biol Chem *261*, 7433-7439.

Hampton, R. Y., Golenbock, D. T., Penman, M., Krieger, M., and Raetz, C. R. (1991). Recognition and plasma clearance of endotoxin by scavenger receptors. Nature *352*, 342-344.

Hart, J. R. (2000). Ethylenediaminetetraacetic Acid and Related Chelating Agents. In Ullmann's Encyclopedia of Industrial Chemistry, J. Roger Hart, ed. (Weinheim, Germany: Wiley-VCH Verlag GmbH & Co. KGaA).

Hawiger, J., Steckley, S., Hammond, D., Cheng, C., Timmons, S., Glick, A. D., and Des Prez, R. M. (1979). Staphylococci-induced human platelet injury mediated by protein A and immunoglobulin G Fc fragment receptor. J Clin Invest *64*, 931-937.

Haworth, R., Platt, N., Keshav, S., Hughes, D., Darley, E., Suzuki, H., Kurihara, Y., Kodama, T., and Gordon, S. (1997). The macrophage scavenger receptor type A is expressed by activated macrophages and protects the host against lethal endotoxic shock. J Exp Med *186*, 1431-1439.

Hayashi, F., Means, T. K., and Luster, A. D. (2003). Toll-like receptors stimulate human neutrophil function. Blood *102*, 2660-2669.

Hayashi, F., Smith, K. D., Ozinsky, A., Hawn, T. R., Yi, E. C., Goodlett, D. R., Eng, J. K., Akira, S., Underhill, D. M., and Aderem, A. (2001). The innate immune response to bacterial flagellin is mediated by Toll-like receptor 5. Nature *410*, 1099-1103.

Helmy, K. Y., Katschke, K. J., JR, Gorgani, N. N., Kljavin, N. M., Elliott, J. M., Diehl, L., Scales, S. J., Ghilardi, N., and van Lookeren Campagne, M. (2006). CRIg: a macrophage complement receptor required for phagocytosis of circulating pathogens. Cell *124*, 915-927.

Hemmi, H., Takeuchi, O., Kawai, T., Kaisho, T., Sato, S., Sanjo, H., Matsumoto, M., Hoshino, K., Wagner, H., and Takeda, K.*, et al.* (2000). A Toll-like receptor recognizes bacterial DNA. Nature *408*, 740-745.

Henn, V., Slupsky, J. R., Gräfe, M., Anagnostopoulos, I., Förster, R., Müller-Berghaus, G., and Kroczek, R. A. (1998). CD40 ligand on activated platelets triggers an inflammatory reaction of endothelial cells. Nature *391*, 591-594.

Heymann, F., Peusquens, J., Ludwig-Portugall, I., Kohlhepp, M., Ergen, C., Niemietz, P., Martin, C., van Rooijen, N., Ochando, J. C., and Randolph, G. J.*, et al.* (2015). Liver inflammation abrogates immunological tolerance induced by Kupffer cells. Hepatology.

Hinglais, N., Kazatchkine, M. D., Mandet, C., Appay, M. D., and Bariety, J. (1989). Human liver Kupffer cells express CR1, CR3, and CR4 complement receptor antigens. An immunohistochemical study. Lab Invest *61*, 509-514.

Hof, H., Nichterlein, T., and Kretschmar, M. (1997). Management of listeriosis. Clin Microbiol Rev *10*, 345-357.

Holmsen, H. (1989). Physiological functions of platelets. Ann Med *21*, 23-30.

Hughes, D. A., Fraser, I. P., and Gordon, S. (1995). Murine macrophage scavenger receptor: in vivo expression and function as receptor for macrophage adhesion in lymphoid and non-lymphoid organs. European journal of immunology *25*, 466-473.

Ikarashi, M., Nakashima, H., Kinoshita, M., Sato, A., Nakashima, M., Miyazaki, H., Nishiyama, K., Yamamoto, J., and Seki, S. (2013). Distinct development and functions of resident and recruited liver Kupffer cells/macrophages. J Leukoc Biol *94*, 1325-1336.

Ikeda, K., Sannoh, T., Kawasaki, N., Kawasaki, T., and Yamashina, I. (1987). Serum lectin with known structure activates complement through the classical pathway. J. Biol. Chem. *262*, 7451-7454.

Ireton, K., Payrastre, B., Chap, H., Ogawa, W., Sakaue, H., Kasuga, M., and Cossart, P. (1996). A role for phosphoinositide 3-kinase in bacterial invasion. Science *274*, 780-782.

Ishiguro, T., Naito, M., Yamamoto, T., Hasegawa, G., Gejyo, F., Mitsuyama, M., Suzuki, H., and Kodama, T. (2001). Role of macrophage scavenger receptors in response to Listeria monocytogenes infection in mice. Am J Pathol *158*, 179-188.

Jackson, C. W., Hutson, N. K., Steward, S. A., and McDonald, T. P. (1990). Megakaryocytopoiesis in man and laboratory animals. Conclusions derived from comparative studies and recently discovered animal models with megakaryocyte anomalies. Prog. Clin. Biol. Res. *356*, 11-23.

Jackson, S. P., Nesbitt, W. S., and Kulkarni, S. (2003). Signaling events underlying thrombus formation. J. Thromb. Haemost. *1*, 1602-1612.

Jin, R., Yu, S., Song, Z., Zhu, X., Wang, C., Yan, J., Wu, F., Nanda, A., Granger, D. N., and Li, G. (2013). Soluble CD40 ligand stimulates CD40-dependent activation of the β2 integrin Mac-1 and protein kinase C zeda (PKCζ) in neutrophils: implications for neutrophil-platelet interactions and neutrophil oxidative burst. PLoS ONE *8*, e64631.

Johanson, W. G., Kennedy, M. G., and Bonte, F. J. (1973). Use of technetium (99m Tc) as a bacterial label in lung clearance studies. Appl Microbiol *25*, 592-594.

Jones, A. L., and Spring-Mills, E. (1984). The liver and the gallbladder. In Modern Concepts of Gastrointestinal Histology, L. Weiss, ed. (New York: Elsevier), pp. 707–748.

Joseph, B., Przybilla, K., Stuhler, C., Schauer, K., Slaghuis, J., Fuchs, T. M., and Goebel, W. (2006). Identification of Listeria monocytogenes genes contributing to intracellular replication by expression profiling and mutant screening. J Bacteriol *188*, 556-568.

Kabha, K., Nissimov, L., Athamna, A., Keisari, Y., Parolis, H., Parolis, L. A., Grue, R. M., Schlepper-Schafer, J., Ezekowitz, A. R., and Ohman, D. E. (1995). Relationships among capsular structure, phagocytosis, and mouse virulence in Klebsiella pneumoniae. Infect Immun *63*, 847-852.

Kanaji, T., Russell, S., and Ware, J. (2002). Amelioration of the macrothrombocytopenia associated with the murine Bernard-Soulier syndrome. Blood *100*, 2102-2107.

Karygianni, L., Wiedmann-Al-Ahmad, M., Finkenzeller, G., Sauerbier, S., Wolkewitz, M., Hellwig, E., and Al-Ahmad, A. (2012). Enterococcus faecalis affects the proliferation and differentiation of ovine osteoblast-like cells. Clin Oral Investig *16*, 879-887.

Kerrigan, A. M., and Brown, G. D. (2009). C-type lectins and phagocytosis. Immunobiology *214*, 562-575.

Kerrigan, S. W., Douglas, I., Wray, A., Heath, J., Byrne, M. F., Fitzgerald, D., and Cox, D. (2002). A role for glycoprotein Ib in Streptococcus sanguis-induced platelet aggregation. Blood *100*, 509-516.

Kessler, C. M., Nussbaum, E., and Tuazon, C. U. (1987). In vitro correlation of platelet aggregation with occurrence of disseminated intravascular coagulation and subacute bacterial endocarditis. J Lab Clin Med *109*, 647-652.

Khandoga, A., Biberthaler, P., Enders, G., Teupser, D., Axmann, S., Luchting, B., Hutter, J., Messmer, K., and Krombach, F. (2002). P-selectin mediates platelet-endothelial cell interactions and reperfusion injury in the mouse liver in vivo. Shock (Augusta, Ga.) *18*, 529-535.

Kim, D. D., Miwa, T., Kimura, Y., Schwendener, R. A., van Lookeren Campagne, M., and Song, W.-C. (2008). Deficiency of decay-accelerating factor and complement receptor 1-related gene/protein y on murine platelets leads to complement-dependent clearance by the macrophage phagocytic receptor CRIg. Blood *112*, 1109-1119.

Kim, K. H., Choi, B. K., Song, K. M., Cha, K. W., Kim, Y. H., Lee, H., Han, I.-S., and Kwon, B. S. (2013). CRIg signals induce anti-intracellular bacterial phagosome activity in a chloride intracellular channel 3-dependent manner. Eur J Immunol *43*, 667-678.

Kinoshita, M., Uchida, T., Sato, A., Nakashima, M., Nakashima, H., Shono, S., Habu, Y., Miyazaki, H., Hiroi, S., and Seki, S. (2010). Characterization of two F4/80-positive Kupffer cell subsets by their function and phenotype in mice. J Hepatol *53*, 903-910.

Kjaer, T. R., Thiel, S., and Andersen, G. R. (2013). Toward a structure-based comprehension of the lectin pathway of complement. Mol Immunol *56*, 413-422.

Klein, I., Cornejo, J. C., Polakos, N. K., John, B., Wuensch, S. A., Topham, D. J., Pierce, R. H., and Crispe, I. N. (2007). Kupffer cell heterogeneity: functional properties of bone marrow derived and sessile hepatic macrophages. Blood *110*, 4077-4085.

Ko, Y.-P., Kuipers, A., Freitag, C. M., Jongerius, I., Medina, E., van Rooijen, W. J., Spaan, A. N., van Kessel, Kok P M, **Höök, M., and Rooijakkers, S. H. M.** (2013). Phagocytosis escape by a Staphylococcus aureus protein that connects complement and coagulation proteins at the bacterial surface. PLoS Pathog. *9*, e1003816.

Kolaczkowska, E., Jenne, C. N., Surewaard, B. G. J., Thanabalasuriar, A., Lee, W.-Y., Sanz, M.-J., Mowen, K., Opdenakker, G., and Kubes, P. (2015). Molecular mechanisms of NET formation and degradation revealed by intravital imaging in the liver vasculature. Nature communications *6*, 6673.

Kolb, W. P., Haxby, J. A., Arroyave, C. M., and Muller-Eberhard, H. J. (1972). Molecular analysis of the membrane attack mechanism of complement. J Exp Med *135*, 549-566.

Kolb, W. P., and Muller-Eberhard, H. J. (1973). The membrane attack mechanism of complement. Verification of a stable C5-9 complex in free solution. J Exp Med *138*, 438-451.

Krijgsveld, J., Zaat, S. A., Meeldijk, J., van Veelen, P. A., Fang, G., Poolman, B., Brandt, E., Ehlert, J. E., Kuijpers, A. J., and Engbers, G. H.*, et al.* (2000). Thrombocidins, microbicidal proteins from human blood platelets, are C-terminal deletion products of CXC chemokines. The Journal of biological chemistry *275*, 20374-20381.

Krych-Goldberg, M., and Atkinson, J. P. (2001). Structure-function relationships of complement receptor type 1. Immunol Rev *180*, 112-122.

Kupffer, K. (1899). Über die sogennanten Sternzellen der Säugethierleber. Archiv für Mikroskopische Anatomie, 254-288.

Kurtz, C. B., O'Toole, E., Christensen, S. M., and Weis, J. H. (1990). The murine complement receptor gene family. IV. Alternative splicing of Cr2 gene transcripts predicts two distinct gene products that share homologous domains with both human CR2 and CR1. J Immunol *144*, 3581-3591.

Lachmann, P. J., and Nicol, P. (1973). Reaction mechanism of the alternative pathway of complement fixation. Lancet *1*, 465-467.

Lambris, J. D. (1988). The multifunctional role of C3, the third component of complement. Immunol. Today *9*, 387-393.

Langer, H. F., Daub, K., Braun, G., Schonberger, T., May, A. E., Schaller, M., Stein, G. M., Stellos, K., Bueltmann, A., and Siegel-Axel, D.*, et al.* (2007). Platelets recruit human dendritic cells via Mac-1/JAM-C interaction and modulate dendritic cell function in vitro. Arterioscler Thromb Vasc Biol *27*, 1463-1470.

Langnaese, K., Colleaux, L., Kloos, D. U., Fontes, M., and Wieacker, P. (2000). Cloning of Z39Ig, a novel gene with immunoglobulin-like domains located on human chromosome X. Biochim Biophys Acta *1492*, 522-525.

Lecuit, M., Vandormael-Pournin, S., Lefort, J., Huerre, M., Gounon, P., Dupuy, C., Babinet, C., and Cossart, P. (2001). A transgenic model for listeriosis: role of internalin in crossing the intestinal barrier. Science *292*, 1722-1725.

Lee, M.-Y., Kim, W.-J., Kang, Y.-J., Jung, Y.-M., Kang, Y.-M., Suk, K., Park, J.-E., Choi, E.-M., Choi, B.-K., and Kwon, B. S.*, et al.* (2006). Z39Ig is expressed on macrophages and may mediate inflammatory reactions in arthritis and atherosclerosis. J Leukoc Biol *80*, 922-928.

Lee, W.-Y., Moriarty, T. J., Wong, C. H. Y., Zhou, H., Strieter, R. M., van Rooijen, N., Chaconas, G., and Kubes, P. (2010). An intravascular immune response to Borrelia burgdorferi involves Kupffer cells and iNKT cells. Nat. Immunol. *11*, 295-302.

Lemaitre, B., Nicolas, E., Michaut, L., Reichhart, J.-M., and Hoffmann, J. A. (1996). The Dorsoventral Regulatory Gene Cassette spätzle/Toll/cactus Controls the Potent Antifungal Response in Drosophila Adults. Cell *86*, 973-983.

Leslie, M. (2010). Cell biology. Beyond clotting: the powers of platelets. Science *328*, 562-564.

Leslie, R. G. Q., and Nielsen, C. H. (2004). The classical and alternative pathways of complement activation play distinct roles in spontaneous C3 fragment deposition and membrane attack complex (MAC) formation on human B lymphocytes. Immunology *111*, 86-90.

Ley, K., Laudanna, C., Cybulsky, M. I., and Nourshargh, S. (2007). Getting to the site of inflammation: the leukocyte adhesion cascade updated. Nat. Rev. Immunol. *7*, 678-689.

Li, G., Sanders, J. M., Bevard, M. H., Sun, Z., Chumley, J. W., Galkina, E. V., Ley, K., and Sarembock, I. J. (2008). CD40 ligand promotes Mac-1 expression, leukocyte recruitment, and neointima formation after vascular injury. Am. J. Pathol. *172*, 1141-1152.

Li, Z., Delaney, M. K., O'Brien, K. A., and Du, X. (2010). Signaling during platelet adhesion and activation. Arterioscler. Thromb. Vasc. Biol. *30*, 2341-2349.

Løvik, M., and North, R. J. (1985). Effect of aging on antimicrobial immunity: old mice display a normal capacity for generating protective T cells and immunologic memory in response to infection with Listeria monocytogenes. Journal of immunology (Baltimore, Md. : 1950) *135*, 3479-3486.

Ludwig, W., Seewaldt, E., Kilpper-Balz, R., Heinz, K., Magrum, L., WOESE, C. R., Fox, G. E., and Stackerbrandt, E. (1985). The Phylogenetic Position of Streptococcus and Enterococcus. Microbiology *131*, 543-551.

Machado, G.-B. S., Assis, M.-C. de, **Leao, R., Saliba, A. M., Silva, M. C. A., Suassuna, J. H., Oliveira, A. V.** de, and **Plotkowski, M.-C.** (2010). ExoU-induced vascular hyperpermeability and platelet activation in the course of experimental Pseudomonas aeruginosa pneumosepsis. Shock *33*, 315-321.

MacKenzie, M. R., Creevy, N., and Heh, M. (1971). The interaction of human IgM and C1q. J. Immunol. *106*, 65-68.

Maletto, B. A., Ropolo, A. S., Alignani, D. O., Liscovsky, M. V., Ranocchia, R. P., Moron, V. G., and Pistoresi-Palencia, M. C. (2006). Presence of neutrophil-bearing antigen in lymphoid organs of immune mice. Blood *108*, 3094-3102.

Markiewski, M. M., Nilsson, B., Ekdahl, K. N., Mollnes, T. E., and Lambris, J. D. (2007). Complement and coagulation: strangers or partners in crime? Trends Immunol. *28*, 184-192.

Marshall-Clarke, S., Downes, J. E., Haga, I. R., Bowie, A. G., Borrow, P., Pennock, J. L., Grencis, R. K., and Rothwell, P. (2007). Polyinosinic Acid Is a Ligand for Toll-like Receptor 3. J. Biol. Chem. *282*, 24759-24766.

Massberg, S., Grahl, L., Bruehl, M.-L. von, **Manukyan, D., Pfeiler, S., Goosmann, C., Brinkmann, V., Lorenz, M., Bidzhekov, K., and Khandagale, A. B.***, et al.* (2010). Reciprocal coupling of coagulation and innate immunity via neutrophil serine proteases. Nature medicine *16*, 887-896.

Matsumoto, A., Kinoshita, M., Ono, S., Tsujimoto, H., Majima, T., Habu, Y., Shinomiya, N., and Seki, S. (2006). Cooperative IFN-gamma production of mouse liver B cells and natural killer cells stimulated with lipopolysaccharide. J Hepatol *45*, 290-298.

Matsumoto, A. K., Kopicky-Burd, J., Carter, R. H., Tuveson, D. A., Tedder, T. F., and Fearon, D. T. (1991). Intersection of the complement and immune systems: a signal transduction complex of the B lymphocyte-containing complement receptor type 2 and CD19. J Exp Med *173*, 55-64.

Matsumoto, M., Fukuda, W., Circolo, A., Goellner, J., Strauss-Schoenberger, J., Wang, X., Fujita, S., Hidvegi, T., Chaplin, D. D., and Colten, H. R. (1997). Abrogation of the alternative complement pathway by targeted deletion of murine factor B. Proc. Natl. Acad. Sci. U.S.A. *94*, 8720-8725.

Matsushita, M., and Fujita, T. (2002). The role of ficolins in innate immunity. Immunobiology *205*, 490-497.

Maugeri, N., Campana, L., Gavina, M., Covino, C., Metrio, M. de, **Panciroli, C., Maiuri, L., Maseri, A., D'Angelo, A., and Bianchi, M. E.***, et al.* (2014). Activated platelets present high mobility group box 1 to neutrophils, inducing autophagy and promoting the extrusion of neutrophil extracellular traps. Journal of thrombosis and haemostasis : JTH *12*, 2074-2088.

Mayer, M. M., Osler, A. G., Bier, O. G., and Heidelberger, M. (1946). The activating effect of magnesium and other cations on the hemolytic function of complement. J. Exp. Med. *84*, 535-548.

McDonald, B., Urrutia, R., Yipp, B. G., Jenne, C. N., and Kubes, P. (2012). Intravascular neutrophil extracellular traps capture bacteria from the bloodstream during sepsis. Cell host & microbe *12*, 324-333.

McGuill, M. W., and Rowan, A. N. (1989). Biological Effects of Blood Loss. Implications for Sampling Volumes and Techniques * Commentary: H. Richard Adams. ILAR Journal *31*, 5-20.

McNicol, A., Zhu, R., Pesun, R., Pampolina, C., Jackson, E. C., Bowden, G. H. W., and Zelinski, T. (2006). A role for immunoglobulin G in donor-specific Streptococcus sanguis-induced platelet aggregation. Thromb Haemost *95*, 288-293.

Melo, M. D., Catchpole, I. R., Haggar, G., and Stokes, R. W. (2000). Utilization of CD11b knockout mice to characterize the role of complement receptor 3 (CR3, CD11b/CD18) in the growth of Mycobacterium tuberculosis in macrophages. Cell. Immunol. *205*, 13-23.

Mestas, J., and Hughes, C. C. W. (2004). Of mice and not men: differences between mouse and human immunology. J. Immunol. *172*, 2731-2738.

Metchnikoff, E. (1893). Lectures on the Comparative Pathology of Inflammation. Keegan Paul, Trench, Trubner.

Miajlovic, H., Loughman, A., Brennan, M., Cox, D., and Foster, T. J. (2007). Both complement- and fibrinogen-dependent mechanisms contribute to platelet aggregation mediated by Staphylococcus aureus clumping factor B. Infect Immun *75*, 3335-3343.

Michelson, A. D. (2012). Platelets (s.l.: Elsevier Reference Monographs).

Miller, L. S., Pietras, E. M., Uricchio, L. H., Hirano, K., Rao, S., Lin, H., O'Connell, R. M., Iwakura, Y., Cheung, A. L., and Cheng, G.*, et al.* (2007). Inflammasome-mediated production of IL-1beta is required for neutrophil recruitment against Staphylococcus aureus in vivo. J Immunol *179*, 6933-6942.

Mills, D. C., Puri, R., Hu, C. J., Minniti, C., Grana, G., Freedman, M. D., Colman, R. F., and Colman, R. W. (1992). Clopidogrel inhibits the binding of ADP analogues to the receptor mediating inhibition of platelet adenylate cyclase. Arterioscler Thromb *12*, 430-436.

Miniño, A. M., Murphy, S. L., Xu, J., and Kochanek, K. D. (2011). Deaths: final data for 2008. Natl Vital Stat Rep *59*, 1-126.

Misra, U. K., and Pizzo, S. V. (1998). Ligation of the alpha2M signaling receptor with receptor-recognized forms of alpha2-macroglobulin initiates protein and DNA synthesis in macrophages. The effect of intracellular calcium. Biochim. Biophys. Acta *1401*, 121-128.

Mitchell, D. A., Pickering, M. C., Warren, J., Fossati-Jimack, L., Cortes-Hernandez, J., Cook, H. T., Botto, M., and Walport, M. J. (2002). C1q deficiency and autoimmunity: the effects of genetic background on disease expression. J. Immunol. *168*, 2538-2543.

Moghimi, S. M., Hedeman, H., Christy, N. M., Illum, L., and Davis, S. S. (1993). Enhanced hepatic clearance of intravenously administered sterically stabilized microspheres in zymosan-stimulated rats. Journal of leukocyte biology *54*, 513-517.

Molina, H., Holers, V. M., Li, B., Fung, Y., Mariathasan, S., Goellner, J., Strauss-Schoenberger, J., Karr, R. W., and Chaplin, D. D. (1996). Markedly impaired humoral

immune response in mice deficient in complement receptors 1 and 2. Proc Natl Acad Sci U S A *93*, 3357-3361.

Moore, P. L., Bank, H. L., Brissie, N. T., and Spicer, S. S. (1978). Phagocytosis of bacteria by polymorphonuclear leukocytes. A freeze-fracture, scanning electron microscope, and thin-section investigation of membrane structure. J Cell Biol *76*, 158-174.

Moreno, S. E., Alves-Filho, J. C., Alfaya, T. M., da Silva, J. S., Ferreira, S. H., and Liew, F. Y. (2006). IL-12, but not IL-18, is critical to neutrophil activation and resistance to polymicrobial sepsis induced by cecal ligation and puncture. J Immunol *177*, 3218-3224.

Morgan, B. P., and Gasque, P. (1997). Extrahepatic complement biosynthesis: where, when and why? Clin Exp Immunol *107*, 1-7.

Moriwaki, H., Blaner, W. S., Piantedosi, R., and Goodman, D. S. (1988). Effects of dietary retinoid and triglyceride on the lipid composition of rat liver stellate cells and stellate cell lipid droplets. J Lipid Res *29*, 1523-1534.

Movita, D., Kreefft, K., Biesta, P., van Oudenaren, A., Leenen, P. J. M., Janssen, H. L. A., and Boonstra, A. (2012). Kupffer cells express a unique combination of phenotypic and functional characteristics compared with splenic and peritoneal macrophages. J Leukoc Biol *92*, 723-733.

Muraille, E., Giannino, R., Guirnalda, P., Leiner, I., Jung, S., Pamer, E. G., and Lauvau, G. (2005). Distinct in vivo dendritic cell activation by live versus killed Listeria monocytogenes. Eur. J. Immunol. *35*, 1463-1471.

Muramatsu, M., Kinoshita, K., Fagarasan, S., Yamada, S., Shinkai, Y., and Honjo, T. (2000). Class switch recombination and hypermutation require activation-induced cytidine deaminase (AID), a potential RNA editing enzyme. Cell *102*, 553-563.

Murphy, K. M., Travers, P., Walport, M., Janeway, C. A., and Ehrenstein, M. (2014). Janeway Immunologie (Berlin: Springer Spektrum).

Naito, M., Hasegawa, G., Ebe, Y., and Yamamoto, T. (2004). Differentiation and function of Kupffer cells. Med Electron Microsc *37*, 16-28.

Naito, M., Hasegawa, G., and Takahashi, K. (1997). Development, differentiation, and maturation of Kupffer cells. Microsc Res Tech *39*, 350-364.

Naito, M., Suzuki, H., Mori, T., Matsumoto, A., Kodama, T., and Takahashi, K. (1992). Coexpression of type I and type II human macrophage scavenger receptors in macrophages of various organs and foam cells in atherosclerotic lesions. The American journal of pathology *141*, 591-599.

Naito, M., and Takahashi, K. (1991). The role of Kupffer cells in glucan-induced granuloma formation in the liver of mice depleted of blood monocytes by administration of strontium-89. Lab Invest *64*, 664-674.

Nakashima, M., Kinoshita, M., Nakashima, H., Habu, Y., Miyazaki, H., Shono, S., Hiroi, S., Shinomiya, N., Nakanishi, K., and Seki, S. (2012). Pivotal advance: characterization of mouse liver phagocytic B cells in innate immunity. J Leukoc Biol *91*, 537-546.

Nemeth, E., Baird, A. W., and O'Farrelly, C. (2009). Microanatomy of the liver immune system. Semin Immunopathol *31*, 333-343.

Neuenhahn, M., Kerksiek, K. M., Nauerth, M., Suhre, M. H., Schiemann, M., Gebhardt, F. E., Stemberger, C., Panthel, K., Schroder, S., and Chakraborty, T.*, et al.* (2006). CD8alpha+ dendritic cells are required for efficient entry of Listeria monocytogenes into the spleen. Immunity *25*, 619-630.

Nicoletti, I., Migliorati, G., Pagliacci, M. C., Grignani, F., and Riccardi, C. (1991). A rapid and simple method for measuring thymocyte apoptosis by propidium iodide staining and flow cytometry. J. Immunol. Methods *139*, 271-279.

Nunez, D., Charriaut-Marlangue, C., Barel, M., Benveniste, J., and Frade, R. (1987). Activation of human platelets through gp140, the C3d/EBV receptor (CR2). Eur J Immunol *17*, 515-520.

Ochsenbein, A. F., Fehr, T., Lutz, C., Suter, M., Brombacher, F., Hengartner, H., and Zinkernagel, R. M. (1999). Control of early viral and bacterial distribution and disease by natural antibodies. Science *286*, 2156-2159.

Oldenburg, M., Kruger, A., Ferstl, R., Kaufmann, A., Nees, G., Sigmund, A., Bathke, B., Lauterbach, H., Suter, M., and Dreher, S.*, et al.* (2012). TLR13 recognizes bacterial 23S rRNA devoid of erythromycin resistance-forming modification. Science *337*, 1111-1115.

Ono, K., Nishitani, C., Mitsuzawa, H., Shimizu, T., Sano, H., Suzuki, H., Kodama, T., Fujii, N., Fukase, K., and Hirata, K.*, et al.* (2006). Mannose-binding lectin augments the uptake of lipid A, Staphylococcus aureus, and Escherichia coli by Kupffer cells through increased cell surface expression of scavenger receptor A. J Immunol *177*, 5517-5523.

Orlova, V. V., Choi, E. Y., Xie, C., Chavakis, E., Bierhaus, A., Ihanus, E., Ballantyne, C. M., Gahmberg, C. G., Bianchi, M. E., and Nawroth, P. P.*, et al.* (2007). A novel pathway of HMGB1-mediated inflammatory cell recruitment that requires Mac-1-integrin. The EMBO journal *26*, 1129-1139.

Orsini, J., Mainardi, C., Muzylo, E., Karki, N., Cohen, N., and Sakoulas, G. (2012). Microbiological Profile of Organisms Causing Bloodstream Infection in Critically Ill Patients. J Clin Med Res *4*, 371-377.

Paidassi, H., Tacnet-Delorme, P., Garlatti, V., Darnault, C., Ghebrehiwet, B., Gaboriaud, C., Arlaud, G. J., and Frachet, P. (2008a). C1q binds phosphatidylserine and likely acts as a multiligand-bridging molecule in apoptotic cell recognition. J Immunol *180*, 2329-2338.

Paidassi, H., Tacnet-Delorme, P., Lunardi, T., Arlaud, G. J., Thielens, N. M., and Frachet, P. (2008b). The lectin-like activity of human C1q and its implication in DNA and apoptotic cell recognition. FEBS Lett *582*, 3111-3116.

Pamer, E. G. (2004). Immune responses to Listeria monocytogenes. Nature Reviews Immunology *4*, 812.

Pampolina, C., and McNicol, A. (2005). Streptococcus sanguis-induced platelet activation involves two waves of tyrosine phosphorylation mediated by FcgammaRIIA and alphaIIbbeta3. Thromb Haemost *93*, 932-939.

Pangburn, M. K., and Muller-Eberhard, H. J. (1984). The alternative pathway of complement. Springer Semin Immunopathol *7*, 163-192.

Pangburn, M. K., Schreiber, R. D., and Muller-Eberhard, H. J. (1981). Formation of the initial C3 convertase of the alternative complement pathway. Acquisition of C3b-like activities by spontaneous hydrolysis of the putative thioester in native C3. J Exp Med *154*, 856-867.

Pasche, B., Kalaydjiev, S., Franz, T. J., Kremmer, E., Gailus-Durner, V., Fuchs, H., Hrabé de Angelis, M., Lengeling, A., and Busch, D. H. (2005). Sex-dependent susceptibility to Listeria monocytogenes infection is mediated by differential interleukin-10 production. Infection and immunity *73*, 5952-5960.

Peerschke, E. I., and Ghebrehiwet, B. (1997). C1q augments platelet activation in response to aggregated Ig. J Immunol *159*, 5594-5598.

Peerschke, E. I., and Ghebrehiwet, B. (2001). Human blood platelet gC1qR/p33. Immunol Rev *180*, 56-64.

Peerschke, E. I., Reid, K. B., and Ghebrehiwet, B. (1993). Platelet activation by C1q results in the induction of alpha IIb/beta 3 integrins (GPIIb-IIIa) and the expression of P-selectin and procoagulant activity. J. Exp. Med. *178*, 579-587.

Peiser, L., De Winther, Menno P J, **Makepeace, K., Hollinshead, M., Coull, P., Plested, J., Kodama, T., Moxon, E. R., and Gordon, S.** (2002a). The class A macrophage scavenger receptor is a major pattern recognition receptor for Neisseria meningitidis which is independent of lipopolysaccharide and not required for secretory responses. Infect Immun *70*, 5346-5354.

Peiser, L., and Gordon, S. (2001). The function of scavenger receptors expressed by macrophages and their role in the regulation of inflammation. Microbes Infect *3*, 149-159.

Peiser, L., Gough, P. J., Kodama, T., and Gordon, S. (2000). Macrophage class A scavenger receptor-mediated phagocytosis of Escherichia coli: role of cell heterogeneity, microbial strain, and culture conditions in vitro. Infect Immun *68*, 1953-1963.

Peiser, L., Mukhopadhyay, S., and Gordon, S. (2002b). Scavenger receptors in innate immunity. Curr Opin Immunol *14*, 123-128.

Petrik, M., Haas, H., Schrettl, M., Helbok, A., Blatzer, M., and Decristoforo, C. (2012). In vitro and in vivo evaluation of selected 68Ga-siderophores for infection imaging. Nucl. Med. Biol. *39*, 361-369.

Phillips, M. J., Poucell, S., Patterson, J., and Valencia, P. (1987). An Atlas and Text of Ultrastructural Pathology (New York: Raven Press).

Phillipson, M., and Kubes, P. (2011). The neutrophil in vascular inflammation. Nat. Med. *17*, 1381-1390.

Pickering, M. C., Jorge, E. G. de, **Martinez-Barricarte, R., Recalde, S., Garcia-Layana, A., Rose, K. L., Moss, J., Walport, M. J., Cook, H. T., and Córdoba, S. R.** de*, et al.* (2007). Spontaneous hemolytic uremic syndrome triggered by complement factor H lacking surface recognition domains. J. Exp. Med. *204*, 1249-1256.

Pillay, J., den Braber, I., Vrisekoop, N., Kwast, L. M., Boer, R. J. de, **Borghans, J. A. M., Tesselaar, K., and Koenderman, L.** (2010). In vivo labeling with 2H2O reveals a human neutrophil lifespan of 5.4 days. Blood *116*, 625-627.

Pinto, A. J., Stewart, D., van Rooijen, N., and Morahan, P. S. (1991). Selective depletion of liver and splenic macrophages using liposomes encapsulating the drug dichloromethylene diphosphonate: effects on antimicrobial resistance. J Leukoc Biol *49*, 579-586.

Pizarro-Cerdá, J., Kühbacher, A., and Cossart, P. (2012). Entry of Listeria monocytogenes in mammalian epithelial cells: an updated view. Cold Spring Harb Perspect Med *2*.

Platt, N., and Gordon, S. (2001). Is the class A macrophage scavenger receptor (SR-A) multifunctional? - The mouse's tale. J Clin Invest *108*, 649-654.

Pluddemann, A., Hoe, J. C., Makepeace, K., Moxon, E. R., and Gordon, S. (2009). The macrophage scavenger receptor A is host-protective in experimental meningococcal septicaemia. PLoS Pathog *5*, e1000297.

Polley, M. J., and Nachman, R. L. (1983). Human platelet activation by C3a and C3a des-arg. J. Exp. Med. *158*, 603-615.

Poros-Gluchowska, J., and Markiewicz, Z. (2003). Antimicrobial resistance of Listeria monocytogenes. Acta Microbiol Pol *52*, 113-129.

Quigg, R. J., Alexander, J. J., Lo, C. F., Lim, A., He, C., and Holers, V. M. (1997). Characterization of C3-binding proteins on mouse neutrophils and platelets. J Immunol *159*, 2438-2444.

Ramadori, G., Rasokat, H., Burger, R., Meyer Zum Büschenfelde, K H, and **Bitter-Suermann, D.** (1984). Quantitative determination of complement components produced by purified hepatocytes. Clin. Exp. Immunol. *55*, 189-196.

Reynes, M., Aubert, J. P., Cohen, J. H., Audouin, J., Tricottet, V., Diebold, J., and Kazatchkine, M. D. (1985). Human follicular dendritic cells express CR1, CR2, and CR3 complement receptor antigens. J Immunol *135*, 2687-2694.

Richards, A., Kemp, E. J., Liszewski, M. K., Goodship, J. A., Lampe, A. K., Decorte, R., Müslümanoğlu, M. H., Kavukcu, S., Filler, G., and Pirson, Y.*, et al.* (2003). Mutations in human complement regulator, membrane cofactor protein (CD46), predispose to development of familial hemolytic uremic syndrome. Proc. Natl. Acad. Sci. U.S.A. *100*, 12966-12971.

Robinson, M. J., Osorio, F., Rosas, M., Freitas, R. P., Schweighoffer, E., Gross, O., Verbeek, J. S., Ruland, J., Tybulewicz, V., and Brown, G. D.*, et al.* (2009). Dectin-2 is a Syk-coupled pattern recognition receptor crucial for Th17 responses to fungal infection. J Exp Med *206*, 2037-2051.

Rodriguez, P. C., Ernstoff, M. S., Hernandez, C., Atkins, M., Zabaleta, J., Sierra, R., and Ochoa, A. C. (2009). Arginase I-producing myeloid-derived suppressor cells in renal cell carcinoma are a subpopulation of activated granulocytes. Cancer Res. *69*, 1553-1560.

Rosen, H., Gordon, S., and North, R. J. (1989). Exacerbation of murine listeriosis by a monoclonal antibody specific for the type 3 complement receptor of myelomonocytic cells. Absence of monocytes at infective foci allows Listeria to multiply in nonphagocytic cells. J Exp Med *170*, 27-37.

Ross, G. D. (2000). Regulation of the adhesion versus cytotoxic functions of the Mac-1/CR3/alphaMbeta2-integrin glycoprotein. Crit Rev Immunol *20*, 197-222.

Ross, G. D., and Medof, M. E. (1985). Membrane complement receptors specific for bound fragments of C3. Adv Immunol *37*, 217-267.

Ross, G. D., and Vetvicka, V. (1993). CR3 (CD11b, CD18): a phagocyte and NK cell membrane receptor with multiple ligand specificities and functions. Clin Exp Immunol *92*, 181-184.

Ruggeri, Z. M., Marco, L. de, **Gatti, L., Bader, R., and Montgomery, R. R.** (1983). Platelets have more than one binding site for von Willebrand factor. J Clin Invest *72*, 1-12.

Salkowski, C. A., Neta, R., Wynn, T. A., Strassmann, G., van Rooijen, N., and Vogel, S. N. (1995). Effect of liposome-mediated macrophage depletion on LPS-induced cytokine gene expression and radioprotection. J Immunol *155*, 3168-3179.

Savage, B., Saldivar, E., and Ruggeri, Z. M. (1996). Initiation of platelet adhesion by arrest onto fibrinogen or translocation on von Willebrand factor. Cell *84*, 289-297.

Scaffidi, P., Misteli, T., and Bianchi, M. E. (2002). Release of chromatin protein HMGB1 by necrotic cells triggers inflammation. Nature *418*, 191-195.

Schlesinger, P. H., Doebber, T. W., Mandell, B. F., White, R., DeSchryver, C., Rodman, J. S., Miller, M. J., and Stahl, P. (1978). Plasma clearance of glycoproteins with terminal mannose and N-acetylglucosamine by liver non-parenchymal cells. Studies with beta-glucuronidase, N-acetyl-beta-D-glucosaminidase, ribonuclease B and agalacto-orosomucoid. Biochem J *176*, 103-109.

Schmitt, A., Guichard, J., Massé, J. M., Debili, N., and Cramer, E. M. (2001). Of mice and men: comparison of the ultrastructure of megakaryocytes and platelets. Exp. Hematol. *29*, 1295-1302.

Schror, K. (1997). Aspirin and platelets: the antiplatelet action of aspirin and its role in thrombosis treatment and prophylaxis. Semin Thromb Hemost *23*, 349-356.

Schuchat, A., Swaminathan, B., and Broome, C. V. (1991). Epidemiology of human listeriosis. Clin Microbiol Rev *4*, 169-183.

Semple, J. W., Aslam, R., Kim, M., Speck, E. R., and Freedman, J. (2007). Platelet-bound lipopolysaccharide enhances Fc receptor-mediated phagocytosis of IgG-opsonized platelets. Blood *109*, 4803-4805.

Semple, J. W., Italiano, J. E., JR, and Freedman, J. (2011). Platelets and the immune continuum. Nat Rev Immunol *11*, 264-274.

Sengelov, H., Kjeldsen, L., Kroeze, W., Berger, M., and Borregaard, N. (1994). Secretory vesicles are the intracellular reservoir of complement receptor 1 in human neutrophils. J Immunol *153*, 804-810.

Shattil, S. J., and Newman, P. J. (2004). Integrins: dynamic scaffolds for adhesion and signaling in platelets. Blood *104*, 1606-1615.

Shen, Y., Naujokas, M., Park, M., and Ireton, K. (2000). InIB-dependent internalization of Listeria is mediated by the Met receptor tyrosine kinase. Cell *103*, 501-510.

Shi, J., Kokubo, Y., and Wake, K. (1998). Expression of P-selectin on hepatic endothelia and platelets promoting neutrophil removal by liver macrophages. Blood *92*, 520-528.

Shimazu, R., Akashi, S., Ogata, H., Nagai, Y., Fukudome, K., Miyake, K., and Kimoto, M. (1999). MD-2, a molecule that confers lipopolysaccharide responsiveness on Toll-like receptor 4. J Exp Med *189*, 1777-1782.

Singer, J. M., Adlersberg, L., Hoenig, E. M., Ende, E., and Tchorsch, Y. (1969). Radiolabeled latex particles ithe investigation of phagocytosis in vivo: clearance curves and histological observations. J Reticuloendothel Soc *6*, 561-589.

Singh, B., Doane, K. J., and Niehaus, G. D. (1998). Ultrastructural and cytochemical evaluation of sepsis-induced changes in the rat pulmonary intravascular mononuclear phagocytes. J Anat *192 (Pt 1)*, 13-23.

Skamene, E., and Chayasirisobhon, W. (1977). Enhanced resistance to Listeria monocytogenes in splenectomized mice. Immunology *33*, 851-858.

Skattum, L., van Deuren, M., van der Poll, T., and Truedsson, L. (2011). Complement deficiency states and associated infections. Mol. Immunol. *48*, 1643-1655.

Smith, S. N., Hagan, E. C., Lane, M. C., and Mobley, H. L. T. (2010). Dissemination and systemic colonization of uropathogenic Escherichia coli in a murine model of bacteremia. MBio *1*.

Snyderman, R., Phillips, J., and Mergenhagen, S. E. (1970). Polymorphonuclear leukocyte chemotactic activity in rabbit serum and Guinea pig serum treated with immune complexes: evidence for c5a as the major chemotactic factor. Infect Immun *1*, 521-525.

Sontheimer, R. D., Racila, E., and Racila, D. M. (2005). C1q: its functions within the innate and adaptive immune responses and its role in lupus autoimmunity. J Invest Dermatol *125*, 14-23.

Sreeramkumar, V., Adrover, J. M., Ballesteros, I., Cuartero, M. I., Rossaint, J., Bilbao, I., Nácher, M., Pitaval, C., Radovanovic, I., and Fukui, Y.*, et al.* (2014). Neutrophils scan for activated platelets to initiate inflammation. Science (New York, N.Y.) *346*, 1234-1238.

Stahl, P. D., Rodman, J. S., Miller, M. J., and Schlesinger, P. H. (1978). Evidence for receptor-mediated binding of glycoproteins, glycoconjugates, and lysosomal glycosidases by alveolar macrophages. Proc Natl Acad Sci U S A *75*, 1399-1403.

Stark, M. A., Huo, Y., Burcin, T. L., Morris, M. A., Olson, T. S., and Ley, K. (2005). Phagocytosis of apoptotic neutrophils regulates granulopoiesis via IL-23 and IL-17. Immunity *22*, 285-294.

Stewart, C. R., Bagnaud-Baule, A., Karpala, A. J., Lowther, S., Mohr, P. G., Wise, T. G., Lowenthal, J. W., and Bean, A. G. (2012). Toll-like receptor 7 ligands inhibit influenza A infection in chickens. J. Interferon Cytokine Res. *32*, 46-51.

Su, G. L., Klein, R. D., Aminlari, A., Zhang, H. Y., Steinstraesser, L., Alarcon, W. H., Remick, D. G., and Wang, S. C. (2000). Kupffer cell activation by lipopolysaccharide in rats: role for lipopolysaccharide binding protein and toll-like receptor 4. Hepatology *31*, 932-936.

Suarez, M., Gonzalez-Zorn, B., Vega, Y., Chico-Calero, I., and Vazquez-Boland, J. A. (2001). A role for ActA in epithelial cell invasion by Listeria monocytogenes. Cell Microbiol *3*, 853-864.

Suzuki, H., Kurihara, Y., Takeya, M., Kamada, N., Kataoka, M., Jishage, K., Ueda, O., Sakaguchi, H., Higashi, T., and Suzuki, T.*, et al.* (1997). A role for macrophage scavenger receptors in atherosclerosis and susceptibility to infection. Nature *386*, 292-296.

Tacchini-Cottier, F., Zweifel, C., Belkaid, Y., Mukankundiye, C., Vasei, M., Launois, P., Milon, G., and Louis, J. A. (2000). An immunomodulatory function for neutrophils during the induction of a CD4+ Th2 response in BALB/c mice infected with Leishmania major. J. Immunol. *165*, 2628-2636.

Takeuchi, O., and Akira, S. (2010). Pattern recognition receptors and inflammation. Cell *140*, 805-820.

Takeuchi, O., Kawai, T., Muhlradt, P. F., Morr, M., Radolf, J. D., Zychlinsky, A., Takeda, K., and Akira, S. (2001). Discrimination of bacterial lipoproteins by Toll-like receptor 6. Int Immunol *13*, 933-940.

Takeuchi, O., Sato, S., Horiuchi, T., Hoshino, K., Takeda, K., Dong, Z., Modlin, R. L., and Akira, S. (2002). Cutting edge: role of Toll-like receptor 1 in mediating immune response to microbial lipoproteins. J Immunol *169*, 10-14.

Tanabe, Y., Xiong, H., Nomura, T., Arakawa, M., and Mitsuyama, M. (1999). Induction of Protective T Cells against Listeria monocytogenes in Mice by Immunization with a Listeriolysin O-Negative Avirulent Strain of Bacteria and Liposome-Encapsulated Listeriolysin O. Infect Immun *67*, 568-575.

Taylor, P. R., Brown, G. D., Reid, D. M., Willment, J. A., Martinez-Pomares, L., Gordon, S., and Wong, S. Y. C. (2002). The beta-glucan receptor, dectin-1, is predominantly expressed on the surface of cells of the monocyte/macrophage and neutrophil lineages. J Immunol *169*, 3876-3882.

Taylor, P. R., Reid, D. M., Heinsbroek, S. E. M., Brown, G. D., Gordon, S., and Wong, S. Y. C. (2005). Dectin-2 is predominantly myeloid restricted and exhibits unique activation-dependent expression on maturing inflammatory monocytes elicited in vivo. Eur J Immunol *35*, 2163-2174.

Taylor, R. P., Ferguson, P. J., Martin, E. N., Cooke, J., Greene, K. L., Grinspun, K., Guttman, M., and Kuhn, S. (1997). Immune complexes bound to the primate erythrocyte complement

receptor (CR1) via anti-CR1 mAbs are cleared simultaneously with loss of CR1 in a concerted reaction in a rhesus monkey model. Clin Immunol Immunopathol *82*, 49-59.

Tepper, R. I., Coffman, R. L., and Leder, P. (1992). An eosinophil-dependent mechanism for the antitumor effect of interleukin-4. Science *257*, 548-551.

Terpstra, V., and van Berkel, T. J. (2000). Scavenger receptors on liver Kupffer cells mediate the in vivo uptake of oxidatively damaged red blood cells in mice. Blood *95*, 2157-2163.

Thomas, C. A., Li, Y., Kodama, T., Suzuki, H., Silverstein, S. C., and El Khoury, J. (2000). Protection from lethal gram-positive infection by macrophage scavenger receptor-dependent phagocytosis. J Exp Med *191*, 147-156.

Tilney, L. G., and Portnoy, D. A. (1989). Actin filaments and the growth, movement, and spread of the intracellular bacterial parasite, Listeria monocytogenes. J Cell Biol *109*, 1597-1608.

Timmons, S., Huzoor-Akbar, **Grabarek, J., Kloczewiak, M., and Hawiger, J.** (1986). Mechanism of human platelet activation by endotoxic glycolipid-bearing mutant Re595 of Salmonella minnesota. Blood *68*, 1015-1023.

Uematsu, S., and Akira, S. (2006). Toll-like receptors and innate immunity. J. Mol. Med. *84*, 712-725.

Urban, C. F., Reichard, U., Brinkmann, V., and Zychlinsky, A. (2006). Neutrophil extracellular traps capture and kill Candida albicans yeast and hyphal forms. Cell Microbiol *8*, 668-676.

van der Laan, L J, **Dopp, E. A., Haworth, R., Pikkarainen, T., Kangas, M., Elomaa, O., Dijkstra, C. D., Gordon, S., Tryggvason, K., and Kraal, G.** (1999). Regulation and functional involvement of macrophage scavenger receptor MARCO in clearance of bacteria in vivo. J Immunol *162*, 939-947.

van Furth, R. (1980). Cell of the mononuclear phagocyte system. Nomenclature in terms of sites and conditions. In Mononuclear phagocytes. Functional aspects., R. van Furth, ed. (Hague: Nijhoff), pp. 1–30.

van Furth, R. (1989). Origin and turnover of monocytes and macrophages. Curr Top Pathol *79*, 125-150.

van Furth, R., Cohn, Z. A., Hirsch, J. G., Humphrey, J. H., Spector, W. G., and Langevoort, H. L. (1972). The mononuclear phagocyte system: a new classification of macrophages, monocytes, and their precursor cells. Bull World Health Organ *46*, 845-852.

van Kessel, K. P., Antonissen, A. C., van Dijk, H., Rademaker, P. M., and Willers, J. M. (1981). Interactions of killed Listeria monocytogenes with the mouse complement system. Infect Immun *34*, 16-19.

van Lookeren Campagne, M., Wiesmann, C., and Brown, E. J. (2007). Macrophage complement receptors and pathogen clearance. Cell Microbiol *9*, 2095-2102.

van Rooijen, N., and van Nieuwmegen, R. (1984). Elimination of phagocytic cells in the spleen after intravenous injection of liposome-encapsulated dichloromethylene diphosphonate. An enzyme-histochemical study. Cell Tissue Res *238*, 355-358.

Vermaelen, K., and Pauwels, R. (2004). Accurate and simple discrimination of mouse pulmonary dendritic cell and macrophage populations by flow cytometry: methodology and new insights. Cytometry. Part A : the journal of the International Society for Analytical Cytology *61*, 170-177.

Verschoor, A., Neuenhahn, M., Navarini, A. A., Graef, P., Plaumann, A., Seidlmeier, A., Nieswandt, B., Massberg, S., Zinkernagel, R. M., and Hengartner, H.*, et al.* (2011). A platelet-mediated system for shuttling blood-borne bacteria to CD8alpha+ dendritic cells depends on glycoprotein GPIb and complement C3. Nat Immunol *12*, 1194-1201.

Vieira, S. M., Lemos, H. P., Grespan, R., Napimoga, M. H., Dal-Secco, D., Freitas, A., Cunha, T. M., Verri, W. A., JR, Souza-Junior, D. A., and Jamur, M. C.*, et al.* (2009). A crucial role for TNF-alpha in mediating neutrophil influx induced by endogenously generated or exogenous chemokines, KC/CXCL1 and LIX/CXCL5. Br J Pharmacol *158*, 779-789.

Vik, D. P., and Fearon, D. T. (1987). Cellular distribution of complement receptor type 4 (CR4): expression on human platelets. J Immunol *138*, 254-258.

Vogt, L., Schmitz, N., Kurrer, M. O., Bauer, M., Hinton, H. I., Behnke, S., Gatto, D., Sebbel, P., Beerli, R. R., and Sonderegger, I.*, et al.* (2006). VSIG4, a B7 family-related protein, is a negative regulator of T cell activation. J Clin Invest *116*, 2817-2826.

Wake, K. (1980). Perisinusoidal stellate cells (fat-storing cells, interstitial cells, lipocytes), their related structure in and around the liver sinusoids, and vitamin A-storing cells in extrahepatic organs. Int Rev Cytol *66*, 303-353.

Wake, K., Decker, K., Kirn, A., Knook, D. L., McCuskey, R. S., Bouwens, L., and Wisse, E. (1989). Cell biology and kinetics of Kupffer cells in the liver. Int Rev Cytol *118*, 173-229.

Wautier, J. L., Souchon, H., Reid, K. B., Peltier, A. P., and Caen, J. P. (1977). Studies on the mode of reaction of the first component of complement with platelets: interaction between the collagen-like portion of C1q and platelets. Immunochemistry *14*, 763-766.

Weis, J. J., Tedder, T. F., and Fearon, D. T. (1984). Identification of a 145,000 Mr membrane protein as the C3d receptor (CR2) of human B lymphocytes. Proc Natl Acad Sci U S A *81*, 881-885.

Weis, W. I., Taylor, M. E., and Drickamer, K. (1998). The C-type lectin superfamily in the immune system. Immunol Rev *163*, 19-34.

Weisman, H. F., Bartow, T., Leppo, M. K., Marsh, H. C., JR, Carson, G. R., Concino, M. F., Boyle, M. P., Roux, K. H., Weisfeldt, M. L., and Fearon, D. T. (1990). Soluble human complement receptor type 1: in vivo inhibitor of complement suppressing post-ischemic myocardial inflammation and necrosis. Science *249*, 146-151.

Wessels, M. R., Butko, P., Ma, M., Warren, H. B., Lage, A. L., and Carroll, M. C. (1995). Studies of group B streptococcal infection in mice deficient in complement component C3 or C4 demonstrate an essential role for complement in both innate and acquired immunity. Proc. Natl. Acad. Sci. U.S.A. *92*, 11490-11494.

Weyrich, A. S., and Zimmerman, G. A. (2004). Platelets: signaling cells in the immune continuum. Trends in immunology *25*, 489-495.

Widmann, J. J., Cotran, R. S., and Fahimi, H. D. (1972). Mononuclear phagocytes (Kupffer cells) and endothelial cells. Identification of two functional cell types in rat liver sinusoids by endogenous peroxidase activity. J Cell Biol *52*, 159-170.

Wiegand, S., Heinen, T., Ramaswamy, A., Sesterhenn, A. M., Bergemann, C., Werner, J. A., and Lübbe, A. S. (2009). Evaluation of the tolerance and distribution of intravenously applied ferrofluid particles of 250 and 500 nm size in an animal model. Journal of drug targeting *17*, 194-199.

Wiesmann, C., Katschke, K. J., Yin, J., Helmy, K. Y., Steffek, M., Fairbrother, W. J., McCallum, S. A., Embuscado, L., DeForge, L., and Hass, P. E.*, et al.* (2006). Structure of C3b in complex with CRIg gives insights into regulation of complement activation. Nature *444*, 217-220.

Willekens, F. L. A., Werre, J. M., Kruijt, J. K., Roerdinkholder-Stoelwinder, B., Groenen-Dopp, Y. A. M., van den Bos, Annegeet G, Bosman, Giel J C G M, and van Berkel, Theo J C (2005). Liver Kupffer cells rapidly remove red blood cell-derived vesicles from the circulation by scavenger receptors. Blood *105*, 2141-2145.

Wisse, E. (1970). An electron microscopic study of the fenestrated endothelial lining of rat liver sinusoids. J Ultrastruct Res *31*, 125-150.

Wisse, E. (1974). Kupffer cell reactions in rat liver under various conditions as observed in the electron microscope. J Ultrastruct Res *46*, 499-520.

Wisse, E., Zanger, R. B. de, **Charels, K., van der Smissen, P., and McCuskey, R. S.** (1985). The liver sieve: considerations concerning the structure and function of endothelial fenestrae, the sinusoidal wall and the space of Disse. Hepatology *5*, 683-692.

Wolfs, E., Struys, T., Notelaers, T., Roberts, S. J., Sohni, A., Bormans, G., van Laere, K., Luyten, F. P., Gheysens, O., and Lambrichts, I.*, et al.* (2013). 18F-FDG labeling of

mesenchymal stem cells and multipotent adult progenitor cells for PET imaging: effects on ultrastructure and differentiation capacity. J. Nucl. Med. *54*, 447-454.

Wong, C. H. Y., Jenne, C. N., Petri, B., Chrobok, N. L., and Kubes, P. (2013a). Nucleation of platelets with blood-borne pathogens on Kupffer cells precedes other innate immunity and contributes to bacterial clearance. Nat Immunol *14*, 785-792.

Wong, C. H. Y., Jenne, C. N., Petri, B., Chrobok, N. L., and Kubes, P. (2013b). Nucleation of platelets with blood-borne pathogens on Kupffer cells precedes other innate immunity and contributes to bacterial clearance. Nat Immunol *14*, 785-792.

Wong, J., Johnston, B., Lee, S. S., Bullard, D. C., Smith, C. W., Beaudet, A. L., and Kubes, P. (1997). A minimal role for selectins in the recruitment of leukocytes into the inflamed liver microvasculature. J. Clin. Invest. *99*, 2782-2790.

Wood, W. B., Smith, M. R., Perry, W. D., and Berry, J. W. (1951). Studies on the cellular immunology of acute bacteriemia. I. Intravascular leucocytic reaction and surface phagocytosis. J Exp Med *94*, 521-534.

Wu, H., Gower, R. M., Wang, H., Perrard, X.-Y. D., Ma, R., Bullard, D. C., Burns, A. R., Paul, A., Smith, C. W., and Simon, S. I.*, et al.* (2009). Functional role of CD11c+ monocytes in atherogenesis associated with hypercholesterolemia. Circulation *119*, 2708-2717.

Wu, J., Meng, Z., Jiang, M., Zhang, E., Trippler, M., Broering, R., Bucchi, A., Krux, F., Dittmer, U., and Yang, D.*, et al.* (2010). Toll-like receptor-induced innate immune responses in non-parenchymal liver cells are cell type-specific. Immunology *129*, 363-374.

Xia, Y., Vetvicka, V., Yan, J., Hanikýrová, M., Mayadas, T., and Ross, G. D. (1999). The beta-glucan-binding lectin site of mouse CR3 (CD11b/CD18) and its function in generating a primed state of the receptor that mediates cytotoxic activation in response to iC3b-opsonized target cells. Journal of immunology (Baltimore, Md. : 1950) *162*, 2281-2290.

Xiong, H., Tanabe, Y., Ohya, S., and Mitsuyama, M. (1998). Administration of killed bacteria together with listeriolysin O induces protective immunity against Listeria monocytogenes in mice. Immunology *94*, 14-21.

Yamada, M., Naito, M., and Takahashi, K. (1990). Kupffer cell proliferation and glucan-induced granuloma formation in mice depleted of blood monocytes by strontium-89. J Leukoc Biol *47*, 195-205.

Yan, J., Vetvicka, V., Xia, Y., Hanikyrova, M., Mayadas, T. N., and Ross, G. D. (2000). Critical role of Kupffer cell CR3 (CD11b/CD18) in the clearance of IgM-opsonized erythrocytes or soluble beta-glucan. Immunopharmacology *46*, 39-54.

Youn, J.-I., and Gabrilovich, D. I. (2010). The biology of myeloid-derived suppressor cells: the blessing and the curse of morphological and functional heterogeneity. Eur. J. Immunol. *40*, 2969-2975.

Yuasa, H., and Watanabe, J. (2003). Are novel scavenger-like receptors involved in the hepatic uptake of heparin? Drug Metab Pharmacokinet *18*, 273-286.

Zawrotniak, M., and Rapala-Kozik, M. (2013). Neutrophil extracellular traps (NETs) - formation and implications. Acta biochimica Polonica *60*, 277-284.

Zhang, D., Zhang, G., Hayden, M. S., Greenblatt, M. B., Bussey, C., Flavell, R. A., and Ghosh, S. (2004). A toll-like receptor that prevents infection by uropathogenic bacteria. Science *303*, 1522-1526.

Zhang, J., Zhu, J., Bu, X., Cushion, M., Kinane, T. B., Avraham, H., and Koziel, H. (2005). Cdc42 and RhoB activation are required for mannose receptor-mediated phagocytosis by human alveolar macrophages. Mol. Biol. Cell *16*, 824-834.

Zhu, Y., Li, X., Schuchman, E. H., Desnick, R. J., and Cheng, S. H. (2004). Dexamethasone-mediated up-regulation of the mannose receptor improves the delivery of recombinant glucocerebrosidase to Gaucher macrophages. J Pharmacol Exp Ther *308*, 705-711.

Zundel, E., and Bernard, S. (2006). Listeria monocytogenes translocates throughout the digestive tract in asymptomatic sheep. J. Med. Microbiol. *55*, 1717-1723.

9 Acknowledgements

First of all I would like to thank Dr. Admar Verschoor for offering me this interesting project his supervision throughout my thesis, incredibly interesting and insightful brainstorming-session and for giving me the freedom to follow my own interests on the side.

Prof. Dr. Dirk Busch I would like to thank for giving me the opportunity to work at this institute, as well as important input during the thesis and acting as first examiner for this thesis. In the same line I would like to thank Prof. Dr. Thilo Fuchs for being the second examiner of this thesis.

I must also extend my thanks to the group of Prof. Dr. Steffen Maßberg, especially Raffaele Coletti and Christin Lehmann for being integral for the setup and the execution of the intravital experiments, as well as Prof. Markus Schwaiger, Iina Laitinen, Sybille Reder, Marco Lehmann and Markus Mittelhäuser for cooperating with us to establish the PET-CT model.

I would furthermore like to acknowledge the SFB914 and the associated IRTG for funding and continued education during my thesis.

Thank you to all fellow group members (Amelie, Andy, Ann, Julia, Patrick, Ronny and Shanshan) and also the students who I had the pleasure to supervise (Eva and Martin) for the pleasant atmosphere in the lab. I also want to extend this thanks to all of the people on the 2nd floor. Some of the worst evenings turned out to be the best, simply by sitting in the kitchen with a beer and an open ear to talk to.

And finally, my heartfelt thanks goes to my family and especially Christin, for being there in times of need, encouraging me and also giving me the needed distraction to stay mostly sane throughout the last years.

Publication: (in revision at *Cell Host & Microbe*)

Dual-track clearance of bacteremia balances rapid restoration of blood-sterility with adaptive immune-induction

Steven P. Broadley*, Ann Plaumann*, Raffaele Coletti, Christin Lehmann, Andreas Wanisch, Amelie Seidlmeier, Knud Esser, Shanshan Luo, Patrick C. Rämer, Steffen Massberg, Menno van Lookeren Campagne, Dirk H. Busch, Admar Verschoor

*Equal contribution